INTEGRATION OF TRIGENERATION AND CO_2 BASED REFRIGERATION SYSTEMS FOR ENERGY CONSERVATION

A thesis submitted for the degree of
Doctor of Philosophy

By

I Nyoman Suamir, M.Sc.

Department of Mechanical Engineering
School of Engineering and Design
Brunel University

September 2012

ABSTRACT

Food retail with large supermarkets consumes significant amounts of energy. The environmental impact is also significant because of the indirect effect from CO_2 emissions at the power stations and due to the direct effect arising from refrigerant leakage to the atmosphere. The application of trigeneration (local combined heat, power and refrigeration) can provide substantial improvements in the overall energy efficiency over the conventional supermarket energy approach of separate provision of electrical power and thermal energy.

The use of natural refrigerants such as CO_2 offers the opportunity to reduce the direct impacts of refrigeration compared to conventional systems employing HFC refrigerants that possess high global warming potential. One approach through which the overall energy efficiency can be increased and the environmental impacts reduced, is through the integration of trigeneration and CO_2 refrigeration systems where the cooling generated by the trigeneration system is used to condense the CO_2 refrigerant in a cascade arrangement. This research project investigates experimentally and theoretically, through mathematical modelling and simulation, such a system and its potential application to supermarkets.

A small size CO_2 refrigeration system for low and medium food temperature applications was designed and constructed to enable it to be integrated with an existing trigeneration system in the refrigeration laboratory at Brunel University to form an integrated trigeneration and CO_2 refrigeration test facility. Prior to the construction, the design of the system was investigated using mathematical models developed for this purpose. The simulations included the CO_2 refrigeration system, CO_2 evaporator coils and the integration of the trigeneration and CO_2 refrigeration systems. The physical size of the design and component arrangement was also optimised in a 3D AutoCAD model.

A series of experimental tests were carried out and the results showed that the medium temperature system could achieve a very good COP, ranging from 32 to 60 due to the low pumping power requirement of the liquid refrigerant. The low temperature system performed with average steady state COP of 4, giving an overall refrigeration system COP in the range between 5.5 and 6.

Mathematical models were also developed to investigate the application of the integrated trigeneration and CO_2 refrigeration system in a case study supermarket. The models were validated against test results in the laboratory and manufacturers' data. The fuel utilisation efficiency and environmental impacts of different trigeneration and CO_2 refrigeration arrangements were also evaluated. The results indicated that a system comprising of a sub-critical CO_2 refrigeration system integrated with a trigeneration system consisting of a micro-turbine based Combined Heat and Power (CHP) unit and ammonia-water absorption refrigeration system could provide energy savings of the order of 15% and CO_2 emission savings of the order of 30% compared to conventional supermarket energy systems. Employing a trigeneration system with a natural gas engine based CHP and Lithium Bromide-Water sorption refrigeration system, could offer energy savings of 30% and CO_2 emission savings of 43% over a conventional energy system arrangement. Economic analysis of the system has shown a promising payback period of just over 3 years compared to conventional systems.

PUBLICATIONS

Published journal papers:

Suamir, IN., Tassou, S.A., Marriott, D., 2012. Integration of CO_2 refrigeration and trigeneration systems for energy and GHG emission savings in supermarkets. *Int. J. Refrigeration* 35, 407-417.

Suamir, IN., Tassou, S.A., 2012. Performance evaluation of integrated trigeneration and CO_2 refrigeration systems. *Appl. Therm. Eng.* doi:10.1016/j.applthermaleng. 2011. 11.055.

Published conference papers:

Suamir, IN., Tassou, S.A., 2011. Modelling and performance analyses of CO_2 evaporator coils for chilled and frozen food display cabinets in supermarket applications. *23rd IIR International Congress of Refrigeration*: Refrigeration for Sustainable Development, Prague, Czech Republic, ISBN 978-2-913149-89-2, paper no. 742, 8 pgs.

Suamir, IN., Tassou, S.A., 2011. Performance evaluation of integrated trigeneration and CO_2 refrigeration systems. *2nd European Conference on Polygeneration*, Tarragona, Spain, ISBN 978-8-461498-44-4, paper no. 47, 12 pgs.

Tassou, S.A., **Suamir, IN.**, 2010. Trigeneration – a way to improve food industry sustainability. *Proc. SEEP 2010 Conference*, Bari, ITALY, 14 pgs.

Suamir, IN., Tassou, S.A., Hadawey, A., Marriott, D., 2010. Integration of CO_2 refrigeration and trigeneration systems for supermarket application. *Proc. 1st IIR Conference on Sustainability and the Cold Chain*, Cambridge, UK, ISBN 978-2-9193149-75-5, paper no. 203, 8 pgs.

Suamir, IN., Tassou, S.A., Hadawey, A., Chaer, I., Marriott, D., 2009. Investigation of the performance characteristics of an ammonia-water absorption chiller in a trigeneration system arrangement. *Proc. Heat and Power Cycle Conference*, Berlin, Germany, ISBN 978-0-956332-90-5, paper no. HPC-430, 6 pgs.

Tassou, S.A., Chaer, I., Sugiartha, N., Marriott, D., **Suamir, IN.**, 2008. Trigeneration - a solution to efficient use of energy in the food industry. *Proc. Inst. R.* 2007-08 7/1-16.

Other published conference papers:

Suamir, IN., Tassou, S.A., Arrowsmith, P., Bushell, M., 2012. Performance of integral hydrocarbon cabinets for supermarket applications. *Proc. 10th IIR Gustav Lorentzen Conference on Natural Refrigerants*, Delft, The Netherlands, ISBN 978-2-913149-90-8, paper no. GL-203, 8 pgs.

Hadawey, A., Tassou, S.A., **Suamir, IN.**, Jouhara, H., 2010. Performance optimization of a secondary refrigerant display cabinet using tests and CFD modelling. *Proc. 1st IIR International Cold Chain Conference*, Cambridge, ISBN 978-2-913149-75-5, paper no. 214, 8 pgs.

Presented material:

Suamir, IN., Tassou, S.A., 2010. Trigeneration and its integration with CO_2 refrigeration systems for supermarket applications. In: *the SIRAC meeting*, Brunel University, 23rd June 2010, 17 pgs, available from http://www.sirac.org.uk/.

CONTENTS

LIST OF FIGURES

LIST OF TABLES

ACKNOWLEDGEMENTS

Integration of trigeneration and CO_2 based refrigeration systems for energy conservation in the food industry was a research project in the Centre for Energy and Built Environment Research (CEBER), School of Engineering and Design, Brunel University. The project was managed by Prof. Savvas Tassou and financially supported by DEFRA under the Advanced Food Manufacturing LINK Programme. This thesis is based on the work carried out for this project.

I am really grateful for the opportunity to be the researcher on this project. The project has appreciably broadened my knowledge and has considerably improved my practical skill and research experience in the areas of CO_2 refrigeration and trigeneration.

I would like to express my special appreciation and gratitude to Prof. Savvas Tassou for his guidance and enthusiastic support throughout the project. His advice and encouragement have strongly inspired me to complete the project successfully and this thesis. I would also like to thank Dr. Yunting Ge, a member of the academic team, for his assistance as well as the refrigeration laboratory technical team and all my colleagues in the Mechanical Engineering Department of Bali State Polytechnic for all their support and encouragement.

It is my great pleasure to acknowledge the financial support received from the Food Technology Unit of DEFRA and the contribution of the industrial collaborators: Tesco Stores Ltd, A&N Shilliday & Company Ltd, ACDP (Integrated Building Services) Ltd, Apex Air Conditioning Ltd, Bock Kältemaschinen GmbH, the Bond Group, Bowman Power group, Cambridge Refrigeration Technology, Cogenco, CSA Consulting Engineers Ltd, Danfoss, Doug Marriott Associates, George Baker & Co (Leeds) Ltd and Somerfield Property Co Ltd.

Finally, I would like to express my very special gratitude to my wife, Ni Made Kuerti, and my daughters, Ni Wayan Engginia and Ni Made Ticheyani, for their patience and fortitude during the most arduous time. I would like to dedicate my thesis to them. I also express my gratitude to my parents and relatives for their support and encouragement.

NOMENCLATURE

A	Area (m^2)
COP	Coefficient of performance (-)
C_p	Specific heat (kJ/kg.K)
CR	Circulation ratio (-): defined as the ratio of refrigerant mass flow rate circulated through the evaporator to the mass flow rate of refrigerant vaporised, described in page 50 and equation (5.6)
d	Diameter (m or mm)
D_h	Hydraulic diameter at air side of a finned tube coil (m)
E_f	Fuel energy consumption (kWh)
E_{annual}	Energy consumption (kWh)
$FESR$	Fuel energy saving ratio (%)
$FEUR$	Fuel energy utilization ratio (%)
Fo	Fourier number (-)
G	mass velocity ($kg/s.m^2$)
GWP	Global warming potential ($kgCO_2/kg$)
H	Specific enthalpy (kJ/kg)
h	Heat transfer coefficient ($kW/m^2.K$ or $W/m^2.K$)
j	Colburn j-factor (-)
L	Length (m)
L_{annual}	Annual refrigerant leakage (kg)
m_{charge}	Mass of refrigerant charge (kg)
m	Mass (kg); a fin efficiency parameter (1/m) defined by equation (4.33)
$\dot{m}$	mass flow rate (kg/s)
M	Molecular weight (kg/mol)
n	System operating time (years)
N	Number of rows or circuits
$NPSH$	Net positive suction head (mLC: metre liquid column)
P	Pressure (kPa or Pa or bar or bar_a)
Pr	Prandtl number (-)
Q	Discharge capacity (kg/h); heating or refrigerating load (kW or kWh)
q	Heat flux (W/m^2)
R	Thermal resistance ($m^2.K/kW$)
Re	Reynolds number (-)
RH	Relative Humidity (%)
R_p	Pressure ratio (-)
S	Suppression factor (-), spacing (m)
T	Temperature (^oC or K)
t	Time (s)
u	Refrigerant velocity (m/s)

U	Overall heat transfer coefficient (kW/m^2.K)
W	Electrical power/energy (kW or kWh)
x	Vapour quality (-)

Greek symbols

α	Recovery factor; thermal diffusivity (m^2/s)
β	CO_2 emissions factor (kgCO_2/kWh)
Δ	Difference
δ	Thickness (m or mm), liquid film thickness (m)
ε	Cross sectional vapour void fraction (-)
φ	Density of heat flowrate (kW/m^2)
η	Efficiency
λ	Thermal conductivity (kW/m.K or W/m.K)
μ	Dynamic viscosity (N.s/m^2)
ρ	Density (kg/m^3)
θ	Dry angle (rad)
ϕ	Fin efficiency parameter (-) defined by equation (4.34)
ω	Humidity ratio (kg/kg$_{da}$)

Subscript

a	Air or air-side
abs	Absorption chiller
add	Additional load
amb	Ambient
c	Cooling, convective, circuit, cold
cab	Display cabinet
cb	Convective boiling
ChW	Chilled water
comp	Compressor
cond	Condensing, condenser
conv	Conventional
crit	Critical point
CW	Cooling water
d	Diagonal
de	Dry out completion
df	Defrost cycle
Dh	Calculated at hydraulic diameter
di	dry out inception
e	Electrical
eq	Equivalent
evap	Evaporating, evaporator
f	Fin or fuel
ff	Free flow sectional
fl	Fouling
fr	Frictional

H	Homogenous
h	Heating, hydraulic, hot
htf	Heat transfer fluid
i	Inlet, in, width axis
int	Integrated system, intermediate
j	Depth axis
k	Height axis
L	Liquid phase
lat	Latent
lm	Logarithmic mean
m	Mean, momentum
M	Mist flow region
md	Maximum discharge
nb	Nucleate boiling
o	Outlet, out, overall
others	Other than refrigeration and electric chiller
r	Refrigeration, refrigerant, refrigerant-side
SG	Standby generator
sp	Single phase
s	Isentropic, surface
sc	Sub-cooling
sh	Superheating
t	Tube
th	Thermal
tp	Two phase
tri	Trigeneration
trigen	integrated trigeneration and CO_2 refrigeration energy system
trip	Triple point
V	Vapour phase
v	Volumetric
vap	Vaporization
w	Water-glycol mixture

ABBREVIATION AND GLOSSARY

AK-CC	Adap-Kool cabinet controller: a cabinet controller manufactured by Danfoss
AKV	Adap-Kool valve: an electrically operated expansion valve manufactured by Danfoss
ARI	Air conditioning and refrigeration institute
ASHRAE	American society of heating refrigerating and air-conditioning engineers
BV	Ball valve
CCC	Committee of the climate change
CCHP	Combined cooling heating and power
CFC	Chloro-fluoro-carbon
CHRP	Combined heating refrigeration and power
CHP	Combined heat and power
CIBSE	Chartered Institution of building services engineers
CO_2	Carbon dioxide
CO_2e	Carbon dioxide equivalent
CP grade	Chemically pure
DEFRA	Department for environment, food and rural affairs
EES	Engineering equation solver
EC	Evaporator coil
EIA	Energy information administration
ETS	Electrically operated expansion valve, manufactured by Danfoss
EXV	Electronic expansion valve
DX	Direct expansion
FPI	Number of fins per inch
FPM	Number of fins per metre
Fossil fuel	An energy source formed in the earths crust from decayed organic material. The common fossil fuels are petroleum, coal and natural gas.
Food refrigeration	Application of a refrigeration system on the prevention and retardation of microbial, physiological, and chemical changes in foods. It also plays a major role in maintaining a safe food supply, nutritional content and retaining characteristics such as flavour, colour and texture (ASHRAE, 2010)
GHG	Green House Gases: gaseous constituents of the atmosphere, both natural and anthropogenic, that absorb and emit radiation at specific wavelengths within the spectrum of infrared radiation emitted by the Earth's surface, the atmosphere, and clouds (PAS 2050, 2008)

GAX	Generator absorber heat exchange
HC	Hydrocarbon
HCFC	Hydro-chloro-fluoro-carbon
HFC	Hydro-fluoro-carbon
HT	High stage of a cascade system/High temperature
HTF	Heat transfer fluid
HVAC	Heating ventilation and air conditioning
HX	Heat exchanger
ICM	Industrial control motor valve
ICMT	High pressure expansion valve
IHX	Internal heat exchanger
IEA	International energy agency
IPCC	Intergovernmental panel on climate change
Isenthalpic expansion	Expansion which takes place without any change in enthalpy
kW	Kilowatt
kWh	Kilowatt hour
LRLM	Load ratio low to medium temperatures of a refrigeration plant
LT	Low temperature
MO	Mineral oil
MOP	Maximum operating pressure
MOPD	Maximum operating pressure difference
MT	Medium temperature
MTP	Market transformation programme
MWh	Megawatt hour = 1000 kilowatt hour
N/A	Not applicable
NG	Natural Gas (primarily methane)
NRV	Non-return valve
O&M	Operational and maintenance
ODP	Ozone depleting potential
PAO	Poly-alpha olefin (oil)
PAS	Publicly available specification
PHX	Plate type heat exchanger
POE	Polyol ester (oil)
Primary fuel	All fuels consumed by end users, including the fuel consumed at electric utilities to generate electricity
ppm	Part per million
PTC	Positive temperature coefficient
Refrigerated display cabinet: a cabinet cooled by a refrigerating system which enables chilled and frozen foodstuffs placed therein for display to be maintained within prescribed temperature limits (ISO 23953-1, 2005)	

RCD	Residual current device
RV	Regulator valve
SCA	Solution cooled absorber
SG	Sight glass
SRC	Specific refrigerant charge defined as refrigerant mass per unit refrigerating capacity, or heating capacity for heat pumps (MTP, 2008); Super radiator coils
SV	Solenoid valve
Sustainability	Sustainable development is development that meets the needs of the present without compromising the ability of future generations to meet their own needs (Evans, 2010)
TOC	Technical options Committee (UNEP)
TXV	Thermostatic expansion valve
Uncertainty	A concept to describe the degree of goodness of a measurement, experimental result, or analytical result (Coleman and Steele, 2009); lack of confidence
UNEP	United Nations Environment Programme

Chapter 1

INTRODUCTION

Global energy demand has been increasing alongside the growth of world population and economy. The increase of energy demand, especially energy from fossil fuel, increases emissions to atmosphere which contributes to the deterioration of ambient air quality with serious public health and environmental effects. World energy demand related greenhouse gas emissions, on the basis of current policies, will be 40% higher in the year 2030 relative to 2007 (IEA, 2009). In order to deal with increases in fossil fuel use, industrialised countries such as the UK and the European Union have been developing an ambitious energy policy to tackle carbon dioxide emissions and climate change. In the UK, the targets are a 60% reduction in greenhouse gas emissions by 2030 compared to 1990 levels and a reduction of at least 80% by 2050 (CCC, 2008 and CCC, 2010).

In developed countries, there is also a trend of increasing consumption of food products which in them has an impact on greenhouse gas emissions. It is estimated that for Western Europe the food industry is responsible for between 20% and 30% of GHG emissions (Tassou and Suamir, 2010). A major source of emissions is energy use by manufacturing processes, food distribution and retail. In the UK, food distribution and retail are responsible for approximately 7% of total GHG emissions (DEFRA, 2005). Refrigeration, which is increasingly important in the processing and preservation of food, is potentially responsible for significant GHG emissions. As described by Coulomb (2008), refrigeration technology is responsible for 15% of all electricity consumed worldwide. Approximately 72% of the global warming impact of

refrigeration plant is due to energy consumption (Cowan et al., 2010). Reducing the energy consumption of refrigeration plant has therefore become one of the key priorities in the reduction of GHG emissions of the food sector.

Another important source of GHG emissions from refrigeration is refrigerant leakage from the refrigeration plant. Extensive pipe-work with associated pipe joints used in refrigeration plant increases the potential for refrigerant losses. HFC refrigerants, currently used in food refrigeration systems, have zero impact on ozone depletion (ODP) and provide comparable performance to CFC and HCFC refrigerants. Leakage of HFC refrigerants to the atmosphere, however, has significant impact on GHG emissions due to their high global warming potential (GWP). This has prompted the introduction of the F-gas regulations by the European Union which are designed to contain, prevent and thereby reduce emissions of fluorinated gases including all HFC refrigerants, such as R-134A, R-407C, R-410A, and R-404A. Replacement of F-gas based refrigerants with negligible or no GWP refrigerants (often called 'natural refrigerants') such as hydrocarbons, ammonia and CO_2 can reduce direct impacts to the environment and present significant challenges to the food refrigeration industry.

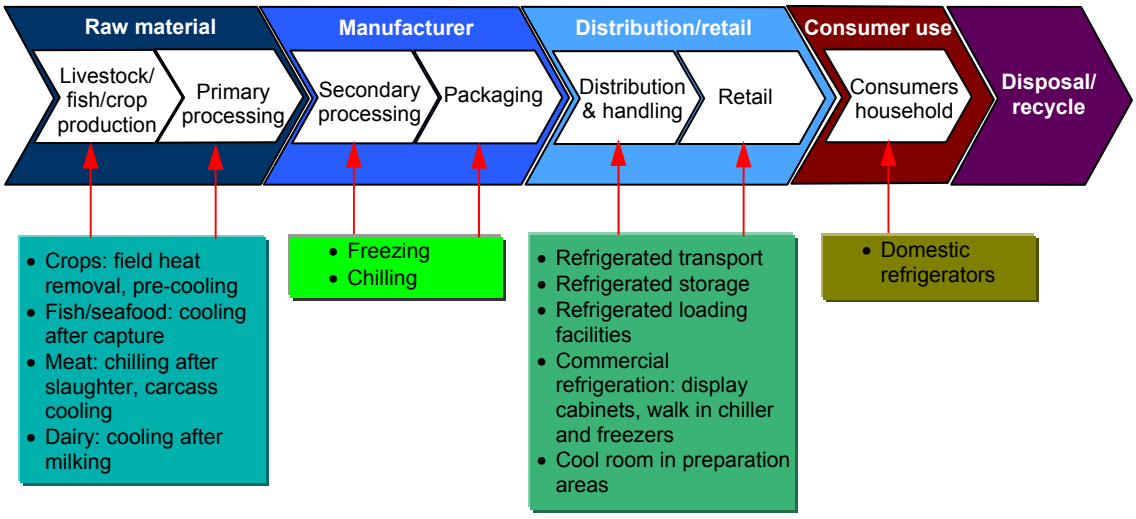

Figure 1.1 Cold chain and refrigeration technology in the life cycle stages of food products
(Source: Estrada-Flores, 2010 and PAS 2050, 2008)

In order to asses GHG emissions in the food industry, it is necessary to consider all stages across the entire life cycle of a food product. These stages are illustrated in Figure 1.1. Refrigeration is employed in almost all the stages of the life cycle to control

the temperature required to maintain food quality from harvest to consumption in the home. A study of the energy used by refrigeration systems across the cold chain has shown that the most significant energy usage for refrigeration in the UK is from the retail sector. This sector was responsible for energy use in the range between 35% and 52% of the estimated energy usage of the top ten food refrigeration sectors (Swain, 2006). A similar study in Australia revealed that the retail sector makes the most significant contributions to cold chain electricity consumption after domestic sector of about 44% (Estrada-Flores, 2010).

1.1 Energy consumption of the food retail industry

In the UK, food retail consumes significant amounts of energy with large supermarkets accounting for between 3% and 5% of total electrical energy consumption (Tassou et al., 2007). Electricity consumption of food retail varies from one store to another depending on the size and format of the store, equipment used, building fabric, sales activity, internal environment, energy and control systems deployed. The variation of electricity consumption per net sales area (also known as electricity intensity) of different types of stores is shown in Table 1.1. It can be seen that the electricity intensity of supermarkets can vary widely from around 500 kWh/m^2 in hypermarkets to over 2900 kWh/m^2 in convenience stores (Tassou et al., 2009). The baseline electricity intensity of the UK's supermarkets was reported by CIBSE to be 915 kWh/m^2 (CIBSE Guide F, 2004).

Table 1.1 Electricity intensity of different size of the food retail stores

Type of stores	No. of stores	Sales area	Electrical energy intensity (kWh/m^2)	
		m^2	Range*	Average
Convenience stores	640	80-280	2900-700	1540
Mid-range stores	1360	280-1400	2600-500	1000
Superstores	420	1400-5000	1500-500	920
Hypermarket	150	5000-10000	1180-500	770

*Electrical energy intensity reduces as the sales area increases
Source: Tassou et al. (2009)

Segmentation of electricity usage in supermarkets also varies. Investigation of several medium size supermarkets in the UK found that the refrigeration systems consume most electricity in the range between 30% and 60%. Lighting accounts for between 15% and 30% and the heating ventilating and air conditioning (HVAC) equipment accounts for

about 10%. Preparation food and services (PFS) and other store utilities account for the remainder. Investigation was based on the energy meter data from Tesco (2009). Similar breakdown of electricity consumption for supermarkets in the UK can also be found in Evans (2008) and Tassou et al. (2009). The breakdown of electricity consumption of a typical medium size retail store is shown in Figure1.2.

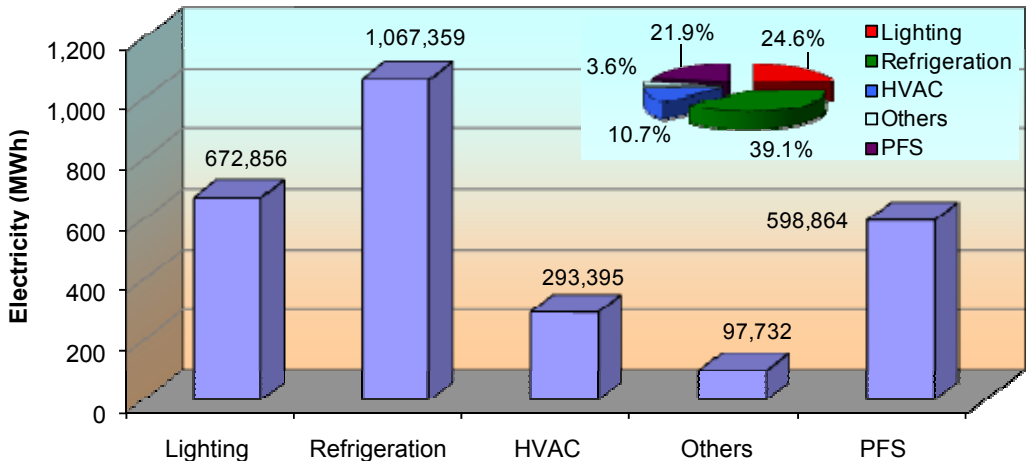

Figure 1.2 Annual electricity consumption of typical 50,000 ft^2 UK supermarket
(Data source: Tesco, 2009)

Electricity for refrigeration in retail food stores is normally distributed through two separate distribution circuit. One circuit is used to power the refrigeration packs which include compressors, pumps and condensers. The second circuit supplies the chilled and frozen food display cabinets for lights, fans, controls, etc. in the sales area. Comparative amounts of electricity consumed by refrigeration in some F-50 stores are shown in Figure 1.3. It can be seen that the electricity supplied to the medium temperature (MT), low temperature (LT) packs and display cabinets can vary from one store to another with average values around 42% for MT, 20% for LT and 38% for cabinets. These comparative figures are slightly different from those of Lawrence and Gibson (2010) for which display cabinets were reported to consume 42%, MT pack systems 35% and LT pack systems 23% of total refrigeration energy. The amount of electricity used by the packs depends on the type of the system used, refrigeration load, control strategy employed and ambient temperature. The electrical energy consumption of display cabinets is related to all electric components in the cabinet such as fans, lights, anti sweat heaters and defrost heaters.

Supermarkets also have a need for space heating and domestic hot water. These heating needs are normally satisfied by gas fired boilers. Gas consumption varies during the year; it is high in the winter and very low in the summer. The annual gas consumption of an F-50 store with a sales area of 4700 m^2 was approximately 880 MWh, equivalent to 187 kWh/m^2 (Tesco, 2009). A wider range of gas consumption in different type of retail food stores is reported by Tassou et al. (2009). The baseline figure in CIBSE Guide F (2004) is 200 kWh/m^2.

Figure 1.3 Electricity consumption of refrigeration packs and display cabinets of some F-50 supermarkets in the UK (Data source: Tesco, 2009)

1.2 Environmental impacts

As described in the preceding section food retail is one of the most energy intensive sectors of the food cold chain. Supermarkets, particularly, have significant environmental impacts due to indirect emissions of greenhouse gases (GHG) from electricity generation in power stations (Tassou et al., 2011). In the UK, the indirect CO_2 emissions from the energy use account for 4.01 $MtCO_2e$ of which 88% is emissions from electrical energy consumption and the remainder is from natural gas (Tassou et al., 2009).

Supermarkets are also responsible for direct greenhouse gas emissions from refrigerant leakage with high global warming potential (GWP) to the environment (Tassou et al., 2011). Walravens et al. (2009) reported that supermarkets are the biggest source of HFC

emissions in the UK with their refrigeration and air conditioning equipment being responsible for 2 $MtCO_2e$ emissions per year.

The environmental impact of refrigerant leakage depends on the type of refrigerant, amount of refrigerant charge and leak tightness of the refrigeration systems. Typical values for specific refrigerant charge (SRC) are provided in MTP (2008). For centralised supermarket systems charged with HFC/HCFC and R-744 refrigerants, the average SRCs are in the region of 3.5 and 1.8 kg per kW refrigerating capacity respectively. Estimates of refrigerant leakage from centralised supermarket refrigeration systems vary in the range between 10% and 25% of charge per annum (MTP, 2008). The author also summarised refrigerant leak rates from four different studies. Detailed specific refrigerant charge and refrigerant leakage for different types of refrigerants and equipment are also presented in Appendix K.

Evans (2008) reported refrigerant leakage from supermarkets to be in the range between 18% and 35% of refrigerant charge per year. It was also reported that leakage of HFC and HCFC refrigerants from Canadian supermarkets was in the range between 10% and 30% of charge per year (CanmetENERGY, 2009). United Nations Environment Programme (UNEP) reported annual supermarket emission rates in the range 15 to 30% of their charge (TOC, 2006). Alongside the direct emissions, refrigerant leakage can also have a significant impact on the energy consumption of the refrigeration systems, since a low charge reduces sub-cooling and increases the superheat, resulting in lower system performance as noted in MTP (2008) and Cowan et al. (2010).

1.3 Approach towards sustainability

The energy plant in a supermarket generally comprises refrigeration systems, heating and cooling systems and electrical supply which is derived from the National Grid. The efficiency of the overall energy system is also low below 55%, because of seasonal variations in demand and the relatively low electricity generation efficiency in power stations as well as distribution losses in the grid (Tassou and Suamir, 2010).

One option of increasing the energy utilisation efficiency of supermarket facilities is through local combined heat and power generation (CHP) also known as co-generation. CHP is a highly efficient method of simultaneously generating electricity and heat at or

near the point of use. CHP can achieve overall efficiencies of up to 85% (CIBSE CHP Group, 2005), which is significantly higher than the separate production of electricity and heat. CHP can offer reduced energy costs and can employ a wide range of fuels, including gas, oil, biogas, bio-fuel, biomass and waste.

The efficiency of CHP varies depending on the type of system, fuel, electrical power output and most importantly the availability of sufficient demand for the generated electricity and thermal energy. Figure 1.4 shows the variation of fuel utilisation efficiency of gas engine based CHP for different size of power output and 100% utilisation (availability). It can be seen that the overall efficiency of CHP can exceed 70% and can sometimes reach 90%, almost 50% higher than the electrical efficiency of electricity generated from the grid.

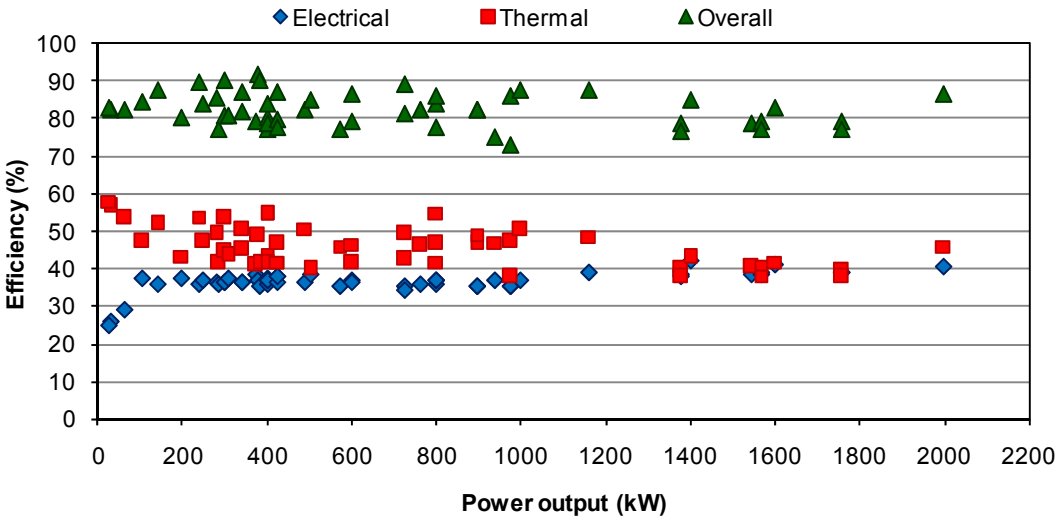

Figure 1.4 Efficiency of different module types of gas engine based CHP
(Data source: Cogenco, 2008)

In supermarket applications, steady demand for the generated electricity and thermal energy is not available throughout the year. The heat demand varies considerably between summer and winter. The efficiency of the CHP, therefore, drops significantly in the summer which also reduces the overall seasonal efficiency. During the summer time, consideration can be made to export thermal energy to neighbouring facilities, but this approach introduces complexities and costs. Where it is not feasible to export heat, a heat following strategy can be adopted in which the heat output is modulated to follow

the site heat demand. This strategy, however, results in fluctuations in the electrical power generation which results in the import of electricity from the National Grid. This strategy leads to a lower efficiency compared with full load operation (Sugiartha et al., 2006).

In order to achieve high efficiencies, CHP systems have to operate at maximum load for the vast majority of time and make maximum utilization of the generated electrical power and heat. One way of ensuring the high energy conversion efficiencies of CHP systems are maintained throughout the year is to use some of the excess heat available in periods of low heat demand to drive sorption refrigeration systems and provide cooling or refrigeration. The integration of CHP and sorption refrigeration or other technologies to provide simultaneously electrical power, heating and cooling or refrigeration is called trigeneration (Tassou et al., 2007). Trigeneration is also known as CCHP (Combined Cooling, Heating and Power) or CHRP (Combined Heating, Refrigeration and Power) as in Bassols et al. (2002) and Maidment and Prosser (2000). The term polygeneration is also sometimes used for the combined and simultaneous production of electricity, heat, cold and other useful forms of energy (PolySMART, 2008).

Trigeneration systems have been used in a number of applications including commercial buildings and industrial facilities. Most of these have been for space cooling applications with a smaller number for refrigeration applications in the food processing industry which requires temperatures below 0 ^{o}C. A number of investigations into the application of trigeneration in the food industry have been reported in the last 10 years. Bassols et al. (2002), illustrated examples of typical ammonia-water plant in the food industry. Theoretical evaluation of trigeneration for supermarket applications has shown that the system can provide 20% energy saving with attractive payback periods (Maidment et al., 1999; 2001; Maidment and Tozer, 2002). Tassou et al. (2007) and Sugiartha et al. (2008) showed that trigeneration technology based on a micro gas turbine integrated with an ammonia water absorption refrigeration system can provide promising economic and environmental benefits when used in supermarket applications. The authors indicated that payback periods of between 3 and 5 can be achieved. Arteconi et al. (2009) reported that trigeneration systems in supermarket applications can produce primary energy savings of 56% with payback period of less than 5 years.

The economic viability of trigeneration for supermarket applications is very sensitive to the price of grid electricity relative to the price of natural gas which is also known as spark ratio. A gas powered trigeneration system will be economically attractive when the spark ratio is greater than 3.3 (Tassou et al., 2007; Sugiartha et al., 2006; 2008). In the UK, the recent increases in electricity and fuel prices have increased the spark ratio and price gap between grid electricity and natural gas (spark gap) as shown in Figure 1.5. The good trend of spark ratio and spark gap together with increased concerns about the environmental impacts of the retail food industry have increased interest in the application of trigeneration technology to supermarkets in the UK.

As indicated earlier the main environmental impact of refrigeration systems are from energy use and from refrigerant leakage. Alternative solutions to reduce the emissions from refrigerant leakage are to use environmentally friendly refrigerants, such as natural refrigerants or secondary refrigerants. Melinder and Granryd (2010) showed that indirect refrigeration systems can reduce refrigerant charge drastically down to 5 - 15% of that of traditional DX-systems.

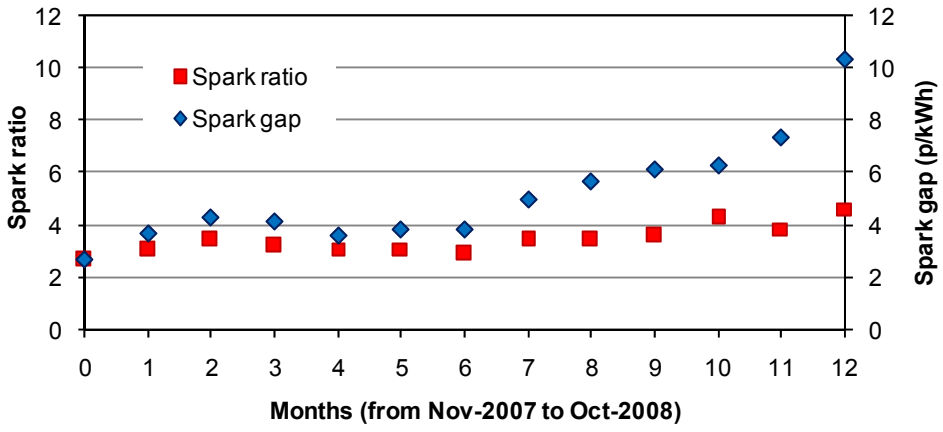

Figure 1.5 Comparison of electricity and gas price in the UK
(Source: Moorjani, 2009)

CO_2 is natural refrigerant that has received considerable attention in the last 10 years. Research and development particularly in Scandinavia, USA and Japan is aimed at developing CO_2 systems for a wide range of applications ranging from small commercial refrigeration and air conditioning systems to car air conditioners and larger commercial and industrial systems, including supermarkets. Most of the development work on CO_2 systems for supermarkets has taken place in Scandinavia and Germany.

However significant interest in CO_2 refrigeration has also been demonstrated in some supermarkets in the UK, Australia, Canada and the Latin America.

In the UK, there is increasing interest by supermarket chains to move towards sustainable and environmentally friendly refrigeration technologies including CO_2 refrigeration. In 2009 there were 46 stores across the UK using CO_2 based technology, increasing from just 14 stores in 2008. Sainsbury's is committed to phasing HCFCs and HFCs and plans to switch to CO_2 in all of its stores by 2030 with the first 135 stores set to be converted by 2014. Tesco plans to introduce CO_2 refrigeration in 150 stores by 2012. M&S and Morrisons converted 34 stores to CO_2 by 2009 and Waitrose is implementing an innovative system based on HC refrigerant (Walravens et al. 2009).

Most of the early systems operate on the subcritical cycle where CO_2 is used in a cascade arrangement with a conventional refrigeration system operating with ammonia, HCs or HFCs. Such arrangements keep the pressures in the CO_2 system relatively low, but still suffer the disadvantage of using another refrigerant such as HFC with its associated global warming implications.

Another way of improving the performance of CO_2 refrigeration as well as totally avoiding the use of HFC refrigerants is by using cascade CO_2 refrigeration with HC or ammonia refrigerant in the high stage system. Bellstedt (2008) indicated that CO_2/NH_3 systems can achieve yearly energy savings of up to 35% over conventional R-404A systems. However, most retailers in the UK have been reluctant to use HC and ammonia in supermarkets due to their flammability and toxicity. Another option is to use absorption/adsorption refrigeration for the high stage in a cascade CO_2 refrigeration arrangement. This solution can be particularly advantageous when the sorption refrigeration system is driven by waste heat or is integrated with a CHP system in a trigeneration system arrangement.

1.4 Research project description

Trigeneration can provide substantial improvement in the overall energy efficiency over the conventional supermarket energy approach of separate provision of electrical power and heat energy. Trigeneration can also make significant contributions to the reduction of the environmental impacts of food factories and supermarkets. This research aims to

increase further the energy and CO_2 emission savings potential of trigeneration through its integration with CO_2 refrigeration systems.

The experimental part of the research programme is based on a trigeneration system that incorporates three main modules; CHP module, sorption refrigeration system module, and a refrigeration load module. The approach employed is to use the exhaust gases of a microturbine CHP unit to drive an ammonia-water absorption refrigeration system, which cool a secondary fluid for refrigeration purposes. The heat transfer between the microturbine exhaust heat exchanger and the generator of the absorption system is performed by a heat transfer fluid in a closed heat transfer loop arrangement. A schematic diagram of the trigeneration arrangement test facility using thermal oil as the heat transfer medium between the microturbine and absorption refrigeration system is as shown in Figure A-1 (Appendix-A). It can also be found in Tassou et al. (2008).

The CHP module is a Bowman 80 kWe recuperated microturbine generation package MTG80RC-G with in-built boiler heat exchanger (exhaust heat recovery heat exchanger). The microturbine consists of a single stage centrifugal compressor, single radial turbine within an annular combustor and a permanent magnet rotor (alternator) all on the same rotor shaft. Other systems in the engine bay include the fuel management system and the lubrication/cooling system. Heat recovery from the exhaust gases is performed in a stainless steel flue-gas/liquid heat exchanger. The heat recovery fluid is Diphyl-THT high performance synthetic heat transfer fluid that can operate at temperatures up to 340 ^{o}C.

The sorption refrigeration system employed is a packaged gas fired ROBUR ACF-60LB chiller. The performance of the unit in its gas fired format was established from tests in the laboratory. For brine flow temperatures between -11 ^{o}C and +3 ^{o}C, the refrigeration capacity of the unit was found to vary from 8.5 kW to 15 kW and the *COP* from 0.32 to 0.57 (Tassou et al., 2008). The modified unit performed as well if not better than the gas fired unit. At brine flow temperature of -8.0 ^{o}C both units had a refrigeration capacity of 12 kW and a *COP* of around 0.53. The optimum *COP* of the absorption chiller was achieved at oil temperature of 195 ^{o}C (Suamir et al., 2009).

The use of secondary fluid such as propylene glycol, potassium-formate and sodium chloride for supermarket applications is one disadvantage of the previous trigeneration

system. The high energy consumption of the secondary fluid pumps due to the high viscosity and poor thermodynamic performance of available secondary fluids was the main disadvantage of the previous trigeneration system. Another disadvantage of the system was the relatively low *COP* of sorption refrigeration systems particularly when they operate at low refrigeration temperatures. The system would be more applicable for chilled food refrigeration applications. Thus a separated system would be required to satisfy the frozen food refrigeration demand. The approach followed in this research to overcome the disadvantages of the secondary single phase fluid system is to integrate the trigeneration system with a CO_2 refrigeration system. For medium temperature applications the CO_2 can be used as a volatile secondary fluid with the cooling produced by the trigeneration system providing the heat rejection medium for the condensation of CO_2. For low temperature frozen food applications cooling from the trigeneration system can be used for the condensation of CO_2 which can be used as a primary refrigerant in a low temperature vapour compression system.

The utilisation of CO_2 as a secondary refrigerant can minimise the use of conventional secondary fluids and increase further the energy savings potential of trigeneration systems. The pressure drop and consequently the pump power required for the secondary fluid through the distribution pipe-work and cooling coils in the display cabinets is primarily a function of the viscosity of the secondary fluid. The viscosity of liquid CO_2 is much less than the viscosity of common secondary fluids and thus the power that will be required to circulate CO_2 from the trigeneration system to the display cabinets will be very small compared to the power required for conventional secondary refrigerants. It is therefore estimated that the energy savings for the integrated CO_2 - trigeneration system will be higher than the trigeneration system with conventional secondary fluids. Other advantages of using CO_2 as secondary refrigerant are excellent heat transfer properties, good material compatibility and smaller pipe size requirements.

1.5 Research objectives

The main objective of this research project is, to design, develop and evaluate proof of concept integrated trigeneration and CO_2 refrigeration systems for food refrigeration applications. Such systems should combine the efficiency advantages of trigeneration with the advantages of CO_2 as a primary refrigerant in low temperature systems and as

secondary refrigerant in medium temperature systems. The project will also investigate heat transfer phenomena of the evaporator coils to ensure maximum thermodynamic performance for the CO_2 system.

1.6 Structure of the thesis

The thesis comprises of eight chapters. Chapter 1 provides an introduction of the work in the thesis. Following the introduction in Chapter 1, Chapter 2 presents an overview of CO_2 as a refrigerant and describes the concept of subcritical and transcritical CO_2 refrigeration systems. The chapter also outlines recent development and applications of CO_2 refrigeration system for food preservation in supermarkets.

Chapter 3 discusses the design and construction of the test facility implemented for the experimental investigation of the integration of CO_2 refrigeration and trigeneration systems. Chapter 4 presents modelling and performance analyses of CO_2 evaporator coils which covers heat transfer, pressure drop as well as simulation of frost formation and its effect on the heat transfer performance of the coils. The chapter also describes the application of the models for design and simulation of finned tube flooded and direct expansion coils using CO_2 and R-404A as refrigerants.

Chapter 5 provides experimental test results for the medium and low temperature refrigeration systems as well as the performance of the overall CO_2 refrigeration system as a whole. This chapter also describes temperature and frost performance of the CO_2 display cabinets as well as the validation of the numerical models.

A case study approach of the integration of volatile-DX CO_2 refrigeration and micro-turbine based trigeneration systems in supermarket applications is discussed in Chapter 6. The chapter describes briefly the case study supermarket in respect of its energy consumption and emphasises the energy as well as environmental performance of the supermarket energy system. Alternative solutions of integrated trigeneration and CO_2 refrigeration systems are presented in Chapter 7. Economic analyses of the energy system alternatives are also provided in this chapter.

Finally, Chapter 8 concludes the research work and identifies further investigations and development required to improve system performance and optimisation.

Chapter 2

CO_2 REFRIGERATION IN SUPERMARKETS

The choice of refrigerants in commercial refrigeration systems has been undergoing a rapid change. One approach gaining popularity is the use of natural refrigerants. Natural refrigerants such as ammonia, hydrocarbons (HC) and CO_2 which were known earlier are now experiencing resurgence after the problems to the environment have been rising due to the use of the non-natural refrigerants. Natural refrigerants are environmentally benign. They have been demonstrated to be a complete solution to synthetic refrigerants such as CFC, HCFC and HFC (Lorentzen, 1995; Riffat et al., 1997). The interest to use natural refrigerants in commercial sector varies amongst countries. CO_2 and HC are more attractive especially in Europe and Japan. In Northern European countries all of those natural refrigerants are used. Applications of natural refrigerants in commercial refrigeration are also widespread in Asia, USA, Australia, Canada and other countries can be expected to follow (TOC, 2006).

The use of natural refrigerants has been resurfacing since about the last two decades, but to implement them in supermarket refrigeration systems is still facing some barriers. "Safety and technology" is considered as the most important barrier followed by regulation, training and availability of the components. Some countries are probably still facing a variety of challenges such as policy and situation as regards the phase out of ODP and GWP refrigerants (ATMOsphere, 2010).

With respect to the local safety, CO_2 is an excellent alternative among the natural refrigerants, especially in supermarket refrigeration applications. CO_2 is in group A1 of

the safety classification which is neither flammable nor toxic (BS EN 378-1, 2008; ASHRAE Standard 34, 2007). On the other hand, ammonia carries a B2 safety classification which indicates that it has a high toxicity and also carries a medium flammability risk. Ammonia may be used in supermarket refrigeration systems with several challenges in order to achieve significant acceptance (Pearson, 2008). Combining ammonia with either a cascade CO_2 or a secondary fluid CO_2 is one opportunity to apply it in supermarket as highlighted by Hinde (2011). Such refrigeration system has been implemented in France (Rivet, 2002) and in Australia (Bellstedt, 2008). HC, which is in group A3 (high flammability), may also have some constrains. Possible leakage of HC refrigerant to the occupied area has to be restricted below its lower flammability limit. However, with currently available safety devices, better system tightness, and advanced design strategy in minimising refrigerant charge some supermarkets in the UK and Germany have also employed HC in their refrigeration systems (Gartshore and Benton, 2010; Lidl, 2011).

2.1 CO_2 as refrigerant

CO_2 is a natural substance that has been used in the refrigeration industry since 1866. After reaching peak use for comfort cooling in the 1920s, its use declined to almost zero with the introduction of chlorofluorocarbon (CFC) refrigerants in the 1930s (Bellstedt et al., 2002; Bodinus, 1999). The rapid decline of CFC systems since last decade of the 20^{th} century has resulted in a remarkable increase in refrigeration research for new alternative refrigerants. The research includes the use of old natural refrigerants including CO_2 and ammonia. Since that period, CO_2 has returned as practicable options for various refrigeration applications (Pearson, 2005).

CO_2 (R-744) is an environmentally benign refrigerant. It has an ODP of zero and a very low global warming potential (GWP) of 1. The main advantages of CO_2 compared to other natural refrigerants are that it is non-toxic and non-flammable, which often limits the application of other natural refrigerants such as hydrocarbons and ammonia. CO_2 also has attractive thermo-physical properties: low viscosity, high thermal conductivity, high specific heat capacity and high vapour density. These lead to good heat transfer in evaporators, condensers, and gas coolers, allowing selection of smaller equipment compared to HFC refrigerants.

One distinguishing characteristic of CO_2 is its phase change properties; the triple point is relatively high at -56.6 ^oC (5.2 bar_a) and the critical temperature is 31 ^oC (73.8 bar_a) which is considered to be relatively low (ASHRAE, 2010). This may limit the application flexibility of CO_2 refrigeration systems and the phase change properties from solid, liquid, and vapour as illustrated in Figure 2.1 should be thoroughly considered in any potential applications.

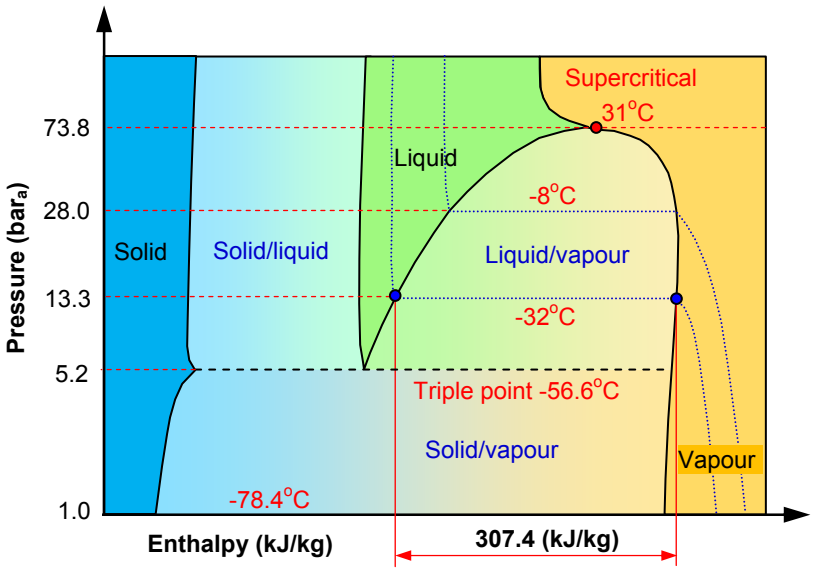

Figure 2.1 CO_2 expansion and phase change
(Adapted from: ASHRAE, 2010)

Comparative performance of CO_2 and selected refrigerants for medium and low temperature refrigeration applications with the same operating conditions are shown in Table 2.1. The refrigeration effect of CO_2 is higher than R-404A but lower than other natural refrigerants. This directly influences the amount of refrigerant that needs to be circulated in a refrigeration system. The table also shows that CO_2 has the lowest pressure ratio among the selected refrigerants which is about 5 to 30% lower for MT system and 15 to 50% for LT system. Having a lower pressure ratio indicates that CO_2 can give greater volumetric and isentropic efficiencies. Another advantage of CO_2 refrigerant which can clearly be seen in the table is that it has a very small suction gas specific volume about 3 to 30 times lower than the other refrigerants for the MT system and even lower for the LT system. This means that a CO_2 refrigeration system will need smaller size compressors and require smaller suction pipe diameters for the same operating conditions.

Table 2.1 Comparative refrigerant performance per kW for MT and LT refrigeration

Refrigerant	P_{evap} (bar_a)	P_{cond} (bar_a)	Pressure ratio	Refrigeration effect (kJ/kg)	Refrigerant mass flow rate x 10^{-3} (kg/s)	Suction gas specific volume x 10^{-3} (m^3/kg)
MT refrigeration system application						
R-22	3.8	11.3	3.0	170.1	5.9	62.6
R-404A	4.7	13.6	2.9	124.2	8.1	42.8
R-290	3.7	10.3	2.9	300.5	3.3	126.1
R-1270	4.6	12.5	2.7	306.4	3.3	105.4
R-717	3.2	11.0	3.5	1134.1	0.9	396.8
R-744	28.0	68.9	2.6	153.1	6.5	13.9
LT refrigeration system application						
R-22	1.5	11.3	7.5	159.4	6.3	150.3
R-404A	1.9	13.6	7.0	110.1	9.1	101.3
R-290	1.5	10.3	6.6	271.7	3.7	285.4
R-1270	2.0	12.5	6.3	281.3	3.6	234.4
R-717	1.1	11.0	10.2	1100.1	0.9	1082.2
R-744	13.3	68.9	5.2	153.3	6.5	29.9

Operating conditions:
Refrigeration capacity 1 kW, degree of superheat 5 K, no sub-cooling, evaporating temperatures of -8 and -32 ^{o}C for MT and LT refrigeration systems respectively and condensing temperature of 28 ^{o}C for both systems.
(Derived using EES, 2010)

CO_2 also shows a very favourable pressure drop performance compared to most other refrigerants. To demonstrate the advantage of CO_2 refrigerant with regards to pressure drop, three different graphs has been plotted as shown in Figures 2.2 and 2.3. The pressure drops data of CO_2 and other selected refrigerants were derived using EES programme for the same geometry, operating conditions and refrigeration load.

Figure 2.2 (a) shows the comparisons of saturated liquid pressure drop of other refrigerants to the pressure drop of CO_2. It can be seen that the liquid pressure drop of the CO_2 refrigerant is significantly smaller than R-404A specifically at lower saturation temperatures but it is about 1.7 to 2.5 times higher than R-1270, R-290 and R-22. Ammonia (R-717) gives the lowest saturated liquid pressure drop for given evaporating temperature range. The acceptable saturated liquid pressure drop of the CO_2 is, however, 5 to 9 times greater than the other refrigerants. This shows that CO_2 can perform better compared to other selected refrigerants except ammonia in term of saturated liquid pressure drop which also make it suitable for use as a secondary fluid.

The saturated vapour pressure drop ratios of other refrigerants to CO_2 refrigerant are presented in Figure 2.2 (b). CO_2 has considerably lower vapour pressure drop than the other refrigerants apart from ammonia. The figure also shows that the lower the

saturation temperature the more favourable the CO_2 refrigerant compared to other selected refrigerants in respect of saturated vapour pressure drop.

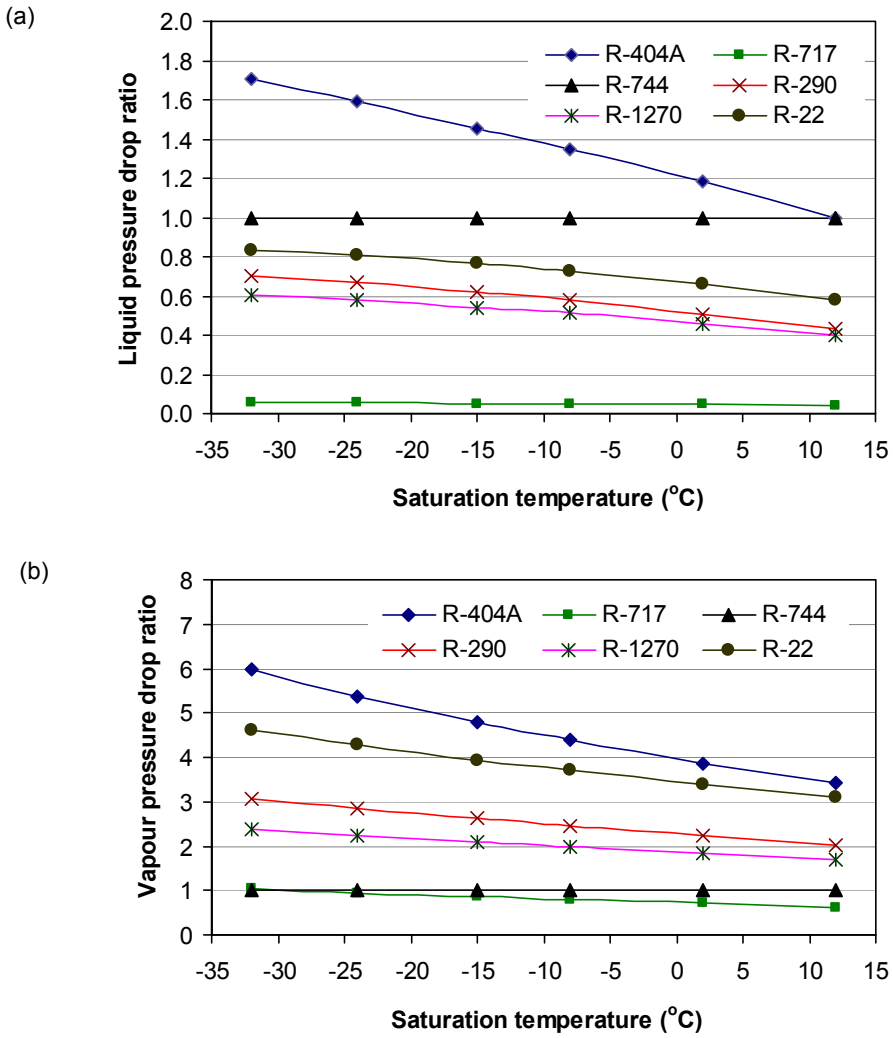

(a) Saturated liquid pressure-drop ratio (b) Saturated vapour pressure-drop ratio

Figure 2.2 Liquid and gas pressure-drop ratio for selected refrigerants and CO_2 at different saturated temperatures, investigated at the same operating conditions
(Obtained using EES, 2010)

Figure 2.3 describes the acceptable pressure drop of saturated liquid and gas line which is equivalent to 1 K saturated temperature drop. For the same saturation temperature, the acceptable pressure drop of CO_2 is significantly higher than the other selected refrigerants. CO_2 can tolerate pressure drop of approximately 45 kPa for LT systems and 80 kPa for MT applications. While the other refrigerants can accept pressure drop as high as 5 kPa and 15 kPa for respectively LT and MT applications. The fact that

higher pressure drop can be tolerated with CO_2 in the evaporator and suction line before system performance is seriously affected, higher evaporating temperature can be achieved and smaller pipe diameter can be used compared to other refrigerants.

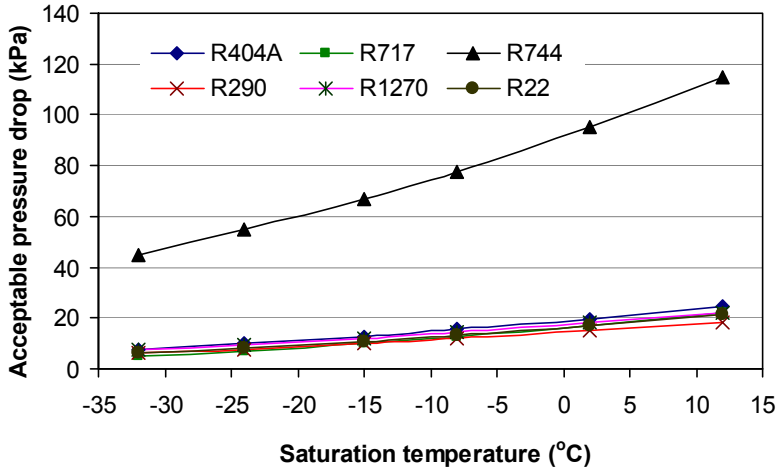

Figure 2.3 Acceptable pressure drop for CO_2 and selected refrigerants in gas and liquid lines of a refrigeration system (Obtained using EES, 2010)

The smaller components and pipe diameter that can be employed with CO_2 lead to a significant reduction in the refrigerant charge required for a given refrigeration load compared to HCFC and HFC refrigerants. For centralised supermarket refrigeration systems, refrigerant charge of CO_2 is expected to be approximately 50% of that of HCFC and HFC refrigerants. The specific refrigerant charge of CO_2 in supermarket applications is in the range 1 to 2.5 kg/kW as shown in Table K-1 (Appendix K). CO_2 is also a relatively cheap refrigerant. Its price is about 50% lower than that of ammonia and approximately 6 to 9 times lower compared to the price of HCFC, HFC and HC refrigerants as can be seen in Table 2.2.

Table 2.2 Price comparison of selected refrigerants

Refrigerants	Price (£/kg)	Price ratio
R-22	17.00	7.3
R-404A	13.20	5.7
R-290	19.25	8.3
R-1270	22.10	9.5
R-717	5.60	2.4
R-744	2.31	1.0

(Source: Dean & Wood, 2011)

As with all other refrigerants, the choice of lubricant is very important with CO_2 refrigeration systems. The primary function of lubricants is to reduce friction and

minimise wear in the compressor. A lubricant achieves this by interposing an oil film between sliding surfaces to reduce direct solid to solid contact and lower the coefficient of friction. A compatible lubricant will be able to continuously keep the lubrication film in the compressor. Lubricants being considered suitable for CO_2 include mineral oils (MO), poly alpha olefin (PAO) and hydro treated mineral oil. Polyol ester (POE) oil which is commonly used for HFC refrigerants also has good miscibility with CO_2 (Lommers, 2003).

In spite of the above advantages, CO_2 also has some disadvantages. One main drawback of CO_2 as a refrigerant is its high working pressures compared to those of natural and synthetic refrigerants. This means that for CO_2 systems, components must be designed to withstand the high pressures and to reduce the safety risk due to high pressure particularly for systems with high refrigerant charge such as supermarket systems (IIR, 2000).

Since CO_2 offers a much higher volumetric capacity, the problem of the higher working pressure can be overcome by optimal design involving smaller and stronger components. Moreover, modern material development, design techniques and technology in manufacturing processes have dramatically reduced the risks associated with the high pressure (Proklima, 2008). However, to reduce costs some components in CO_2 plant such as in indirect systems and low temperature of cascade systems are usually designed for maximum operating pressure (MOP) of 40 to 46 bars. In practice, the most common and easiest way to protect against high pressure is to release some of the CO_2 charge from the plant through relief valves when the pressure reaches a certain set value. This temporarily reduces the pressure and temperature of CO_2 in the system. If the system remains at standstill, then the relief valves will repeatedly open and close to keep the pressure low. In such cases, the plant can significantly lose the charge and need to be recharged to compensate for the lost CO_2. For a CO_2 refrigeration system which is designed for possibly long downtime, a small independent refrigeration unit can be fitted to cool down the CO_2 liquid to levels where saturated pressure is less than the design pressure. Another technique is to employ a receiver which can withstand pressures higher than the saturated pressure of CO_2 at high ambient temperatures. In the event of stoppage, the plant is pumped down and all CO_2 charge is stored in the

receiver. For UK weather conditions (Met Office, 2009) a 75 bar design pressure for the receiver is considered safe.

Another safety issue with CO_2 refrigerant is the concentration level of CO_2 gas in the occupied area in the event of leakage. CO_2 is heavier than air and tends to displace the air from an occupied area close to the floor. CO_2 is also odourless and cannot be smelled by people. Leakage from the CO_2 system could make the level of CO_2 concentration too high which can risk health damage to the persons in the confined space such as in the plant room. A similar risk exists with CFC, HCFC and HFC refrigerants. In practice, this is considered to be a controlled risk which can be prevented with proper leak detection and space ventilation. A reliable CO_2 detector is required to ensure the plant room is safe for people and to keep the concentration level of CO_2 in the range of good indoor air quality (human comfort) which should not exceed 1000 ppm (ASHRAE Standard 62.1, 2007).

2.2 Different types of CO_2 refrigeration systems

In supermarket applications three types of refrigeration systems are mainly employed which include stand-alone (integral), condensing units and centralised supermarket systems (IPCC, 2005). In centralised systems, a number of different design approaches can be adopted that fall into two major categories: subcritical cascade systems and transcritical systems. Subcritical cascade systems operate at moderate pressures and employ two refrigerants one for refrigeration and another for heat rejection whereas transcritical systems operate at high pressures at high ambient temperatures but employ only CO_2 as refrigerant.

2.2.1 Subcritical CO_2 refrigeration systems

As discussed earlier, the CO_2 refrigerant has a low critical point which limits the maximum condensing temperature to around 25 ^{o}C (Rhiemeier et al., 2009). In order to keep the cycle in the subcritical region all year round, it is necessary to use a cascade system to absorb the heat rejected in the condenser of the low pressure system. A schematic diagram of a simple cascade system using CO_2 as the low stage cycle is shown in Figure 2.4. The cascade system is constituted by two single stage systems

connected by a heat exchanger. The high pressure system which rejects heat to the ambient or cooling medium can employ a variety of refrigerants.

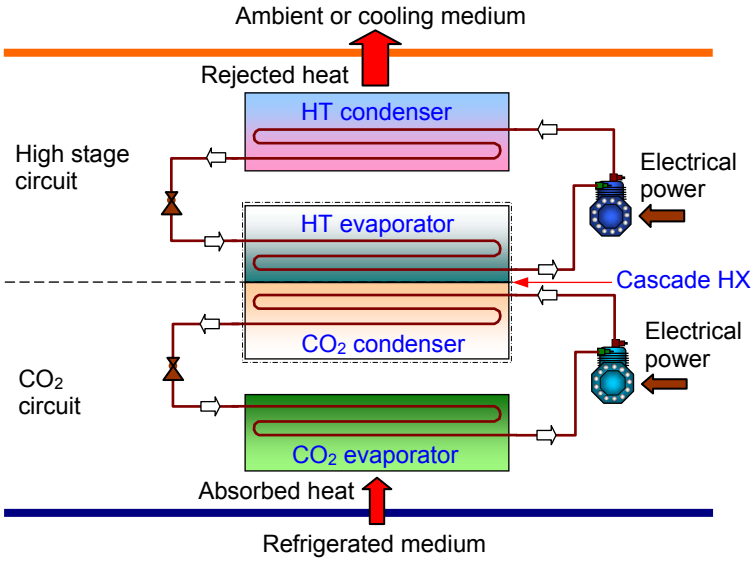

Figure 2.4 Schematic diagram of a cascade arrangement using CO_2 as the low stage cycle

The performance of subcritical cascade systems in supermarket applications has been reported by a number of investigators (Campbell et al., 2006; Hinde et al., 2009). Other investigations have also been conducted on the use of all natural refrigerants in cascade arrangements. Fernandez-Seara et al. (2006) studied a compression–absorption cascade refrigeration system using CO_2 and ammonia as the refrigerants at the lower stage. Sawalha et al. (2006) evaluated theoretically and experimentally the performance of an ammonia/CO_2 cascade refrigeration system for a supermarket application. The authors have reported that the cascade arrangement could provide better *COP* compared to a conventional R-404A system. Similar cascade ammonia/CO_2 systems have also been investigated by Lee et al. (2006); Getu and Bansal (2008); Bingming et al. (2009) and Dopazo et al. (2009). Bansal and Jain (2007) reviewed cascade refrigeration systems and analysed systems using CO_2 in the low stage cycle, while the high stage employed a variety of refrigerants including propane, propylene, ammonia and R-404A.

2.2.1.1 All-volatile systems

Figure 2.5 shows a simplified all-volatile subcritical CO_2 system arrangement. With this arrangement CO_2 works as secondary fluid for both chilled and frozen food systems

which are arranged as parallel units. The CO_2 circuits are connected to primary refrigeration systems which act as the high pressure stages of the arrangement. The evaporating temperature of the high stage system must be lower than the saturation temperature of the corresponding secondary loop system. The temperature difference depends on the effectiveness of the cascade condenser. At the same time, the saturation temperatures of the secondary loops should be low enough to keep the chilled food in the range between -1 ^oC to +4 ^oC and frozen food from between -15 ^oC and -18 ^oC. Supermarkets commonly use saturation temperatures in the range between -30 ^oC and -35 ^oC for the LT loop and from -7 ^oC to -10 ^oC for the MT loop. With the pressures corresponding to these temperatures, it is possible to use conventional refrigeration pipes and components to handle CO_2.

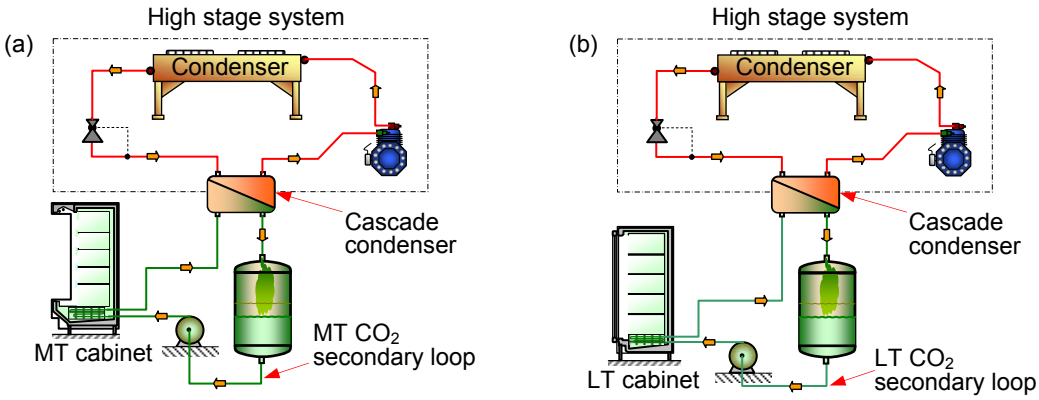

Figure 2.5 Parallel MT and LT indirect system with CO_2 as secondary fluid

The CO_2 circuit contains a receiver that the CO_2 returning from the cascade condenser. The receiver also functions as a liquid reservoir for the CO_2 pump. The level of liquid in the receiver can be connected to the pump controller to ensure the pump works at an acceptable net positive suction head (*NPSH*). The size of the receiver should, therefore, be carefully designed to be able to accommodate the fluctuations of the liquid CO_2 caused by variation in the load.

The pump circulates the liquid CO_2 in the secondary loop from the receiver to the evaporator and keeps the evaporator wet (flooded) for all load conditions. In the evaporator, liquid CO_2 absorbs heat and some of it evaporates. The saturated mixture then flows to the cascade condenser where it rejects heat to the high stage system and

becomes liquid again. From the condenser the CO_2 returns back to the receiver for the repetition of the cycle.

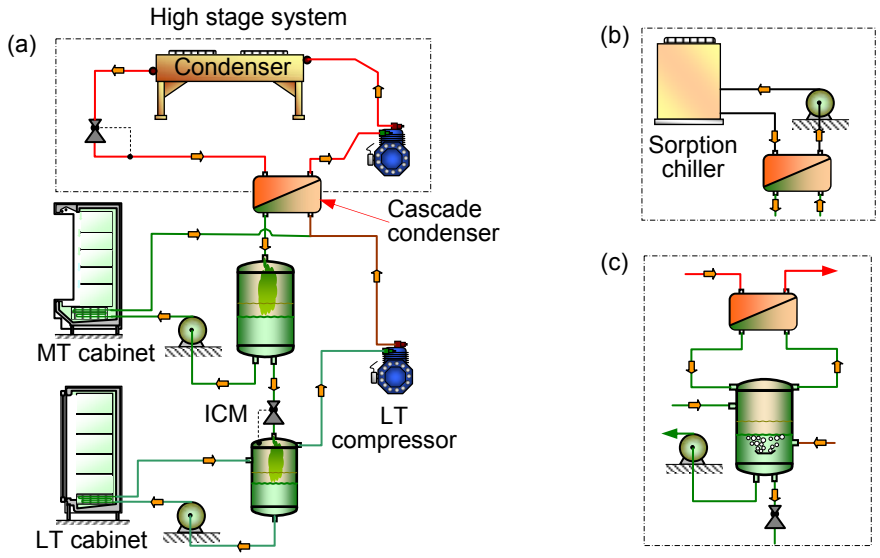

Figure 2.6 All-volatile CO_2 subcritical system with LT DX circuit; (a) cascade arrangement with vapour compression cycle on HT section, (b) alternative arrangement for HT system with sorption chiller, (c) Other arrangement for cascade joint

Another arrangement for all-volatile subcritical CO_2 system is shown in Figure 2.6. The system employs an LT DX circuit and LT secondary loop for the low temperature system. The arrangement uses only one high stage system which can minimise the refrigerant charge and safety risk if other natural refrigerants such as HC and ammonia are used. The liquid CO_2 from the MT receiver is distributed to both the MT secondary loop and the LT system. For the LT system the liquid CO_2 flows through a valve (ICM) where it is expanded to the low stage evaporating pressure. The ICM valve is modulated to maintain the temperature and liquid level of the LT secondary loop relatively constant. From the ICM valve the two phase mixture enters the LT receiver where it is separated into two phases. The liquid phase flows through the LT secondary loop and the saturated gas enters the LT compressor and is compressed to the MT pressure level. The hot gas from the LT compressor then mixes with the two phase mixture. The mixture then enters the cascade condenser and returns back to the MT receiver to complete the cycle. An internal heat exchanger (IHX) might be required between the suction line of the LT compressor and the liquid line upstream of the ICM valve to ensure there is no liquid at suction line of the compressor.

The above arrangement can also employ a sorption chiller on the high stage as an alternative solution to a vapour compression system as shown in Figure 2.6 (b), particularly where there is waste heat available, as is the case with local power generation to drive the sorption chiller. Different arrangement for the CO_2 cascade coupling can also be applied as can be seen in Figure 2.6 (c).

The volatile subcritical CO_2 solutions are relatively simple systems to implement and offer advantages over conventional water based brine systems. They require considerably smaller pipes and components, and installation cost savings can reach 12% (Danfoss, 2010). With respect to energy consumption, the author stated that the secondary CO_2 solutions can be more energy efficient by about 30% for the LT system and 20% for the MT system. Rogstam (2010) reported that the secondary CO_2 could provide energy reduction for pumping of the order of 90% compared to fixed speed brine pumps and 50% reduction compared to variable speed brine pumps. Another possibility is to operate the CO_2 system on gravity circulation.

2.2.1.2 Volatile-DX system

A volatile-DX system is a subcritical CO_2 system with MT secondary loop cascaded with a LT DX circuit as shown in Figure 2.7. The advantage of this system is that it is a simple system without LT pump or LT receiver for the LT circuit.

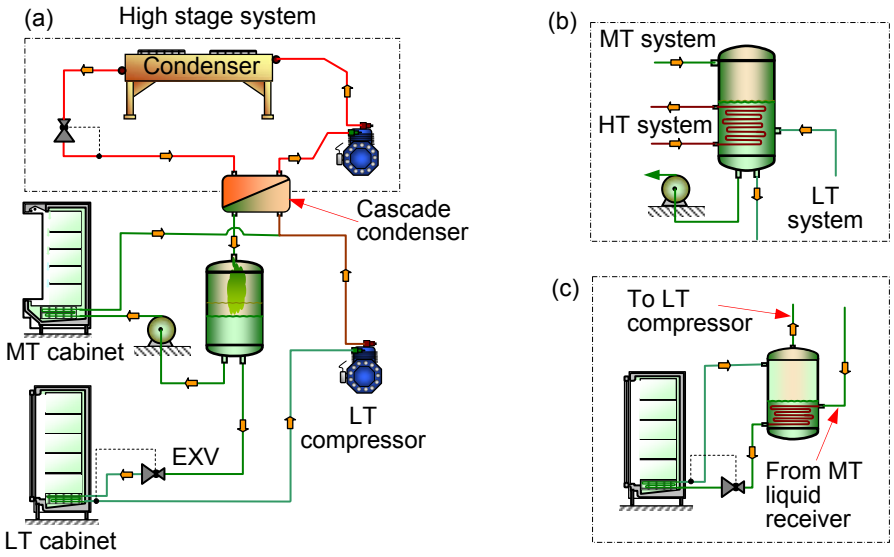

Figure 2.7 Cascade CO_2 refrigeration with MT secondary loop and LT DX system; (b) Alternative cascade coupling arrangement for HT system, (c) Alternative LT evaporator arrangement. (Adapted from: Sawalha et al., 2006)

Subcritical CO_2 system solutions in supermarket applications provide several advantages over conventional systems. The HFC refrigerant charge on the high stage system can be significantly reduced which reduces impact on the environment. The high stage system can be located in a secured machine room with no public access. This gives possibility to employ other natural refrigerants such as ammonia and hydrocarbons with minimum safety risk. It has also been reported that the energy consumption of subcritical CO_2 supermarket solutions can be comparable to that of R-404A DX systems (Sawalha et al., 2006; Hinde et al., 2009; Rhiemeier et al., 2009).

To date many subcritical CO_2 systems have been implemented in EU countries such as Denmark, Germany, Norway, Sweden, Italy and the UK (Rhiemeier et al., 2009). Such systems have also been reported in supermarket applications in Australia, Canada and the Latin America as reported (Bellstedt, 2008; CanmetENERGY, 2009; Verdemar, 2010).

2.2.2 All-CO_2 systems

All-CO_2 systems employ CO_2 as the only working fluid without the need of a second refrigerant on the high pressure side of a cascade arrangement for heat rejection. This minimises the environmental impact from the refrigerant leakage but requires the system to operate above the critical temperature of CO_2 (transcritically) at high ambient temperatures. At temperatures above the critical point, heat rejection occurs whilst CO_2 in the gaseous state and takes place in a gas cooler. This necessitates high pressures which can lead to high power consumption. Therefore, the pressure of the gas cooler becomes very important operating parameters which need to be controlled in order to obtain best performance.

In transcritical stage the operating pressure of the gas cooler becomes independent of the gas cooler exit temperature. Figure 2.8 shows that different operating pressures can be selected at a particular gas cooler exit temperature. The figure also illustrates optimum operating pressures at different exit temperatures of the gas cooler.

The temperature of CO_2 exits the gas cooler depends on the ambient temperatures and the heat rejected from the gas cooler. The exit temperatures can be maintained close to the ambient temperatures by modulating the speed of the cooling fans. The pressure of

the gas cooler is regulated by a high pressure expansion device (ICMT valve) and the optimum operating pressure can be achieved by modulating the ICMT valve which incorporates a proportional integral differential (PID) controller. Control parameters of this controller include the exit temperature and the actual pressure of the gas cooler.

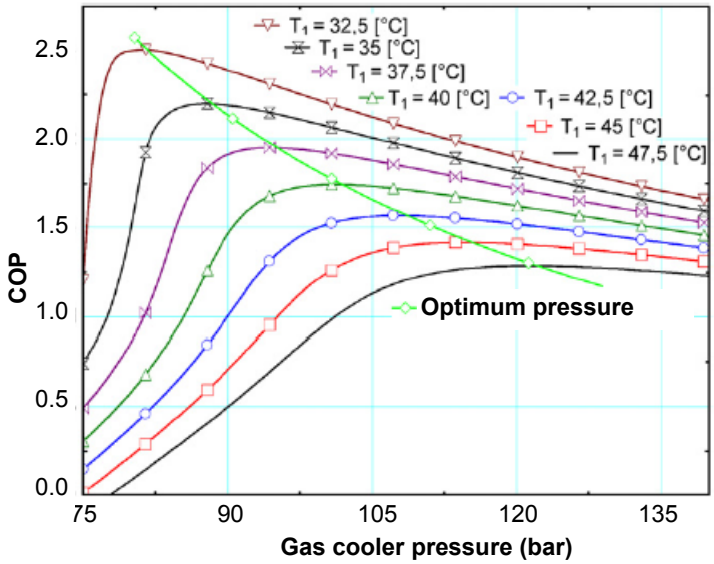

Figure 2.8 ***COP*** **of a CO_2 transcritical cycle vs. pressures of the gas cooler at different exit gas temperatures (T_1)** (Source: Sawalha, 2008)

2.2.2.1 Parallel CO_2 system arrangement

Figure 2.9 illustrates a parallel CO_2 system which constitutes two separate DX circuits. One circuit is for chilled food (MT) display cabinets and another for frozen food (LT) cabinets. The MT system uses single stage compression whereas two-stage compression with intercooler is normally used for the LT system. In practice, both systems normally use multi-compressor packs. Internal heat exchangers (IHX) are also commonly employed to ensure the systems have superheated CO_2 vapour at the suction line of the compressors.

The use of two-stage compression with intercooler can reduce the pressure ratio and discharge temperature of the LT compressors. The intercooler de-superheats the CO_2 vapour before the second stage of compression. This can keep the discharge temperature of the LT CO_2 system below 140 ^oC which is considered as an acceptable value for the CO_2 compressors (Girotto et al., 2004). The two stage compression can also improve volumetric and isentropic efficiencies of the LT compressors.

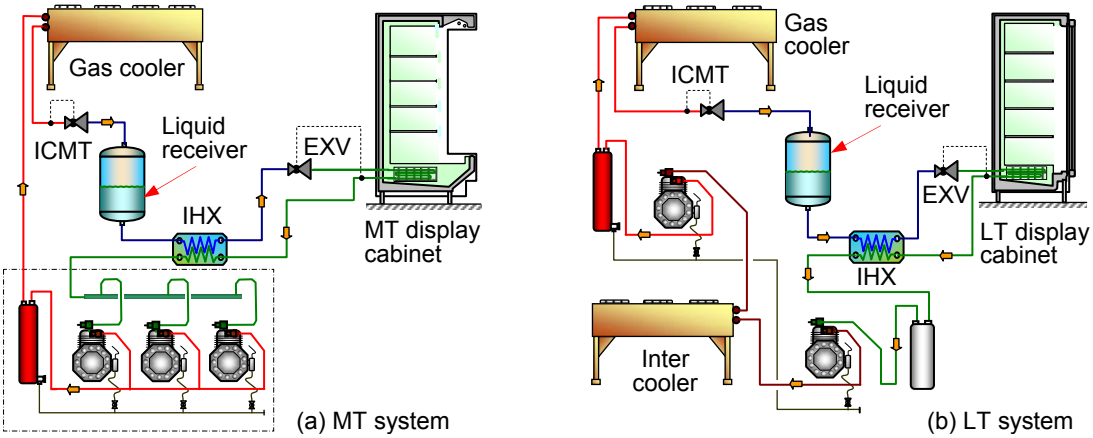

Figure 2.9 Simplified parallel CO_2 refrigeration systems

2.2.2.2 Integrated CO_2 system solutions

In the integrated system solutions, both MT and LT circuits are connected to the same heat rejection circuit. The arrangement of the three circuits depends on the system solutions chosen. These are described in the following sections.

- *Transcritical CO_2 booster system*

A simplified diagram of a transcritical CO_2 booster system is shown in Figure 2.10. The system is divided into 4 pressure levels. The high pressure is in the range between 60 and 90 bar_a. It incorporates the discharge of HT compressor, gas cooler and high pressure expansion device (ICMT). The intermediate pressure is from 30 to 40 bar_a. This section begins from downstream the ICMT valve incorporates the liquid receiver and the bypass valve (ETS) and ends at the expansion valves of the MT and LT circuits. The medium pressure level ranges from 26 to 29 bar_a and includes the discharge of the LT compressor, the MT evaporator and suction of the HT compressor. The low pressure section in the pressure range from 12 to 14 bar_a incorporates the LT evaporator and suction line to the LT compressor.

The main function of the bypass valve (ETS) is to keep the pressure in the intermediate pressure section relatively constant by bypassing saturated gas from the receiver to the medium pressure section. The bypass valve also ensures a differential pressure exists

between the liquid line after the liquid receiver and the MT evaporator coils for the proper operation of the MT expansion valve.

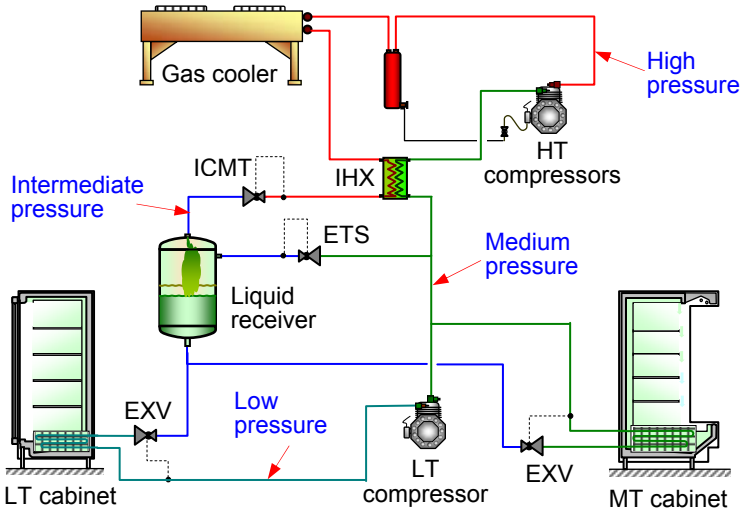

Figure 2.10 All-CO_2 booster system with gas bypass
(Adapted from: Danfoss, 2008a)

In a CO_2 booster system, the lower the intermediate pressure the better it is for system efficiency which can be explained as follows: The intermediate pressure does not influence the pressure ratio of the LT and HT compressors which means the power consumption of the compressors remains constant. The refrigeration effect of the MT and LT evaporators, however, will increase when the intermediate pressure reduces. This will improve the refrigeration capacity of the systems which leads to a higher system efficiency.

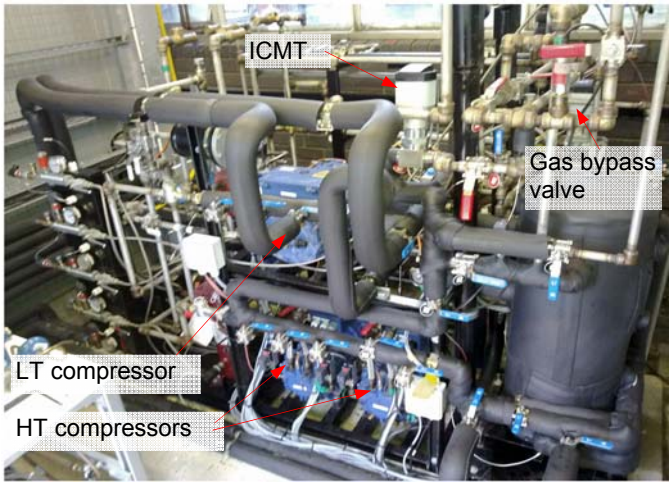

Figure 2.11 All-CO_2 booster system installed in the Refrigeration Laboratory, Brunel University

For the operation of the MT expansion valve, at least a 4 bar pressure difference is maintained over the MT evaporator pressure (Danfoss, 2008a). Other factors that influence the operation of the bypass valve and control of the intermediate pressure include the gas cooler exit pressure and temperature and the requirement to have superheated CO_2 vapour at the entry to the HT compressor.

Figure 2.11 shows a small size plant with integrated all-CO_2 booster system. The CO_2 system employs an air cooled gas cooler, two parallel compressors for the high pressure system and a single compressor for the low pressure cycle. ICMT and ICM valves are utilised for the high pressure expansion device and the gas bypass valve respectively. The CO_2 plant incorporates a Danfoss controller for the system control and monitoring.

- *Cascade CO_2 system with flash gas bypass*

A cascade CO_2 system with flash gas bypass is shown in Figure 2.12. The high stage or heat rejection section is similar to the booster system. The difference is that the LT system is cascaded as an individual circuit with the HT system for heat rejection. The MT evaporators are divided into two groups: one provides refrigeration to the MT display cabinets and the other condenses the CO_2 gas for the LT systems.

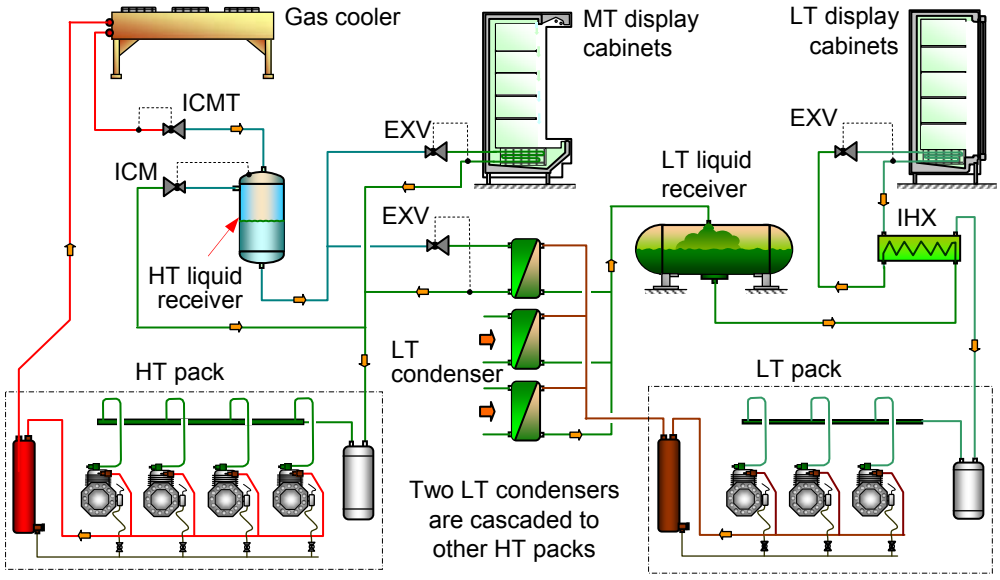

Figure 2.12 Integrated cascade all-CO_2 system with flash gas bypass

This solution has been implemented in a number of UK supermarkets (Campbell, 2009). Performance investigations have shown its seasonal energy performance to be about the

same as that of conventional R-404A systems (Suamir and Tassou, 2010). In order to gain full advantage of subcritical operation when the ambient temperature is low a bypass valve is required in parallel with the ICMT valve (the bypass valve is not shown in the diagram). The bypass valve closes when the ambient temperature is above a certain value (the switching point between subcritical and transcritical operation) to allow the ICMT valve to regulate the flow of CO_2 gas out from the gas cooler and opens below the switching point to allow the liquid CO_2 to freely flow from the condenser (gas cooler) to the liquid receiver.

- *Cascade CO_2 system with a suction receiver*

The cascade CO_2 system with low pressure receiver is an improvement on the cascade system with flash gas bypass. As can be seen in Figure 2.13, a suction receiver is added on the high temperature side of the system. A back pressure valve is used instead of bypass valve to minimise the fluctuation in the intermediate pressure due to pressure and temperature variations at the outlet of the gas cooler.

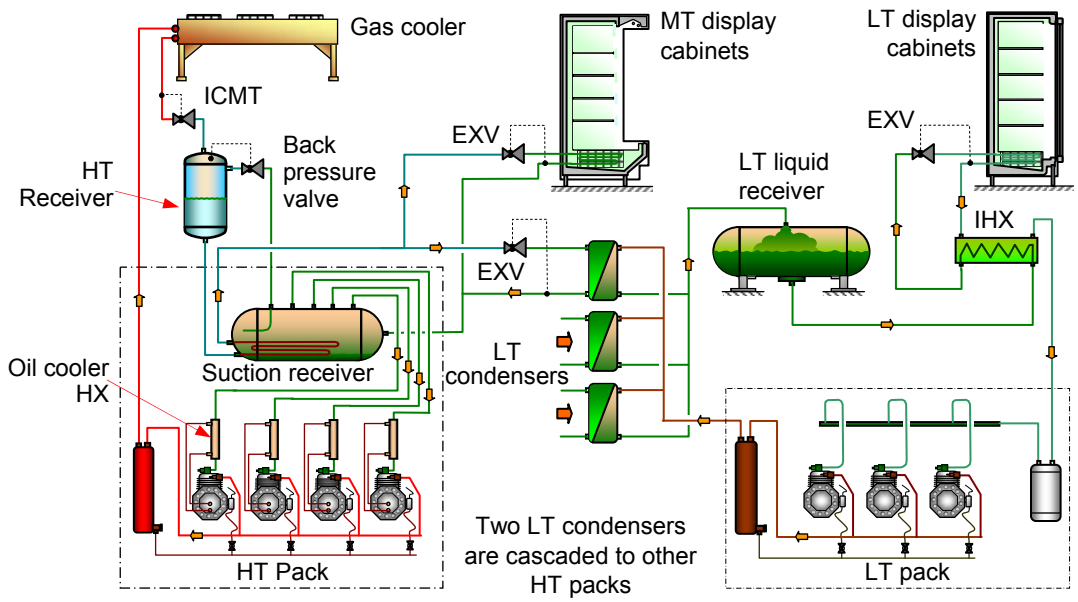

Figure 2.13 Integrated cascade all-CO_2 system with suction receiver

With this arrangement the MT evaporators can be set at zero superheat which can increase the refrigeration capacity and the *COP* of the system. To ensure no liquid enters the compressors, the system is equipped with oil cooler HX at the suction line of

each HT compressor. According to Campbell (2009) this system is adaptable to variable load; is less sensitive to charge and is easy to service.

Figure 2.14 presents an integrated cascade all-CO_2 system with suction receiver implemented in a UK supermarket. The store has sales area of 2,300 m^2. The CO_2 refrigeration plant of this store constitutes 4 HT packs and 2 LT packs. Every single HT pack comprises 3 compressors, an air cooled gas cooler and a suction receiver (0.26 m^3 volume). The LT pack incorporates 3 LT compressors, a liquid receiver (0.13 m^3 volume) and 3 condensers. For reliability of the LT refrigeration system, each LT pack is cascaded to three different HT packs as shown in Figure 2.13.

Figure 2.14 Integrated cascade all-CO_2 plant in Tesco Ramsey, UK

2.3 Summary

This chapter outlines advantages and disadvantages of the CO_2 as a natural refrigerant. The CO_2 refrigerant, with ODP of zero and GWP of one, has lower impact to the environment compared to HCFC and HFC refrigerants. Having attractive thermo-physical properties, the CO_2 refrigerant can provide good heat transfer in heat exchangers of a refrigeration system which allows selection of smaller equipment than HCFC and HFC refrigerants. The CO_2 refrigerant is also non-toxic and non-flammable which make it more advantageous than other natural refrigerants such as ammonia and hydrocarbons. Moreover, the CO_2 refrigerant is relatively cheap.

The main downside of the CO_2 refrigerant is its high working pressures. The problem of the higher working pressure, however, can be overcome by using smaller and stronger components. Some practical techniques to protect a CO_2 refrigeration system against high pressure are also explained in this chapter.

The chapter also describes different solutions and arrangements of the CO_2 refrigeration systems for supermarket applications which fall into two major categories: subcritical cascade systems and transcritical systems. Subcritical cascade systems operate at moderate pressures and employ two refrigerants one for refrigeration and another for heat rejection whereas transcritical systems operate at high pressures at high ambient temperatures but employ only CO_2 as refrigerant. Recent developments of the CO_2 refrigeration systems and their applications in supermarkets are also presented.

The following chapter will explain the design and the construction of the test facility and will include the integration arrangement, system design and modelling, component calculations, the components used, refrigeration load system and the test chamber.

Chapter 3

DESIGN AND CONSTRUCTION OF THE TEST FACILITY

A small size CO_2 refrigeration system for low and medium temperature applications was designed and constructed to enable it to be integrated with the existing trigeneration system to form an overall test facility. Instrumentation and monitoring systems were also fitted to comprehensively monitor the performance of the system for evaluation purposes.

For design purposes, mathematical models were established in the Engineering Equation Solver (EES) platform which include pipe sizing, liquid receiver, evaporator-coil models and system integration. The EES models were used to determine the dimensions and capacity of the components. The models were also used to estimate the performance of the integrated system at different operating conditions. Based on the dimensions of the components a 3D drawing of the system was drawn using AutoCAD.

The CO_2 refrigeration plant and the integration circuit were constructed in the Refrigeration Laboratory of Brunel University. Technical drawings were produced which include piping, instrumentation diagrams, liquid receiver, evaporator coils and electrical control systems.

This chapter presents the mathematical models produced for the design of the CO_2 refrigeration system. The evaporator coil models will be presented separately in Chapter 4. This chapter also details the construction of the test facility which

incorporates mechanical, electrical, control and monitoring systems. The loading systems and the environmental test chamber are also briefly described.

3.1 Integration arrangement

The test facility consists of three main modules; CHP module, absorption refrigeration system module, and a refrigeration load module as described in Section 1.4. The main construction is very similar to the previous trigeneration test facility (see Figure A-1 in the Appendix A). The difference is only on the refrigeration load module. A subcritical CO_2 refrigeration system with chilled and frozen food display cabinets was used to replace the water based secondary loop medium temperature display cabinet.

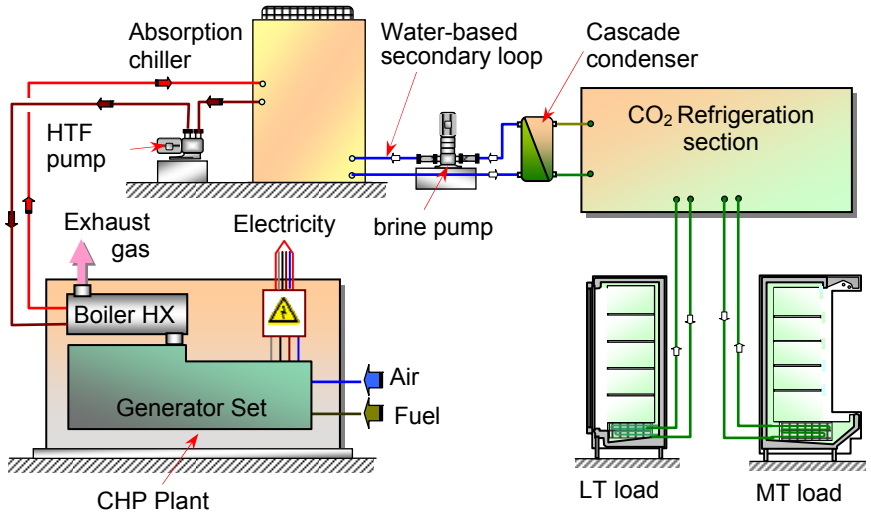

Figure 3.1 Integration arrangement of CO_2 refrigeration and trigeneration systems

Figure 3.1 shows a schematic diagram of the integration arrangement of the CO_2 refrigeration and trigeneration systems. The arrangement employs a water based secondary loop which bridges the CO_2 refrigeration system to the absorption chiller of the trigeneration facility. Main components of the secondary loop include cascade condenser, brine pump and evaporator of the absorption chiller. The CO_2 refrigeration system rejects heat to the secondary loop in the cascade condenser which is a brine/CO_2 heat exchanger. The rejected heat is then released to the atmosphere from the condenser of the absorption chiller which is driven by recovered heat from the CHP system.

3.2 Mathematical models

3.2.1 Integration model

The integration model uses the ambient conditions and required product temperature as boundary conditions. The temperature for the products was assumed to be -1 ^{o}C to 5 ^{o}C for medium temperature (MT) system and -15 ^{o}C to -18 ^{o}C for the low temperature (LT) system. Evaporating temperatures for the medium and low temperature systems were assumed to be -8 ^{o}C and -32 ^{o}C respectively. London weather data was assumed for the purposes of heat rejection.

The integration model involved all components which influenced the performance of the system and each component was treated as a single control volume. Mass and energy balance principles were applied to the control volumes which can be expressed as follows:

$$\sum_{in} m = \sum_{out} \dot{m} \qquad (kg/s) \tag{3.1}$$

$$Q - W + \sum_{in} \dot{m}.H - \sum_{out} \dot{m}.H = 0 \quad (kW) \tag{3.2}$$

3.2.1.1 Trigeneration system model

Figure 3.2 shows the schematic diagram of the CHP module. It can be seen that the fuel energy of the CHP is used to generate electrical power and to produce heat. Some of the heat is recovered in the gas/liquid heat exchanger (boiler HX) and the rest is released to the atmosphere as waste heat. The boiler HX is circuited to the heat transfer fluid (HTF) loop through which the useful heat is utilised to drive the absorption chiller.

The energy balance of the CHP model consists of fuel energy, useful energy (electrical power and useful heat) and energy losses (waste heat and other losses). This energy balance equation using CHP efficiency (η_{CHP}) can be expressed as:

$$\eta_{CHP} E_{f,CHP} = W_{e,CHP} + Q_{h,CHP} \tag{3.3}$$

The useful heat of the CHP can be determined from:

$$Q_{h,CHP} = Q_h + Q_{h,abs} \tag{3.4}$$

$$Q_{h,CHP} = \dot{m}_{gas} C_{p,gas} (T_{i,gas} - T_{o,gas}) \quad (3.5)$$

Equation (3.4) shows that the useful heat of the CHP system can be used to drive the absorption chiller ($Q_{h,abs}$) and for central heating or domestic water supply (Q_h). In this design, the heat for spare or domestic heating (Q_h) was assumed to be zero. The temperature of the hot gas exiting the Boiler HX ($T_{o\text{-}gas}$) was obtained by assuming the temperature difference between the gas and the heat transfer fluid (HTF) at the outlet of the boiler HX to be 14.6 ^{o}C. This was obtained from experimental test results.

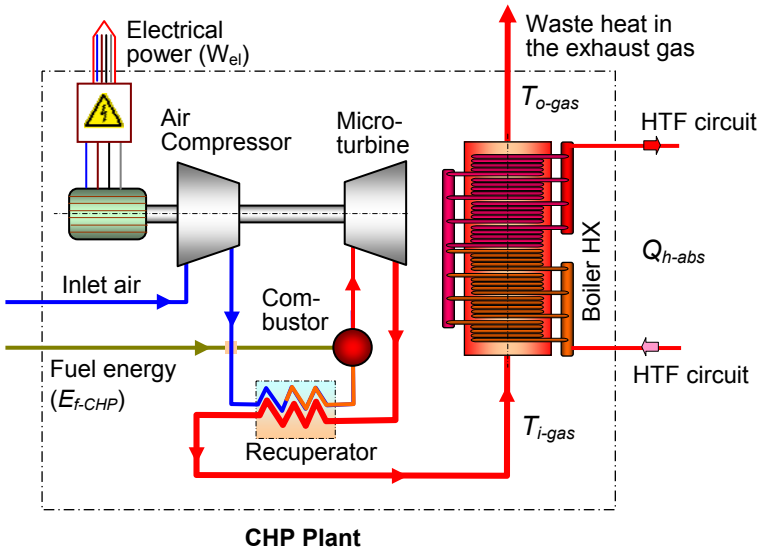

Figure 3.2 Schematic diagram of the microturbine based CHP system

Figure 3.3 shows the schematic diagram of the heat transfer fluid (HTF) driven ammonia-water absorption chiller. The absorption chiller employs a generator absorber heat exchange (GAX) system which comprises main components such as generator, condenser, expansion device, absorber, solution pump and evaporator. An HTF jacket was attached on the generator to enable the unit to be driven by the heat transfer fluid heated up in the exhaust gas HX of the CHP system. The evaporator is connected to a cascade condenser of the CO_2 refrigeration system.

In order to simplify the model, the performance parameters of the absorption system which include refrigeration capacity ($Q_{r,abs}$) and coefficient of performance (COP_{abs}) were determined from best fit equations of manufacturer and experimental data as a

function of delivery brine temperature and ambient temperature. The equations are given below:

$$Q_{r,abs} = A_0 + A_1 T_o + A_2 T_o^{\,2} + A_3 T_o^{\,3} + A_4 T_o^{\,4} + A_5 T_o^{\,5} + A_6 T_o^{\,6} + B_1 T_{amb} + B_2 T_{amb}^{\,2} + B_3 T_{amb}^{\,3} + B_4 T_{amb}^{\,4} + B_5 T_{amb}^{\,5} + B_6 T_{amb}^{\,6} \quad (3.6)$$

$$COP_{abs} = C_0 + C_1 T_o + C_2 T_o^{\,2} + C_3 T_o^{\,3} + C_4 T_o^{\,4} + C_5 T_o^{\,5} + C_6 T_o^{\,6} + D_1 T_{amb} + D_2 T_{amb}^{\,2} + D_3 T_{amb}^{\,3} + D_4 T_{amb}^{\,4} + D_5 T_{amb}^{\,5} + D_6 T_{amb}^{\,6} \quad (3.7)$$

$Q_{r,abs}$ is the refrigeration capacity of the absorption system (kW); T_o and T_{amb} are delivery brine and ambient temperatures (^oC) respectively. Constants of the equations are listed in Table 3.1.

Table 3.1 Constants of the best fit equations

	Parameter order						
	0	**1**	**2**	**3**	**4**	**5**	**6**
A	0.4962	-0.175	-0.06885	-0.01365	-0.001457	-0.000078	-0.0000016
B		0.00029	-0.00021	-2.492×10^{-8}	1.337×10^{-6}	-3.264×10^{-8}	7.881×10^{-11}
C	3.429	-9.55	-4.022	-0.8278	-0.08856	-0.004712	-0.0000985
D		0.008248	-0.004558	0.00000828	0.0000275	-7.190×10^{-7}	2.076×10^{-9}

The coefficient of correlations for the refrigeration capacity $R_Q^2 = 0.9890$ and the coefficient of performance $R_{COP}^2 = 0.9974$

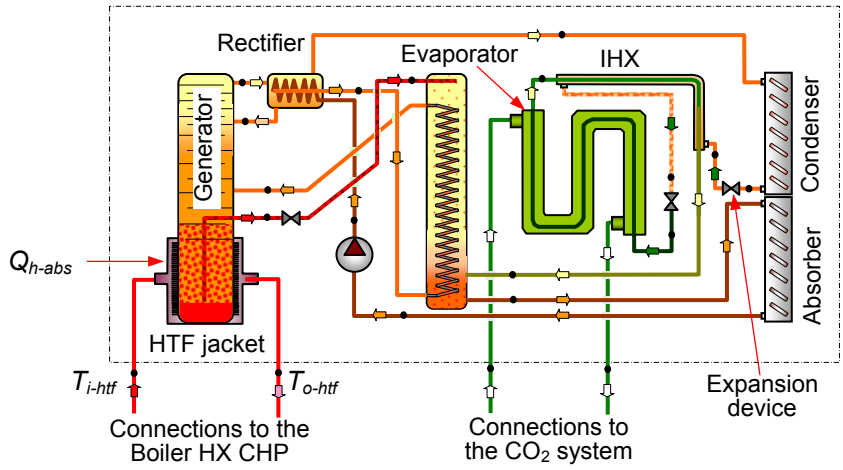

Figure 3.3 Schematic diagram of the ammonia-water absorption chiller

In this model, $Q_{r,abs}$ was used as a boundary condition in simulating the integrated system. The heat rejected from cascade condenser of the CO_2 refrigeration system (Q_{cond}) should be smaller than $Q_{r,abs}$. The results of the simulations are considered invalid if Q_{cond} is higher than $Q_{r,abs}$.

The heat required to drive the generator of the absorption system ($Q_{h,abs}$) can be calculated from:

$$COP_{abs} = \frac{Q_{cond}}{Q_{h,abs}} \tag{3.8}$$

The mass flow rate of the heat transfer fluid and power consumption of the HTF pump can be determined from:

$$Q_{h,abs} = \dot{m}_{htf}\ Cp_{htf}\ (T_{o,htf} - T_{i,htf}) \tag{3.9}$$

$$W_{htf,pump} = \frac{\dot{m}_{htf}\ v_{htf}\ \left(P_{o,htf} - P_{i,htf}\right)}{\eta_{htf,pump}} \tag{3.10}$$

$T_{i\text{-}htf}$ is the temperature of the HTF entering the generator jacket which has been found from the experimental tests to be in the range between 190 and 200 ^{o}C. $T_{o,htf}$ can be determined by assuming the temperature difference of HTF across the generator to be 6 ^{o}C. (P_o - P_i) and ($\eta_{htf,pump}$) are the pressure losses in the HTF circuit and the total efficiency of the HTF-pump. These were determined from tests to be 400 kPa and 0.45 respectively. The properties of the HTF can be determined from equations (B.1) to (B.4) in Appendix B.

3.2.1.2 CO_2 refrigeration model

The CO_2 refrigeration system of the test facility is a volatile-DX system. The basic principle of such system is explained in Section 2.2.1.2.

A simplified diagram of the CO_2 system is shown in Figure 3.4. The system comprises an LT CO_2 compressor, LT and MT evaporators, a CO_2 pump, expansion valve (EXV), regulator valve (RV), liquid receiver, internal heat exchanger (IHX) and a cascade condenser. The condenser is a CO_2/brine HX. To provide flexibility to investigate different arrangements for the LT compressor, the discharge line is split into two branches. One branch is connected to the saturated gas line from the liquid receiver and the other feeds directly into the liquid receiver. The figure also shows a bypass circuit from the CO_2 pump to the liquid receiver which allows the flow of CO_2 refrigerant to the MT evaporator to be varied to enable investigation of the effect of circulation ratio (*CR*) on the performance of the MT evaporator.

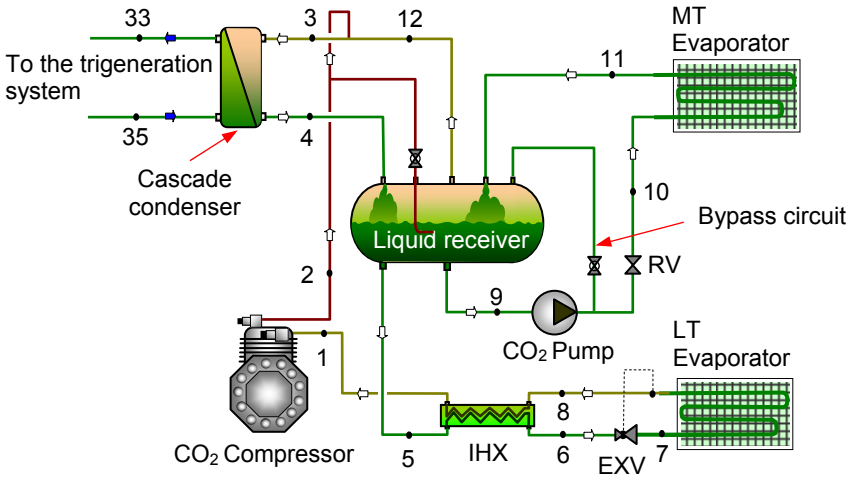

Figure 3.4 Centralised volatile-DX CO_2 section

The refrigeration cycle of the system is shown in Figure 3.5. The cycle refers to the schematic diagram in Figure 3.4. It can be seen that the thermodynamic cycle of the system consists of compression of a low pressure, low temperature superheated CO_2 vapour to medium pressure level, followed by mixing of the superheated gas from the compression process with saturated CO_2 gas from the liquid receiver. The CO_2 gas is de-superheated and condensed in the cascade condenser and exits as saturated liquid. Some of the liquid is pumped to the MT evaporator where evaporation takes place by absorbing heat from air circulating in a refrigerated display cabinet. The CO_2 exiting the MT evaporator is a mixture of vapour and liquid. Liquid from the receiver flows through an internal heat exchanger (IHX) before is expanded isenthalpically in the expansion device (EXV) which results in a low temperature vapour-liquid mixture entering the low temperature evaporator. The low temperature two phase mixture evaporates in the LT evaporator removing heat from the LT refrigerated cabinet. The vapour exiting the LT evaporator is superheated in the IHX and then compressed in the LT compressor to complete the cycle.

To simulate the volatile-DX CO_2 refrigeration system, some assumptions were made as follows: steady state flow conditions; negligible thermal losses to the environment; negligible refrigerant pressure drops in the pipes; degree of superheat of the LT evaporator 5 K; CO_2 leaving the condenser in saturated liquid; vapour quality at the exit of MT evaporator to be 0.8 (it can be varied depending on the circulation ratio); isenthalpic expansion in the EXV; negligible refrigerant pressure drop across the

regulator valve (RV). The isentropic efficiency (η_s) of the CO_2 pump was assumed to be 0.5 and the overall efficiency (η_o) was predicted from manufacturer's data to be 0.1. The compression process in the CO_2 system was non-isentropic. The isentropic and volumetric efficiency of the compressor can be expressed as a function of pressure ratio (R_p) and can be determined from (Lee et al., 2006).

$$\eta_s = 0.00476.R_p^2 - 0.09238.R_p + 0.89810 \quad (3.11)$$

$$\eta_v = 0.00816.R_p^2 - 0.15293.R_p + 1.13413 \quad (3.12)$$

The electrical motor efficiency of the compressor (η_m) was assumed to be 0.86 (Navarro et al., 2007).

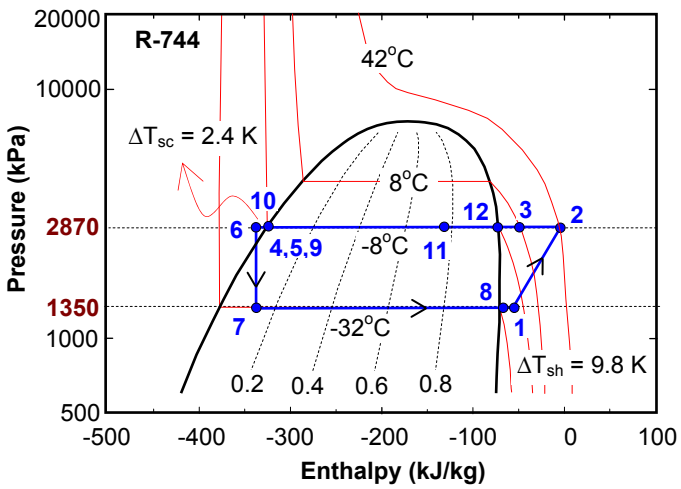

Pressure (kPa) is absolute pressure

Figure 3.5 P-h diagram of the subcritical CO_2 refrigeration cycle

Table 3.2 summarises the main mass and energy balance equations for each component of the CO_2 refrigeration system. The properties of CO_2 refrigerant were derived from the EES software.

In the integrated system arrangement, the CO_2 refrigeration system rejects heat to the secondary loop through the cascade condenser. The temperature of the secondary fluid (brine) should be lower than the temperature of the CO_2 refrigerant. This temperature difference is a function of the effectiveness of the heat exchanger. The effectiveness of the cascade condenser and its temperature losses (ΔT_{cond}) can be calculated from:

$$\varepsilon_{cond} = \frac{T_3 - T_4}{T_3 - T_{35}} \tag{3.13}$$

$$\Delta T_{cond} = T_4 - T_{35} \tag{3.14}$$

The position of each measurement point is shown in Figure 3.4. T_3 and T_4 are temperatures of CO_2 refrigerant entering and leaving the condenser respectively; T_{35} is the temperature of brine entering the condenser.

Table 3.2 Equations for the CO_2 refrigeration system
(Numbers of the parameters refer to Figure 3.4)

Components	Mass balance	Energy balance
LT Compressor	$\dot{m}_1 = \dot{m}_2$	$\dot{m}_1 H_1 + W_{comp.s} = \dot{m}_2 H_2$ $W_{comp.s} = \dot{m}_1 \left(\frac{H_{2s} - H_1}{\eta_s} \right)$ $W_{comp} = \dot{m}_1 \left(\frac{H_{2s} - H_1}{\eta_s . \eta_v . \eta_m} \right)$
Mixing point	$\dot{m}_3 = \dot{m}_2 + \dot{m}_{12}$	$\dot{m}_3 H_3 = \dot{m}_2 H_2 + \dot{m}_{12} H_{12}$
Condenser	$\dot{m}_3 = \dot{m}_4$	$\dot{m}_3 H_3 = \dot{m}_4 H_4 + Q_{cond}$
Expansion valve (EXV)	$\dot{m}_6 = \dot{m}_7$	$H_6 = H_7$
LT Evaporator	$\dot{m}_7 = \dot{m}_8$	$\dot{m}_7 H_7 + Q_{LT} = \dot{m}_8 H_8$
Internal heat exchanger (IHX)	$\dot{m}_1 = \dot{m}_8$ $\dot{m}_5 = \dot{m}_6$	$\dot{m}_5 H_5 + \dot{m}_8 H_8 = \dot{m}_1 H_1 + \dot{m}_6 H_6$ $Q_{IHX} = \dot{m}_5 (H_5 - H_6)$
CO_2 pump	$\dot{m}_9 = \dot{m}_{10}$ *	$W_{CO2,pump} = \frac{\dot{m}_9 v_9 (P_{10} - P_9)}{\eta_s \eta_o}$
MT evaporator	$\dot{m}_{10} = \dot{m}_{11}$	$\dot{m}_{10} H_{10} + Q_{MT} = \dot{m}_{11} H_{11}$

* For simulation purposes mass flow rate of the bypass line was assumed to be 0 kg/s.

The performance of the CO_2 refrigeration system can be determined from:

$$COP_{LT} = \frac{Q_{LT}}{W_{comp}} \tag{3.15}$$

$$COP_{MT} = \frac{Q_{MT}}{W_{CO2,pump}} \tag{3.16}$$

$$COP_{CO2,overall} = \frac{Q_{MT} + Q_{LT}}{W_{CO2,pump} + W_{comp}} \tag{3.17}$$

The coefficient of performance (*COP*) of the integrated system can be calculated from:

$$COP_{\text{int}} = \frac{Q_{MT} + Q_{LT}}{Q_{h,abs} + W_{\text{int}}} \tag{3.18}$$

W_{int} is the electrical power consumption of the various components of the integrated system which can be expressed as:

$$W_{\text{int}} = W_{comp} + W_{CO2,pump} + W_{abs} + W_{htf,pump} + W_{brine,pump} \tag{3.19}$$

Equation (3.19) shows that the integrated system consumes electricity for the LT CO_2 compressor (W_{comp}), CO_2 pump ($W_{CO2,pump}$), absorption chiller (W_{abs}), heat transfer fluid pump ($W_{htf,pump}$) and brine pump ($W_{brine,pump}$).

The electrical power of the brine pump can be determined from:

$$W_{brine,pump} = \frac{\dot{m}_{brine}.v_{brine}.\left(P_{o,brine} - P_{i,brine}\right)}{\eta_{brine,pump}} \tag{3.20}$$

($P_{o,brine}$-$P_{i,brine}$) and ($\eta_{brine,pump}$) are pressure head and total efficiency of the brine pump which were assumed to be 250 kPa and 0.5 respectively. The power consumption of the brine pump can be reduced by minimising the pressure drop of the secondary loop which subsequently reduces the pressure head. This can be achieved by installing the CO_2 refrigeration system near the trigeneration plant.

3.2.1.3 Integration capacity and performance simulations

A simplified schematic diagram of the integrated system displayed in the model is shown in Figure 3.6. A medium temperature vertical multi deck cabinet with refrigeration capacity of 5 kW and a 3 kW low temperature vertical door type cabinet form the loading system of the integrated arrangement. The input parameters of the model include ambient temperature, refrigeration duties and evaporating temperatures of the MT and LT cabinets, circulation ratio, effectiveness of the IHX and delivery brine temperature.

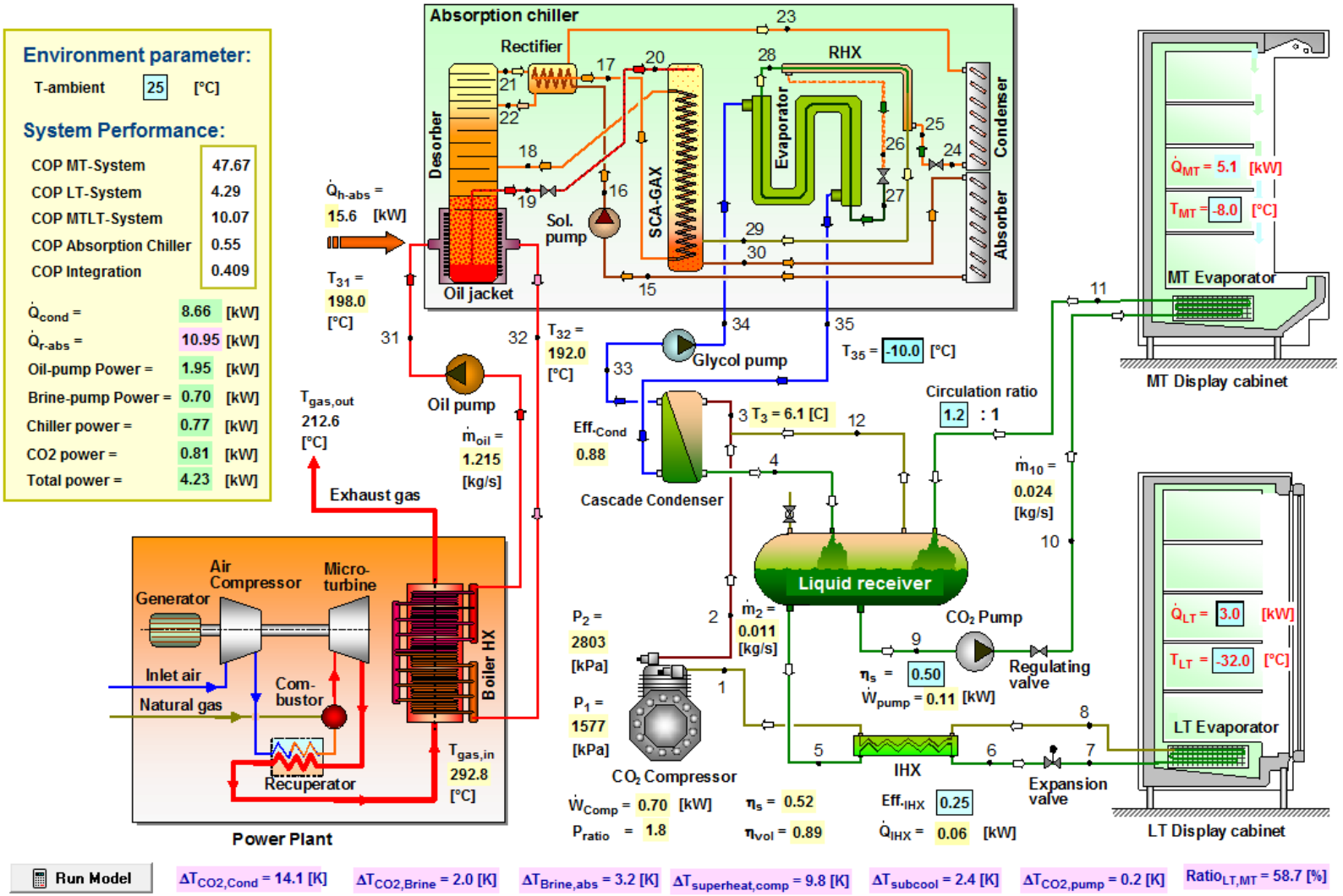

Figure 3.6 A simplified schematic diagram of the integrated arrangement displayed in the model

The main output parameters include *COP* and power consumption of the individual components and systems, refrigeration capacity of the absorption chiller ($Q_{r,abs}$), rejected heat from the cascade condenser (Q_{cond}) and heat required to drive the absorption chiller ($Q_{h,abs}$).

Other parameters such as mass flow rate, degree of sub-cooling and superheating, thermal and flow properties of the CO_2 refrigerant at every point in the cycle can also be obtained from the model.

In order to determine the performance characteristics of the individual and the integrated systems at different operating conditions, the following investigations have been carried out using the model:

- Variation of the system *COP* with ambient temperature
- Effect of the condensing temperature on the system *COP*
- Effect of the LT evaporating temperature on the system *COP*
- Variation of the *COP* with load ratio of LT to MT systems
- Influence of the use of internal heat exchanger (IHX).
- Variation of the *COP* with circulation ratios

- *Variation of the system COP with ambient temperature*

Figure 3.7 presents the influence of the ambient temperature on the *COP* of the absorption chiller and the integrated system at different delivery brine temperatures. The minimum condensing temperature of the absorption system and the temperature difference between condensing and ambient temperatures were assumed to be 25 ^{o}C and 5 ^{o}C respectively. The system was simulated with cascade condenser effectiveness (ε_{cond}) 0.88 and LT evaporating temperature ($T_{evap,LT}$) -32 ^{o}C. The LT and MT loads were maintained constant of 3 and 5.0 kW respectively. Circulation ratio of the MT system was set at CR = 1.2. The condensing temperature of the CO_2 refrigeration system varied from -6 ^{o}C to -8 ^{o}C when the delivery brine temperatures changed from -8 ^{o}C to -10 ^{o}C.

The *COP* of the absorption system (COP_{abs}) decreased with increased ambient temperature but increased with brine temperature as can be seen in Figure 3.7. The results show a good agreement with test data Robur (2006) and Suamir et al. (2009).

The COPs of the absorption and integrated systems are stable at ambient temperature below 20 °C but they begin to reduce at ambient temperatures above 20 °C. This is mainly because the condensing temperature of the absorption system was kept constant at 25 °C at ambient temperatures below 20 °C. Figure 3.7 also shows that the *COP* of the integrated system (COP_{int}) was determined to be 25% lower than COP_{abs} due to the power consumption of the HTF pump as well as the refrigerant pump and compressor of the CO_2 refrigeration system. As can be seen in Figure 3.6 the power consumption of HTF pump (oil pump) is nearly 2.5 times that of the CO_2 refrigeration system. This indicates that optimisation of the HTF circuit can reduce the electrical energy consumption of the HTF pump which subsequently will improve the *COP* of the integrated system.

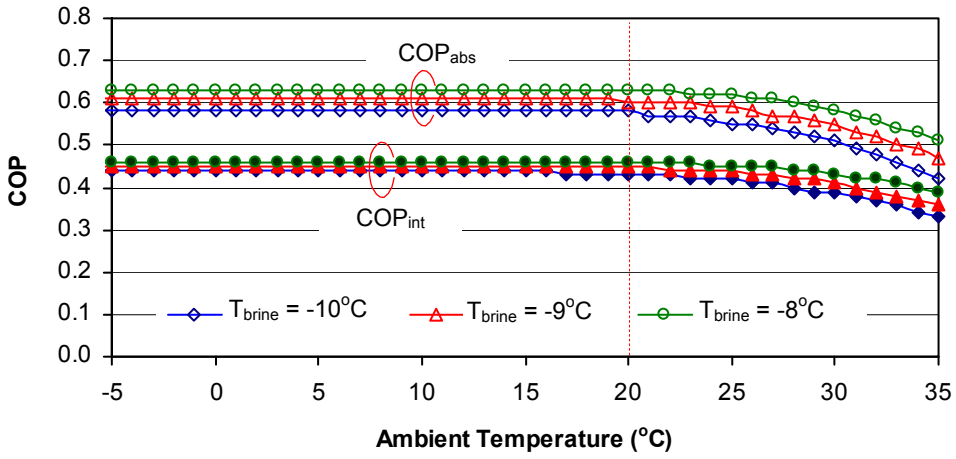

Figure 3.7 Effect of the ambient temperature on the *COP* of the absorption and integrated systems

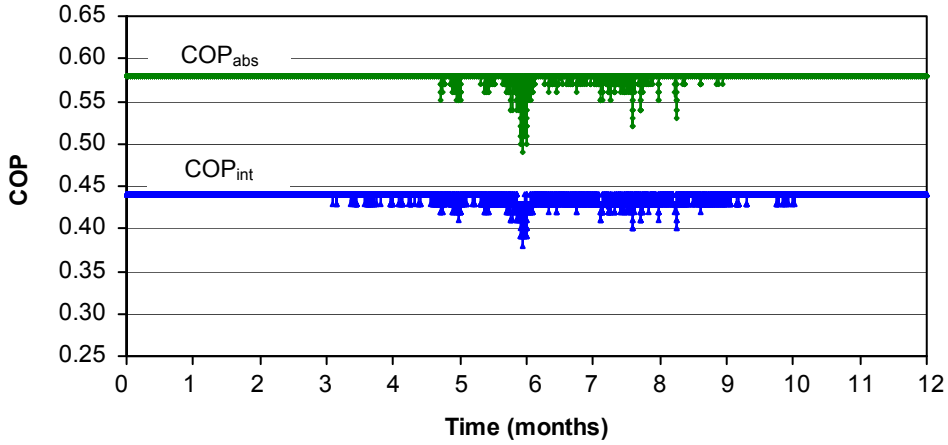

Figure 3.8 Seasonal performance of the absorption and the integrated systems

The seasonal COPs of the absorption and integrated systems are shown in Figure 3.8. The simulation results were obtained using London weather data (Met Office, 2009) and MT and LT evaporating temperatures of -8 °C and -32 °C respectively. It can be seen that the COPs are steady in the winter because the minimum condensing temperature is fixed at 25 °C but reduce in the summer due to higher ambient and condensing temperatures.

- *Effect of the condensing temperature on the system COP*

The condensing temperature of the DX-volatile CO_2 system is the same as the evaporating temperature of the MT system which can be varied by modulating the delivery brine temperature. The effect of the condensing temperature on the performance of the CO_2 refrigeration and integrated systems is shown in Figure 3.9. The simulations were carried out at constant refrigerant mass flow rate for both LT and MT systems; $\varepsilon_{cond} = 0.88$; $T_{evap,LT} = -32$ °C; $CR = 1.2$ and $T_{amb} = 25$ °C.

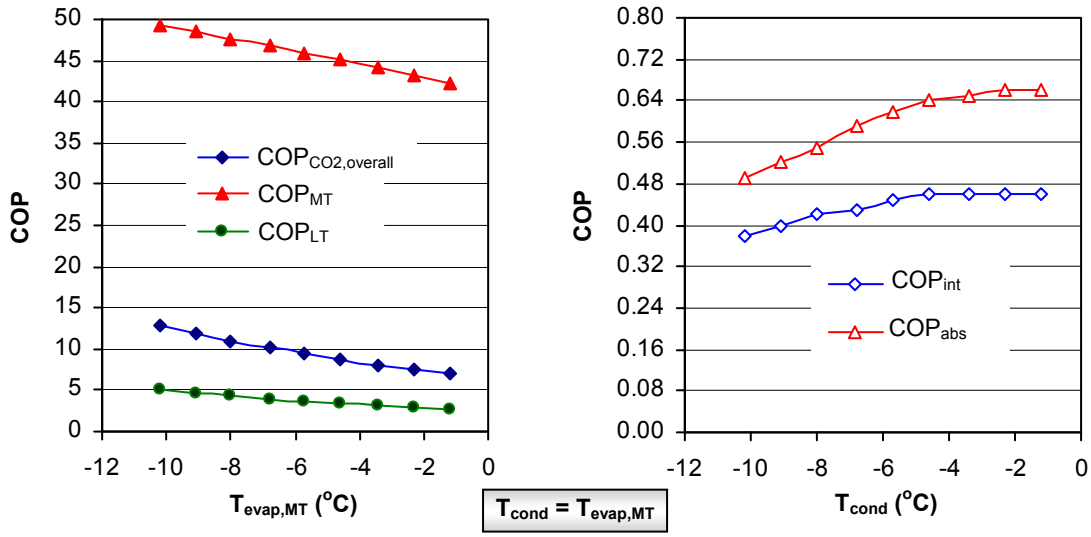

(a) COP of the CO_2 refrigeration system

(b) COP of the absorption and integrated systems

Figure 3.9 Variation of system *COP* with condensing temperature

Figure 3.9a shows that increasing the condensing temperature from -10 °C to -1 °C reduced the *COP* of the MT refrigeration system (COP_{MT}) by 14%. This is because the MT refrigeration capacity reduced from 5.2 to 4.7 kW (about 9.6% reduction) and increased the pump power by 5%. The increase of the condensing temperature also

significantly reduced the *COP* of the LT system (COP_{LT}) and the overall *COP* ($COP_{CO2,overall}$) by 47% and 46% respectively. This is mainly due to the increase in the compressor power consumption due to the higher discharge pressure and temperature.

Figure 3.9b shows that increasing the condensing temperature, however, enables the absorption system to operate at higher delivery brine temperature which improves the COP_{abs} and COP_{int} by approximately 35% and 21% respectively. This shows that the integrated arrangement will be more efficient if a higher MT evaporating temperature is used to satisfy the refrigeration requirements.

- *Effect of the LT evaporating temperature on the system COP*

Figure 3.10 shows the effect of the LT evaporating temperature on the *COP* of the individual and the integrated systems. The simulation was carried out at $T_{evap,MT}$ = -8 °C, CR = 1.2, T_{amb} = 25 °C and at constant refrigerant mass flow rate. Two interesting simulation results are noted. Firstly, increasing the LT evaporating temperature can considerably improve the COP_{LT} and $COP_{CO2\text{-}overall}$ but it does not influence the COP_{MT}. This indicates that operating at higher LT evaporating temperatures will improve the overall system efficiency.

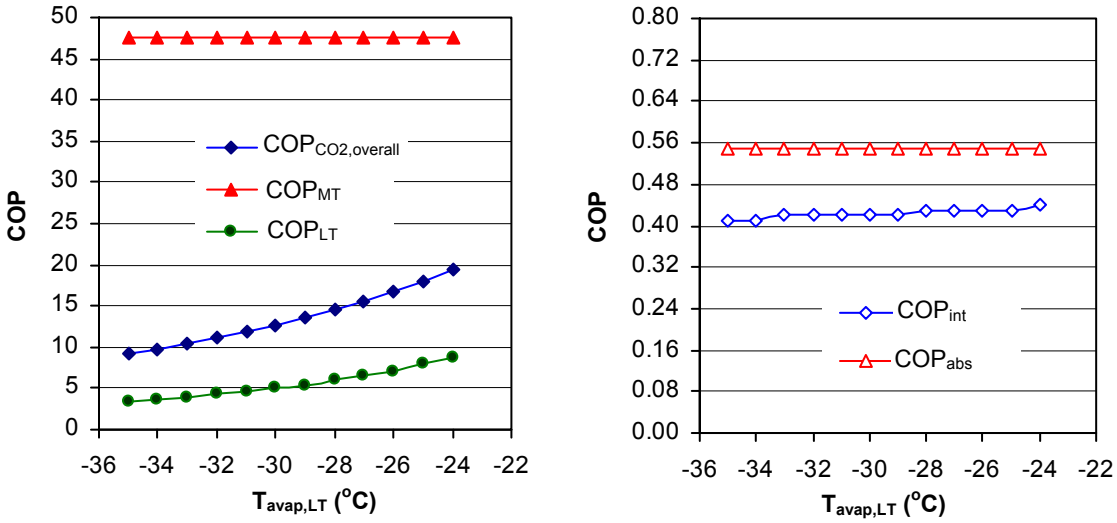

(a) COP of the CO_2 refrigeration system

(b) COP of the absorption and integrated systems

Figure 3.10 Variation of system *COP* with LT evaporating temperature

Secondly, the LT evaporating temperature has insignificant effect on the COP_{abs}. It just slightly increases the COP_{int} (Figure 3.10b) even though the increase of the $COP_{CO2,overall}$ is significant (Figure 3.10a).

- *Variation of the COP with load ratio of LT to MT systems*

The load ratio of LT and MT refrigeration systems (LRLM) may vary in each supermarket. For medium size supermarkets the LRLM can range from 14% to 52% with the average for Tesco (Tesco, 2009) being 32% representing average electrical energy consumption ratio for the LT and MT systems to the overall refrigeration system including display cabinets of 20% and 42% respectively as described in Section 1.1 (Chapter 1).

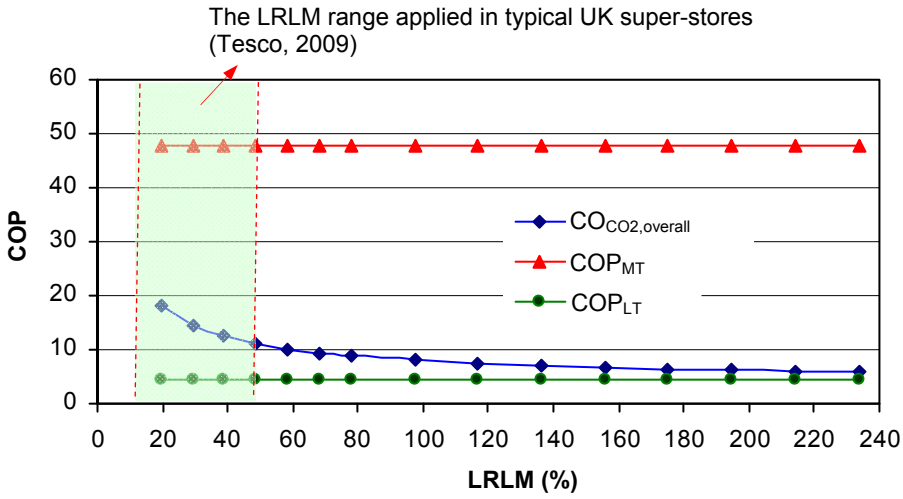

Figure 3.11 Variation of *COP* with load ratio of LT and MT systems (LRLM)
(Investigated at: $T_{evap,MT}$ = -8 °C, $T_{evap,LT}$ = -32 °C, *CR* = 1.2, T_{amb} = 25 °C)

Figure 3.11 illustrates the influence of LRLM on the *COP* of the CO_2 system. The overall *COP* ($COP_{CO2,overall}$) reduces when the *LRLM* increases even though the COP_{MT} and COP_{LT} are maintained constant. The overall *COP* of the CO_2 system was found to be more sensitive to load ratio below LRLM of 80%.

- *Influence of the use of internal heat exchanger (IHX)*

The CO_2 system was designed with a liquid-suction heat exchanger (IHX) to enable the system to be evaluated at different suction superheating and liquid line subcooling. The

model was used to simulate the effect of the suction superheating and liquid line subcooling on the *COP* of the LT DX system. The model was also used to determine a suitable effectiveness for the IHX to provide suction superheating below 20 K as recommended by Bock (2009). For design purposes, the suction superheating and liquid line subcooling were assumed to be in the range 8 to 12 K and 2 to 3 K respectively.

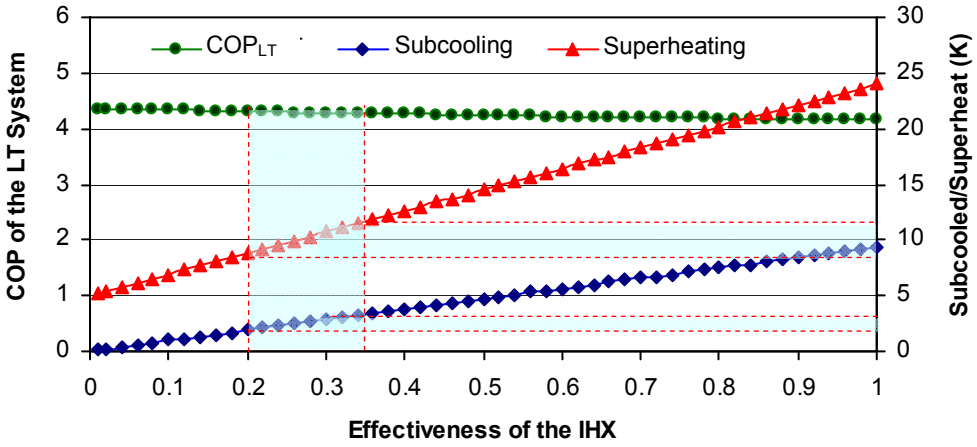

Figure 3.12 Variation of superheating, subcooling and COP_{LT} with different IHX effectiveness
(Investigated at: LT refrigeration duty 3 kW, T_{cond} = -8 °C, $T_{evap,LT}$ = -32 °C, T_{amb} = 25 °C)

The simulation results are presented in Figure 3.12. It can be seen that the suction superheating and liquid line subcooling increase with the effectiveness of the IHX. The effectiveness of the IHX which could provide the designed superheating and subcooling was found to be in the range between 0.2 and 0.35. The figure also shows that increasing the suction superheating and liquid line subcooling slightly reduces the COP_{LT}. The COP_{LT} will drop by less than 5% when the suction superheating and liquid line subcooling increase to 20 K and 8 K respectively.

- *Variation of the COP with circulation ratio*

The circulation ratio (*CR*) indicates the amount of refrigerant flowing through a flooded evaporator coil. Stoecker (1998) defines the circulation ratio as the ratio of refrigerant flow rate circulated through the evaporator to the flow rate of refrigerant vaporised. *CR* = 1 means that just enough refrigerant circulates to provide complete evaporation without superheating. *CR* = 2 means that the mass flow rate of refrigerant that flows through the evaporator is twice that required for complete evaporation. To investigate

the effects of the circulation ratio on the system *COP*, a correlation between *CR* and refrigeration duty of the MT evaporator coil ($Q_{evap,MT}$) was applied. The correlation, which is presented in Figure 4.7 (Chapter 4), was established using the CO_2 evaporator model.

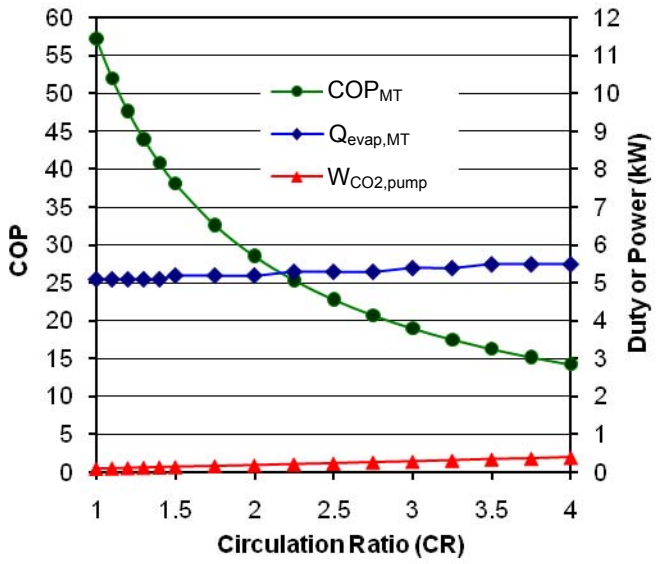

Figure 3.13 Effect of circulation ratio (*CR*) on the *COP*, refrigeration duty and power consumption of the MT refrigeration system

Figure 3.13 shows the influence of the circulation ratio on the *COP*, refrigeration duty and pump power of the MT CO_2 system at $T_{evap,MT}$ = -8 °C, $T_{evap,LT}$ = -32 °C and T_{amb} = 25 °C. The load ratio of LT to MT systems (LRLM) was in the range between 58% and 61%. It can be seen that the CO_2 pump power ($W_{CO2,pump}$) increases linearly with the circulation ratio. The MT refrigeration duty ($Q_{evap,MT}$) increases slightly up to *CR* = 2.5 but then remains relatively constant. The COP_{MT} reduces sharply as the *CR* increases above 1.0.

A circulation ratio was also found to influence the $COP_{CO2,overall}$ as shown in Figure 3.14. Increasing the circulation ratio from 1.0 to 4.0 reduced the $COP_{CO2,overall}$ from 11.0 to 8.0. The *CR* has only a very small effect on the *COP* of the integrated system.

To enable investigation of the effect of the circulation ratio on the system performance, the test rig was designed to provide a circulation ratio of up to 2. Other design conditions for the system and estimated performance parameter are listed in Table 3.3.

A display of the EES model developed for the design is shown in Figure B-1 (Appendix B).

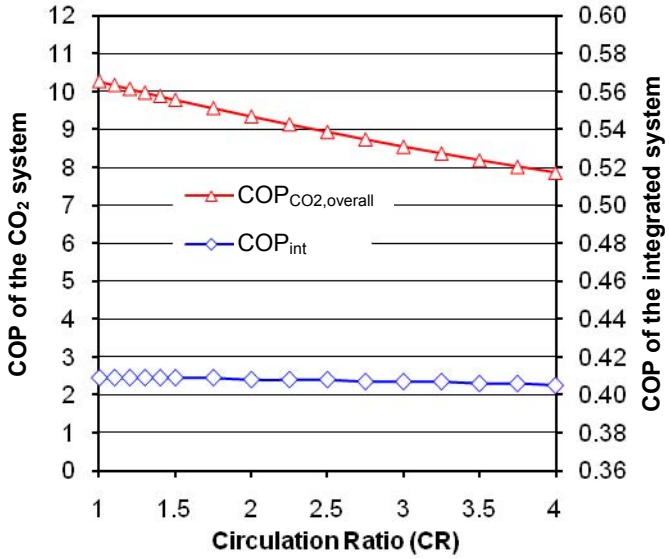

Figure 3.14 Effect of the circulation ratio (*CR*) on the overall COPs of the CO_2 system and the integrated arrangement

Table 3.3 Design conditions and estimated performance parameters

Design conditions		**Estimated performance parameters**	
Parameters	*Value*	*Parameters*	*Value*
Ambient temperature (°C)	25	MT refrigeration capacity (kW)	5
Delivery brine temperature (°C)	-10	LT refrigeration capacity (kW)	3
Condensing temperature (°C)	-8	*COP* of MT CO_2 system	28.6
MT evaporating temperature (°C)	-8	*COP* of LT CO_2 system	4.3
LT evaporating temperature (°C)	-32	*COP* overall CO_2 system	9.2
Circulation ratio	2	*COP* of the absorption system	0.55
Load ratio LT to MT (LRLM) (%)	60	*COP* of the integrated system	0.41
LT evaporator superheat (K)	5	LT compressor power (kW)	0.70
LT compressor suction superheat (K)	9.8	CO_2 pump power (kW)	0.18
LT liquid line subcooling (K)	2.4	Brine pump power (kW)	0.69
Condenser effectiveness (%)	88	HTF pump power (kW)	1.93
Max. capacity of the absorption chiller (kW)	10.95	Heat rejected in the condenser (kW)	8.56
Mass flow rates			
Brine mass flow rate (kg/s)*	0.725	MT CO_2 mass flow rate (kg/s)	0.040
HTF mass flow rate (kg/s)	1.20	LT CO_2 mass flow rate (kg/s)	0.011
CHP exhaust gas mass flow rate (kg/s)	0.81		

* Water-glycol mixture: propylene glycol with 40% mass fraction in water solution was considered.

3.2.2 Piping system design and pressure drop simulation

A CO_2 refrigerant piping system requires the same general design considerations as any refrigerant flow system. One factor that critically influences system design is the pressure drop since pressure losses decrease the thermal capacity and increase the power requirement in a refrigeration system. Pressure drop at suction line of the compressor causes suction pressure at the inlet of the compressor lower than evaporating pressure. As a result, density of refrigerant vapour reduces, pressure ratio and discharge temperature increases. This in turn reduces volumetric efficiency, refrigerant mass flow rate, refrigeration (thermal) capacity and increases work of compression.

The piping systems of the test rig have been designed to provide practical line sizes without excessive pressure drop. The pressure drop of the liquid and gas lines were designed to be well below 78 kPa and 55 kPa respectively which represent 1 K equivalent saturation temperature drop as recommended by ASHRAE (2010). To simulate the pressure drop in the piping system, a model was developed within EES. The maximum operating pressure was considered to be 35 bar.

When the system is in operation, most of the refrigerant pipes contain single phase flow, either liquid or gas. One section with two phase flow is that downstream of the MT evaporator. The pressure drop (ΔP) of single phase section was calculated from the equation below:

$$\Delta P = 4f \frac{L}{d_i} \frac{G^2}{2\rho} \tag{3.21}$$

where d_i = internal diameter of the pipe (m), L = pipe length (m), G = mass velocity (kg/s.m^2), ρ = refrigerant density (kg/m^3) and f = friction factor. For turbulent flow with Reynolds number (Re) up to 10^5, CO_2 friction factor of the single phase section was calculated from the Blasius equation (Cheng et al., 2008a):

$$f = \frac{0.079}{\mathrm{Re}^{0.25}} \tag{3.22}$$

where Reynolds number was calculated from:

$$\mathrm{Re} = \frac{G\, d_i}{\mu} \tag{3.23}$$

For flow conditions where Re ≤ 2300 the CO_2 friction factor was calculated from:

$$f = \frac{16}{\mathrm{Re}} \tag{3.24}$$

The pressure drop of the refrigerant pipe downstream of the MT evaporator was determined using the procedure of two phase CO_2 pressure drop described by Cheng et al. (2008a). A vapour quality x = 0.5 was used which results from a circulation ratio (CR) = 2.

Table 3.4 presents the resulting nominal outside diameter of the pipe and the pressure drop determined from the simulation. It can be seen that the pressure losses in the suction and liquid lines of the LT compressor are low at 1.42 kPa (0.026 K) and 0.33 kPa (0.004 K) respectively. The table also shows that the pipe section after the MT evaporator has the highest pressure drop of 24.7 kPa, equivalent to 0.32 K. This pressure drop, however, is still within the acceptable range.

Table 3.4 Specified pipe sizes of the CO_2 refrigeration system

Pipe number	Position in the system	d_o (mm)	L (m)	ΔP (kPa)
1,8	Suction LT compressor after and before IHX	15.87	15	1.42
5,6	LT Liquid line before and after IHX	12.7	14	0.33
2	Discharge LT compressor	12.7	7	1.77
9,10	MT liquid line before and after the CO_2 pump	12.7	16	3.30
11	After MT evaporator	12.7	20	24.71
12	Saturated gas line from liquid receiver	12.7	1	0.47
3	Common line before condenser	12.7	1	1.19
4	Liquid line after condenser	12.7	1	0.14

Note: d_o is nominal outside diameter conforming to BS EN 12735-1 (2001).

The calculation screen of the EES model is shown in Figure B-2 (Appendix B). The display also shows the internal volume and flow velocity in each section of the pipe circuit. The estimated total volumes of gas and liquid CO_2 in the pipe circuit were also estimated to be 2.2 and 3.8 litres respectively.

Besides pressure drop, the design also considered other refrigeration-piping basic principles such as protection of the pipes from excessive vibration of the compressor and to prevent liquid refrigerant or oil slugs from entering the compressor during operation and shutdown. Thus, the system was equipped with vibration eliminators, a suction line accumulator and a non-return valve on the discharge line of the compressor.

To minimise leakage, brazed joints were used. The pipes were also insulated with 25 mm thick insulation to prevent sweating or frosting and minimise heat transfer with the surroundings which can be significant in CO_2 systems and adversely affect performance (Bertelsen and Christensen, 2003).

3.2.3 EES model to determine the optimum size of the liquid receiver

The liquid receiver has been designed for three main purposes. One is to provide pump-down storage capacity when other components of the system must be serviced or the system must be shut down due to the tests having been completed. The second is to accommodate a fluctuating refrigerant demand which varies with load conditions. The third is to provide adequate liquid flow at the suction line of the CO_2 pump.

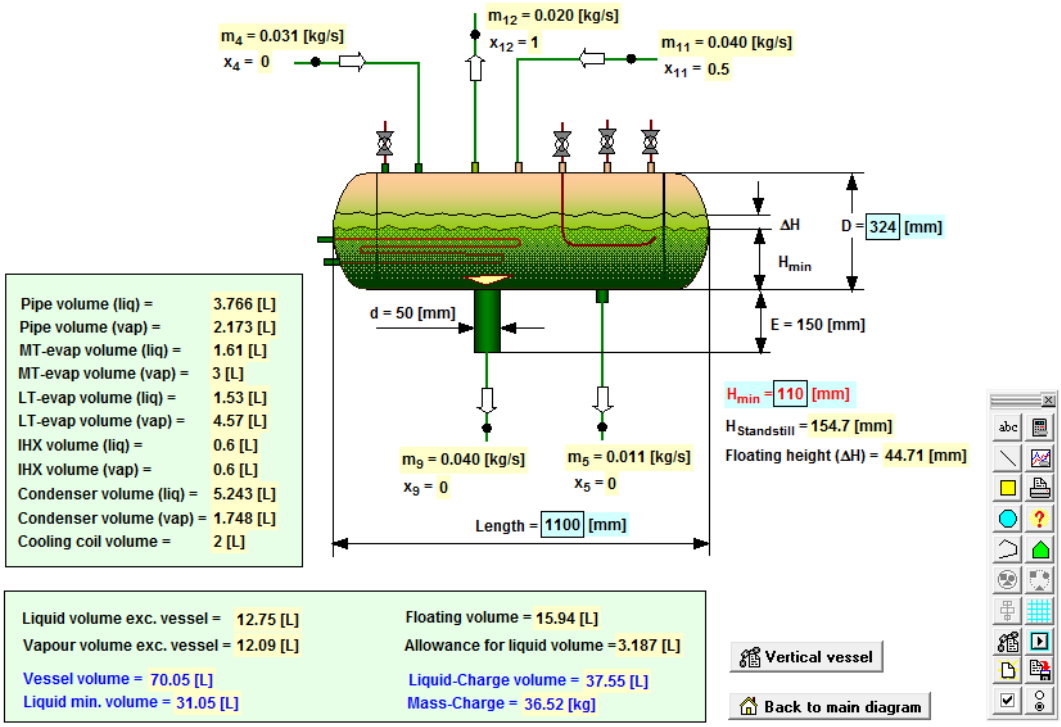

Figure 3.15 Simulation results from liquid receiver model

To determine the optimum size of the liquid receiver, two EES models were established: model of horizontal receiver and model of vertical receiver. By considering the volume of all components of the CO_2 refrigeration system including piping, the dimensions of the liquid receiver and fluctuation of the liquid level in the vessel were investigated. Figure 3.15 shows dimensions of the horizontal liquid receiver. The optimum volume of the vessel was found to be 70 L with external surface area 1.12 m^2

and total mass charge 37 kg. The simulation results for the vertical receiver are given in Figure B-3 (Appendix B). For the same volume, the horizontal liquid receiver requires slightly higher refrigerant charge but reduces the fluctuations in the liquid level compared to the vertical receiver.

The horizontal liquid receiver was chosen for the test rig. A technical drawing was produced shown in Figure C-2 (Appendix C) and the receiver was manufactured by Klimal-Italia Srl. Figure 3.16 shows the liquid receiver placed on a steel frame. The receiver has several connections to the CO_2 refrigeration circuit including down pipe to the CO_2 pump and connections to a standstill condensing unit. It is also completed with a vertical small tube which houses a liquid level transmitter.

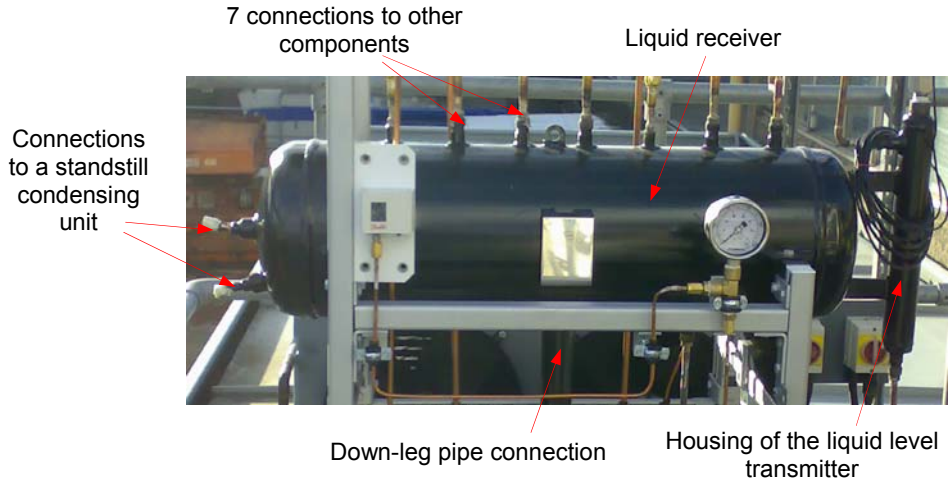

Figure 3.16 The liquid receiver (manufactured by Klimal-Italia Srl.)

The liquid receiver was tested at 71.5 bar. It was specified with maximum allowable pressure of 50 bar at temperature range from 50 ^{o}C to -10 ^{o}C.

3.2.4 3D drawing of the CO_2 refrigeration plant

A 3D-AutoCAD drawing was prepared to facilitate dimensioning and construction of the CO_2 refrigeration plant (Figure 3.17). Installation requirements of system components, positive gravity flow, available space in the plant room and accessibility to the components for operation and maintenance were also taken into considerations.

For clarity, the components and piping are shown without insulation. It can be seen that the test rig consists of two main sections: the compressor-pump section and liquid

receiver section. The compressor-pump section incorporates the LT CO_2 compressor, CO_2 pump, oil management system (oil separator, oil reservoir, oil filter and oil level controller), suction accumulator, filter drier, mass flow-meters and control panel. The liquid receiver section includes liquid receiver, CO_2 condenser, CO_2 liquid level controller and safety device. All system components are properly mounted on steel frames.

.

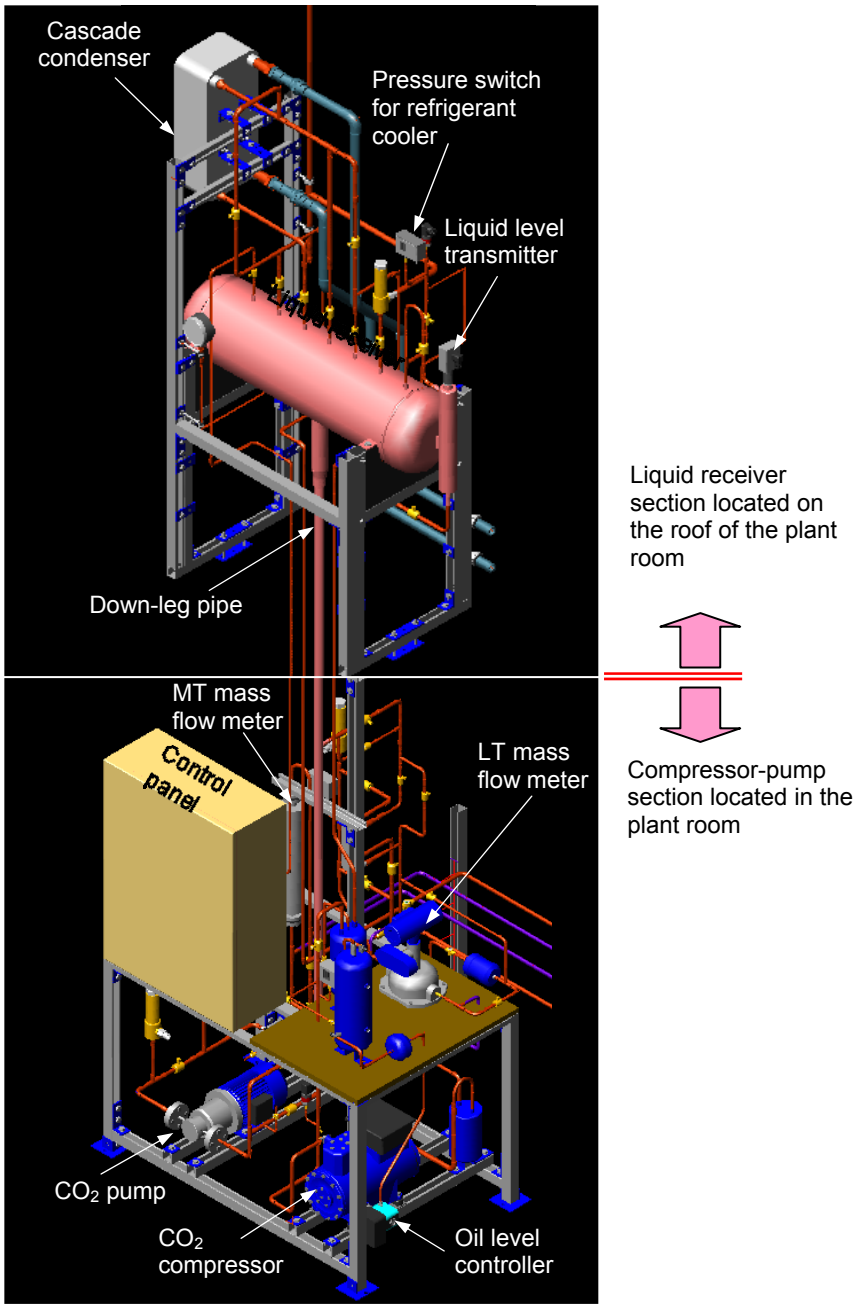

Figure 3.17 The subcritical CO_2 refrigeration test plant in a 3D drawing

3.3 Mechanical system design and component selection

A detailed schematic diagram of mechanical system design is shown in Figure 3.18. Components identification and numbering of the mechanical system especially the flow control valves can be found in Figure C-1 (Appendix C).

The MT system has been designed so that the liquid CO_2 for the medium temperature cabinet can be either pumped with a CO_2 pump or gravity fed to the MT coil. The system is also designed to enable the coil to be fed with different mass flow rates or circulation ratios (*CR*). In order to facilitate the design requirements, as can be seen in Figure 3.18, a bypass valve is fitted parallel to the CO_2 pump. The valve allows the liquid CO_2 flowing to the MT coil by gravity. Another control valve is added to bypass some of the liquid CO_2 from discharge line of the CO_2 pump to the liquid receiver. This valve in combination with a regulator valve upstream of the MT coil can be used to vary the flow rate of liquid CO_2. In order to determine a CO_2 flow rate at a particular test condition which provides just enough refrigerant without superheat ($CR = 1$), the system is equipped with a sight glass at downstream of the MT coil and a mass flow meter at the liquid line.

The LT system comprises three main components which include an expansion valve, an LT evaporator coil and a CO_2 compressor as illustrated in Figure 3.18. The figure also shows that the LT system is equipped with some accessories as commonly found on a DX conventional refrigeration system such as an accumulator on the suction line of the LT compressor; a filter drier and a sight glass situated between the liquid receiver and expansion valve. Parallel to the IHX, a bypass valve was fitted to allow flexibility for testing with and without heat exchange between the liquid line and the outlet of the LT evaporator. The LT circuit is also equipped with an oil management system to maintain the oil level in the compressor relatively constant.

One common component of the LT and MT systems is the cascade condenser where condensation of the CO_2 from both systems takes place. The condensation of the CO_2 gas is provided by the absorption refrigeration system of the trigeneration facility through a secondary refrigerant circuit using a water-glycol mixture to transfer thermal energy between the CO_2 system and the absorption refrigeration system.

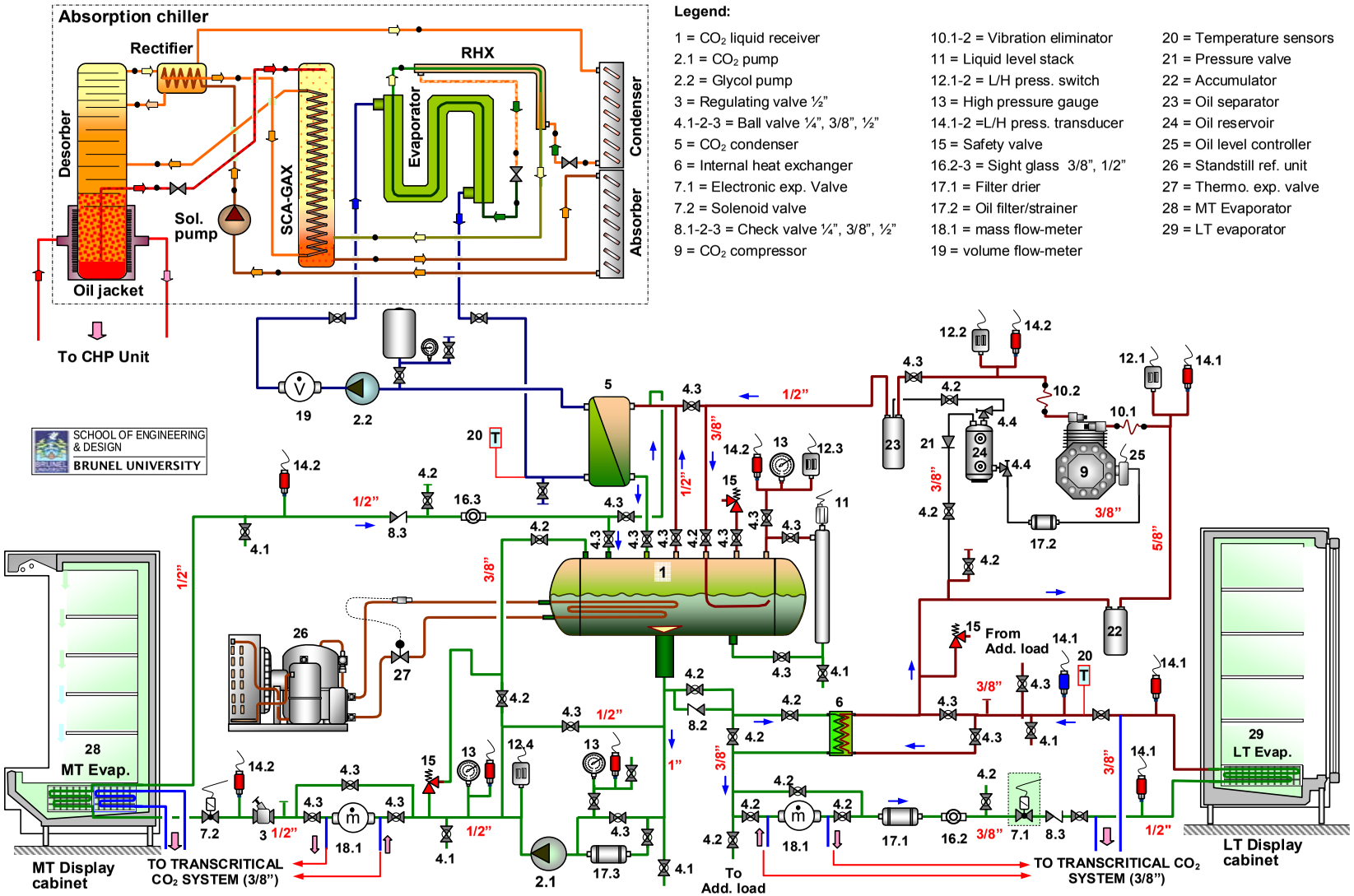

Figure 3.18 Piping diagram of the integrated trigeneration and CO_2 refrigeration system

Another common component is the liquid receiver where most of the CO_2 refrigerant charge is stored. The receiver and associated piping provide free flow of liquid from the condenser. Pressures between the two are equalized so that the receiver cannot build up a higher pressure than the condenser. To facilitate the flow of liquid CO_2 from the condenser by gravity, the condenser is placed just above the liquid receiver. A pipe from the bottom of the receiver feeds liquid CO_2 to the pump and LT DX systems. The pipe has been sized to provide sufficient head for the CO_2 pump and minimum pressure drop. The liquid receiver is also equipped with an evaporator coil connected to a small conventional condensing unit, as shown in Figure 3.18. The condensing unit is used to keep the pressure of the liquid CO_2 refrigerant low during standstill.

Figure 3.18 also shows pipe connections and flow control valves so that the loading system and flow meters can also be used by a transcritical CO_2 system. For safety, the CO_2 refrigeration system is equipped with safety relief valves. The location of the valves can also be seen in Figure 3.18. Detailed description of the safety relief valves is presented in Section 3.3.8. In addition, the piping system and components of the CO_2 refrigeration system are also selected to be compatible with the CO_2 refrigerant and maximum pressure of at least 40 bar.

3.3.1 CO_2 compressor

Selecting a CO_2 compressor at the early stage of the development of the CO_2 refrigeration technology was challenging due to limited range of capacities available. Figure 3.19 shows the CO_2 compressor selected for the test rig. It is a two-piston low temperature semi-hermetic reciprocating compressor. It can be seen that at designed conditions, T_{evap} = -32 ^{o}C and T_{cond} = -8 ^{o}C, the compressor has a refrigeration capacity more than three times the designed load of the LT cabinet. Consequently, an additional LT load was added to the test system to balance the load and to avoid the compressor cycling on and off frequently. The compressor was also equipped with a variable speed controller to enable some variation of capacity. Having a large capacity, the compressor significantly increased the LT and MT load ratio. This subsequently reduced the overall *COP* of the refrigeration system as previously demonstrated in Figure 3.11.

To ensure safe operation, the compressor was equipped with several safety controls which included oil safety switch, low and high pressure switches, motor temperature

switch and a time delay relay. The oil safety switch protects the compressor from running without sufficient lubrication by switching it off if the oil level drops below a certain limit. The low and high pressure switches are used to stop the compressor when the suction pressure drops below 7 bar and the discharge pressure rises above 33 bar respectively. The motor temperature switch which is integrated with the motor compressor switches the compressor off, when the temperature in the motor windings becomes excessive. A time delay relay is used to prevent the starting of the compressor just after the compressor has been shut down due to action of LT cabinet controller or one of the safety controls. The relay used is an 'on time delay' which elapsed time is set for 3 minutes.

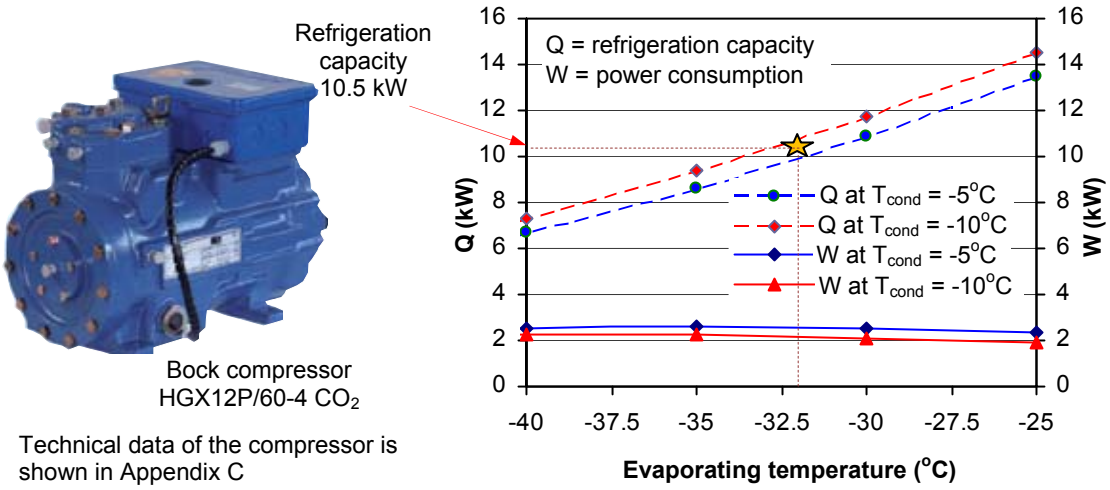

Figure 3.19 CO_2 compressor with specified performance data
(Data source: Bock, 2009)

3.3.2 CO_2 pump

A rotary vane type pump was selected for the test rig. The pump has a rated flow of 0.44 m^3/h (approximately 108 g/s) liquid CO_2 at -8 ^oC which can provide a circulation ratio up to 4 for the MT secondary circuit. The pump requires a net positive suction head (*NPSH*) of 3.5 mLC (metre of liquid column). Figure 3.20 shows the selected CO_2 pump with and without insulation. Detailed specifications of the pump are given in Appendix C.

Cavitation in a CO_2 refrigeration application is not a major problem due to energy released during cavitation is much smaller compared to other refrigerants (Heerup, 2009). Cavitation, however, can reduce the specified flow capacity of a CO_2 pump. In order to avoid cavitation and to achieve the rated flow, the installation of the pump was prepared to provide *NPSH* at least 3.7 mLC. In addition, heat transfer with the surroundings on the suction pipe and the pump itself was also minimised by insulating them with appropriate insulation as shown in Figure 3.20.

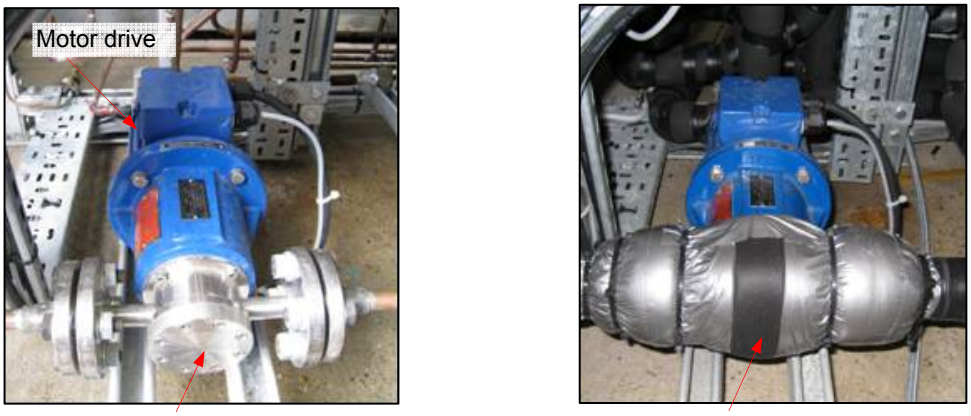

Figure 3.20 CO_2 pump (Hermetic HTP 1-400)

The pump is also equipped with a safety control system which consists of a liquid level relay, high pressure switch which switches the pump off when the discharge pressure rises to 33 bar and a motor temperature switch. The liquid level relay is used to protect the pump from cavitation by stopping the pump motor when the liquid level in the liquid receiver drops to 35% of full liquid height.

3.3.3 Condenser

A plate type heat exchanger was selected as the condenser of the CO_2 refrigeration system. This type of heat exchanger has high thermal efficiency and small foot print (Jokar et al., 2010). Figure 3.21 shows the condenser HX and its specifications. Detailed size of the condenser is given in Figure C-3 (Appendix C).

The condenser is mounted in a counter flow configuration between the CO_2 line and the water-glycol line. The CO_2 enters the condenser as a superheated gas at 6.3 ^{o}C and exits

as saturated liquid at -8 °C. The temperature difference between the exiting liquid CO_2 and returning water-glycol can be as low as 2 K (specified by the manufacturer).

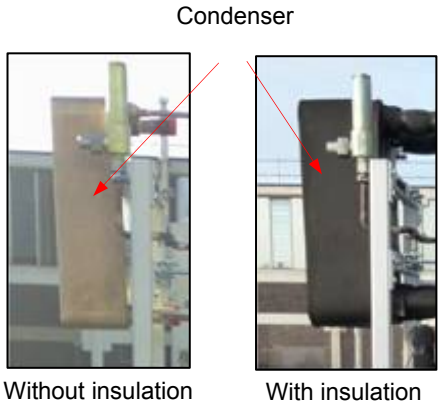

Parameters and specifications	CO_2 side	Water glycol side
Inlet temperature (°C)	6.3	-10
Outlet temperature (°C)	-8	-6.8
Flow rate (kg/s)	0.040	0.725
Heat load (kW)	12	
Heat transfer area (m^2)	7.66	
Over surface (%)	40	
Number of channel	29	30
Test pressure (bar)	75	75
Max. working pressure (bar)	45	45
Hold up volume (L)	6.99	7.23

Figure 3.21 CO_2 condenser (SWEP B120THx60/1P-SC-M2)

3.3.4 Evaporators

Evaporator coils used in the loading system are standard finned coils which have been designed to operate with CO_2 refrigerant. The evaporator coil of the medium temperature cabinet is a flooded coil whereas the coil for the low temperature cabinet is a direct expansion coil.

Figure 3.22 shows the MT flooded coil fitted at the bottom of the MT cabinet. The coil is made from copper tubes of 12.7 mm nominal outside diameter and corrugated aluminium fins of 0.22 mm thickness and fin spacing of 158 fins per metre (FPM). The coil consists of 4 circuits in staggered arrangement with 4 rows high, 6 rows deep and total tube length of approximately 50 m. The MT coil can contain about 4.6 litres CO_2 refrigerant.

Figure 3.22 also shows that the MT flooded evaporator coil is placed adjacent to the MT DX evaporator coil which is used for transcritical CO_2 refrigeration tests. The two evaporator coils which are not used simultaneously are separated by a 25 mm air gap.

The size of the MT flooded coil is 152 x 198 x 2085 mm (height x depth x length). It is relatively compact compared with a HFC evaporator coil of the same capacity. As it can be seen from Figure 3.22, two CO_2 MT evaporator coils could be fitted into the space originally utilised by a single R-404A evaporator coil.

The LT DX evaporator coil is also made from copper tube of 12.7 mm nominal outer diameter with corrugated aluminium fins of 0.22 mm thickness. The fin spacing is 118 fins per metre (FPM). The coil comprises 3 circuits in staggered arrangement with 4 rows high and 8 rows deep and its size is 152 x 264 x 2030 mm (height x depth x length). The total tube length is approximately 65 m which gives refrigerant volume of about 6.1 litres. The LT evaporator coil is also utilised by the loading system of the transcritical CO_2 system. Both systems use a direct expansion coil for the low temperature system and thus, only one LT evaporator coil is used. However, separate evaporator controllers are employed for the two systems.

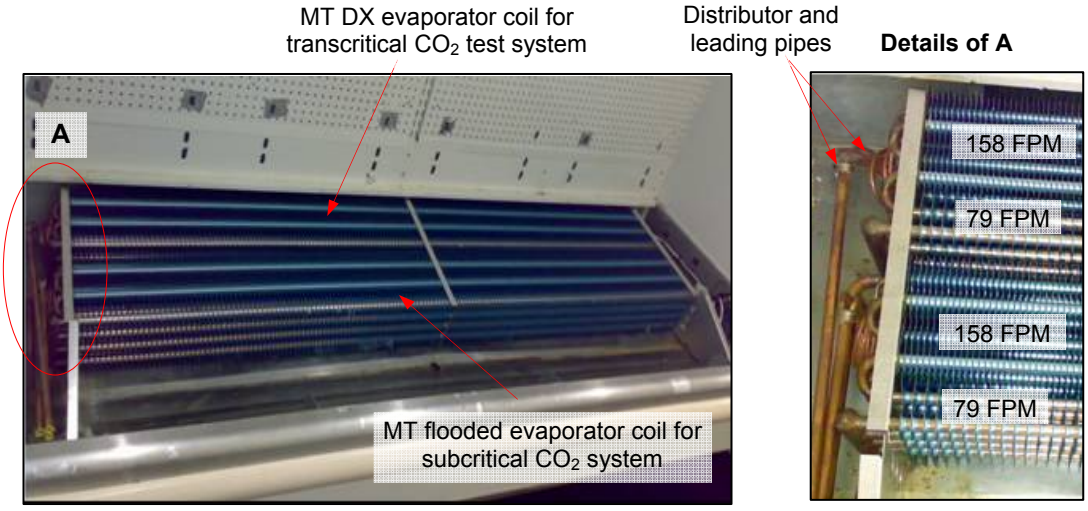

FPM = number of fins per metre; FPI = number of fins per inch; 158 FPM = 4 FPI; 79 FPM = 2 FPI

Figure 3.22 MT CO_2 evaporator coils fitted in the display cabinet

The MT and LT evaporator coils were tested at 52 bar with specified maximum allowable working pressure of 40 bar. Detailed information of the coils is given in the technical drawings in Figures C-4 and C-5 (Appendix C).

To reduce the effect of frost formation on the coils the free flow area of the front part of the coils was increased by reducing the fin density from 158 fins per metre to 79 fins per metre for the MT coil (Figures 3.22 and C-4) and from 118 fins per metre to 59 fins per metre for the LT coil (Figure C-5). The coils also utilise a hydrophilic coating on the fins to improve condensate drainage and ease of separation of frost from the coil during defrosting.

The main design parameters for the MT flooded coil are: CO_2 saturated liquid enters the coil at 28 bar_a (-8 ^oC); evaporation temperature in the coil at -8 ^oC; CO_2 exits the coil as liquid and vapour mixture at vapour quality of 0.5 (at designed circulation ratio CR = 2). For the LT evaporator coil, CO_2 enters the EXV as liquid with 2.4 K subcooling at 28 bar_a. After expansion CO_2 enters the LT coil as a liquid-vapour mixture at evaporation pressure of 13 bar_a (-32 ^oC) and exits with 5 K superheating. Detailed designs of the CO_2 evaporator coils including simulation programmes which have been established to evaluate their performance are presented in Chapter 4.

3.3.5 Expansion valve

Parameters considered in selecting and sizing the expansion valve for the low temperature DX circuit were pressure drop across the valve of 15 bar, full load refrigeration capacity of 3 kW and part load of 2 kW.

An electrically operated expansion valve has been chosen for the DX evaporator as shown in Figure 3.23. It has a wider range and flexibility for refrigerant flow control compared to the traditional thermostatic expansion valve (TXV). It also offers the possibility to integrate its control with the cabinet controller to make it easier to change the operational settings for system investigations.

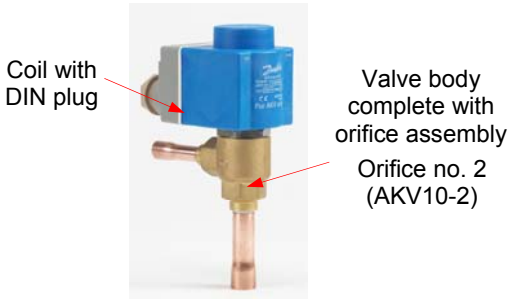

Figure 3.23 Electronic expansion valve
(Source: Danfoss, 2008)

The valve is of the pulse-width-modulated type which is an on/off solenoid valve with special features that allow it to operate as a variable metering device by rapidly pulsing the valve open and closed. For example, if the evaporator needs 75% flow, the valve is open 75% and closed 25% of the time. The duration of each pulse is regulated by an electronic controller. Thus, the application of this valve requires a controller and control sensors which include a pressure transducer and a temperature sensor. The controller of the valve is integrated with the evaporator controller which is described in Sections 3.5 and 3.6.

The expansion valve was specified to have a maximum operating pressure difference (MOPD) across it of 18 bar and maximum operating pressure (MOP) of 52 bar.

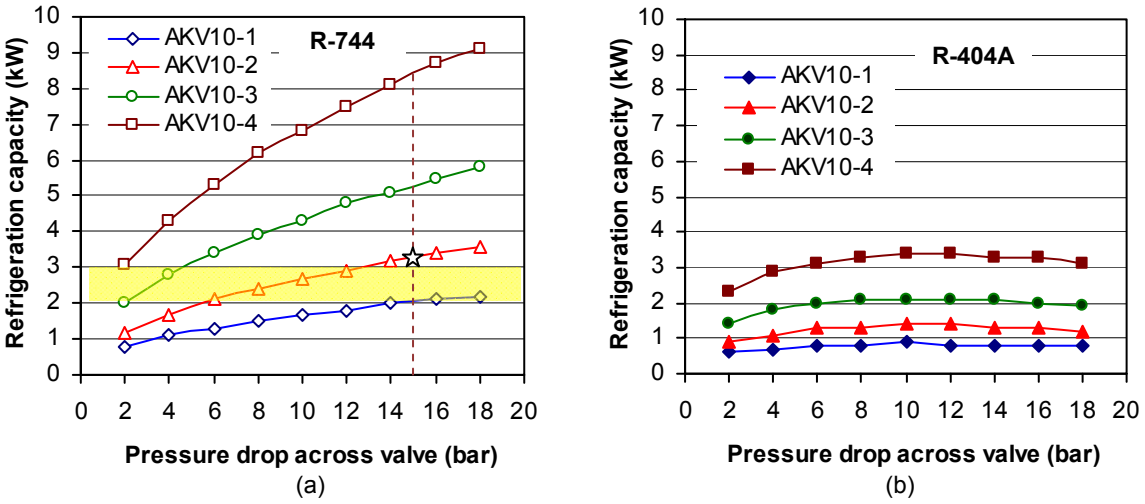

Figure 3.24 Performance data of electronic expansion valves type AKV10
(Data source: Danfoss, 2008b)

Figure 3.24(a) shows the performance characteristics of the AKV10 range of valves. It can be seen that the AKV10-2 is the closest AKV valve to satisfy the design requirements. It can also be seen that the capacity of the AKV10 valve is much higher when used with CO_2 refrigerant compared to R-404A.

3.3.6 Internal heat exchanger

The internal or suction line heat exchanger (IHX) is shown in Figure 3.25. It is a plate heat exchanger and was installed in counter flow configuration between the liquid supply line and suction line of the LT compressor. The IHX can increase the degree of superheat of the CO_2 gas exiting the LT evaporator to achieve suction superheating in the range 8 to 12 K. It can also reduce the risk of liquid entering the LT compressor. In the liquid line, the IHX subcools CO_2 liquid entering the expansion valve and this can improve the *COP* of the LT system.

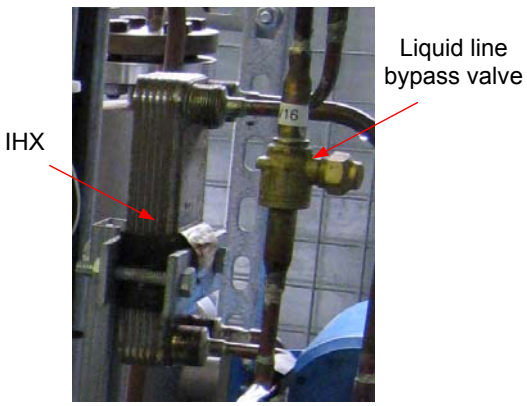

Figure 3.25 Internal heat exchanger
(SWEP: B5Hx10/1P-SC-M4)

The IHX has a heat transfer capacity of 0.2 kW. The amount of subcooling can be varied by using a bypass valve to bypass some of the refrigerant round the heat exchanger.

3.3.7 Refrigerant flow control devices

Four types of flow control valves are used in the test system shown in Figure 3.26. They are Danfoss products which are compatible with CO_2 refrigerant. The solenoid and ball valves are stop valves also commonly referred to as shutoff valves. The solenoid valve was used to automatically prevent liquid CO_2 flowing to the MT flooded evaporator when no flow is required, such as during the defrost cycle and when the cabinet has reached the set point. The ball valves are manually operated and used to isolate the system components such as: compressor, pump, condenser, liquid receiver, IHX and evaporators for servicing and safety (ASHRAE Standard 15, 2007).

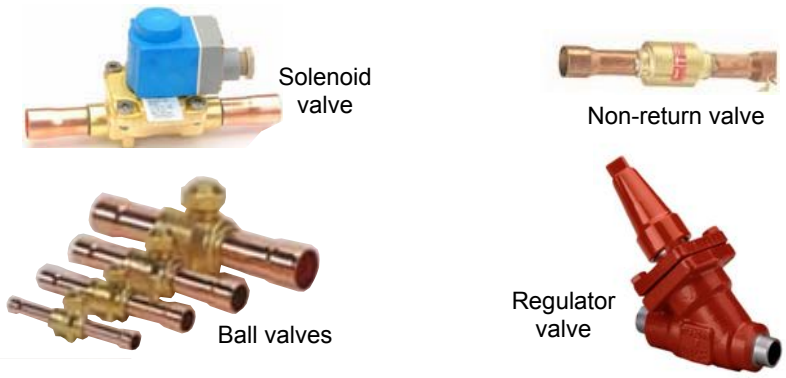

Figure 3.26 Refrigerant flow control valves
(Source: Danfoss, 2008b)

Ball valves were also installed on long lengths of pipe to isolate the system in case of leaks and to facilitate pump down. The ball valves were also used to vary the flow through components such as: IHX, pump and flow meters, by bypassing some of the flow round the components.

A regulator valve is used in the MT circuit to regulate liquid CO_2 flow to the MT flooded evaporator. The valve is manually operated. Non-return valves are used to prevent liquid from becoming trapped in pipe sections because when heated it can expand rapidly and can reach pipe rupture pressure. A non-return valve is also fitted

downstream of the MT evaporator to prevent liquid CO_2 from flowing back to the evaporator when the system stops.

3.3.8 Pressure relief valves

The system is protected from high pressures with 3 pressure relief valves. Two are fitted on the LT and MT circuits respectively and another one on the liquid receiver. The valves discharge is open to the atmosphere apart from the valves in the MT circuit which is vented to the liquid receiver because the protected line mainly contains liquid CO_2.

The minimum required discharge capacity of the pressure relief valves especially the one for the liquid receiver can be determined by following BS EN 13136 (2001) as follows:

$$Q_{md} = \frac{3600.\varphi.A_o}{H_{vap}} \tag{3.25}$$

Where Q_{md} = minimum required discharge capacity of the pressure relief valve (kg/h); φ = density of heat flow rate (kW/m^2); for the standard vessel used this is 10 kW/m^2; A_o = external surface area of the liquid receiver (m^2) and H_{vap} = heat of vaporization (kJ/kg) at the set pressure.

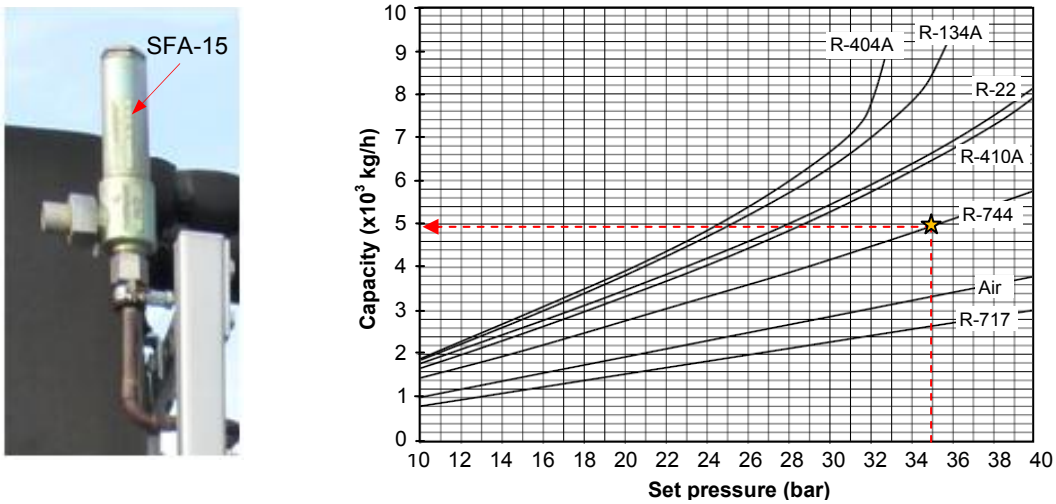

Figure 3.27 Pressure relief valve and its discharge capacity
(Danfoss: SFA-15 T335)

The pressure relief valve was set at a pressure 25% higher than the operating pressure of the system giving a burst pressure of 35 bar. At this set pressure, the minimum discharge capacity was determined to be 177 kg/h.

The characteristics of the pressure relief valve chosen for the application are shown in Figure 3.27. The valve has a factory setting of 35 bar. It can be seen that discharge capacity of the valve for CO_2 application at this pressure is nearly 5000 kg/h which is considerably higher than the 177 kg/h required.

3.3.9 Oil management system

The LT compressor inevitably loses some lubricating oil from the oil sump during normal operation as some mixes and circulates with the refrigerant through the system. In order to ensure that the majority of oil returns back to the compressor and to ensure that the compressor is always properly lubricated; the CO_2 refrigeration system is equipped with an oil management system.

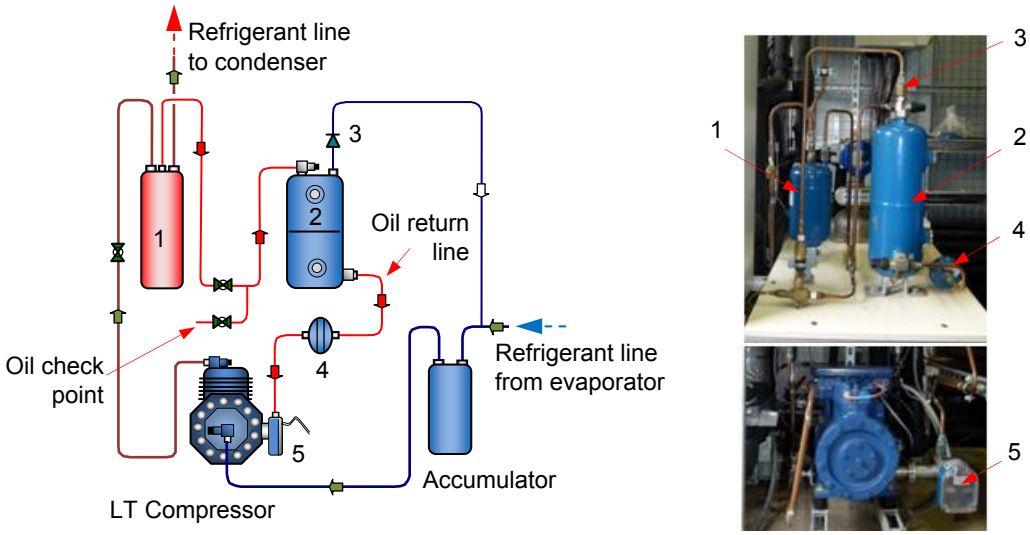

1 = Oil separator (OS-16-CD)
2 = Oil reservoir (OSA-3.8-CD)
3 = Pressure valve (RV-10B/1.5)
4 = Oil strainer (F-10L-CD)
5 = Oil level regulator (ERM2-0-BC-CD)
= Ball valve

Figure 3.28 Schematic diagram and selected components of the oil management system

Figure 3.28 shows a schematic diagram of the oil management system and pictures of the main components which include an oil separator, oil reservoir, oil strainer, oil level regulator and a pressure valve. These components were specified for subcritical CO_2

refrigeration applications with a maximum operating pressure (MOP) 40 bar except from the oil separator which was specified for a MOP of 45 bar (ESK Schultze, 2008).

The oil separator has a capacity of 2.3 L with a first oil charge 0.6 L. The oil separator removes some oil from the refrigerant and reduces the rate of oil circulation through the refrigeration system. It is equipped with a built-in float valve which opens when the oil level rises above the first charge level and the excess oil is drained back to the compressor trough the oil reservoir.

The oil reservoir has a total volume of 3.8 L. It receives the returned oil from the oil separator and also provides a reserve supply of oil for the compressor. It incorporates a pressure valve (RV-10B/1.5) which maintains the pressure in the reservoir 1.5 bar above the suction pressure. If the pressure rises above this value, the valve opens and vents any refrigerant trapped with the oil back to the suction line of the compressor. The oil reservoir also incorporates two sight glasses and two service valves. The sight glasses are used to ensure that there is enough oil in the reservoir, while the service valves are used for charging/draining the oil to/from the reservoir.

The oil supply to the compressor is regulated by the oil level regulator. The regulator comprises an oil level sensor and a solenoid valve. The solenoid valve allows the lubricating oil to flow to the compressor from the oil reservoir when the oil level reaches its lower limit and stops the oil supply when the oil level reaches the upper limit. The oil level regulator is also equipped with a relay which is integrated with the compressor controller. The relay switch stops the compressor when the oil level drops below the lower limit. The integration of the oil regulator relay with the compressor controller is described in Section 3.5. The oil regulator relay is also used to activate an alarm in the event the oil management system has failed to feed the lubrication oil into the compressor.

3.3.10 Auxiliary components

Several auxiliary components associated with the main mechanical components of the CO_2 refrigeration system have been described previously. Other auxiliary components are shown in Figure 3.29. These include an accumulator, sight glass, filter drier and pressure gauges.

The suction line accumulator is an ESK product (FA-12-CD) specified for use with CO_2 refrigerant. It has a 0.8 litre and a MOP of 40 bar. The accumulator protects the compressor from damage by preventing liquid droplets from entering the compressor.

The system is also equipped with two sight glasses. One was installed on the liquid line of the LT DX circuit to monitor the presence of flash gas upstream of the expansion valve. Another sight glass was fitted on the MT secondary circuit to monitor the refrigerant flow downstream of the MT flooded evaporator. Both sight glasses are Danfoss products (type SGN) which are compatible with the CO_2 refrigerant.

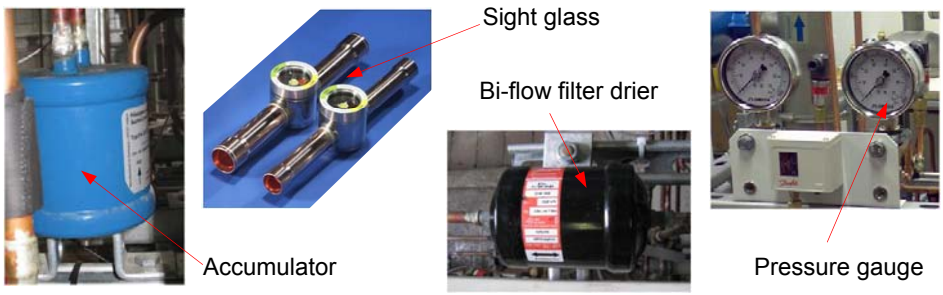

Figure 3.29 The auxiliary components

The filter driers used in the system are also Danfoss products (DCB bi-flow type). They contain a mixture of silica gel and molecular sieves and are suitable for CO_2 refrigerant applications. They were installed on the liquid line, one upstream of the expansion valve and another one upstream of the CO_2 pump (Figure 3.18). The main purpose was to limit any debris within the system from reaching the expansion valve and the CO_2 pump. Using bi-flow type filter driers enables the liquid CO_2 to flow in both directions which can reduce the possibility of liquid being trapped in the system during standstill conditions.

In order to monitor the pressure fluctuations during charging and operation, the test system was also equipped with three pressure gauges. One was installed on the liquid receiver and the other two upstream and downstream of the CO_2 pump. The gauges are Omega Engineering products (PG63-70S) compatible with CO_2 refrigerant. They have a measurement range from 0 to 70 bar. The gauges are very useful particularly when

charging the CO_2 system with refrigerant. The only way to immediately monitor the pressure of the system is from the pressure gauges.

3.4 Refrigeration load system

The test rig was originally designed for a full load refrigeration capacity of 8 kW provided by two refrigerated display cabinets: a medium temperature cabinet of full load capacity of 5 kW and a low temperature cabinet of full load capacity of 3 kW. Because the lowest LT compressor capacity commercially available at the time the system was designed was far bigger than the capacity of the LT cabinet as well as the application of a variable speed controller could not reduce the compressor capacity as low as the designed LT load; a low temperature additional load was added to the loading system to balance the capacity of the compressor.

The effect of the additional load on the pressure drop of the LT piping system has also been evaluated using the EES model. The pressure drops were still in the acceptable range with pressure losses in the suction and liquid lines equivalent to saturation temperatures 0.25 K and 0.04 K respectively.

3.4.1 Display cabinets

The refrigerated display cabinets used are a chilled open vertical multi-deck cabinet and a glass door frozen food cabinet. They were originally designed for R-404A refrigerant and were modified by replacing the evaporator coil and controls, to operate with CO_2 refrigerant. The evaporator coil of the low temperature cabinet is a direct expansion coil whereas the coil of the medium temperature cabinet is a flooded evaporator coil which was designed to operate with CO_2 as a secondary (volatile) refrigerant.

The chilled or MT cabinet is a Carter ELFM 2.54 m long cabinet with an open length 2.47 m. The height of the cabinet is 2.05 m and the depth 1.13 m. The cabinet has a total display area (TDA) of 4.2 m^2. The flooded evaporator coil and circulation fans are located below the base shelf. A schematic diagram of the MT cabinet is shown in Figure 30 (a). It can be seen that the cabinet has two evaporator coils as previously explained in Section 3.3.4.

Figure 3.30 (b) shows a schematic diagram of the glass door frozen food cabinet. It is a 2.4 m long display cabinet with glazing height of 1.9 m and display area of 2.7 m^2. The

three glass doors of the cabinet incorporate anti-sweat heaters to prevent condensation (sweating) on the glass surface.

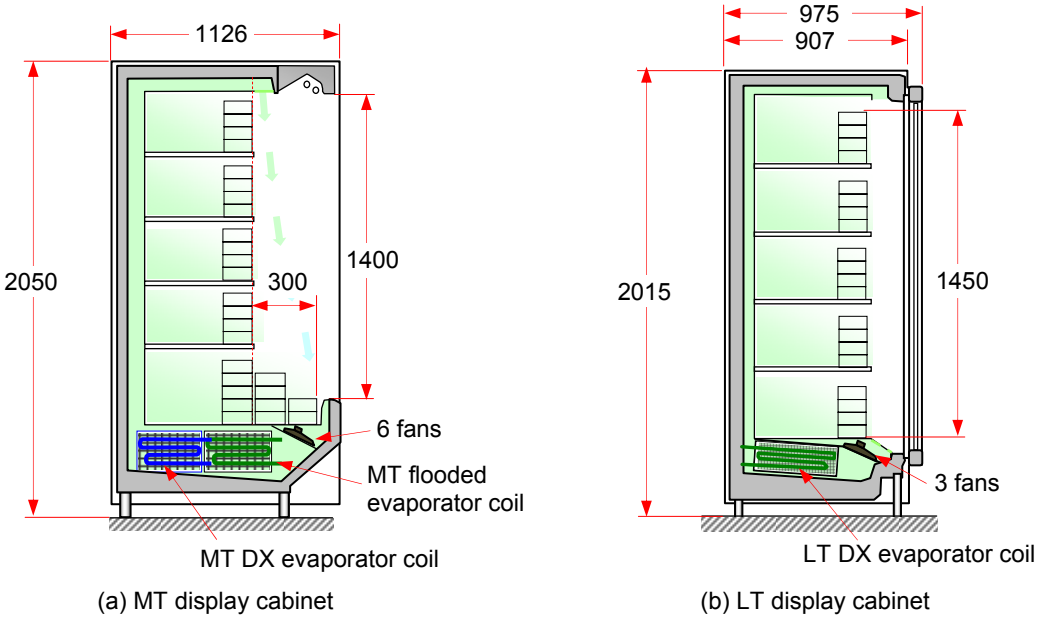

Figure 3.30 Refrigerated display cabinets

The cabinets were loaded with test packages stacked on the shelves. The test packages of the MT cabinet were 0.8 litre plastic containers filled with water. For the LT cabinet, one litre plastic containers filled with 50% propylene glycol in water solution were used. The solution has a freezing temperature of -33 ^{o}C. At the positions where product temperatures were measured, M-packages were used according to ISO 23953-2 (2005). Each M-package had a calibrated T-type thermocouple inserted into the geometric centre of the package.

3.4.2 Low temperature additional load

The additional load comprises an evaporator heat exchanger, water-glycol circuit and auxiliary components. The loading system is also used for additional load of the transcritical CO_2 system. A schematic diagram of the additional load, including the connections to the subcritical and transcritical CO_2 test systems, is shown in Figure 3.31.

The evaporator HX of the additional load system is a plate type heat exchanger (PHX) SWEP-B15Hx30/1P-SC-M of 8 kW refrigeration capacity at evaporating temperature -32 ^{o}C and 10 K superheat. The cold-stream of the heat exchanger functions as a CO_2

LT DX evaporator which absorbs heat from water-glycol solution at the hot-stream of the heat exchanger. The evaporator HX incorporates a “Danfoss” cabinet controller AK-CC 550A, electronic expansion valve (AKV10-4), pressure transducer (AKS-32) and temperature sensors type PTC-1000 (AKS-11). Operational settings of the evaporator including the refrigerant superheat can be set in the AK-CC 550A controller.

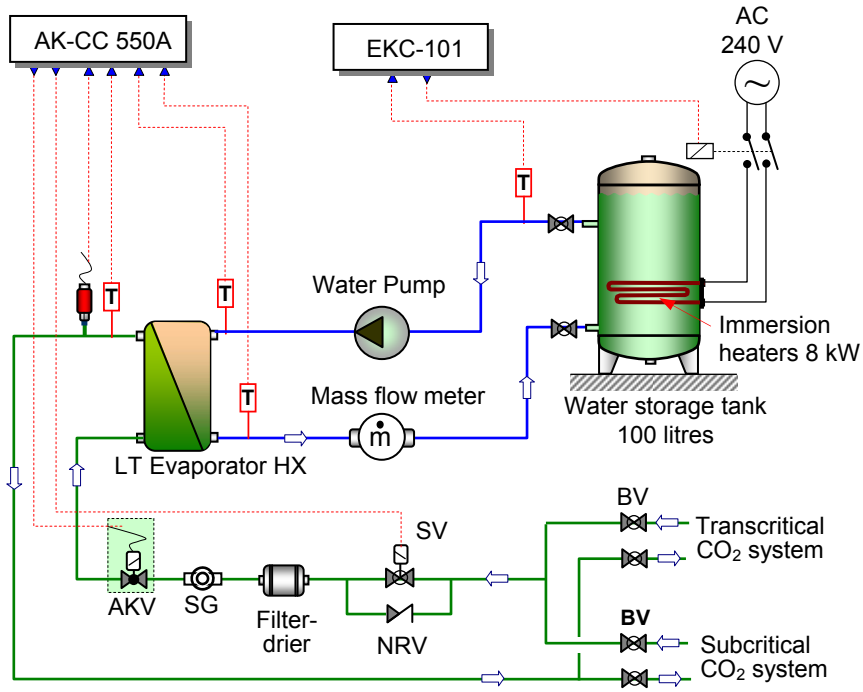

Figure 3.31 Schematic diagram of the LT additional load

The refrigerant circuit of the additional load also incorporates auxiliary components such as sight glass, filter-drier and flow control valves (SV, NRV and BV) as shown in Figure 3.31. The solenoid valve (SV) is used to regulate the flow to the evaporator HX. This valve automatically closes when the temperature set point has been achieved. The non-return valve (NRV), also known as check valve, is fitted in parallel with the solenoid valve to allow the liquid CO_2 to escape when the valve is closed. This protects the circuit from damage that may be caused by liquid CO_2 trapped in the pipe. The ball valves (BV) are utilised to enable the additional load to be used by both the subcritical and transcritical CO_2 test systems.

The water-glycol circuit consists of a circulation pump and a water storage tank. The circuit was filled with propylene glycol of 55% mass fraction in water solution.

The solution has a freezing temperature of -38 ^{o}C. The purpose of using this high concentration solution is to prevent ice blockage in the channels of the evaporator plate heat exchanger due to low evaporating temperature.

The circulation pump used in the water-glycol circuit is a Grundfos CH-2-30 specified for a flow capacity of 1.5 m^3/h; total head 30 m and minimum operating temperature -20 ^{o}C. Water storage is provided by a 100 litre copper tank insulated with polyurethane foam of 50 mm thickness. The storage incorporates two immersion heaters of heating capacity 4 kW each and a temperature controller Danfoss EKC 101. The temperature of the water-glycol mixture at the outlet of the storage tank is maintained relatively constant by regulating the power supply to the immersion heaters. In addition, the circuit also incorporates a flow meter to measure the flow rate of the water-glycol mixture. This flow rate was used to determine the refrigeration duty of the additional load system.

3.5 Control system

Figure 3.32 shows a schematic diagram of the control system which consists of electrical and electronic control systems. The electrical control system comprises an LT control circuit (C-1), MT control circuit (C-2) and standstill control circuit (C-3). The main function of the electrical control system is to connect and to disconnect power supply to the electrical components as well as the electronic control system. The LT control circuit (C-1) automatically regulates the operation of the LT compressor based on inputs from the LT cabinet controller, high and low pressure switches and oil level regulator. The MT control circuit (C-2) drives the CO_2 pump including the solenoid valve upstream of the MT evaporator. The control circuit receives input from the MT cabinet controller, discharge pressure switch and liquid level controller. The standstill control circuit (C-3) energises the standstill condensing unit based on the pressure of the liquid receiver during standby conditions. The following sections detail the electrical and electronic control systems including the control strategy applied to the test rig.

3.5.1 The electrical control system

Wiring diagrams of the electrical control system are given in Figures D-1 to D-5 (Appendix D) which detail the electrical installation of the main control circuit followed by LT, MT, standstill and additional load control circuits respectively.

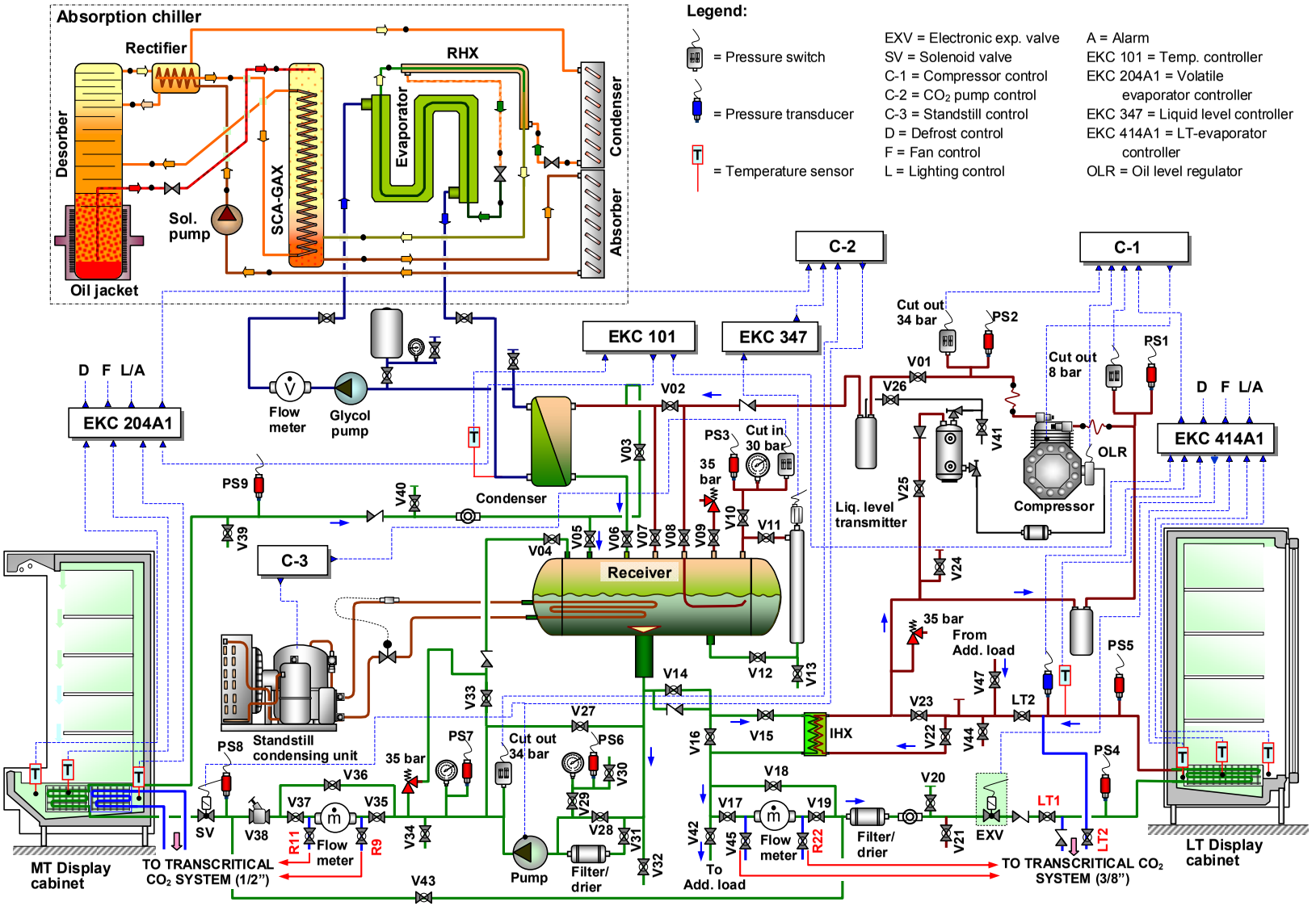

Figure 3.32 Schematic diagram of the electrical and electronic control systems

Figure D-1 (Appendix D) shows the wiring diagram of the power supply to the compressor, CO_2 pump, LT, MT and standstill control circuits. Each circuit is protected against overload or short circuit conditions using a circuit breaker. The whole circuit is isolated by a main switch and an emergency switch. The electrical system also incorporates a residual current device (RCD) which is an electrical wiring device that disconnects the main power supply to the whole system whenever it detects current leakage through the human body that is grounded and accidentally touching the energised part of the circuits.

The LT and MT control circuits are detailed in Figures D-2 and D-3 (Appendix D). It can be seen that the operation of the LT compressor and the CO_2 pump are regulated through using contactor relays. The relay of the LT compressor is circuited in series with the control switches of the LT cabinet controller; high and low pressure switches and oil regulator (Figure D-2). The CO_2 pump relay (Figure D-3) is energised by the contact switches of the MT cabinet controller, discharge pressure switch and liquid level regulator. Both contactor relays can also be manually overridden by on/off switches. The figures also show that the controls of the LT and MT cabinets have been modified to incorporate the installation of a selector switch in each display cabinet to switch over the connection of the cabinet controller either to the subcritical or transcritical CO_2 systems. The modified control also incorporates three switches to override the automatic on/off inputs from the cabinet controller to the fans, lights and defrost heater respectively.

3.5.2 The electronic control system

The system employed is a commercially available electronic control system manufactured by Danfoss. Figure 3.33 shows the electronic controllers used which consist of an LT cabinet controller (EKC-414A1), MT cabinet controller (EKC-204A1), water-glycol temperature controller (EKC-101) and liquid level controller (EKC-347). The system also uses an AK-CC 550 controller to control the additional load evaporator as explained in Section 3.4.2.

The cabinet controller EKC-414A1 automatically regulates the operation of the LT cabinet based on parameter settings and input signals from the sensors. The operational parameter settings, which can be set by using a panel mounted display EKA-162,

include temperature set point, temperature range, degree of superheat and defrost parameters (type, frequency, duration and temperature termination). The controller receives input signals from a suction line pressure transducer and temperature sensor fitted on the outlet of the evaporator. The controller also detects temperatures of the air in the LT cabinet from PTC-1000 type temperature sensors which were placed on the air-on, air-off and on the free surface of LT evaporator coil. The controller modulates the opening of the expansion valve to provide the specified degree of superheat at the outlet of the LT evaporator. To ensure the controller can provide an accurate modulation to the expansion valve, the refrigerant used in the system (R-744) and the pressure range of the pressure transducer must be specified correctly in the controller. The controller also provides an on/off signal to the LT control circuit to control the operation of the LT compressor. A wiring diagram showing the controller, location of the sensors and their connections is shown in Figure D-6 (Appendix D).

Figure 3.33 Control components
(Source: Danfoss, 2008b)

The MT cabinet controller (EKC-204A1) is simpler compared to the DX evaporator controllers. The controller provides on/off signal to the fans, lights and defrost heater of the cabinet without controlling the degree of superheat of the refrigerant. Thus, it requires only input signals from temperature sensors which include air on, air off and MT evaporator coil surface. Together with the liquid level controller (EKC-347), the EKC-204A1 regulates the operation of the CO_2 pump and the solenoid valve upstream of the MT evaporator coil.

The electrical power of both LT and MT controllers (EKC-414A1 and EKC-204A1) is supplied from the electrical control system through selector switches. These switches

can be used to drive the controllers either manually or automatically. For the automatic control operation, the switches were fitted in series with contact switches of a temperature controller EKC-101. This temperature controller is used to prevent the CO_2 system from operating when the temperature of the water-glycol, which cools the CO_2 condenser, is still high, above -3 ^{o}C. This setting can, however, be varied to allow CO_2 system performance investigations at different condensing temperatures.

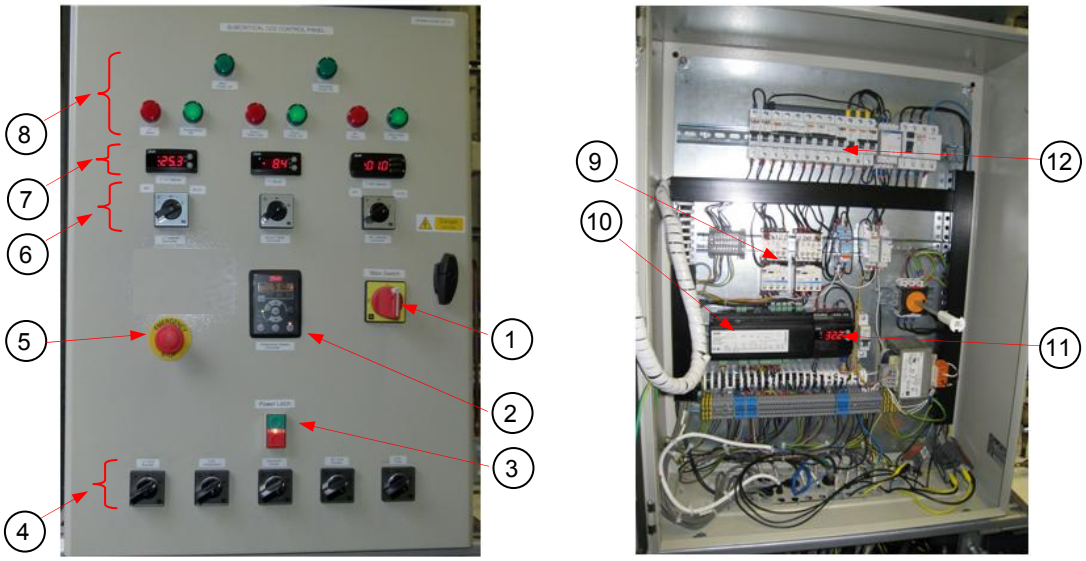

(a) (b)

Legend:

1 = main switch
2 = compressor speed controller
3 = power latch
4 = switches for: LT control system, compressor, standstill condensing unit, MT control system and CO_2 pump
5 = emergency switch
6 = switches for EKC-414A1, EKC-204A1, EKC-101
7 = controllers' display
8 = power supply indicators
9 = contactor relays
10 = LT cabinet controller EKC-414A1
11 = liquid level controller EKC-347
12 = circuit breakers and RCD

Figure 3.34 Electrical control panel

The electrical and electronic control systems were installed in an electrical control panel on the compressor-pump section of the test rig. A front view of the control panel showing controller displays, switches and indicator lights is shown in Figure 3.34 (a) and the arrangement of the components inside the panel can be seen in Figure 3.34 (b).

3.5.3 Control strategy

Figure 3.35 shows the control strategy applied to the test rig. The flow temperature delivery from the trigeneration system is maintained relatively constant by using the

temperature controller (thermostat) of the absorption system. In normal operation, the delivery water-glycol temperature was set at -10 ^{o}C with 0.5 K temperature differential.

The MT system control strategy involves the control actions of the pump control circuit, EKC-347 and EKC-204A1. The EKC-347 modulates the pump control circuit to allow the pump to operate when the liquid level in the liquid receiver above 35% of full liquid height. The EKC-204A1 also provides signal to the pump control circuit to regulate the pump operation based on air temperatures in the MT cabinet which were set at -3 ^{o}C weighting 100% air-off temperature with 2 K differential. The pump control circuit switches the pump off when the air-off temperature reaches -3 ^{o}C and allows it to operate again when the air-off temperature rises to -1 ^{o}C. The MT system incorporates a solenoid valve upstream of the MT evaporator. The pump will operate after the solenoid valve to be energised with a time delay of 1 minute and the pump will turn off 1 minute before the valve is deenergised.

Figure 3.35 also shows the control strategy for the LT system which comprises compressor and LT load control. The compressor control strategy is based on the suction pressure of the LT compressor. The main parameters that affect the suction pressure are the LT refrigeration load and the compressor flow capacity. At full load conditions, the flow capacity of the compressor can maintain the target pressure at 12.2 bar. At part load conditions, however, the flow capacity of the compressor must be modulated by varying its speed using a frequency inverter.

The LT load control strategy involves the control of the LT cabinet and LT evaporator for additional load involving controller EKC-414A1 and AK-CC 550 respectively. The controllers modulate the opening of the respective expansion valves to maintain a degree of superheat in the range 5 K to 12 K. At full load conditions, the valve opening was set at 80% of maximum represented by the pulsing frequency of the valve solenoid.

The EKC-414A1 also provides input signal to the compressor control circuit to regulate the speed of the compressor. The control regulation is based on average air on and air off temperature of the evaporator of -23 ^{o}C and a differential of 4 K. The AK-CC 550 controls the solenoid valve upstream of the additional load evaporator. The valve is closed when the temperature of the water-glycol exiting the evaporator drops below -27 ^{o}C.

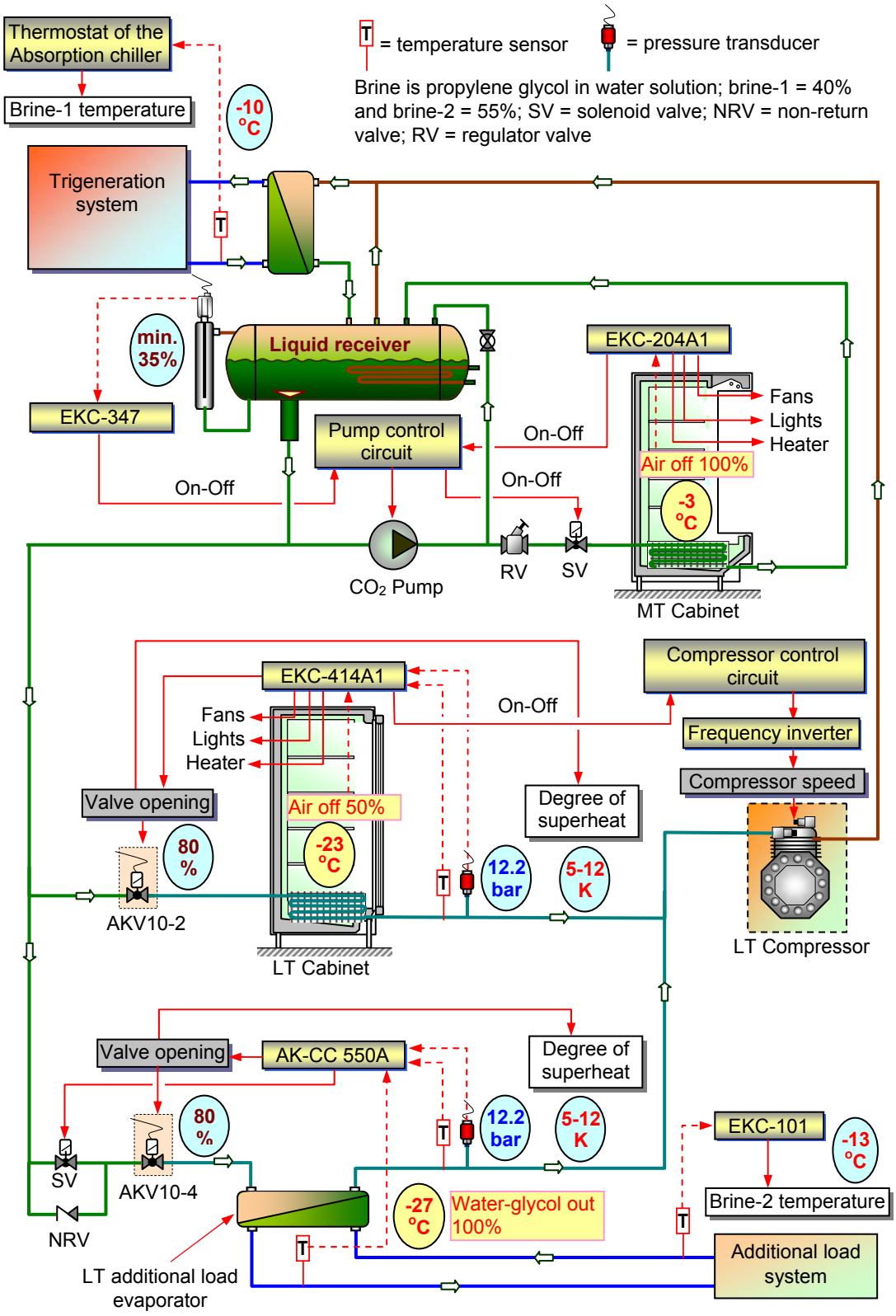

Figure 3.35 Operational control strategy

3.6 Instrumentation and data logging system

The instrumentation is used for both control and performance monitoring. For control, the instrumentation is mainly used to provide signal inputs to the controllers. For monitoring, the instrumentation is used to establish the state and flow conditions of the CO_2 refrigerant such as pressure, temperature and flow rate at different points in the system. The instrumentation is also used to monitor the liquid level in the liquid receiver, temperature and relative humidity of the loading system and test chamber as well as power consumption of the test rig. To enable the information to be read and recorded for system analyses and evaluation, the instrumentation is connected to a data logging system.

3.6.1 Instrumentation devices

The instrumentation devices used on the test rig are temperature and pressure measurements, liquid level transducer, relative humidity sensor, flow meter, and power meter. A velocity meter was also used to measure air velocity in the test chamber and MT display cabinet. The following sections provide a brief description of each device.

3.6.1.1 Temperature and pressure measurements

T-type thermocouples were used for most of the temperature measurements. The thermistors (thermally sensitive resistor) type PTC-1000 were used for the sensors of the control system and RTDs (resistance temperature detector) for the air temperature sensor of the test chamber. T-type thermocouples have a temperature measurement range -250 ^{o}C to 350 °C with specific error (specified by manufacturer) of ± 0.5 ^{o}C. The thermocouples were calibrated using a calibration bath and precision thermometer (ASL type F250 MK II, probe J 100-250-10-NA) of uncertainty ± 0.04 ^{o}C. The temperature range of calibration was -30 ^{o}C to 100 ^{o}C. It was found that all thermocouples had calibration error within the specifications.

Positions of the temperature measurements on the test rig are indicated in Figure E-1 (Appendix E). The number and explanation of each measurement point are listed in Table E-1 and the calibration equations of the thermocouples including their calibration errors are given in Table E-2 (Appendix E).

Ten pressure transducers (Danfoss products) were installed on the test rig. One type AKS 32 with output voltage 0-10 V d.c. is used for the control system. The others are used to measure the pressures in the suction and discharge lines of the compressor and CO_2 pump, upstream and downstream of the LT and MT cabinets as well as the pressure in the liquid receiver. Measurement points of the pressure transducers are shown in Figure E-1 (Appendix E).

The pressure transducers of the monitoring system have different measurement ranges with input voltage of 24 V d.c. and output current 4 mA to 20 mA. The output cables of the transducer have to be circuited with a resistor to change the output current to become an output voltage since the data logging system requires a voltage input. The pressure range of the transducers and the resistors used are given in Table E-3 (Appendix E). Each pressure transducer of the monitoring system was calibrated using a deadweight pressure gauge calibrator. The voltage outputs were recorded for a series of known pressures. The graphs of the voltage against the pressure were drawn and the best-fit linear equations were derived and used in the data logging system to enable an automatic recording of the measured pressures. The coefficient of correlations of the pressure transducers were above 99.9% with manufacturer uncertainty of ± 0.3%. The graphs and calibration equations of the transducers are given in Figure E-3 (Appendix E).

3.6.1.2 Liquid level transducer

The transducer used is AKS 41U-15.3 which is a Danfoss control component. It has an insertion rod length of 389 mm and was calibrated for water (R-718) with 4 to 20 mA output across the whole measuring range. Before installation, the transducer was recalibrated using water to set the minimum and maximum levels which provided a measurement range as high as the internal diameter of the liquid receiver (310 mm). The setting was then adjusted for CO_2 (R-744). Figure 3.36 shows the transducer and its electrical connection to the liquid level controller EKC 347. The level of the liquid CO_2 in the receiver can be read on the display of the controller as a percentage of the total measurement range. The reading can also be recorded and displayed on the screen of the data logging system.

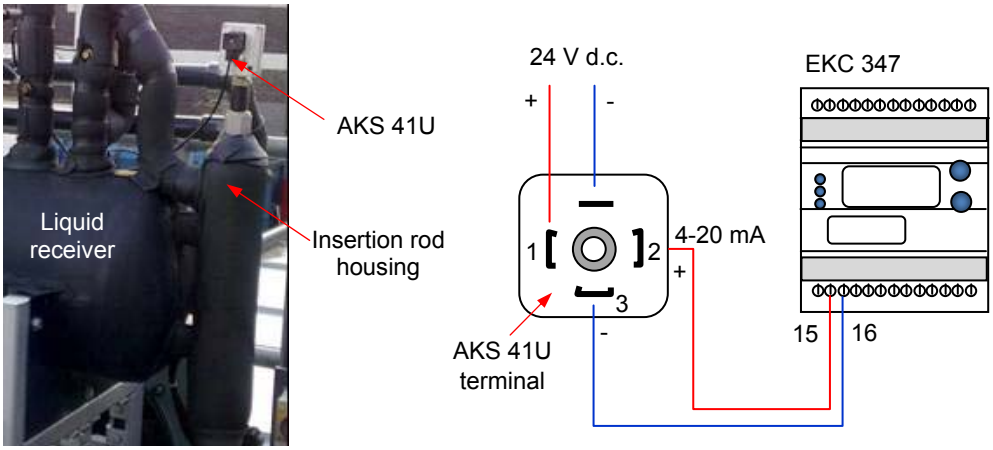

Figure 3.36 Liquid level transducer and the electrical connections to controller (EKC 347)

3.6.1.3 Relative humidity measurements

The relative humidity within the environmental test chamber was monitored by using a 'Rotronic' humidity and temperature probe. The probe incorporates a humidity sensor (Hygrometer IN-1) and an RTD temperature sensor PT100 which have measurement range 0% to 100% and -40 ^{o}C to 60 ^{o}C for relative humidity and temperature respectively. The output voltage range is 0 to 1 V d.c. The relative humidity sensor has a measurement uncertainty of ± 1.5% and ± 0.5 ^{o}C for the temperature sensor. Similar probes were also installed in the LT and MT display cabinets to measure the relative humidity of air before and after the evaporator coils.

3.6.1.4 Flow meter

The refrigeration capacity of the MT and LT display cabinets is determined by calculating the amount of heat absorbed by the evaporator coils. The calculations involve the enthalpies of the refrigerant before and after the evaporators and mass flowrate of the refrigerant circulating through the evaporator coils. For the LT additional load where the load is provided by a water-glycol solution, the refrigeration capacity is determined by calculating the heat absorbed by the refrigerant from the water-glycol mixture assuming the heat transfer in the evaporator is an adiabatic process. This calculation requires mass flow rate, specific heat and temperature drop of the water-glycol mixture before and after the evaporator.

To ensure that the mass flow rates are measured with reasonable accuracy, a coriolis type flow meter was chosen for the CO_2 refrigerant and an electromagnetic flow meter was used for the water-glycol mixture. Figure 3.37 shows the flow meters employed in the test rig. For the LT display cabinet which requires a CO_2 mass flow rate of about 0.011 kg/s, the Optimass-3050C-S03 (Figure 3.37a) is used which has a flow rate capacity up to 0.028 kg/s. The Optimass-MFM-4065 (Figure 3.37b) with a measurement range up to 0.342 kg/s is used for the MT display cabinet. Both flow meters were manufactured by Krohne-Germany and have a measurement uncertainty of ± 0.035%. The flow meters, however, are also subject to inaccuracies arising from the presence of gas bubbles in the liquid line. To minimise the risk of this occurring, the liquid line was insulated with 25 mm of insulation (Armaflex class 0) and a liquid suction HX was installed in the LT system.

(a) Coriolis flow meter, Optimass-3050C-S03

(b) Coriolis flow meter, Optimass-MFM-4065

(c) Electromagnetic flow meter Aquaflux 2010-IFC 010D

Figure 3.37 Flow meter of the LT, MT and additional load systems

The Aquaflux-2010-IFC-010D meter shown in Figure 3.37c, also from Krohne, is used to measure the volume flow rate of the water-glycol mixture. The volume flow rate was converted to mass flow rate by multiplying it with the density of the water-glycol mixture determined using the bulk mean temperature of the mixture in the evaporator. The flow meter has a capacity range 0.5 to 21 m^3/h and uncertainty ± 0.3%.

Each flow meter provides a current output 4-20 mA which is converted into a voltage input in the data logging system. In order to convert the voltage to a flow rate, a

calibration was carried out in the laboratory. Best-fit linear equations from the calibration were used in the logging programme to enable automatic recording of flow rate.

3.6.1.5 Power meter

The power consumption of the CO_2 test rig includes the power of the LT compressor, CO_2 pump, and the control system. In order to measure these, a power meter was installed in the electrical control panel. The power consumption of the control system was determined when both compressor and pump were in off-cycles and the power consumption of the compressor and pump were determined when only one of them was in operation. The power meter used is a Voltech PM-300, shown in Figure 3.38. It is a three phase power analyser which has measurement uncertainty for voltage and current of ± 0.02% and ± 0.03% respectively. The power meter has an LCD screen to display the measured voltage, current, power factor, and instant power. The measured parameters were also logged into the computer via RS232 port.

Figure 3.38 Power meter, Voltech PM-300

3.6.1.6 Velocity meter

The velocity meter was used to map the velocity profile of the air flow in the environmental test chamber to ensure that the air velocity was within the ISO 23953-2 standard. The meter was also used to measure the air velocity at the back tunnel of the MT cabinet which is required for determination of the mass flow rate of the air flow across the MT evaporator coil. The air mass flow rate was used to verify the refrigeration capacity of the MT flooded evaporator coil when the circulation ratio of the MT circuit was equal to 1. The velocity meter is Velocicalc Plus 8386A-M-GB, a TSI product, with measurement range 0 m/s to 50 m/s and uncertainty ± 3%. The meter can also simultaneously measure the temperature and relative humidity of the air with measurement range -10 ^{o}C to 60 ^{o}C and 0% to 90% RH respectively.

3.6.2 Data logging system

The output signals from the instrumentation devices are logged by a data logging system which comprises data acquisition modules and a recording and display system. The data acquisition modules utilise the Datascan 7000 series from MSL (Measurement System Ltd.) which include a Datascan measurement processor 7320 and expansion modules 7020. Each Datascan module contains 16 differential input channels, individually configurable for voltage and thermocouple measurements. To cover all the instrumentation devices used, 1 processor and 11 expansion modules were prepared as shown in Figure 3.39a. The configuration of each module and the channels are detailed in Table E-1 (Appendix E).

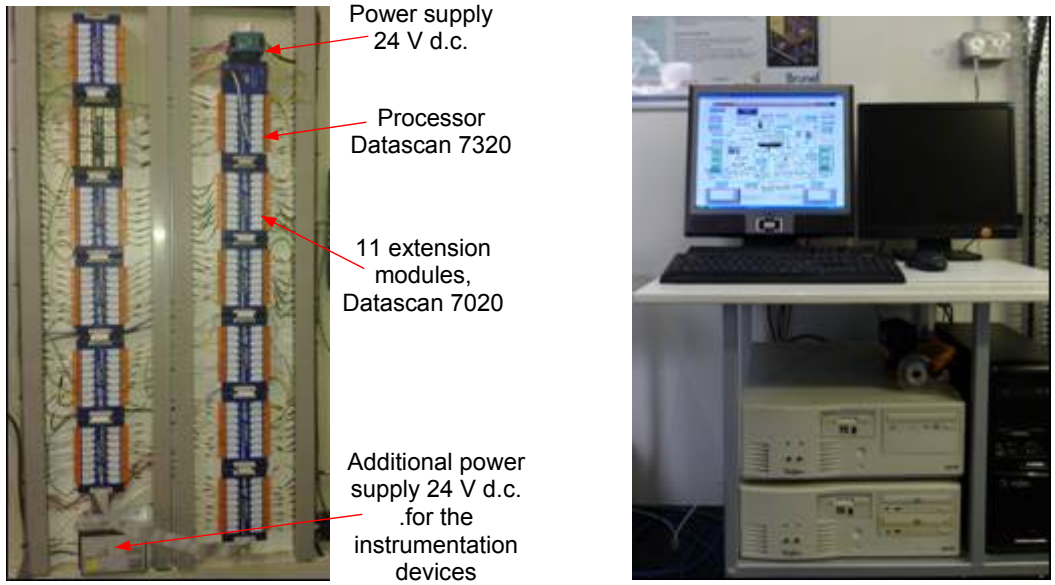

(a) Datascan processor and expansion modules

(b) Computer sets

Figure 3.39 Data logging system

The recording and display system is a standard desk top computer. Communication between the Datascan modules and the computer is performed through an RS232 cable. The computer incorporates Labtech software which is fully compatible with the Datascan modules and allows a mix of more than 250 analogue and digital channels. The software also has a capability to manipulate a complex measurement system to be an attractive display so that it can be easier to monitor. The power consumption of the test rig was recorded and monitored separately using a second computer set. Both

computer sets are shown in Figure 3.39b. A monitoring display set up in the Labtech software is given in Figure E-2 (Appendix E).

3.7 Refrigerant charge

The test rig is equipped with two charging connections, one is in the suction line of the LT compressor and the other is downstream of the MT evaporator just before the connection to the liquid receiver. This enables the system to be charged in gas or liquid phase. Figure 3.40 shows one of the charging connections and valve. The charging valve is used to isolate the system when the charging process has been completed.

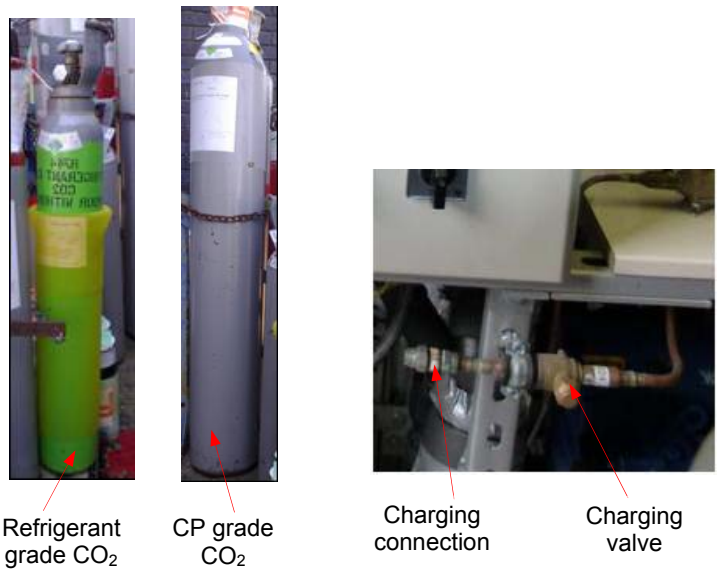

Figure 3.40 CO_2 and charging connection

Before charging, the system was pressure-tested and then evacuated. The system was charged during standstill conditions directly to the liquid receiver. Two methods of charging were used. Firstly, charging in gas when the system was in vacuum conditions until the pressure reached 7 bar (slightly above the triple point of CO_2). This prevents the formation of dry ice which can block the charging line when charging in liquid. The outlet valves of the liquid receiver were open to allow the whole CO_2 system to be pressurised. Secondly, charging in liquid. All outlet valves of the liquid receiver were closed. The standstill condensing unit was set in automatic operation. The condensing unit operates when the pressure in the liquid receiver increases to 30 bar. The level of liquid CO_2 in the liquid receiver can be monitored from the display of the EKC-347.

The amount of refrigerant charge is 37 kg which fills 50% of the receiver volume with liquid CO_2. This gives a specific refrigerant charge of 2.3 kg/kW which is in the range of the charge of a centralised supermarket CO_2 system as reported in MTP (2008).

The CO_2 used in the system is of refrigerant grade. The cylinder of the refrigerant grade CO_2 is shown in Figure 3.40. Alternatively, a CP (Chemically Pure) grade CO_2 with 100% purity can also be used (Figure 3.40). Both have the same characteristics. The price of the CP grade CO_2, however, is 16% lower than the refrigerant grade CO_2.

3.8 Environmental test chamber

The display cabinets of the refrigeration load system were placed in an environmental test chamber which is a self contained unit located near the CO_2 plant room. Figure 3.41 shows a picture of the test chamber and the site where the test chamber is located. It can be seen that the test chamber is situated outside and the fluctuation of ambient conditions can directly affect its thermal load. In order to control the air temperature and relative humidity as well as the air velocity, the chamber incorporates an air handling unit (AHU) which was installed above its roof and supported by a purpose built steel structure. Figure 3.41 also shows other facilities surrounding the test chamber which include CO_2 plant room and CHP chamber.

Figure 3.41 CO_2 test chamber and associated test facilities

The layout and detailed dimensions of the test chamber are given in Figure F-1 (Appendix F). The external walls of the test chamber, also known as non-technical walls, are constructed from steel frames and covered with painted metal skins. The gap between the metal skins was filled with a rock-wool layer which provided a total wall thickness of 80 mm and a U-value (thermal transmittance) of 0.5 W/m^{2}K. The roof and the suspended floor have a similar structure of 125 mm thickness with a U-value of 0.4 W/m^{2}K. The chamber also has a single glazed window of U-value 5.7 W/m^{2}K and a swing door, 0.9 m wide and 2.5 m high. In order to provide access to bring the cabinets into the chamber, an extension door with screw joints was constructed adjacent to the swing door giving a total opening of 2.5 m wide and 2.5 m high.

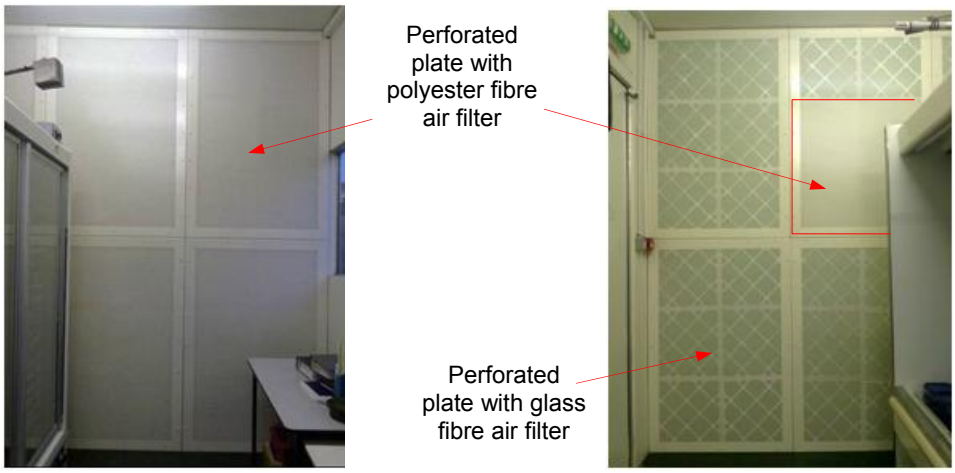

Figure 3.42 Technical walls of the CO_2 test chamber

Both ends of the chamber where the supply and return AHU ducts terminated were partitioned off with technical walls to form supply and return air plenums. This provides a maximum useful test area of 6.14 m long, 3.1 wide and 3.05 m high. The technical walls of the supply and return air plenums were constructed from perforated plate supported by a wooden frame. The walls are also covered with air filters to provide a pressure drop and uniform air velocity across the technical walls as well as within the test area. A polyester fibre air filter giving a pressure drop between 135 Pa and 250 Pa and a glass fibre panel air filter of 10 to 125 Pa pressure drop were used to cover the supply air and return air perforated plates respectively. Figure 3.42 shows the construction of the technical walls viewed from the test area.

3.8.1.1 Positioning the display cabinets in the test chamber

Figure 3.43 shows the positions of the MT and LT cabinets inside the chamber. It can be seen that the MT cabinet is placed near to the return air technical wall and the LT cabinet 0.5 m away from the supply air technical wall. The location of the cabinets in the chamber is given in Figure F-2 (Appendix F).

(a) The MT cabinet and the return air technical wall

(b) The LT cabinet and the supply air technical wall

Figure 3.43 Position of the MT and LT cabinets in the test chamber

3.8.1.2 Air handling unit

Figure 3.44 shows a schematic diagram of the air handling unit (AHU). The AHU is a weatherproof model CAIRplus-128-096AVBV from GEA-Denco Ltd. specified for outdoor installation with a design duty of 1.9 m^3/s and 400 Pa pressure drop. It comprises a mixing section, air filter, cooling coil, electric heater battery, heating coil, humidifier section and a centrifugal fan. The unit is connected to the return air and supply air plenums by return and supply air ducts respectively.

The mixing section of the AHU constitutes a return air damper and a fresh air damper to facilitate control and regulations of the return and fresh air to the unit. The filter section contains cardboard-framed synthetic panel and plastic-framed synthetic bag filters. The section is also completed with two gauge manometers to measure the pressure difference before and after the filters. Start pressure drops of the panel and bag filters

are 58 Pa and 98 Pa respectively and the filters must be replaced when the pressure drop reaches 200 Pa for the panel filter and 300 Pa for the bag filter.

The cooling coil is a DX evaporator coil manufactured from copper tubes and aluminium fins of 3.5 mm fin spacing. The evaporator coil has three circuits and two rows arrangement with refrigerant volume of 6 litres. The cooling capacity of the coil is 32.3 kW specified for R-410A at evaporation temperature 6 ^{o}C. Air pressure drop of the coil is 24 Pa at surface air velocity 1.92 m/s.

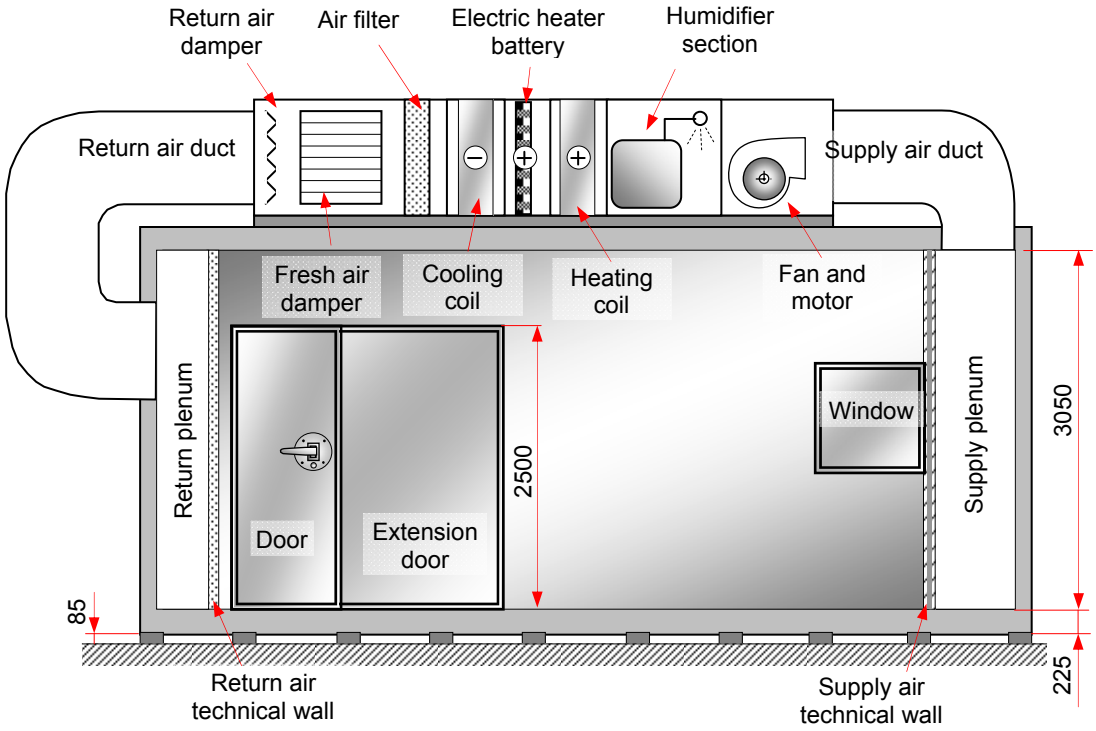

Figure 3.44 Schematic diagram of the air handling unit and font view of the test chamber

The AHU incorporates an electric heater battery of rated power 20 kW. The heater battery has a multi-stage switching capability and a safety temperature limiter to limit the maximum surface temperature to 100 ^{o}C. The air pressure drop of the heater battery is 11 Pa specified at air velocity of 1.57 m/s. The unit also incorporates a low pressure hot water (LPHW) heat exchanger to enable the unit to utilise hot water for heating instead of electric heaters. The heat exchanger (HX) is a fin tube type made from copper tubes and aluminium fins of 2.5 mm fin spacing. The HX coil has two circuits and total

water volume of 4 litres. The coil is specified for 55 kW heating duty and pressure drop at air side of 11 Pa.

The AHU is also completed with a self contained electric steam humidifier to provide humidification when the relative humidity of the air in the chamber is below the set point. The humidifier can produce 15 kg of steam per hour. However the steam production varies based on the humidification demand. The humidifier was manufactured by GEA-Denco Ltd.

In order to circulate the specified air volume through the test area, the unit utilises a centrifugal fan. The fan has backward-curved blade impellers and has been statically and dynamically balanced by the manufacturer. The fan is 'Comefri' THLZ 400 FF with maximum air flow rate capacity of 4.2 m^3/s at total pressure 818 Pa and fan speed 2560 rpm. The flow capacity, however, can be modulated using the frequency inverter of the drive motor.

The AHU was designed to be able to regulate and maintain the ambient conditions in the test chamber from 0 ^oC to 40 °C and 40% to 80% RH for both winter and summer weather conditions. Allowable temperature and RH deviations are within ± 1 ^oC and ± 3% respectively. A display of the AHU design is given in Figure F-3 (Appendix F).

3.8.1.3 Condensing unit

The condensing unit is connected to the cooling coil of the air handling unit by an expansion valve kit to form a complete DX refrigeration system. The condensing unit is 'Daikin' ERQ250AW1 which is an inverter driven condensing unit. It has two hermetic scroll compressors; one compressor is an inverter driven model of maximum speed 6300 rpm and the other is an on-off type compressor with a fixed speed of 2900 rpm. The condensing unit has a nominal cooling capacity of 28 kW and an operating range from -5 ^oC to 43 ^oC. The unit uses refrigerant R-410A and has a refrigerant charge of 8.4 kg.

The condensing unit also incorporates a communication box and interface card to enable the unit to be controlled from a fully integrated 'Trend IQ3' control system. The control system automatically regulates the operation of the condensing unit either for cooling or

dehumidification based on the cooling and dehumidification demand from the test chamber. Capacity control is achieved by modulating the signal input (ranging from 0 to 10 V d.c.) to the communication box. When the cooling demand or dehumidification demand is 100% (signal input 10 V d.c.), the unit operates at full capacity and both compressors run at full speed. The unit is on a standby mode when the signal input indicates no demand (0 V d.c.).

3.8.1.4 Test chamber control system

The air conditioning control system of the test chamber employs a 'Trend' IQ3 controller which is a building management system (BMS) controller that uses Ethernet and networking technologies which enable a system to be monitored and adjusted from any internet access point in the world. For this test chamber application, the controller is used for local control purposes which incorporate a display panel (IQView4), input and output modules, heater controller (thyristor control module), on-off input components and sensors.

Figure 3.45 shows a schematic diagram of the control system. It can be seen that the control receives signal inputs directly from the sensors and indirectly from the input components through the input modules. These signal inputs are compared to the desired control parameters (set points) and then the controller provides signal outputs which are used to modulate the controlled devices which include heater battery, inverter and fan, humidifier and the condensing unit.

Three main parameters are controlled and maintained in a specified range and specified point of measurement. The parameters are temperature, relative humidity and velocity of the air in the test chamber. The air temperature and relative humidity are dependent on the climate class tests but the air velocity is independent and should be maintained in the range between 0.1 m/s to 0.2 m/s (ISO 23953-2, 2005). In order to control these parameters, the controller uses a proportional control algorithm (mode). The controller decreases the average signal outputs to the controlled devices as the controlled parameters approach the set points. These affect a slowing down of the modulations so that the controlled parameter does not overshoot or undershoot the set point. The proportional action occurs within a "proportional band" around the set point. Outside

the proportional band, the controller functions as an on-off controller. The set points and proportional bands can be set on the display panel (IQView4).

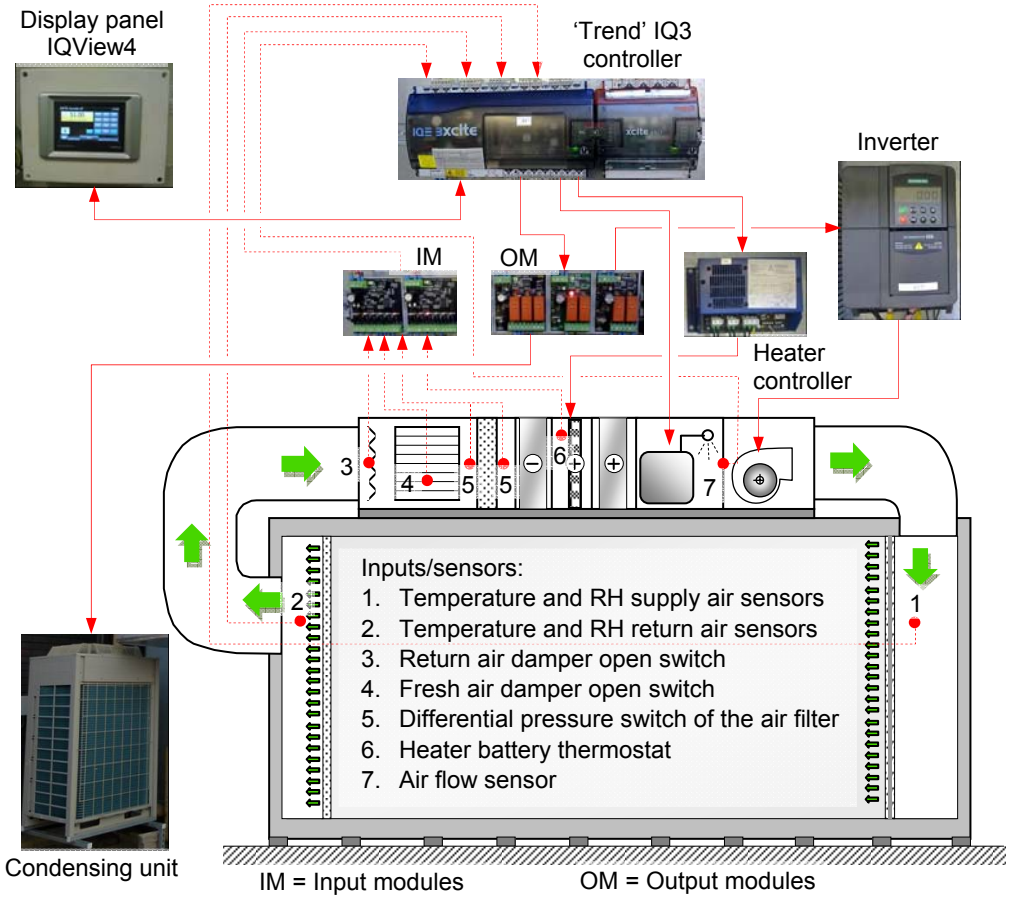

Figure 3.45 Schematic diagram of the test chamber control system

To control the air temperature of the chamber, the controller regulates either the heater battery or the condensing unit. The controller compares the set point with the measured temperature and modulates the heater battery when the temperature is below the set point or the condensing unit when cooling is required. The relative humidity (RH) is controlled by modulating the humidifier when the RH is below the set point and the condensing unit when the RH value is above the set point to affect dehumidification. The velocity of the air in the chamber can be varied by regulating the speed of the fan through modulation of the frequency inverter.

3.8.1.5 Test chamber commissioning

After the construction of the air conditioning system, a series of tests were carried out to evaluate the test chamber performance and its compliance to the conditions and tolerances recommended in ISO 23953-2 (2005) standard. Three parameter sets were evaluated. One is the uniformity of the air velocity. Figure F-4 (Appendix F) shows the variation of air velocities inside the chamber. It can be seen that the air velocity is relatively uniform. A 3D measurement through the test area indicated 29 points out of 30 measurement points to be within the standard range of between 0.1 m/s and 0.2 m/s.

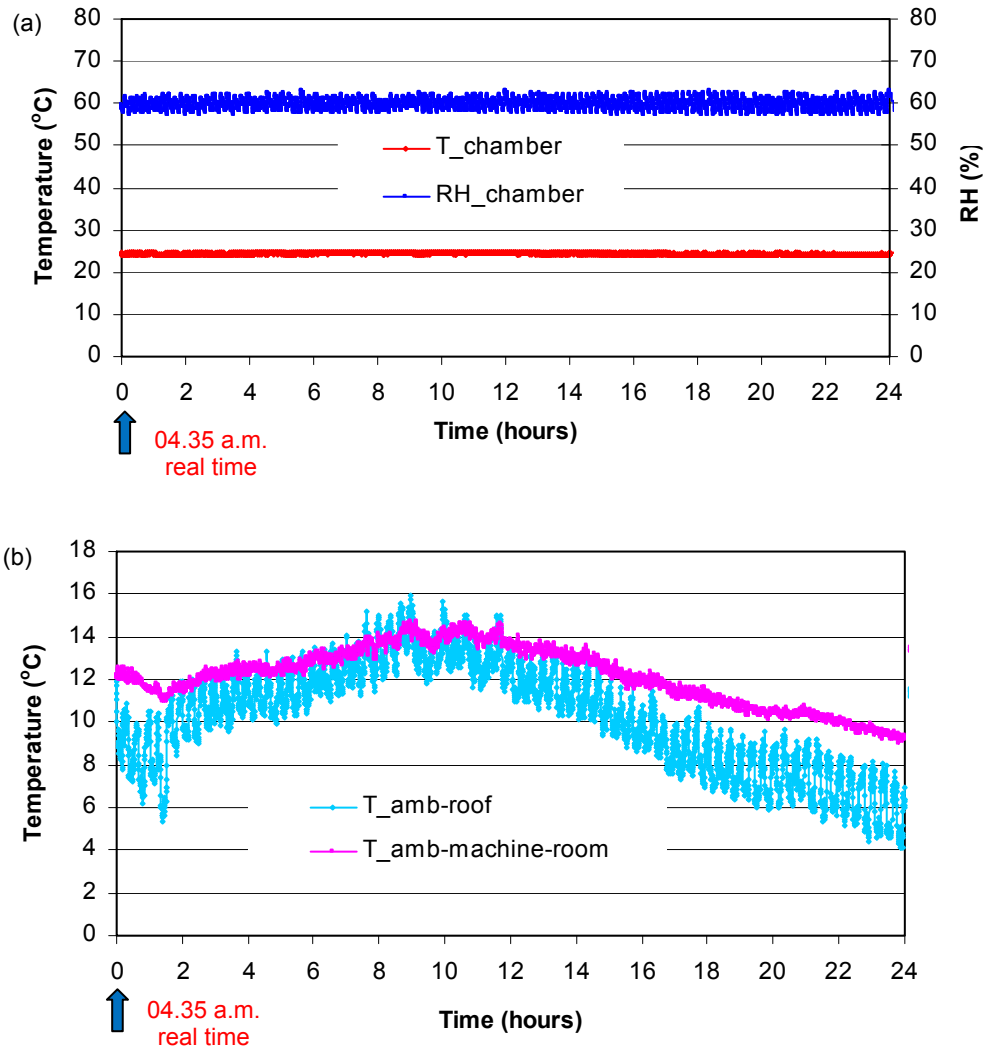

Figure 3.46 Variation of the test chamber conditions and ambient temperatures

Figure 3.46a shows the variation of air temperatures and relative humidity set up for climate class 3 conditions (25 ^{o}C, 60% RH) in the chamber over a period of 24 hours. They were measured at a point in the middle of the MT display cabinet 150 mm above and 300 mm in front of the top edge of the cabinet opening. Even though the ambient temperature varied significantly during the day (Figure 3.46b), the conditions within the chamber remained relatively stable. The temperature and relative humidity could be maintained within ± 1.0 ^{o}C and ± 3.0% respectively.

Another important parameter is the positioning of a display cabinet in the chamber, i.e. the distance from the cabinet to the walls and ceiling. Figures F-5 and F-6 (Appendix F) show that the test chamber can comply with the ISO standard for vertical door type cabinets up to 3.75 m long but it cannot comply with the requirements for vertical open type cabinets. Horizontal open type cabinets up to 2.5 m long, however, can be tested in the chamber with compliance to the standard.

In order to increase the capability of the test chamber, some improvements are required which include better insulation and extension of the width of the chamber. Figure F-7 (Appendix F) shows proposed improvements to the test chamber.

3.9 Commissioning the test facility

Prior to performing experimental tests, the test facility was commissioned in order to set and measure system performance against design parameters. The commissioning was performed after the test system was pressure and leak tested.

Mechanical and electrical checks were carried out to ensure the system run in the safest possible manner during its initial start up. At this stage, the functionality of the mechanical and electrical components including the control system was appropriately tested. The operation and setting of the pressure relief valves and pressure switches were also adjusted and verified. The pressure relief settings were checked by pressurising the system with nitrogen. Electrical components such compressor, pump, solenoid valve and oil management system were checked by switching the control system to the manual mode. Most of the mechanical and electrical components could function as specified. Some components such as the liquid level switch and expansion valve were set and tested during system operation.

The initial set up was configured in the electronic control system in accordance with the designed control strategy described in Section 3.5.3. The initial set up was adjusted further for better system operation and performance. Explanation of the operational procedure of the test facility is detailed in Appendix G.

During the initial operation it was found that at full load conditions the temperature of the water-glycol of the high stage circuit increased from -10 ^{o}C to -5 ^{o}C which indicated that the refrigeration capacity of the absorption unit of the trigeneration system was insufficient to maintain the set point of -10 ^{o}C.

To enable the CO_2 refrigeration system to operate at full load conditions, the high stage system was modified by installing a water chiller condensing unit in parallel with the absorption system. The water chiller is 'Hitema' ESE-045 specified for 18 kW refrigeration capacity at -12 ^{o}C delivery water-glycol temperature. After installation of the chiller, the CO_2 refrigeration system could steadily operate at designed and full load conditions.

3.10 Summary

This chapter has described the mathematical models developed to facilitate the design of the CO_2 refrigeration system and integrated trigeneration facility. The chapter has also detailed the construction of the test facility which incorporates mechanical, electrical, control, instrumentation and data logging systems. The refrigeration loading system and the environmental test chamber have also been briefly described.

Chapter 4 will present the evaporator coil models of the CO_2 chilled and frozen food display cabinets. The chapter will also detail the validation of the models and performance analyses of the CO_2 evaporator coils.

Chapter 4

MODELLING AND PERFORMANCE ANALYSES OF CO_2 EVAPORATOR COILS

4.1 Introduction

An advantage of CO_2 over HFC refrigerants is its better heat transfer properties that can lead to an increase in the evaporating temperature. A consequence of this is a potential increase in the refrigeration capacity of the coil and a reduction in the rate of frost formation on the coil surface.

Refrigeration systems in supermarkets normally operate at two temperature levels, medium temperature (MT) and low temperature (LT). The evaporating temperature of MT refrigeration systems is around -8 ^{o}C and for LT refrigeration system -32 ^{o}C. The refrigeration systems employed can either be of the direct expansion or the secondary refrigeration loop type. In conventional supermarkets, the direct expansion refrigeration system is the most commonly used whereas the secondary loop type is a good option for CO_2 refrigeration applications. As CO_2 has low viscosity, its use as volatile secondary fluid can significantly improve the performance of the refrigeration system due to low pumping power. Analyses of secondary loop refrigeration systems using CO_2 as secondary fluid have been reported by Inlow and Groll (1996) and Melinder and Granryd (2010).

Finned tube heat exchangers are commonly used as forced air evaporator coils in refrigerated display cabinets in supermarkets. The performance of the evaporator coil

directly affects the temperature performance of the display cabinet and the overall performance of the supermarket refrigeration system. The influence of geometry and configuration on the performance of finned tube coils for synthetic refrigerants has been investigated by many researchers. Romero-Mendez et al. (2000) examined the effects of fin spacing on the hydrodynamics and heat transfer of a plate fin and tube heat exchanger. Liang et al. (2001) and Jiang et al. (2006) investigated the impacts of circuit design on the performance of evaporator coils. Getu and Bansal (2007) developed a model of R-404A evaporator coil to analyse the performance of LT supermarket display cabinet coils. Chandrasekharan et al. (2006) developed a design tool for a finned tube display cabinet evaporator to predict the local and overall effects of frost accumulation.

To date, there has not been much research into evaporator coil design specifically for CO_2 refrigerant. Aidoun and Ouzzane (2009) established a numerical model to study the effects of circuitry of CO_2 finned tube evaporators and found that it was possible to use longer circuit lengths, thus reducing the number of circuits for a given refrigeration capacity. Shilliday and Tassou (2010) investigated the impact of the geometry, tube circuitry and tube diameter on the performance of CO_2 evaporators and showed that reducing the number of circuits could increase the velocity of refrigerant and reduce the total length of pipe.

This chapter presents the performance of CO_2 evaporator coils under different geometry, circuit arrangement and different operating conditions for chilled food and frozen food display cabinets for supermarket applications. The design and performance of the CO_2 coils used in the display cabinets of the test rig cabinets are also discussed. Comparison with evaporator coils using R-404A refrigerant is also presented and discussed.

4.2 Evaporator model description

Two main models were established to investigate the performance of CO_2 evaporator coils. The first model was for the investigation of the performance of MT CO_2 flooded evaporator coils. The second model was for the simulation of the performance of CO_2 DX evaporator coils for both chilled and frozen food temperature levels. The models can also be used to design the geometry and tube arrangement of evaporator coils for a given refrigeration capacity. The numerical models apply standard plate fin

specification from SRC (2010) to determine fin and tube pattern, height and width of the coil. The models were developed using the software EES.

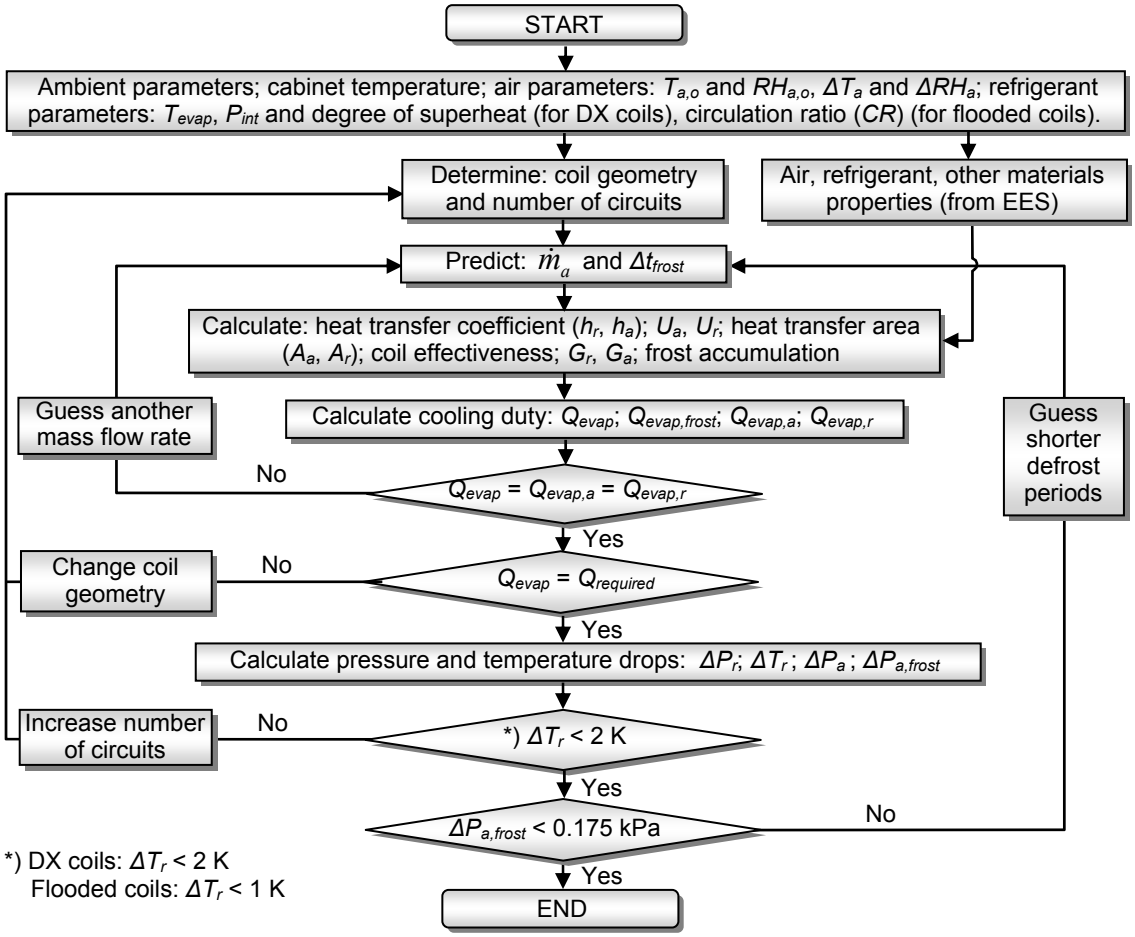

Figure 4.1 Structure of the simulation models for flooded and DX evaporator coils

Figure 4.1 shows a flowchart of the models for flooded and DX evaporator coils. The models consist of four loops. The first loop ensures that the energy balance in the evaporator coil can be satisfied. The loop determines the air mass flowrate at a given display cabinet refrigeration duty. The convergence of the loop is satisfied when the rate of heat transfer on the air side, on the refrigerant side and that determined from the overall heat transfer coefficient become equal. The other two loops verify the geometry and the number of circuits. Another loop determines the optimum defrost period of the coil for given operating conditions. Once the convergence of the first loop has been achieved and the refrigeration duty becomes equal to the design requirement, the geometry of the coil is determined. The key input parameters shown in Figure 4.1 such

as evaporating temperature, circulation ratio and air mass flowrate can also be varied to investigate the comparative heat transfer performance and pressure drop behaviour of different coil geometries and arrangements.

The models make some assumptions as follows: steady state flow conditions; one dimensional flow for refrigerant inside tubes and air across the coil; negligible thermal losses to the environment; uniform temperature and air flow; constant air side convective heat transfer coefficient over the entire coil; intermediate pressure (P_{int}) to be considered as condensing pressure for CO_2 DX evaporator coil; negligible refrigerant pressure drops of less than 2 K saturated temperature equivalent for DX coils (SRC, 2001) and less than 1 K for flooded coils; the same number of tubes in each circuit with the same fraction of total mass flow rate; quasi steady frosting process; maximum pressure drop at air side of the coil to be lower than 0.175 kPa (Bell and Mueller, 2001).

4.3 Mathematical model approach

Figure 4.2 shows the basic geometry of the finned tube evaporator considered in the models. The tubes are arranged in coordinates along width, depth and height axes (i, j, k) as can be seen in the figure. The number of rows and tube pattern can be used to determine the size of the coil and the tube interconnections within the coil circuits. If the coil has more than one circuit, the number of tubes in each circuit should be evenly balanced.

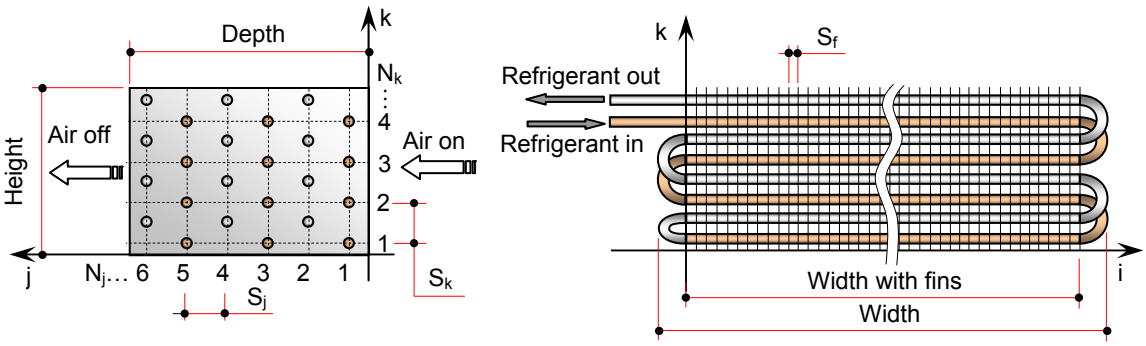

Figure 4.2 Geometry of a finned tube evaporator model

The geometric parameters of the evaporator coil such as tube spacing, height, depth, free flow area, and surface area are associated with the tube arrangement of the coil:

staggered or in-line. The staggered arrangements commonly used are the 30°, 45° and 60° layouts, while the coil with inline arrangement is referred to as the 90° tube layout. The models have been developed to provide the possibility to determine the geometric parameters of a coil for different tube arrangements.

The mathematical models use the lumped element technique by which the evaporator coil can be divided into the superheated and two phase regions. A DX coil has two lumped regions (single and two phase regions), while a flooded evaporator coil only has a one region, the two phase region as shown in Figure 4.3. Each region is considered as a single control volume.

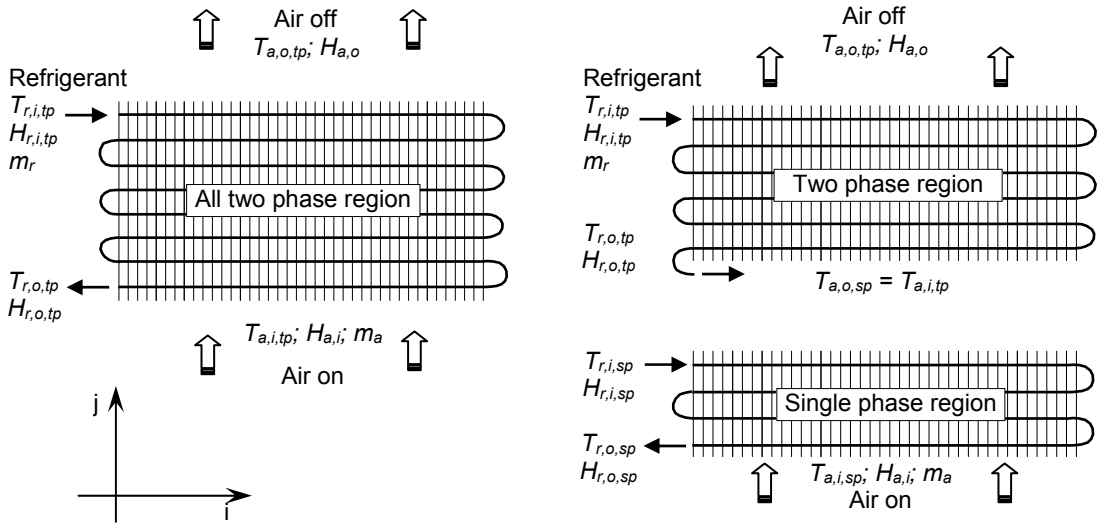

(a) Flooded coil with single lumped region (b) Direct expansion coil with two lumped regions

Figure 4.3 Schematic of flooded and DX evaporator coils with single and two control volumes respectively

The mass and energy balance principles are applied to each control volume, which are summarised in equations (4.1) to (4.3) for DX evaporator coil. For flooded evaporator coil, the equations are also applied but the heat transfer rate components for single phase region ($Q_{evap,r,sp}$) equation (4.1), $\dot{m}_r (H_{r,o,sp} - H_{r,i,sp})$ equation (4.2) and ($U_{a,sp} A_{a,sp} \Delta T_{lm,sp}$) equation (4.3) are omitted due to single phase region does not exist.

$$Q_{evap} = Q_{evap,r,tp} + Q_{evap,r,sp} = Q_{evap,a} \tag{4.1}$$

$$Q_{evap} = \dot{m}_r (H_{r,o,tp} - H_{r,i,tp}) + \dot{m}_r (H_{r,o,sp} - H_{r,i,sp}) = \dot{m}_a (H_{a,i} - H_{a,o}) \tag{4.2}$$

$$Q_{evap} = U_{a,tp} A_{a,tp} \Delta T_{lm,tp} + U_{a,sp} A_{a,sp} \Delta T_{lm,sp} \tag{4.3}$$

The air-side surface area of the coil (A_a) and other geometric parameters such as free flow area and free flow area with frost were calculated as in Shah and Seculic (2003). The fraction of the coil area in each control volume in a DX coil is calculated in proportion to the amount of heat transfer in each control volume.

$$A_{a,tp} = A_a \left(\frac{Q_{evap,r,tp}}{Q_{evap}} \right) \quad \text{and} \quad A_{a,sp} = A_a \left(\frac{Q_{evap,r,sp}}{Q_{evap}} \right) \tag{4.4}$$

The logarithmic mean temperature difference of each control volume (ΔT_{lm}) is defined as:

$$\Delta T_{lm} = \frac{\Delta T_1 - \Delta T_2}{\ln\left(\frac{\Delta T_1}{\Delta T_2} \right)} \tag{4.5}$$

where $\Delta T_1 = T_{h,i} - T_{c,o}$ and $\Delta T_2 = T_{h,o} - T_{c,i}$;

$T_{h,i}$; $T_{h,o}$ and $T_{c,i}$; $T_{c,o}$ are inlet/outlet temperatures of hot and cold streams of the control volume respectively. The hot stream is air and the cold stream is the refrigerant.

When $\Delta T_1 - \Delta T_2 < 0.05$, to avoid errors of division by zero in the EES software the logarithmic mean temperature difference is calculated from (Mattsson, 1997):

$$\Delta T_{lm} = 0.5\ (\Delta T_1 + \Delta T_2) \left[1 - \frac{(\Delta T_1 - \Delta T_2)^2}{12\ \Delta T_1\ \Delta T_2} \left(1 - \frac{(\Delta T_1 - \Delta T_2)^2}{2\ \Delta T_1\ \Delta T_2} \right) \right] \tag{4.6}$$

The overall heat transfer coefficient (U_a) of the coil with frost can be determined from equation (4.7) which is based on the external and internal heat transfer coefficients and frost, wall and fouling resistances. For the frost free coil models the component of frost resistance is not included.

$$\frac{1}{U_a} = R_{tot} = R_a + R_{frost} + R_{fl,a} + R_{wall} + R_{fl,r} + R_r \tag{4.7}$$

The thermal resistances are calculated from the equations in Table 4.1. For the DX coil the internal and external heat transfer areas (A_r, A_a) as well as the internal heat transfer coefficient (h_r) depend on the mode of heat transfer, single or two phase.

Table 4.1 Equations for the thermal resistance of the coil
Calculations refer to the air-side surface area, equation (4.3)

Components	Thermal resistance (m^2K/kW)	References
Air-side (external) resistance	$R_a = \frac{1}{\eta_o h_a}$	
Frost resistance	$R_{frost} = \frac{\delta_{frost}}{\eta_o \lambda_{frost}}$	
Air-side fouling resistance	$R_{fl,a} = \frac{0.000176}{\eta_o}$	Kakac and Liu (2002)
Tube wall resistance	$R_{wall} = \frac{A_a \ln\left(\frac{d_o}{d_i}\right)}{2\pi\lambda_t L_t}$	
Refrigerant-side fouling resistance	$R_{fl,r} = 0.000352 \frac{A_a}{A_r}$	Kakac and Liu (2002)
Refrigerant-side (internal) resistance	$R_r = \frac{A_a}{A_r h_r}$	

Where: A = heat transfer surface area (m^2); d = diameter of tube (m); η_o = overall evaporator HX efficiency (Section 4.3.4); h = heat transfer coefficient (kW/m^2 K); L_t = length of the coil tube (m); δ_{frost} = frost thickness (Section 4.3.3); λ = thermal conductivity (kW/m.K) for λ_{frost} is presented in Section 4.3.3.

4.3.1 Heat transfer coefficient and pressure drop at refrigerant side

The local heat transfer coefficients and pressure drop correlations were selected for each flow regime as it changes with the flow and evaporation of refrigerant in the evaporator. Thus the correlations reliably capture the variation of two phase heat transfer coefficient and frictional pressure drops at different mass velocities and vapour qualities. Figure 4.4 shows the flow regime of the CO_2 refrigerant evaporating inside horizontal tubes.

The approach used in the models to determine the overall two phase heat transfer coefficient and pressure drop of the evaporator coils from local heat transfer coefficient and pressure drop of CO_2 evaporation was to divide the coil into 12 elements (Figure 4.4) from $x = x_{in}$ to $x = 1$ for the DX evaporator and $x = 0$ to $x = x_{out}$ for the flooded evaporator and determine the average value. This approach provides acceptable results and is moderately easy to manage in the model. A larger number of elements did not provide any significant difference to the simulation accuracy.

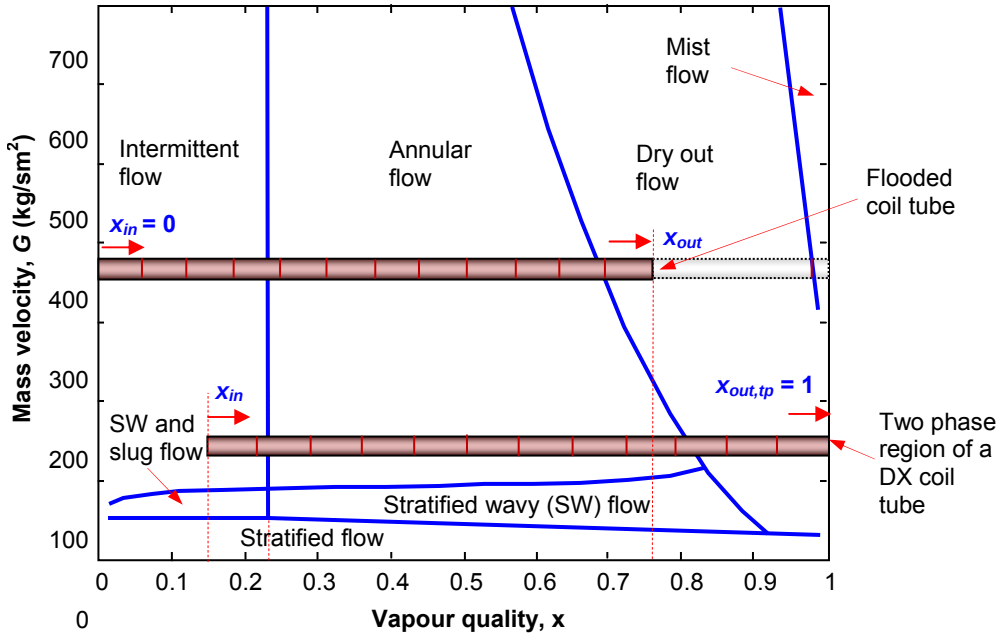

x_{in} = vapour quality at inlet of the evaporator coil
x_{out} = vapour quality at outlet of a flooded evaporator coil
$x_{out,tp}$ = vapour quality at outlet of the two phase region of a DX evaporator coil

Figure 4.4 A flow pattern map of CO_2 evaporation inside DX and flooded evaporator coils
(Source of the CO_2 flow pattern map: Cheng et al., 2008a)

Equations (4.8) to (4.10) show general equations for the local two phase heat transfer coefficient (h_{tp}) and pressure drop (ΔP_r) on the refrigerant side of the evaporator. Key equations are presented in Table 4.2 and more detailed correlations for each flow regime including the transition boundary correlations can be found in Cheng et al. (2008a; 2008b).

$$h_{tp} = \frac{\theta_{dry} h_V + (2\pi - \theta_{dry})\, h_{wet}}{2\pi} \tag{4.8}$$

$$h_{wet} = \left[\left(Sh_{nb} \right)^3 + h_{cb}^3 \right]^{(1/3)} \tag{4.9}$$

$$\Delta P_r = \Delta P_{static} + \Delta P_m + \Delta P_{fr} \tag{4.10}$$

Where θ_{dry} is the dry angle which defines the ratio of the tube perimeter in contact with liquid and vapour; h_V and h_{wet} are respectively heat transfer coefficients on the dry and wet perimeters (W/m^{2}K); h_{nb}, S and h_{cb} are nucleate boiling heat transfer coefficient (W/m^{2}K), nucleate boiling heat transfer suppression factor and convective boiling heat transfer coefficient (W/m^{2}K) respectively.

The static pressure drop (ΔP_{static}) of a horizontal tube is equal to zero; momentum pressure drop (ΔP_m) and frictional pressure drop (ΔP_{fr}) are calculated from:

$$\Delta P_m = G^2 \left(Z_{out} - Z_{in} \right) \tag{4.11}$$

$$\Delta P_{fr} = 4f \frac{L_t}{d_h} \frac{\rho u^2}{2} \tag{4.12}$$

where:

$$Z_{out} = \left[\frac{(1-x)^2}{\rho_L (1-\varepsilon)} + \frac{x^2}{\rho_V \, \varepsilon} \right]_{out};$$

$$Z_{out} = \left[\frac{(1-x)^2}{\rho_L (1-\varepsilon)} + \frac{x^2}{\rho_V \, \varepsilon} \right]_{out};$$

f is the friction factor which depends on the flow region; d_h = hydraulic diameter of the tube (m); G = mass velocity (kg/s.m^2); L_t = tube length (m); u = refrigerant velocity (m/s); x = vapour quality; ε = cross sectional vapour void fraction; and ρ = density (kg/m^3).

Table 4.2 Key equations for two phase heat transfer coefficient and pressure drop for CO_2 inside a horizontal tube

Parameters	Equations
Vapour phase heat transfer coefficient (Dittus-Boelter equation)	$h_V = 0.023 \, \mathrm{Re}_V^{0.8} \, \mathrm{Pr}_V^{0.4} \frac{\lambda_V}{d_h}$
Nucleate boiling heat transfer coefficient	$h_{nb} = 131 \left(\frac{P}{P_{crit}} \right)^{-0.0063} \left(-\log_{10} \frac{P}{P_{crit}} \right)^{-0.55} M^{-0.5} q^{0.58}$
Convective boiling heat transfer coefficient	$h_{cb} = 0.0133 \, \mathrm{Re}_\delta^{0.69} \, \mathrm{Pr}_L^{0.4} \frac{\lambda_L}{\delta}$ where: $\delta = \frac{d_h}{2} - \sqrt{\left(\frac{d_h}{2} \right)^2 - \frac{2A_L}{2\pi - \theta_{dry}}}$
Heat transfer coefficient of the mist flow region	$h_M = 2.10^{-8} \, \mathrm{Re}_H^{1.97} \, \mathrm{Pr}_V^{1.06} \, Y^{-0.183} \frac{\lambda_V}{d_h}$ where: $Y = 1 - 0.1 \left[\left(\frac{\rho_L}{\rho_V} - 1 \right) (1-x) \right]^{0.4}$

Source: Cheng et al, 2008b

Table 4.2 Key equations for two phase heat transfer coefficient and pressure drop for CO_2 inside a horizontal tube (Continued)

Parameters	Equations
	Homogenous Reynolds number: $\mathrm{Re}_H = \frac{G\,d_h}{\mu_V}\left[x + \frac{\rho_L}{\rho_V}(1-x)\right]$
Heat transfer coefficient of the dry out flow region	$h_{dryout} = h_{tp(X_{di})} - \frac{x - x_{di}}{x_{de} - x_{di}}\left(h_{tp,X_{di}} - h_{M,X_{de}}\right)$

Source: Cheng et al, 2008b

A = area (m^2); d_h = diameter hydraulic of tube (m); h = heat transfer coefficient (W/m^2 K); M = molecular weight (kg/mol); Pr = Prandtl number; q = heat flux (W/m^2); Re_H, Re_V and Re_δ are respectively homogeneous, vapour phase and liquid film Reynolds numbers; u = refrigerant velocity (m/s); x = vapour quality; δ = liquid film thickness (m); λ = thermal conductivity (W/m.K); ρ = density (kg/m^3); μ = dynamic viscosity ($N/s.m^2$); θ = dry angle (rad). *Subscripts*: crit = critical; cb = convective boiling; di = dry out inception; de = dry out completion; h = hydraulic; L = liquid phase; M = mist flow region; nb = nucleate boiling; V = vapour phase; tp = two phase.

Results for the prediction of two phase pressure drop of CO_2 in evaporator coils have been verified using data from Cheng et al. (2008a) as shown in Figure 4.5a. The figure shows the variation of the pressure drop for a 7 mm internal diameter tube coil. Figure 4.5b shows two phase pressure drop obtained from the CO_2 evaporator models for the same internal tube diameter. It can be seen that the results from model are in a good agreement with the pressure drop prediction by Cheng et al. (2008a). Both pressure drop increase up to a vapour quality of approximately 0.8 and then drop sharply due to the start of the dry-out region.

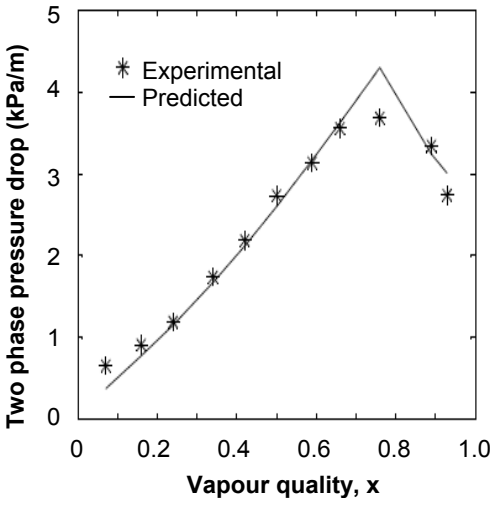

(a) Comparison of CO_2 two phase pressure drop model results and experimental data (Cheng et al., 2008a)

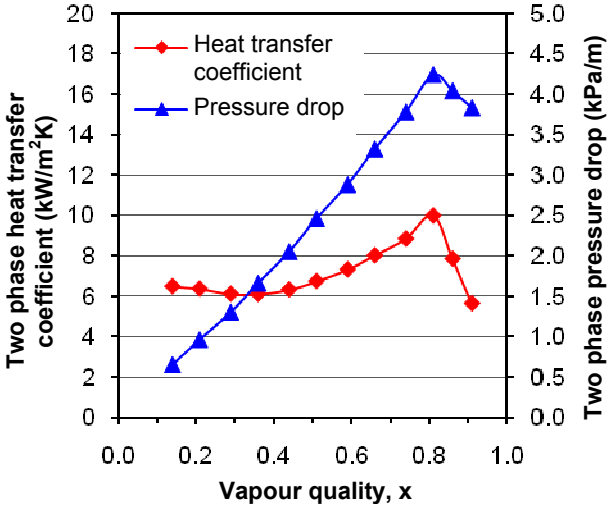

(b) Results from the CO_2 evaporator models

Figure 4.5 Variation of CO_2 two phase pressure drop and heat transfer coefficient (Investigated at T_{evap} = -10 °C, G_r = 400 kg/s m^2 and internal tube diameter 7 mm, q = 9 kW/m^2)

Figure 4.5b also shows the variation of two phase heat transfer coefficient of CO_2 refrigerant at different vapour quality resulted from the evaporator model. It can be seen that two phase heat transfer coefficient also increases up to a vapour quality of 0.8 and then drop sharply in the dry-out region.

For the R-404A evaporator model, the two phase heat transfer coefficient of R-404A was determined from the correlation by Wojtan et al. (2005b). The two phase pressure drop was calculated from Moreno-Quiben and Thome (2007a; 2007b). The heat transfer coefficient and pressure drop correlations were associated with the flow pattern map developed by Wojtan et al. (2005a).

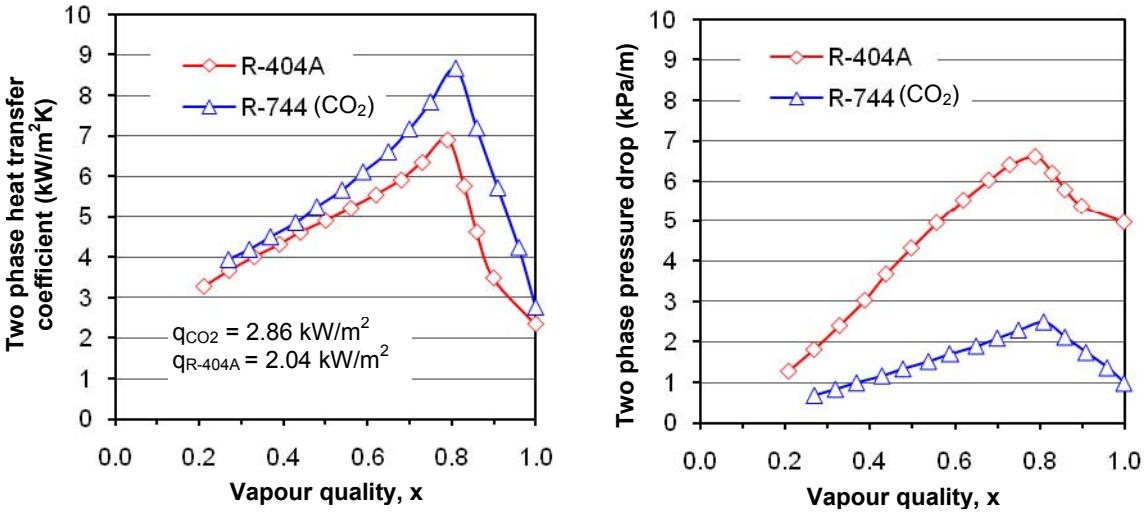

(a) Two phase heat transfer coefficients

(b) Two phase pressure drops

Figure 4.6 Comparison of two phase heat transfer coefficient and pressure drop between CO_2 and R-404A

Figure 4.6 presents the two phase heat transfer coefficient and pressure drop of R-404A in comparison with CO_2 refrigerant. The results were obtained from direct expansion evaporator models at evaporating temperature T_{evap} = -10 °C, condensing temperature T_{cond} = 16.5 °C (without subcooling), mass velocity G_r = 400 kg/s.m^2 and internal diameter of the coil tube d_i = 10.7 mm respectively. The figure shows that the two phase heat transfer coefficient and pressure drop of both refrigerants increase with vapour quality reaching their peak values at the end of the annular flow region (at vapour quality between 0.7 and 0.8) and then decrease sharply in the dry-out region.

From the figure, the advantage of CO_2 over R-404A refrigerant can also be seen. The two phase heat transfer coefficient of CO_2 is about 20% (on average) higher than R-404A. This contributes to better heat transfer on the CO_2 evaporator coil reducing the size of the coil for the same refrigeration duty. Figure 4.6b shows that the two phase pressure drop of CO_2 is much lower, approximately one third, of the pressure drop of R-404A. This offers a number of advantages for CO_2 as a refrigerant which have been described in Section 2.1 (Chapter 2).

4.3.2 Heat transfer coefficient and pressure drop on the air side

The air side heat transfer coefficient (h_a) consists of convective and latent heat transfer coefficients: $h_{c,a}$ and $h_{lat,a}$ respectively (Getu and Bansal, 2007).

$$h_a = h_{c,a} + h_{lat,a} \tag{4.13}$$

The convective heat transfer coefficient was calculated using the Colburn j-factor, Kim *et al.* (1999):

$$h_{c,a} = \frac{j\, C_{p,a}\, G_a}{\mathrm{Pr}^{2/3}} \tag{4.14}$$

The Colburn *j*-factor for evaporator coil having three or more tube rows in the direction of the air flow (rows deep $N_j \geq 3$) can be determined from (Kim et al., 1999):

$$j_{N_j \geq 3} = 0.240\ \mathrm{Re}_{Dh}^{-0.409} \left(\frac{S_k}{S_j}\right)^{0.425} \left(\frac{S_f}{d_o}\right)^{-0.035} \tag{4.15}$$

For less than three rows deep ($N_j < 3$):

$$j_{N_j} = j_{N_j \geq 3} \left\{ 0.931 \left[1.49\, \mathrm{Re}_{Dh}^{-0.162} \left(\frac{S_k}{S_j}\right)^{-0.892} \left(\frac{S_f}{d_o}\right)^{-0.152} \left(\frac{S_k}{d_o}\right) \right]^{(3-N_j)} \right\} \tag{4.16}$$

The air flow Reynolds number of the free flow area is given by:

$$\mathrm{Re}_{Dh} = \frac{G_a\, D_h}{\mu_a} \tag{4.17}$$

The hydraulic diameter of the air side (D_h) can be calculated from:

$$D_h = \frac{4\ A_{ff,a}\ L_j}{A_a} \tag{4.18}$$

where $A_{ff,a}$ is the free flow area at air side of the evaporator coil (m^2); $C_{p,a}$ is the specific heat of air (kJ/kg K); d_o = outside diameter of the evaporator tube (m); G_a is the air mass velocity through the free flow area (kg/s.m^2); S_j, S_k and S_f are tube and fin spacing (Figure 4.2).

The latent heat transfer coefficient can be determined from (Threlkeld, 1970):

$$h_{lat,a} = \frac{h_{c,a}\, H_{sg}\, (\omega_{a,i} - \omega_{a,o})}{Le\, C_{p,a}\, (T_{a,i} - T_{a,o})} \tag{4.19}$$

where the Lewis number (*Le*) is assumed to be 1 and the sublimation latent heat (H_{sg}) is estimated from the correlation proposed by Ismail and Salinas (1999):

$$H_{sg} = 2322\left(-0.04667\ (1.8\ T_{r,m} + 32) + 1220.1\right) \tag{4.20}$$

$T_{r,m}$ is average temperature of the refrigerant.

The air pressure drop over the evaporator is calculated from the pressure drop equation given by Kays and London (1998):

$$\Delta P_a = \frac{G_a^2}{2\rho_{a,i}}\left((1-\sigma^2)\left(\frac{\rho_{a,i}}{\rho_{a,o}} - 1\right) + f_a \frac{A_a}{A_f}\frac{\rho_{a,i}}{\rho_{a,m}}\right) \tag{4.21}$$

where A_f is fin surface area including leading and trailing edge area (m^2); $\rho_{a,i}$, $\rho_{a,o}$, and $\rho_{a,m}$ are inlet, outlet and average air density (kg/m^3) respectively; σ is the ratio of free flow to frontal area; $\omega_{a,i}$ and $\omega_{a,o}$ are the humidity ratio of air-on and air-off the coil respectively.

The total friction factor (f_a) of the evaporator is calculated from (Kim et al., 1999):

$$f_a = f_f \frac{A_f}{A_a} + f_t\left(1 - \frac{A_f}{A_a}\right)\left(1 - \frac{\delta_f}{S_f}\right) \tag{4.22}$$

where δ_f is the fin thickness (m); the friction factors due to fins (f_f) and tube bank (f_t) can be determined from:

$$f_f = 1.435\ \mathrm{Re}_{Dh}^{-0.562}\left(\frac{S_k}{S_j}\right)^{-0.365} + \left(\frac{S_f}{d_o}\right)^{-0.131}\left(\frac{S_k}{d_o}\right)^{1.22} \tag{4.23}$$

$$f_t = \frac{4}{\pi}\left(0.25 + \frac{0.118}{\left(\frac{S_k}{d_o}-1\right)1.08}\,\mathrm{Re}_{Dh}^{-0.16}\right)\left(\frac{S_k}{d_o}-1\right) \tag{4.24}$$

4.3.3 Calculation of frost accumulation

Frost accumulation on the evaporator surface is estimated using the method proposed by Getu and Bansal (2007). The rate of frost accumulation is determined from equation (4.25); the amount of frost accumulated on the surface of the evaporator (Δm_{frost}) from equation (4.26) and the frost thickness (δ_{frost}) from equation (4.27).

$$\dot{m}_{frost} = \dot{m}_a\,(\omega_{a,i} - \omega_{a,o}) \tag{4.25}$$

$$\Delta m_{frost} = \dot{m}_{frost}\,\Delta t_{frost} \tag{4.26}$$

$$\delta_{frost} = \frac{\Delta m_{frost}}{\rho_{frost}\,A_a} \tag{4.27}$$

where $\dot{m}_a$ is the air mass flow rate; $\dot{m}_{frost}$ is the frost accumulation rate; the parameter $\omega_{a,i}$ and $\omega_{a,o}$ are the humidity ratio of air-on and air-off evaporator coil; and Δt_{frost} is the step time of frost accumulation. The frost density and thermal conductivity are calculated from empirical correlations as described in Getu and Bansal (2007):

$$\rho_{frost} = 1.714\,.\,10^{-4}\left(\frac{L_j}{D_h}\right)^{-0.056}\omega_{a,m}^{-0.011}\left(T_{trip,H_2O} - T_s\right)^{0.845}\mathrm{Re}_{Dh}^{0.463}\,Fo_{Dh}^{0.217}\,\rho_{ice} \tag{4.28}$$

$$\lambda_{frost} = 6.534\,.\,10^{-4}\left(\frac{L_j}{D_h}\right)^{-0.048}\omega_{a,m}^{0.004}\left(T_{trp,H_2O} - T_s\right)^{0.737}\mathrm{Re}_{Dh}^{0.375}\,Fo_{Dh}^{0.18}\,\lambda_{ice} \tag{4.29}$$

where $T_{trip,H2O}$ and T_s are the water triple point and the coil surface temperature respectively. The coil surface temperature is assumed to be the average of the refrigerant temperature in the coil. The parameter $\omega_{a,m}$ is the average humidity ratio of the air across the coil. The properties of ice evaluated at the coil surface temperature were determined from the EES software.

The Fourier number is defined as:

$$Fo_{Dh} = \frac{\alpha_a \ \Delta t_{frost}}{D_h^2} \tag{4.30}$$

α_a is the thermal diffusivity of air (m^2/s).

The air pressure drop over the coil was determined by using coil geometric parameters and air mass velocity with frost thickness (δ_{frost}).

4.3.4 Overall surface efficiency of the evaporator coil

The overall surface efficiency of the evaporator coil (η_o) is a function of fin and total surface area ratio and fin efficiency which can be formulated as below (Wang et al., 1996).

$$\eta_o = 1 - \frac{A_f}{A_a}\left(1 - \eta_f\right) \tag{4.31}$$

The estimation of fin efficiency (η_f) is calculated from the equation proposed by Hong and Webb (1996). The correlation is based on a simplified analytical solution for a circular fin by Schmidt (1945) approximation. For the case of rectangular and hexagonal fins, the fin efficiency could be treated as for a circular fin by considering an equivalent circular fin radius (Schmidt, 1949).

$$\eta_f = \frac{\tanh\left(m\ r_o\ \phi\right)}{m\ r_o\ \phi}\cos\left(m\ r_o\ \phi\right) \tag{4.32}$$

where:

$$m = \sqrt{\frac{2h_a}{\lambda_f\ \delta_f}} \tag{4.33}$$

$$\phi = \left(\frac{r_{f,eq}}{r_o} - 1\right)\left(1 + 0.35\ln\left(\frac{r_{f,eq}}{r_o}\right)\right) \tag{4.34}$$

For inline tube arrangement (rectangular fins):

$$\frac{r_{f,eq}}{r_o} = 1.28\ \frac{0.5\,S_k}{r_o}\sqrt{\frac{S_j}{S_k} - 0.2} \tag{4.35}$$

For staggered tube arrangement (hexagonal fins):

$$\frac{r_{f,eq}}{r_o} = 1.27\,\frac{0.5\,S_k}{r_o}\sqrt{\frac{S_d}{S_k} - 0.3} \tag{4.36}$$

$$S_d = \sqrt{S_j^2 + \frac{1}{4}\left(S_k^2\right)} \tag{4.37}$$

where $r_{f,eq}$ is the equivalent circular fin radius of rectangular and hexagonal fins; r_o is the outside radius of the evaporator tube (m); S_d is the diagonal spacing between the tubes.

4.4 Designs and performance of the CO_2 evaporator coils utilised in the MT and LT cabinets of the test rig

The models have been developed and used to design the evaporator coils of the MT and LT cabinets of the test facility. Three evaporator coils were designed: a flooded MT evaporator coil of 5 kW refrigeration capacity; two DX LT evaporator coils of 5 kW and 3 kW capacities respectively.

Table 4.3 Design parameters of the evaporator coils

Parameters	MT flooded coil	MT DX coil	LT DX coil
Ambient temperature (^oC)	25	25	25
Ambient relative humidity (%)	60	60	60
Condensing temperature (^oC)	-	-3	-8
Intermediate/condensing pressure (bar_a)	-	32	28
Evaporating temperature (^oC)	-8	-8	-32
Circulation ratio	2	-	-
Degree of superheat (K)	-	5	5
Liquid line subcooling (K)	-	-	2.4
Air volume flow rate (m^3/s)*	0.275	0.275	0.193
Air mass flow rate (kg/s)	0.35	0.35	0.27
ΔT between air-on and air-off (K)	10	9.2	10
ΔRH between air-off and air-on (%)	23	15	15
Allowable maximum height (m)	0.15 to 0.16	0.15 to 0.16	0.15 to 0.16
Allowable maximum depth (m)	0.21	0.21	0.40

* Estimated using measured air velocity at cross section of the rear air ducts of the MT and LT cabinets.

The designs were based on the parameters detailed in Table 4.3. The main design parameters for the MT flooded coil were evaporation temperature in the coil of -8 ^oC and refrigerant mass flowrate equivalent to circulation ratio (CR) = 2. For the MT DX

coil, CO_2 enters the expansion valve (EXV) as liquid without subcooling at intermediate pressure of 32 bar_a and saturation temperature of -3 ^oC. After expansion the CO_2 enters the evaporator coil at a temperature of -8 ^oC and exits at -3 ^oC giving a superheat of 5 K. For the LT DX evaporator coil, CO_2 enters the EXV as liquid with 2.4 K subcooling at 28 bar_a. The evaporation temperature of this coil is at -32 ^oC (13 bar_a) and CO_2 exits the coil with 5 K superheating. The coils were sized to fit within the available space in the cabinets which were originally built for R-404A coils.

Table 4.4 Coil geometry and estimated performance parameters

Coil Geometry/Parameters	MT flooded coil	MT DX coil	LT DX coil
Coil geometry			
Copper tube diameter, d_o (m)	0.0127	0.0127	0.0127
Tubes arrangement/layout	staggered/30^o	staggered/30^o	staggered/30^o
Transversal tube spacing, S_k (m)	0.038	0.038	0.038
Longitudinal tube spacing, S_j (m)	0.033	0.033	0.033
Fin spacing, S_f (m)	0.0064	0.0064	0.0085
Fin thickness, δ_f (m)	0.00022	0.00022	0.00022
Number of circuits, N_c	4	4	3
Number of rows deep, N_j	6	6	8
Number of rows high, N_k	4	4	4
Coil height, L_k (m)	0.152	0.152	0.152
Coil depth, L_j (m)	0.198	0.198	0.264
Coil width, L_i (m)	2.085	2.085	2.030
Total tube length, L_t (m)	50.0	50.0	65.0
Performance parameters			
Refrigeration capacity (kW)	5.24	5.09	3.0
Refrigerant mass flow rate (kg/s)	0.0410	0.0204	0.0113
Refrigerant mass velocity, G_r (kg/s.m^2)	114.9	56.7	41.7
Refrigerant side pressure drop, ΔP_r (kPa)	9.41	4.81	7.78
Frost free air side pressure drop, ΔP_a (kPa)	0.005	0.005	0.003
Air side pressure drop with 4 (h) frost period, $\Delta P_{a,frost}$ (kPa)	0.011	0.017	0.007*
Overall surface efficiency, η_o	0.87	0.85	0.92
Fin efficiency, η_f	0.85	0.84	0.91
External heat transfer coefficient, h_a (kW/m^2.K)	0.046	0.057	0.029
Internal heat transfer coefficient, h_r (kW/m^2.K)	3.304	2.970	1.336

* Estimated for frost period, Δt = 48 (h) or 2 (days); Design parameters refer to Table 4.3

The coil geometry and tube arrangement including estimated performance parameters are shown in Table 4.4. For the same evaporating temperature, the flooded coil can provide lower air-off temperature and lower air-side pressure drop with four hours between defrost periods. Moreover, the internal heat transfer coefficient of the MT DX coil is lower than for the MT flooded coil. This is because the DX coil has a lower mass flow rate of the same number of circuits which results in a smaller refrigerant mass velocity and does smaller heat transfer coefficient.

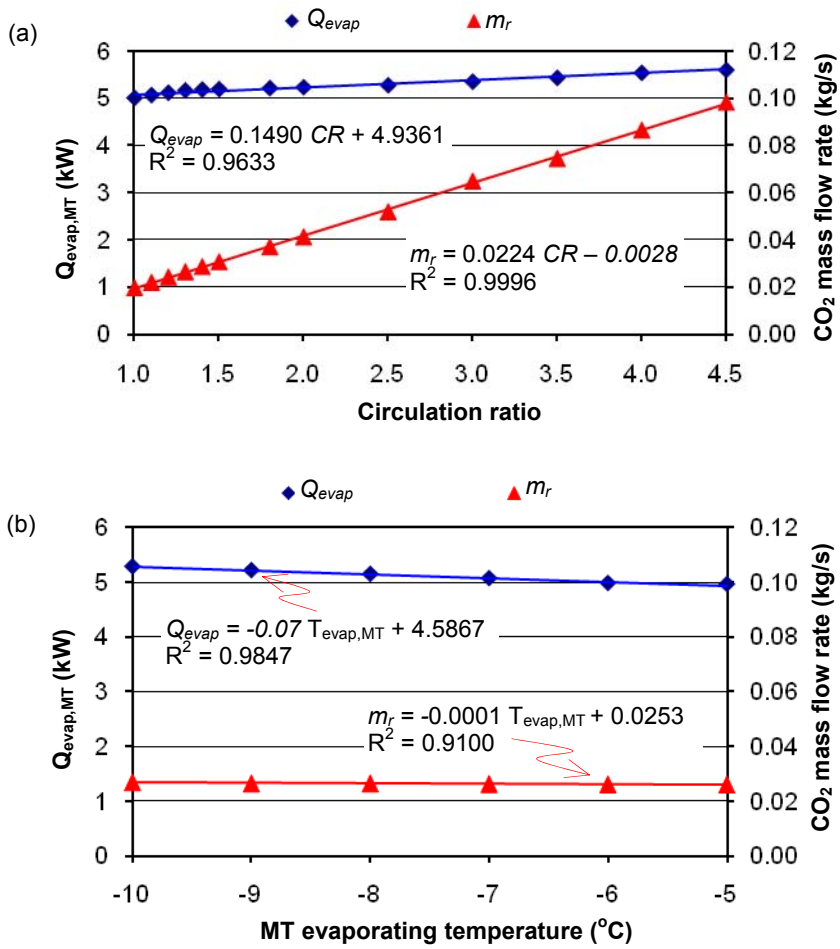

Figure 4.7 The influence of circulation ratio (*CR*) and evaporating temperatures on the flooded coil capacity and refrigerant mass flow rate
(Investigated at: (a) T_{evap} = -8 °C; (b) CR = 1.3)

Simulating the MT DX coil using a single circuit tube arrangement showed the capacity of the coil to improve by 4.1%. The internal pressure drop also increased from 4.8 kPa to 30.8 kPa corresponding to 0.6 K saturation temperature difference. This pressure drop is still within the acceptable range for CO_2 evaporator coils. Simulating the LT DX coil with a single circuit tube arrangement showed an increase the capacity of the coil by 10% and the pressure drop by 28.4 kPa giving a pressure drop of 36.2 kPa (0.96 K). Because the model at this point had not been validated, for safety in terms of pressure drop the MT coils were manufactured with four circuits. The LT DX coil was manufactured with a 3 circuit tube arrangement due to lower pressure drop in this coil. Detailed geometry and estimated performance parameters of the evaporator coils are given in Figures H-1 to H-4 (Appendix H). The construction of the coils has been described in Section 3.3.4 (Chapter 3).

Figure 4.7 shows the variation of refrigeration capacity and refrigerant mass flow rate of the flooded coil at different circulation ratios (Figure 4.7a) and at different evaporating temperatures (Figure 4.7b). It can be seen that the coil capacity increases with circulation ratio but requires significant increase of refrigerant mass flow rate. The refrigeration capacity of the coil slightly reduces when the evaporating temperatures increases with relatively constant mass flow rate. The figure also presents trend-line equations including correlation coefficients between refrigeration capacity, mass flow rate and circulation ratio. These correlations were used to model the influence of the circulation ratio on the performance of the integrated trigeneration and CO_2 refrigeration system as explained in Section 3.2.1.3 (Chapter 3).

4.5 Experimental and theoretical validation of the models

The models were validated using test results from the experimental test facility. The model of the conventional evaporator coil with R-404A refrigerant was validated against data provided by the manufacturer. Comparison between predicted and experimental data under design conditions was found to be satisfactory for the refrigeration capacity as shown in Table 4.5.

Table 4.5 Model and experimental results

Parameters		[a] MT CO_2 Models		[b] DX LT CO_2 model	[c] DX MT R-404A model
		Flooded	DX		
Q_{evap} (kW) full load at ΔT_a range between 9 and 10 K and T_{evap} = -8 °C for MT, -32 °C for LT, CR = 1.3	Model	5.19	5.09	3.00	-
	Experiment	5.10	4.93	2.89	-
Q_{evap} (kW) steady state load at ΔT_a between 8 and 9 K for MT; between 7 and 8 K for LT	Model	4.55	4.46	2.35	3.65
	Experiment	4.42	4.30	2.12	3.60*
ΔP_r (kPa) steady state; for flooded coil CR = 1.3 and ΔT superheat for DX coil between 5 and 12 K	Model	7.91	4.81	7.78	40.92
	Experiment	21.15	16.87	23.32	148.28*

[a] Tube arrangement: staggered; d_o = 0.0127 (m); N_k = 4; N_j = 6; N_c = 4; fins pitch 158 fins/m (4 FPI)
[b] Tube arrangement: staggered; d_o = 0.0127 (m); N_k = 4; N_j = 8; N_c = 3; fins pitch 118 fins/m (3 FPI)
[c] Tube arrangement: inline; d_o = 0.01587 (m); N_k = 2; N_j = 16; N_c = 2; fins pitch 118 fins/m (3 FPI)
* Data from manufacturer

The pressure drop estimates, however, were lower than the experimental results mainly because the pressure drops across the distributor and inlet and outlet effects were not included in the model. For synthetic refrigerants these pressure drops can be as high as 89% of total pressure drop in the evaporator coil (SRC, 2001).

4.6 Performance analyses of CO_2 evaporator coils

The validated models were used to design 8 evaporator coils with different geometry and circuitry. The evaporator coils were simulated at evaporating temperature of -8 ^oC for the MT coils and -30 ^oC for the LT coils. Tubes and fins were assumed to be made of copper and aluminium respectively. Equilateral fin and tube pattern in a staggered arrangement was assumed.

Table 4.6 Geometry of the designed coils and their performance parameters

Parameters	MT evaporator coils					LT evaporator coils		
	DX CO_2		Flooded CO_2		DX R-404A	DX CO_2		DX R-404A
	EC-1	EC-2	EC-3	EC-4	EC-5	EC-6	EC-7	EC-8
d_o (mm)	9.52	12.70	9.52	12.70	15.87	9.52	12.70	15.87
N_k	2	2	2	2	2	2	2	2
N_j	21	17	13	10	20	12	10	12
N_c	2	1	2	1	2	2	1	2
L_t (m)	91.1	73.8	56.4	43.4	86.6	48.7	40.6	48.7
L_k (m)	0.064	0.064	0.064	0.064	0.076	0.064	0.064	0.076
L_j (m)	0.577	0.467	0.358	0.275	0.660	0.330	0.275	0.396
L_i (m)	2.170	2.170	2.170	2.170	2.170	2.030	2.030	2.030
V_r (L)	4.14	6.78	2.56	3.99	13.47	2.22	3.74	7.57
G_r (kg/s.m^2)	171.0	168.7	199.8	198.1	109.0	100.4	99.0	72.2
CR	-	-	1.2	1.2	-	-	-	-
Q_{evap} (kW)	3.75	3.75	3.75	3.76	3.76	2.25	2.25	2.25
$Q_{evap,frost}$ (kW)*	3.26	3.12	3.24	2.96	3.44	2.16	2.14	2.15
η_f**	0.85	0.88	0.85	0.88	0.87	0.89	0.92	0.90
h_r (kW/m^2.K)	2.899	3.107	3.206	3.473	0.482	2.521	2.802	0.337
h_a (kW/m^2.K)	0.062	0.073	0.064	0.075	0.063	0.042	0.050	0.046
ΔP_r (kPa)	65.13	30.89	42.34	19.27	50.47	33.15	16.24	31.79
$\Delta P_{a,frost}$ (kPa)*	0.016	0.024	0.030	0.043	0.013	0.018	0.020	0.010

* After frost accumulation of 4 (h) for MT coils and 48 (h) for LT coils;

** Fin thickness: 0.22 (mm) and fin pitch: 118 (fins/m); V_r is the refrigerant volume of the coils (litre).

Table 4.6 shows the geometry of the evaporator coils together with their performance parameters. It can be seen that the physical sizes of the CO_2 evaporator coils are much smaller compared to the R-404A coils.

For the given refrigeration duty, the flooded MT coil with tube diameter 9.52 mm (EC-3) has the smallest size with refrigerant volume about 62% of the MT DX coil with the same tube diameter (EC-1) and about 19% of the refrigerant volume of the R-404A evaporator coil (EC-5). The CO_2 coils also need less refrigerant charge as shown in

Figure 4.8, assuming 25% and 35% of the evaporator volume was filled with liquid for the DX and flooded evaporator coils respectively.

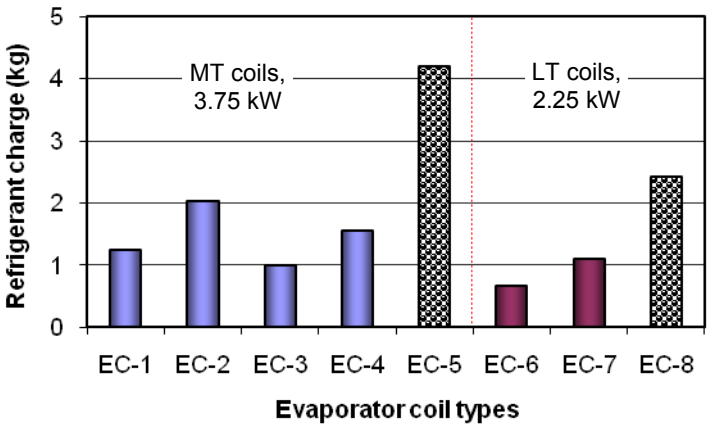

Figure 4.8 Refrigerant charge comparisons

The CO_2 evaporator coils with smaller tube diameter require more tube rows and longer tubes to meet the designed refrigeration duty. Using single circuit arrangement results in high pressure drop particularly for the DX type coils. As can be seen in Table 4.6 the pressure drops of the CO_2 coils (EC-1, EC-3 and EC-6) are higher than the coils with larger tube diameter (EC-2, EC-4 and EC-7) even for the two circuit arrangement. Moreover, the physical size of the coils, except for in the case of the flooded coil EC-3, is larger which will increase their manufacturing cost.

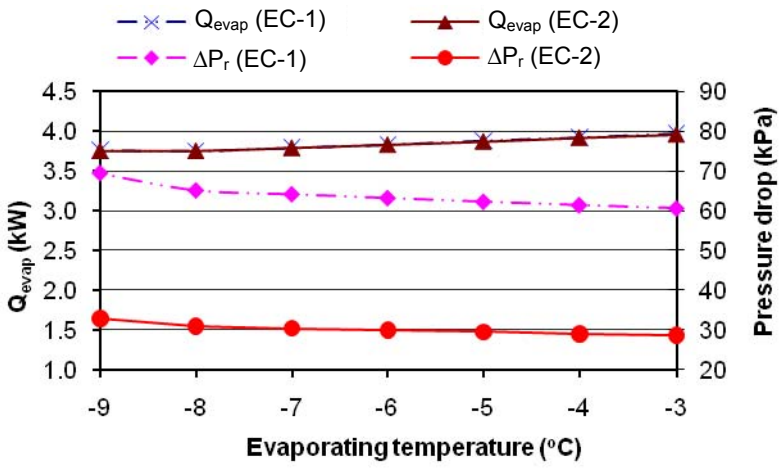

Figure 4.9 The influence of evaporating temperature on the performance of MT DX coils

Figure 4.9 shows the variation of the performance of CO_2 MT DX coils with evaporating temperature. Increasing the evaporating temperature can slightly improve the refrigeration capacity and can reduce the pressure drop. This was also found to apply to LT DX evaporator coils.

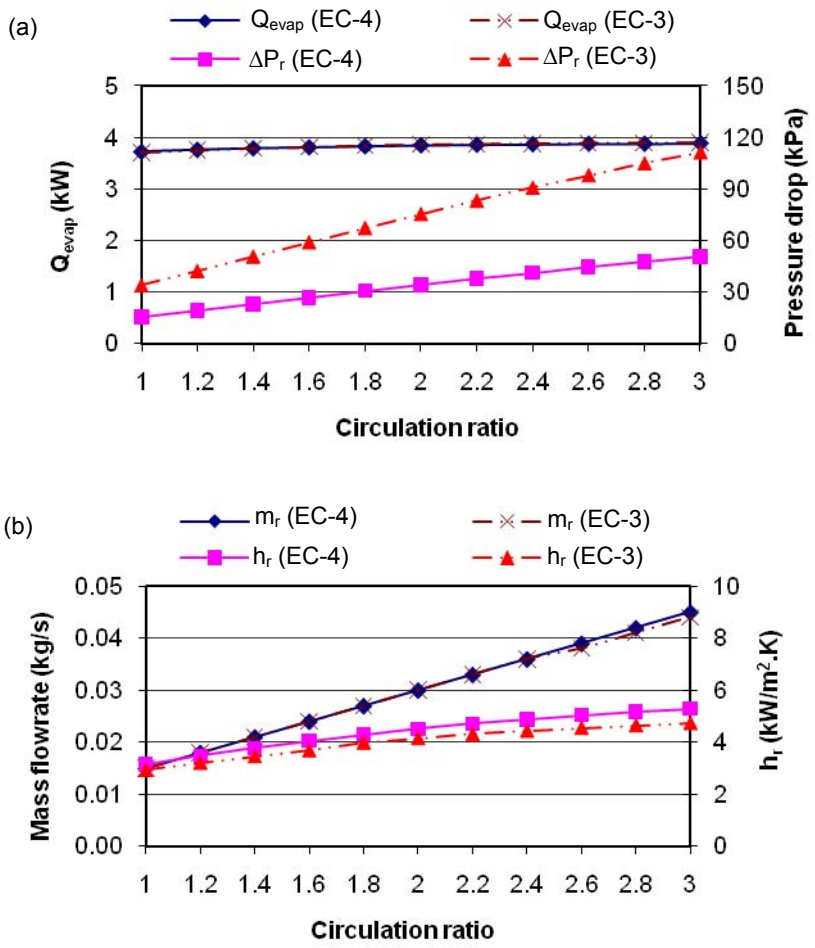

Figure 4.10 The influence of circulation ratio on the performance of the flooded coils

Figure 4.10 shows the performance of the flooded CO_2 evaporator coils at different circulation ratios (*CR*). As the *CR* increases, the refrigeration duty slightly improves due to the enhancement of the evaporation heat transfer coefficient. However, the increase of the *CR* considerably increases the pressure drop and refrigerant mass velocity which increases the power consumption of the CO_2 pump and causes a reduction in the coefficient of performance of the refrigeration system. The *CR*, therefore, should be chosen to be as low as possible in the range of the designed refrigeration capacity. The

experimental tests showed the optimum *CR* to be in the range between 1.1 and 1.3 (Chapter 5).

4.7 Summary

This chapter has detailed numerical models developed for the design of CO_2 evaporator coils. The models have been used to design the evaporator coils of the display cabinets of the test rig. This chapter has also described the validation of the models and their application for design and simulation of finned tube flooded and direct expansion coils with different geometry and circuit arrangements using CO_2 and R-404A as refrigerants. The simulations showed that for a given refrigeration capacity, CO_2 evaporator coils have smaller size and lower refrigerant charge compared to the coils using R-404A refrigerant.

Chapter 5 will present experimental test results for the coils and the whole refrigeration system.

Chapter 5

EXPERIMENTAL TEST RESULTS AND MODEL VALIDATION

This chapter reviews the as-built test facility and reports experimental test results on the performance of volatile medium temperature (MT) CO_2 refrigeration with different circulation ratios and different evaporating temperatures. The performance of low temperature (LT) direct expansion refrigeration as well as the combined MT and LT performance is also considered. This chapter also briefly describes the test conditions and procedure, parameter setting, data collection and processing which includes uncertainty analyses of the test results. Validation of the simulation models is also presented.

5.1 Overview of the as-built test facility

The test facility consists of three main modules: CHP module, absorption refrigeration module and retail refrigeration system module as shown in Figure 5.1. The CHP module is based on an 80 kWe recuperated micro gas turbine generation package with in-built boiler heat exchanger (exhaust heat recovery heat exchanger). The 3-phase electrical power output from the high speed alternator can be modulated in the range 30 kW_e to 80 kW_e.

The absorption refrigeration module currently employed is based on a packaged direct gas fired ROBUR chiller which has been re-engineered to operate with a heat transfer fluid heated by the exhaust gases of the microturbine in the CHP module. The

absorption module was integrated with the CHP module through the in-built boiler heat exchanger and heat transfer fluid (HTF) system (Figure 5.1) to form the trigeneration system.

The capacity of the installed absorption module is about 30% of the possible optimum capacity of the trigeneration system. The refrigeration capacity of the trigeneration system is dependent on the type of thermally driven refrigeration system used. For ammonia-water refrigeration systems providing refrigeration to -10 ^{o}C, the trigeneration system can provide up to 30 kW of refrigeration which recovers approximately 50 kW wasted heat of the CHP module. To achieve this, a new indirectly heated generator was developed and implemented on the absorption chiller. Further performance improvement could be achieved through better integration of the CHP system and absorption chiller to reduce pumping power and pipe heat losses.

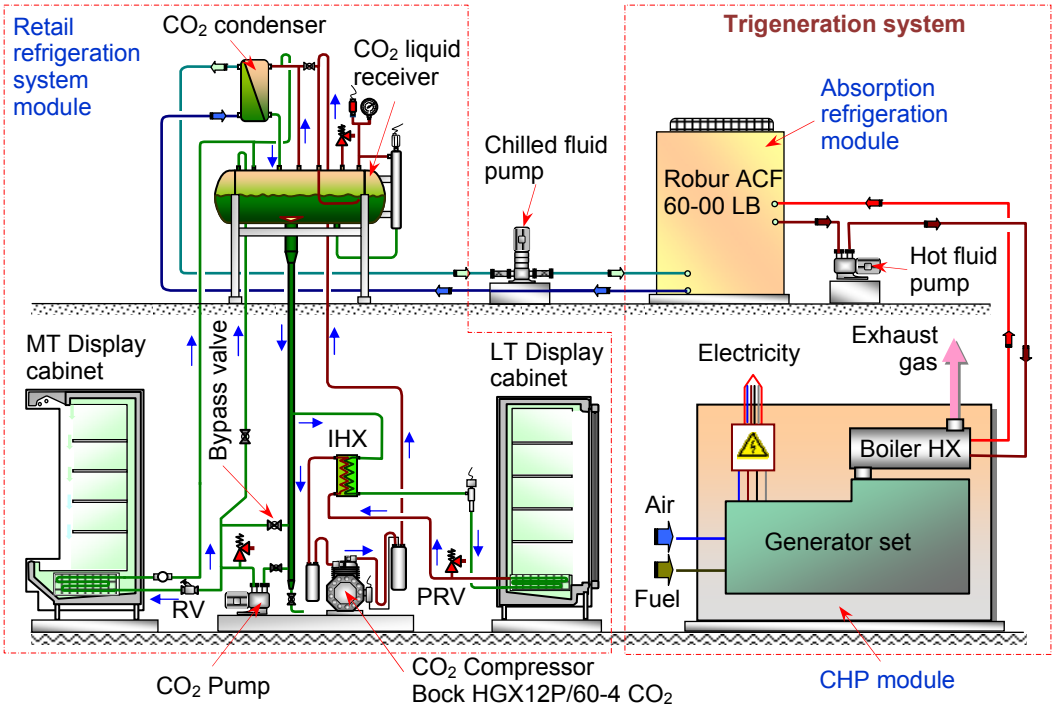

Figure 5.1 Simplified diagram of the integrated volatile-DX CO_2 refrigeration and trigeneration
(Detailed diagram of the integrated system is shown in Figure I-1; Appendix I)

The retail refrigeration system module as shown in Figure 5.2 consists of a cascade volatile MT and direct expansion LT CO_2 refrigeration system and associated test facilities which include an environmental test chamber and chilled and frozen food

display cabinets located in the chamber to provide controlled load to the refrigeration system. The refrigerated display cabinets, chilled open vertical multi-deck, and glass door frozen food which were originally designed with R-404A refrigerant were modified by replacing the evaporator coil and controls, to operate with CO_2 refrigerant. The evaporator coil of the low temperature cabinet is a direct expansion coil whereas the coil of the medium temperature cabinet is a flooded evaporator coil which is designed to operate with CO_2 as a secondary (volatile) refrigerant. Condensation of the CO_2 from both the low and medium temperature sections of the system is provided by the absorption refrigeration system of the trigeneration facility through a CO_2 condenser in the form of a plate heat exchanger. The CO_2 condenser is installed just above the liquid receiver to facilitate the flow of liquid CO_2 from the condenser by gravity. The system was designed so that the CO_2 for the medium temperature cabinet could be either pumped with a centrifugal CO_2 pump or gravity fed to the coil.

(a) CO_2 pump and compressor section

(b) CO_2 condenser and liquid receiver section

(c) MT and LT loading system

Figure 5.2 Retail refrigeration system module with CO_2 refrigeration system

The test facility is equipped with Danfoss controllers and was comprehensively instrumented with power metres, pressure transducers, thermocouples, relative humidity sensors and coriolis refrigerant flow meters to enable detailed investigations of the transient and steady state performance of individual components and the overall system. Monitoring is performed through a data logging system which can scan and store the measured parameters at present time intervals.

5.2 Experimental test conditions and data processing

A series of tests was carried out to evaluate energy performance of the CO_2 refrigeration system which comprised performance of the MT and LT system as well as that of the overall CO_2 refrigeration system. Tests were performed with different circulation ratios (*CR*) and different evaporating temperatures for the MT CO_2 refrigeration system. System performance parameters were recorded and used to determine the refrigeration capacity and coefficient of performance (*COP*) of the LT, MT and overall CO_2 refrigeration system.

5.2.1 Test conditions

The tests on the MT refrigeration system were carried out at three evaporating temperature levels: -6 ^oC, -8 ^oC and -10 ^oC. Each temperature level was tested at different refrigerant mass flow rates or circulation ratios. Tests on the LT circuit and overall system were carried out at circulation ratio *CR* = 1.3, condensing and evaporating temperatures at T_{cond} = -7 ^oC and $T_{evap,LT}$ = -32 ^oC respectively.

The chilled and frozen food display cabinets were placed in the test room as described in Section 3.8 (Chapter 3). The test chamber was conditioned at climate class 3 (25°C and 60% RH). These conditions were measured at a point in the middle of the MT display cabinet 150 mm above and 300 mm in front of the top edge of the cabinet opening. The display cabinets including the product packages and temperature measurement points have been explained in Section 3.4.1 (Chapter 3). On the air side of the MT display cabinet, besides temperatures, the relative humidity (*RH*) of the air-on and air-off the coil was also measured and recorded. The MT and LT cabinets were tested for M1 and L1 classification respectively. An M1 cabinet requires product temperatures ranging from -1 ^oC to +5 ^oC and a cabinet of L1 classification requires the highest temperature of the warmest product to be lower or equal to -15 ^oC and the lowest temperature of this warmest product to be lower or equal to -18 ^oC (ISO 23953-2, 2005).

5.2.2 Experimental test procedure

The test facility was operated according to the mode of tests and following the operational procedure as detailed in Appendix G. In order to investigate the transient performance, the system was monitored from start up to the point it achieved steady

state conditions. Investigations on steady state performance were carried out after the test plant reached the specified steady state conditions.

5.2.3 Operational setting

The control strategy and parameter setting of the test system such as condensing temperature and target pressure (evaporating temperature) have been described in Section 3.5.3 (Chapter 3). For test purposes, steady state conditions and operational parameters of the tests were specified in the controllers as shown in Table 5.1.

Table 5.1 Operational setting of the MT and LT cabinets and the additional load evaporator

Parameters	MT cabinet	LT cabinet	LT additional load
Cut off temperature	-3 °C	-23 °C	-27 °C
Temperature differential	2 K	4 K	4 K
Air-on and air-off weight	100% air-off	50%	100%*
Defrost type	Off-cycle	Electric	N/A
Number of defrost	4 per day	1 per 2 days	N/A
Defrost minimum time	30 minutes	30 minutes	N/A
Defrost termination	7 °C	-4 °C	N/A
Degree of superheat	N/A	5 to 12 K	5 to 12 K

* Water-glycol temperature at the outlet of the evaporator; N/A means not applicable.

5.2.4 Data collection

Measured performance parameters from the instrumentation devices such as temperature, pressure, relative humidity and flow rate were logged by a data logging every 20 seconds. The power consumption of the compressor, pump and controller were measured and recorded every 1 minute. Detailed explanation of the instrumentation, data logging system and the measurement points are given in Section 3.6 (Chapter 3).

5.2.5 Data processing

Collected data were processed in a spread sheet programme. The properties of the refrigerant and humid air were derived from the EES software, while the properties of water-glycol mixture were determined by using the equations from M. Conde Engineering (2002) as described in Appendix B. The energy performance parameters of the refrigeration system were calculated which include refrigeration capacity, power consumption and coefficient of performance (COP). The calculations also involved determination of the circulation ratio and uncertainty analyses of the calculations.

5.2.5.1 Calculation of the refrigeration capacity

The refrigeration capacity of the evaporators of the display cabinets was calculated using the enthalpy difference across the coil and the mass flow rate of refrigerant. For the LT DX evaporator the expansion of the refrigerant was assumed to be isenthalpic. The enthalpy of the refrigerant liquid entering the evaporator, $H_{r,i,LT}$, and the refrigerant vapour leaving the evaporator, $H_{r,o,LT}$, were determined from measurements of temperature and pressure of the refrigerant at inlet of the expansion valve and outlet of the evaporator respectively. For the MT flooded evaporator, the enthalpy of the refrigerant entering the evaporator, $H_{r,i,MT}$, was determined from the MT evaporating temperature and pressure, while the enthalpy of the refrigerant leaving the evaporator, $H_{r,o,MT}$, was determined from the evaporating temperature and vapour quality of the refrigerant at the outlet of the evaporator (x_o), where $x_o = 1/CR$. The calculation of the circulation ratio (CR) is detailed in Section 5.2.5.4. For the LT DX additional load, the refrigeration capacity was calculated from the energy balance between the refrigerant and the water-glycol sides assuming adiabatic heat transfer. The refrigeration capacities of the MT and LT systems were calculated from:

$$Q_{MT} = \dot{m}_{r,MT}\,(H_{r,o,MT} - H_{r,i,MT}) \tag{5.1}$$

$$Q_{LT} = Q_{LT,cab} + Q_{LT,add} \tag{5.2}$$

where:

$$Q_{LT,cab} = \dot{m}_{r,LT}\,(H_{r,o,LT} - H_{r,i,LT}) \tag{5.3}$$

$$Q_{LT,add} = \dot{m}_{w}\,C_{p,w}(T_{w,i} - T_{w,o}) \tag{5.4}$$

$Q_{LT,cab}$ and $Q_{LT,add}$ are the refrigeration capacities of the evaporator of the frozen food display cabinet and additional load respectively; $\dot{m}_w$ is the water-glycol mass flow rate.

5.2.5.2 Power consumption

The total power consumption of the system is the sum of the power consumption of the LT compressor and the power consumption of the CO_2 pump. The power consumption of the LT compressor (W_{comp}) was determined by recording the power when only the LT system was in operation, whereas the power consumption of the CO_2 pump was

determined when only the MT system was in operation. Because the refrigerant flow rate from the pump was partially bypassed to the liquid receiver, the pumping power ($W_{CO2,pump}$) used in the *COP* calculation was assumed to be proportional to the measured refrigerant mass flow rate through the MT evaporator coil.

5.2.5.3 Calculation of the COP

The coefficient of performance (*COP*) of the LT, MT and overall refrigeration system were calculated from the equations described in Chapter 3: (3.15), (3.16) and (3.17) respectively. The COP of the LT system was also compared to the reversed Carnot cycle calculated from:

$$COP_{Carnot} = \frac{T_{evap,LT}}{T_{cond,LT} - T_{evap,LT}} \tag{5.5}$$

where evaporating and condensing temperatures $T_{evap,LT}$ and $T_{cond,LT}$ respectively are in Kelvin (K).

5.2.5.4 Circulation ratio

The flow of CO_2 refrigerant in the MT evaporator coil starts as liquid, gradually evaporates along the coil pipe and then exits the evaporator coil at certain quality (x_o) which is the inverse value of the circulation ratio (*CR*). The circulation ratio, as defined in Section 3.2.1.3 (Chapter 3) can be determined from:

$$CR = \frac{\dot{m}_{r,MT}}{\dot{m}_{vap}} \tag{5.6}$$

where $\dot{m}_{r,MT}$ = total refrigerant mass flow rate in MT evaporator, $\dot{m}_{vap}$ = refrigerant vapour mass flow rate, and CR = 1 occurs when $\dot{m}_{r,MT} = \dot{m}_{vap}$.

In the test system, CR = 1 can be established by adjusting the regulator and bypass valves upstream of the MT evaporator coil while observing the quality of the liquid refrigerant flowing through a sight glass fitted at the outlet of the coil. In order to make the adjustment of the refrigerant flow rate easier, the regulator valve should be installed adjacent to the sight glass as shown in Figure 5.1 and the adjustment should be started from overfeed flow rate so that the liquid refrigerant can be clearly seen in the sight

glass. With the bypass valve slightly open, the regulator valve can be gradually closed until the liquid refrigerant just disappears from the sight glass. The supplied mass flow rate to the evaporator ($\dot{m}_{r,MT}$), can then be measured from the flow meter which is fitted on the liquid line upstream of the MT evaporator coil. The mass flow of refrigerant vapour ($\dot{m}_{vap}$) at a particular evaporating temperature ($T_{evap,MT}$) can be calculated from:

$$\dot{m}_{vap} = \frac{Q_{MT}}{H_{fg}} \tag{5.7}$$

where H_{fg} is the enthalpy of evaporation of the CO_2 refrigerant at evaporating temperature ($T_{evap,MT}$). Q_{MT} is the refrigeration load of the MT cabinet which is equivalent to the heat absorbed from the air crossing the MT coil and can be determined from:

$$Q_{MT} = \dot{m}_a (H_{a,ON} - H_{a,OFF}) \tag{5.8}$$

$\dot{m}_a$ is the mass flow rate of the air flowing through the evaporator coil as a function of air velocity and cross sectional area of the air passage in the cabinet; $H_{a,ON}$ and $H_{a,OFF}$ are the enthalpies of the air entering and leaving the coil respectively.

In a real supermarket application, the circulation ratio can be controlled by integrating the cabinet controller with a motorized valve installed upstream of the evaporator coil and with the speed controller of the CO_2 pump.

5.2.5.5 Uncertainty in the calculation of *CR* and *COP*

Considering the uncertainty of the measured variables which include air mass flow rate, air temperature and relative humidity, refrigerant temperatures, pressures, power and refrigerant mass flowrate and assuming that the individual measurements are uncorrelated and random, the uncertainty in the calculation of *CR* was determined, using the Engineering Equation Solver (EES) software, to be ± 10.8%. The uncertainty in the calculations of the COP_{LT}, COP_{MT}, $COP_{Overall}$ and COP_{Carnot} were found to be ± 0.2% ± 10.8%, ± 3.6% and ± 0.6% respectively. The uncertainty of the COP_{MT} is relatively high because its calculation involved the circulation ratio. Detailed explanation of the uncertainty analysis is given in Appendix J.

5.3 Test results

5.3.1 Thermodynamic cycle of the refrigeration system

Figure 5.3 shows the thermodynamic cycle of the CO_2 refrigeration system obtained from the test results. The cycle refers to the schematic diagram Figure 3.4 (Chapter 3). Pressure drop of MT circuit (9-10-11) was found to be 37.5 kPa which corresponds to 0.5 K temperature drop. The pumping process (9-10) and heat extraction process in the MT cabinet (10-11) can be assumed to be at constant temperature and pressure.

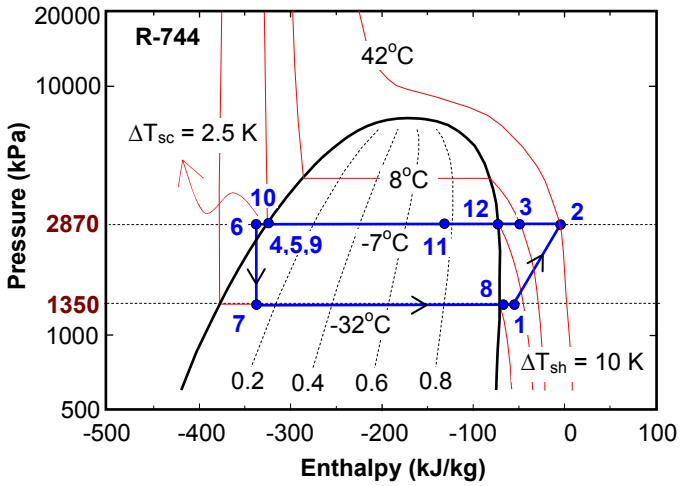

Pressure (kPa) is absolute pressure

Figure 5.3 Pressure-enthalpy diagram of the CO_2 refrigeration cycle based on the test results

Figure 5.3 also shows the LT circuit (1-2-3-4-5-6-7-8) which was integrated with the heat rejection loop of the MT system (12-3-4). The circuit was equipped with an internal heat exchanger (IHX) which exchanged heat from cold stream (8-1) to the hot stream (5-6) of the circuit to provide sub-cooling of around 2.5 K on the CO_2 liquid before being expanded into liquid-vapour mixture through the EXV. This exchanged heat increased the superheat of the CO_2 gas from the LT evaporator (of 5 K superheating at point 8) to be around 10 K superheating (at point 1) before entering the LT compressor. The expansion process in the EXV (6-7) was assumed to be isenthalpic. The compression process (1-2) utilised a semi hermetic reciprocating compressor of isentropic efficiency of around 0.69. This efficiency is discussed further in Section 5.4.

5.3.2 Medium temperature refrigeration system

For the MT CO_2 refrigeration system, investigations were carried out to establish the impact of the circulation ratio on the performance of the coil and the MT CO_2 refrigeration system at different evaporating temperatures. The results showed that the MT system can achieve very high *COPs* ranging from 32 to 60, due to the low power consumption of the CO_2 pump.

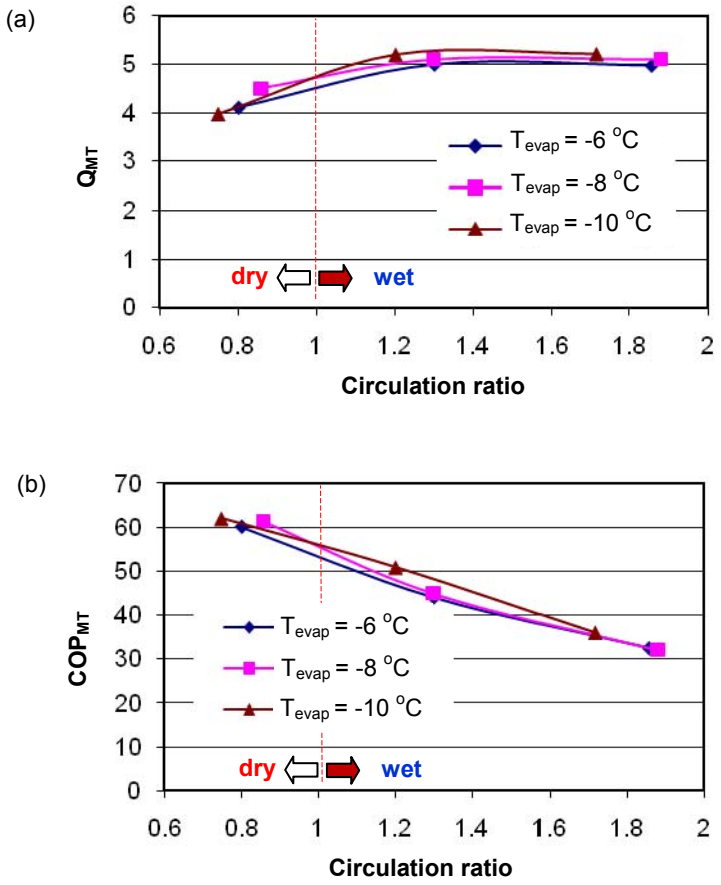

(a) MT refrigeration capacity (b) COP of the MT system

Figure 5.4 Variation of MT refrigeration capacity and COP with circulation ratio for different evaporating temperatures

The COP and refrigeration capacity of the MT refrigeration system vary with circulation ratio and the evaporating temperature as shown in Figure 5.4. Increasing the circulation ratio increases the refrigeration capacity, reaching a maximum at a circulation ratio of 1.3. Because of the increase in pumping power with increasing refrigerant flow rate,

however, the increase in the circulation ratio causes a reduction in the system COP. For the system tested, the optimum *CR* was found to be in the range between 1.1 and 1.3.

Figure 5.4 also shows that at constant circulation ratio, the *COP* slightly increases as the evaporating temperature decreases. This is contrary to what is expected for a direct expansion refrigeration system and can be explained as follows: in a flooded evaporator, reducing the evaporation temperature can improve heat transfer due to the higher temperature difference between the refrigerant and the air. This will enhance the evaporation rate of the refrigerant in the coil which in turn will increase the vapour quality at the exit of the evaporator coil, causing a reduction in the circulation ratio. In order to maintain a constant *CR*, the mass flowrate of refrigerant will have to be increased. This will improve further the heat transfer of the CO_2 refrigerant and will also increase the refrigeration capacity of the evaporator coil which leads to a higher *COP*. These results are in agreement with the results from the flooded evaporator model which have been explained in Section 4.4 (Figure 4.7). For a DX refrigeration system, on the other hand, the refrigeration capacity will decrease when the evaporating temperature reduces. This has been described in Section 4.6 (Chapter 4).

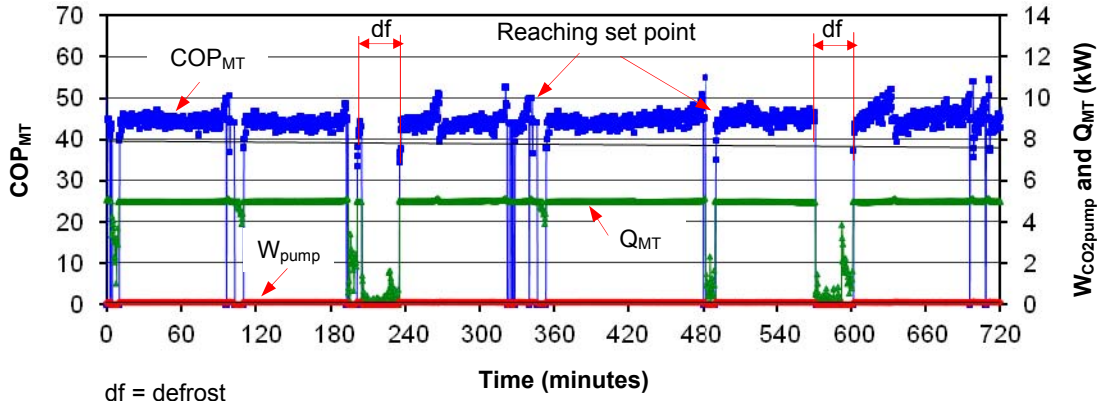

Figure 5.5 Performance of the CO_2 MT refrigeration system
(Investigated at evaporating temperatures of -7 °C and *CR* = 1.3)

The performance of the MT CO_2 refrigeration system with time at circulation ratio *CR* = 1.3 and evaporating temperature -7 °C is shown in Figure 5.5. From the figure it can be seen that the MT system consumes very low pump power of 0.110 kW in average. The *COP* of the MT system which was calculated as the ratio of the cooling done by the

evaporator coil to the pump power consumption was around 45.4. The MT system delivers an average refrigeration capacity of 4.9 kW.

Figure 5.5 also shows the pump cycling off in response to: i) the cabinet coil air-off temperature which was set at -3 ^{o}C and; ii) during the defrost cycle. For the MT system, the off-cycle defrost control was set at 4 defrost cycles per 24 hour period. Defrost termination was controlled on coil air-off temperature of 7 ^{o}C or elapsed time of 30 minutes whichever was reached first.

5.3.3 Low temperature refrigeration system

Figure 5.6 shows performance of the LT CO_2 refrigeration system with time at condensing temperature -7 ^{o}C and evaporating temperature -32 ^{o}C. It can be seen that the LT system can deliver a steady state *COP* of 4.0 with refrigeration capacity (Q_{LT}) of about 10 kW.

Figure 5.6 also shows the compressor cycling off when the air temperature in the cabinet reaches the set point. Defrost cycle of the LT cabinet, however, could not be seen within this test period because the electric defrost of the cabinet was set for 30 minutes every 48 hours. These defrost control settings were found to be satisfactory for the conditions tested.

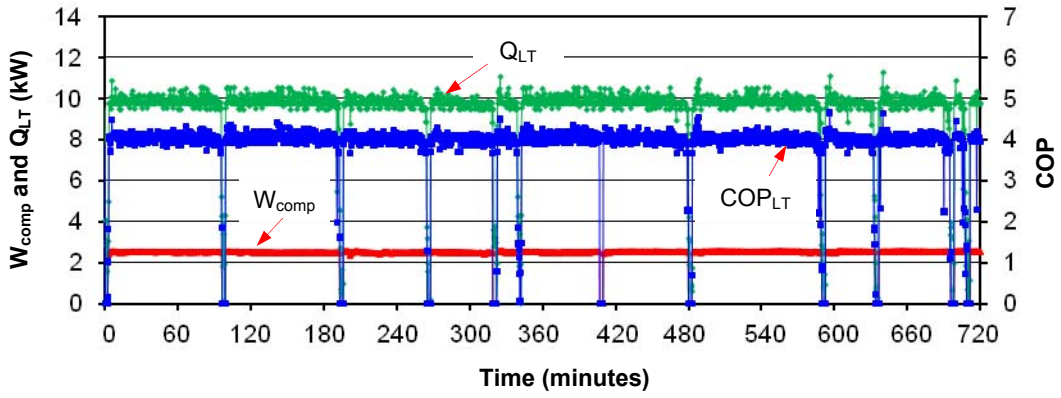

Figure 5.6 Performance of the CO_2 LT refrigeration system
(Investigated at condensing and evaporating temperatures of -7 ^{o}C and -32 ^{o}C)

The variation of evaporating and condensing temperatures of the LT system is shown in Figure 5.7. The evaporating temperature was measured at inlet to the LT evaporator just after the expansion valve, while the condensing temperature was measured at the outlet

of the condenser. The average evaporating and condensing temperatures were -32 °C and -7 °C respectively with average measured pressures of 12.5 bar and 27.7 bar. Figure 5.7 also shows the average reversed Carnot COP of the LT system to be around 9.6. The actual COP is less than half of the Carnot COP due to irreversibilities of expansion and compression processes in the actual cycle as well as electrical, mechanical and volume losses from the compressor.

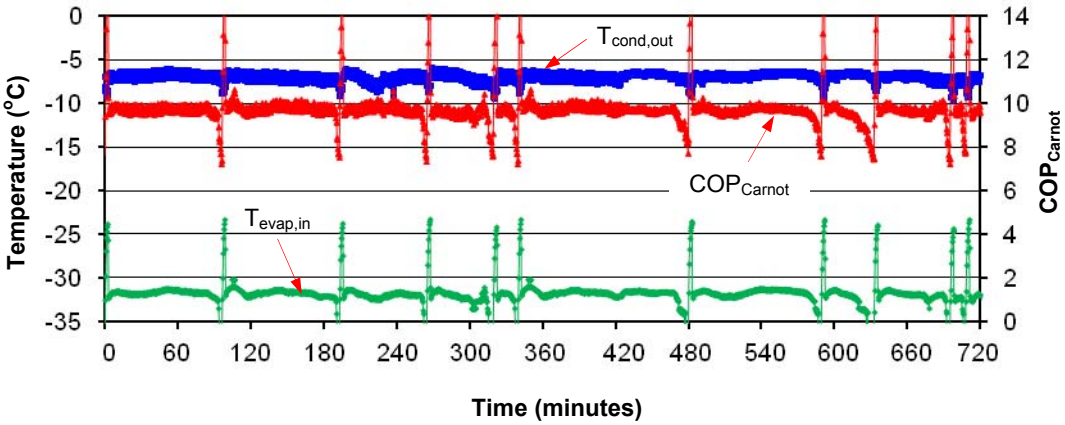

Figure 5.7 Evaporation and condensing temperatures including theoretical COP of the LT system

5.3.4 Overall refrigeration system

Figure 5.8 shows the performance of the MT and LT refrigeration systems and the combined performance of the MT and LT circuits at an evaporating temperature of -7 °C for the MT system and -32 °C for the LT system and a circulation ratio for the refrigerant in the MT evaporator coil of 1.3.

From Figure 5.8 it can also be seen that the average overall *COP* of the CO_2 refrigeration system, MT and LT, varied in the range between 5.5 and 6. The total refrigeration load for the system was 15 kW of which 5 kW was for the MT system and 10 kW for the LT system. In supermarkets the LT load is normally between 20% and 30% of the MT load but in the experimental facility the balance of load for the MT and LT systems was decided by the availability of compressors at the time the facility was constructed. A change in the load balance between the LT and MT to better reflect the actual load balance in a supermarket would have resulted in an even higher overall *COP* for the system.

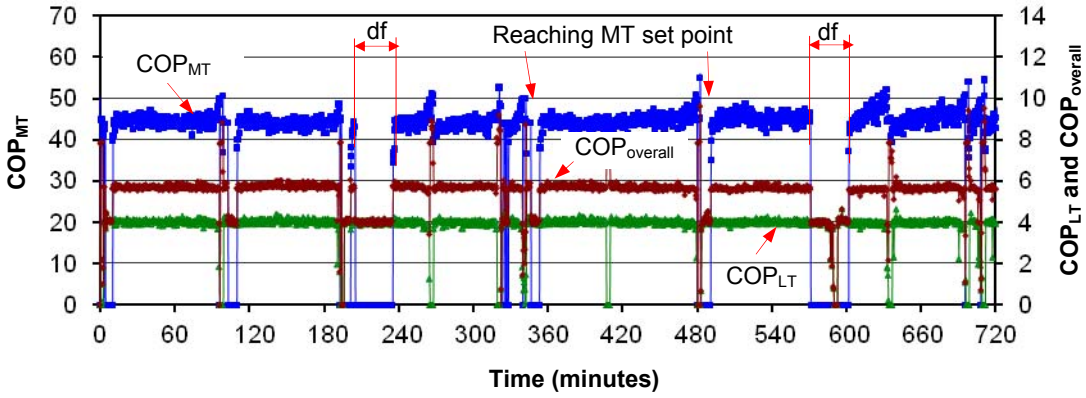

Investigated at circulation ratio of 1.3, condensing and evaporating temperatures of -7 °C and -32 °C; df = defrost

Figure 5.8 Performance of the CO_2 MT and LT refrigeration systems

5.3.5 Product and air temperatures

Product and air temperatures of the MT and LT cabinets were used as a measure of establishing whether the CO_2 refrigeration system had reached steady state condition. When the product temperatures of the MT and LT cabinet were relatively stable in the range M1 and L1 temperature classifications (as specified in Section 5.2.1) respectively, the MT and LT systems were considered to have reached steady state conditions. These conditions were used for the analysis of the CO_2 refrigeration cycle performance as described in the previous sections.

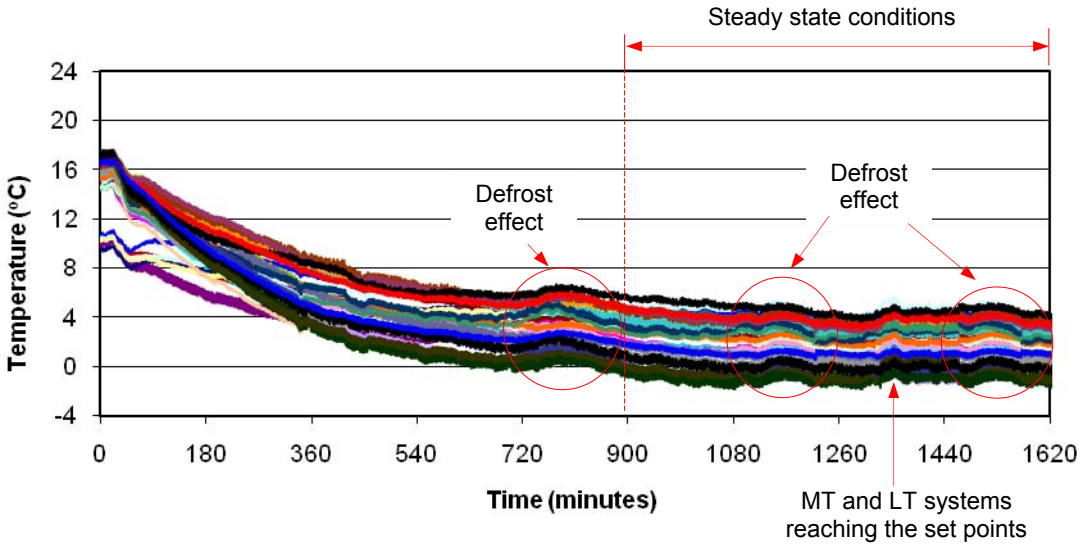

Figure 5.9 Variation of the MT product temperatures with time
(Investigated at circulation ratio of 1.3 and evaporating temperatures of -7 °C)

Figure 5.9 shows product temperature variation of the MT cabinet which includes cooling down and steady state period. These results were obtained with a circulation ratio CR = 1.3 and evaporating temperature $T_{evap,MT}$ = -7 °C. From the figure, it can be seen that the product temperatures can reach the M1 temperature range in 15 hours. The figure also shows that the product temperatures increase during the defrost cycle and when the cabinet reaches the set point.

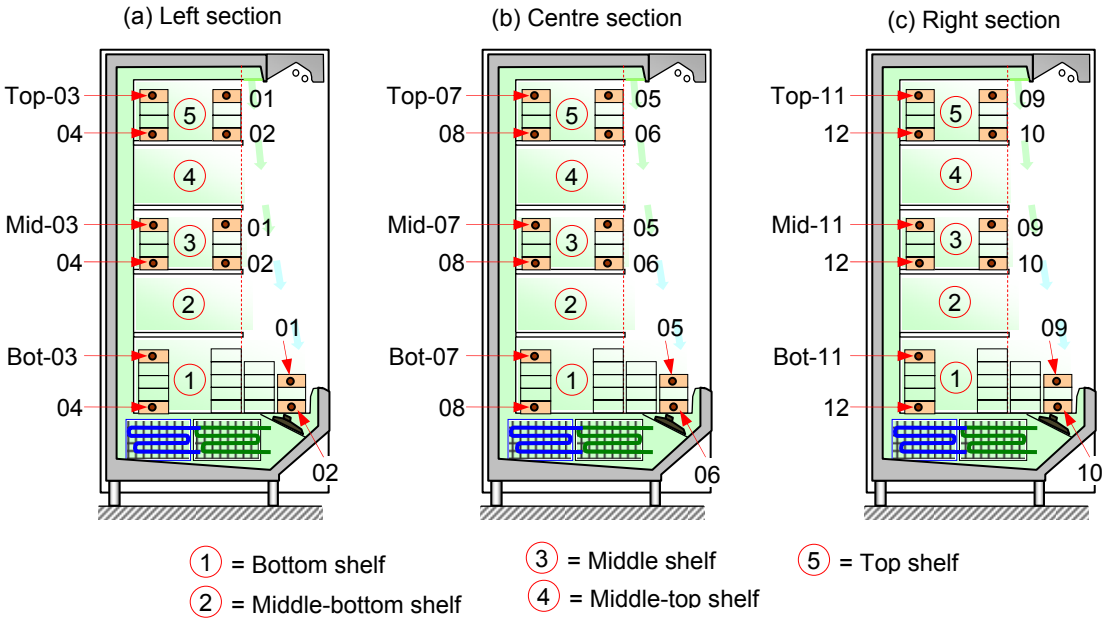

Figure 5.10 Positions of the product temperature measurements for the MT cabinet

The positions of product (M-package) temperature measurements for the MT cabinet are given in Figure 5.10. Mean, maximum and minimum temperatures of the M-packages at all measured positions during the steady state period of 12 hours are presented in Table 5.2. The product temperatures are grouped according to their positions on the shelves: top, middle and bottom. It can be seen that all measured product temperatures are within M1 classification ranging from +5 °C to -1 °C. The products on the middle shelf have the lowest arithmetic mean temperature (AMT) and the bottom shelf has the highest AMT. The maximum MT product temperature was found to be 5.3°C. This product is located on the bottom shelf at position Bot-10 (Figure 5.10). The overall AMT of the MT products was found to be 1.9 °C (Table 5.2).

Table 5.2 Mean, maximum and minimum temperatures of the MT products

Measured positions	Max.	Min.	Mean	Measured positions	Max.	Min.	Mean	Measured positions	Max.	Min.	Mean
Top-01	3.8	1.8	2.9	Mid-01	2.1	0.5	1.2	Bot-01	2.1	1.0	1.6
Top-02	3.7	1.8	2.8	Mid-02	2.3	0.8	1.5	Bot-02	2.8	1.8	2.3
Top-03	0.1	-1.4	-0.5	Mid-03	-0.4	-1.3	-0.9	Bot-03	-0.2	-1.2	-0.7
Top-04	1.0	-1.2	-0.1	Mid-04	0.0	-1.2	-0.5	Bot-04	2.0	0.6	1.3
Top-05	4.7	2.7	3.9	Mid-05	4.1	2.7	3.5	Bot-05	2.9	1.6	2.3
Top-06	4.4	2.8	3.6	Mid-06	3.4	2.1	2.8	Bot-06	4.8	3.4	4.2
Top-07	0.3	-0.8	0.1	Mid-07	0.5	-1.1	-0.2	Bot-07	1.8	0.7	1.3
Top-08	0.8	-0.8	0.0	Mid-08	0.6	-0.8	-0.1	Bot-08	4.0	2.7	3.4
Top-09	5.1	3.6	4.5	Mid-09	4.1	2.9	3.6	Bot-09	4.5	3.4	4.0
Top-10	4.4	3.1	3.8	Mid-10	2.8	1.6	2.2	Bot-10	5.3	4.0	4.7
Top-11	5.0	0.4	2.4	Mid-11	1.6	0.1	0.8	Bot-11	2.5	1.2	1.9
Top-12	1.4	0.5	1.0	Mid-12	1.0	-0.2	0.4	Bot-12	4.0	2.8	3.3
AMT of the top shelf			2.0	AMT of the middle shelf			1.2	AMT of the bottom shelf			2.5
AMT overall of the MT products											**1.9**

AMT = average mean temperature; Bot = bottom shelf; Mid = middle shelf; Top = top shelf; Max. = maximum temperature; Min. = minimum temperature. Measured positions of the MT products refer to Figure 5.10

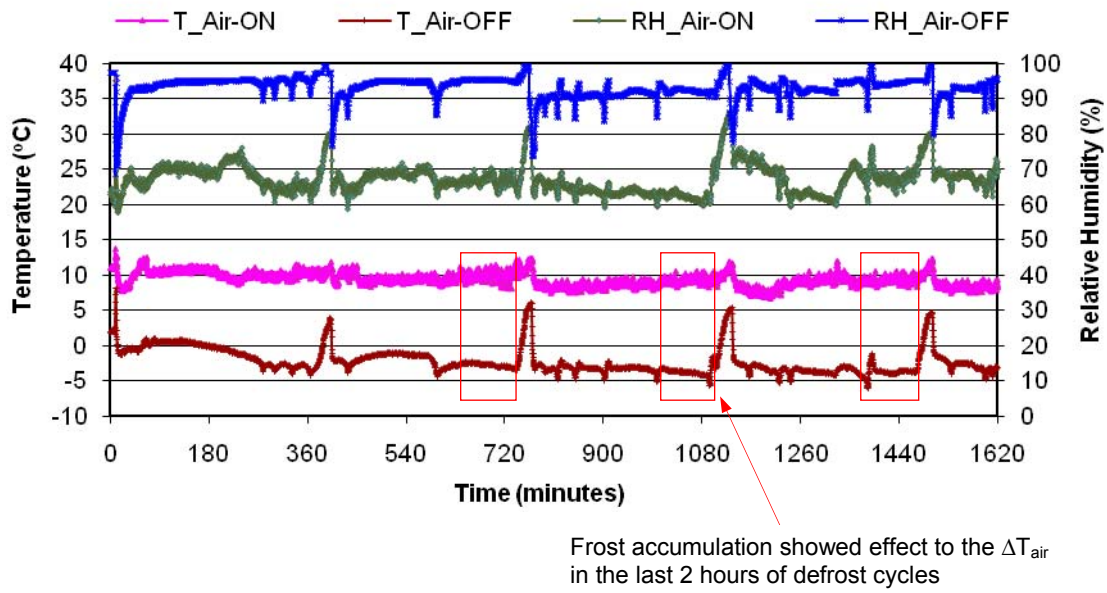

Figure 5.11 Variation of air temperatures and RHs of the MT cabinet

Variations for air temperature entering the MT evaporator coil (air-on) and leaving the coil (air-off) are shown in Figure 5.11. The temperatures are average of three point measurements measured at the right, centre and left hand side of the air passage of the MT cabinet before and after the evaporator coil. It can be seen that the air temperatures vary periodically during the test due to the defrost cycle. The temperature difference

between the air-on and air-off is approximately 10 °C after start up and just after defrost. The temperature difference starts to increase after 4 hours from defrost and reaches more than 12 °C just before the next defrost cycle.

Figure 5.11 also shows the variation of relative humidity (*RH*) at evaporator coil air-on and air-off measured at the centre section of the MT cabinet. It can be seen that the relative humidity of the air-on and off tends to equalise during the defrost cycle when refrigerant is not flowing through the coil. During the cooling cycle the difference between the *RH* value on and off the coil tends to increase with frost accumulation on the coil and reaches maximum just before defrost.

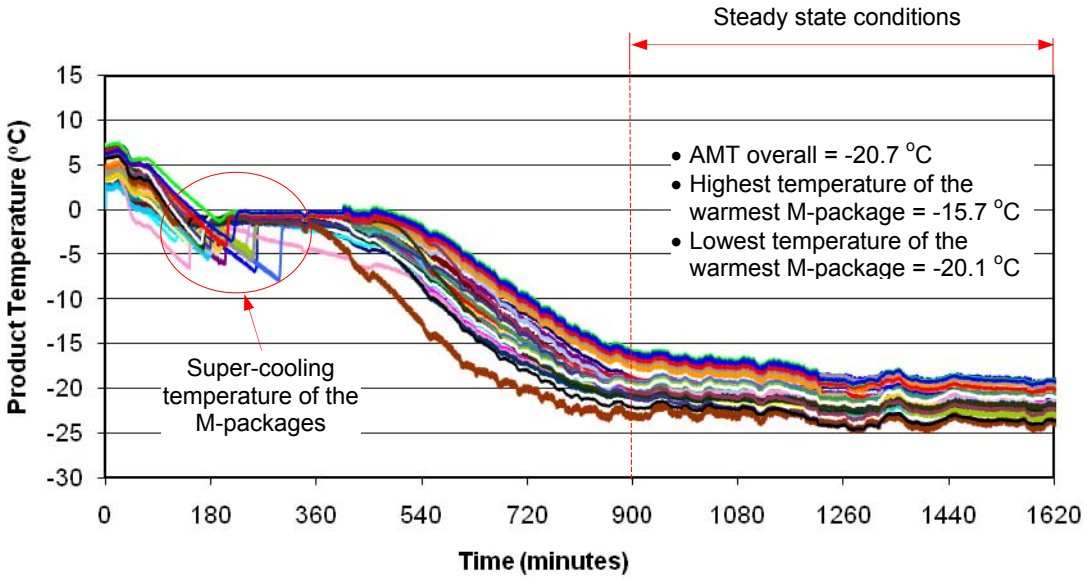

Figure 5.12 Variation of the LT product temperatures with time
(Investigated at condensing and evaporating temperatures of -7 °C and -32 °C respectively)

Figure 5.12 shows the variation of the product temperatures of the LT cabinet. The results were obtained at evaporating and condensing temperatures -32 °C and -7 °C respectively and with the doors of the cabinet closed. The temperatures reached the L1 temperature classification (below -15 °C) in 15 hours. At a stable condition, the difference between the maximum and minimum product temperatures was about 5 °C. Figure 5.12 also shows the super-cooling behaviour of the M-packages when their temperatures first dropped below their freezing point of -1 °C.

Positions of the measured product (M-packages) for the LT cabinet are shown in Figure 5.13. Detailed results of the LT product temperature measurements which include

maximum, minimum and mean temperatures are presented in Table 5.3. It can be seen that all of the measured temperatures were in the range of L1 classification. The highest product temperature was on the top shelf at position Top-11.

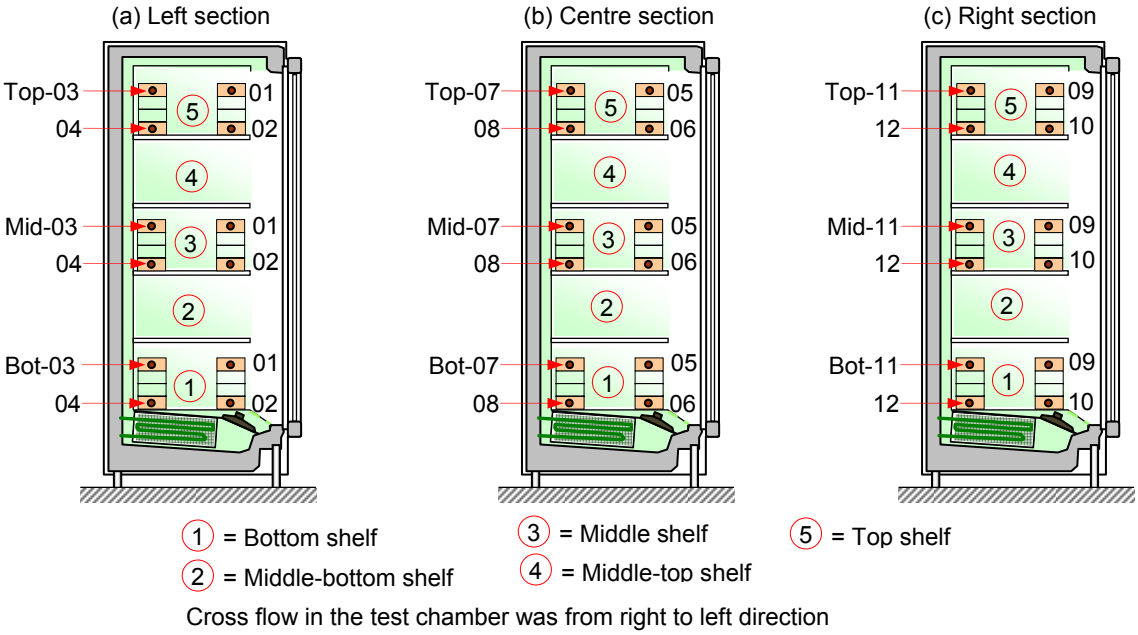

Figure 5.13 Positions of the product temperature measurements for the LT cabinet

Table 5.3 Mean, maximum and minimum temperatures of the LT products

Measured positions	Max.	Min.	Mean	Measured positions	Max.	Min.	Mean	Measured positions	Max.	Min.	Mean
Top-01	-20.3	-22.6	-21.6	Mid-01	-19.2	-22.9	-20.9	Bot-01	-18.8	-22.0	-20.8
Top-02	-19.4	-21.5	-20.4	Mid-02	-19.9	-23.1	-21.2	Bot-02	-19.3	-22.0	-20.7
Top-03	-20.7	-22.8	-21.9	Mid-03	-18.4	-22.1	-20.3	Bot-03	-20.5	-23.3	-22.1
Top-04	-20.3	-22.3	-21.4	Mid-04	-18.4	-22.6	-20.6	Bot-04	-19.8	-22.9	-21.6
Top-05	-21.5	-24.9	-23.4	Mid-05	-18.4	-23.2	-20.9	Bot-05	-19.2	-23.4	-21.5
Top-06	-19.8	-23.6	-21.8	Mid-06	-20.4	-23.2	-21.8	Bot-06	-19.6	-23.0	-21.5
Top-07	-20.7	-24.6	-22.9	Mid-07	-18.7	-23.6	-21.1	Bot-07	-18.8	-22.6	-20.6
Top-08	-21.3	-24.6	-23.0	Mid-08	-17.1	-22.8	-20.2	Bot-08	-19.2	-23.7	-21.5
Top-09	-19.0	-22.1	-20.6	Mid-09	-17.3	-20.4	-19.0	Bot-09	-17.9	-21.5	-19.3
Top-10	-16.4	-20.0	-18.5	Mid-10	-16.5	-20.3	-18.4	Bot-10	-18.6	-21.4	-20.2
Top-11	**-15.7**	**-20.1**	-18.2	Mid-11	-16.1	-20.2	-18.6	Bot-11	-18.4	-21.2	-19.9
Top-12	-16.0	-19.8	-18.2	Mid-12	-16.8	-20.1	-18.6	Bot-12	-19.5	-22.4	-21.1
AMT of the top shelf			-21.0	AMT of the middle shelf			-20.1	AMT of the bottom shelf			-20.9
AMT overall of the LT products											**-20.7**

AMT = average mean temperature; Bot = bottom shelf; Mid = middle shelf; Top = top shelf; Max. = maximum temperature; Min. = minimum temperature.
Measured positions of the LT products refer to Figure 5.13.

Figure 5.14 shows the temperature variation of the air-on and air-off the LT evaporator coil. These temperatures were the averages of three measurements on the right, centre and left sections of the LT cabinet before and after the evaporator coil. The fluctuations in the temperatures that can be observed are due to the closure of the expansion valve which switched the flow of refrigerant off when the cabinet set point temperature was reached. At steady state conditions the difference in temperature between air-on and air-off the coil was around 8 ^{o}C. The figure also presents the variation of the relative humidity on and off the coil measured at the centre section of the LT cabinet. During steady state conditions, the difference between the air-on and air-off relative humidity was approximately 25%.

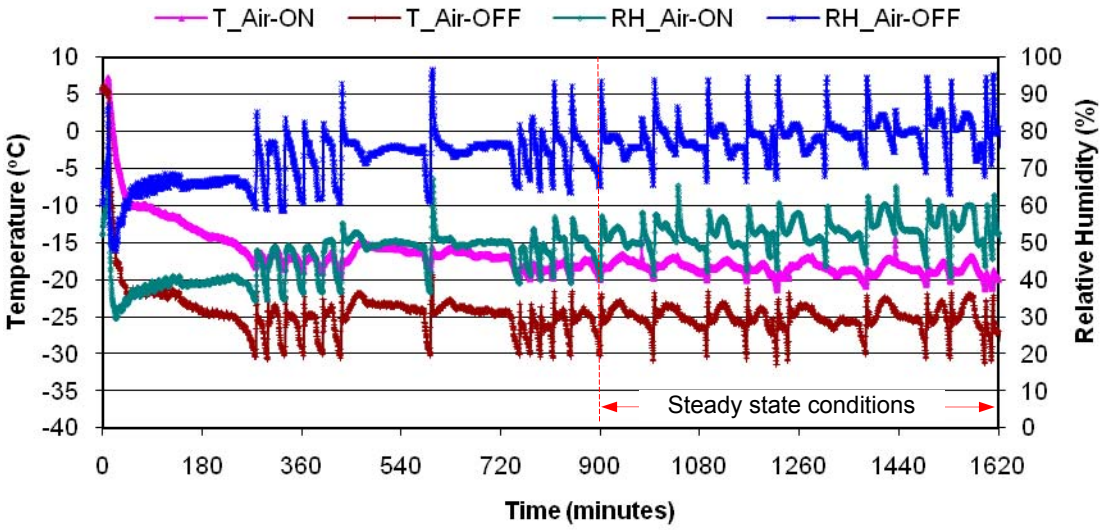

Figure 5.14 Variation of air temperatures and RHs of the LT cabinet

5.3.6 Frost performance of the CO_2 display cabinets

Excessive frost on the surface of the evaporator coil will reduce the air circulation in the cabinet and cause an increase in the product temperature especially in the case of the MT cabinet as previously described. Figure 5.15 shows the accumulation of frost on the surface of the MT evaporator coil after 4 hours from defrost. It can be seen that frost accumulation was fairly uniform across the coil surface.

The amount of frost accumulated on the surface of the MT evaporator coil was measured by collecting the drained water from the cabinet during the defrost cycle. The results are shown in Figure 5.16a. These measurements were taken at different

evaporating temperatures and refrigerant circulation ratios. For these tests, the defrost cycle of the MT cabinet was set at 6 cycles per day (24 hours period). It can be seen that the frost accumulation increases when the evaporating temperature decreases. At evaporating temperature -6 ^{o}C, the frost accumulation was about 4.3 kg and increased to 5.1 kg when the evaporating temperature was reduced to -10 ^{o}C. The circulation ratio, however, did not have a significant effect on the frost behaviour of the cabinet. The amount of frost accumulated on the surface of the MT coil remained relatively constant when the circulation ratio increased from 1.2 to 1.9.

(a) Coil surface with frost

(b) Coil surface without frost

Figure 5.15 MT evaporator coil with frost accumulations and without frost
(Taken 4 hours after defrost at evaporating temperature -7 ^{o}C)

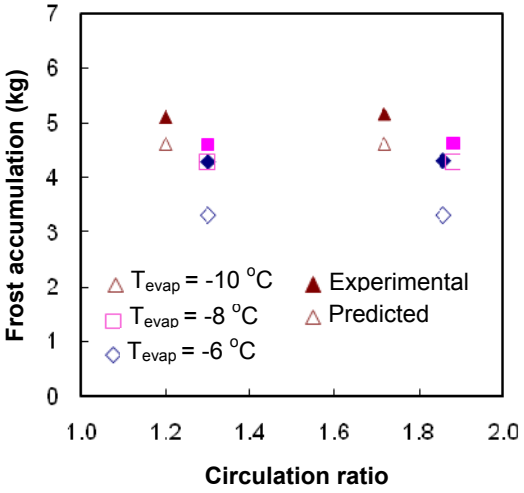

(a) Variation of frost accumulation with circulation ratio and evaporating temperature

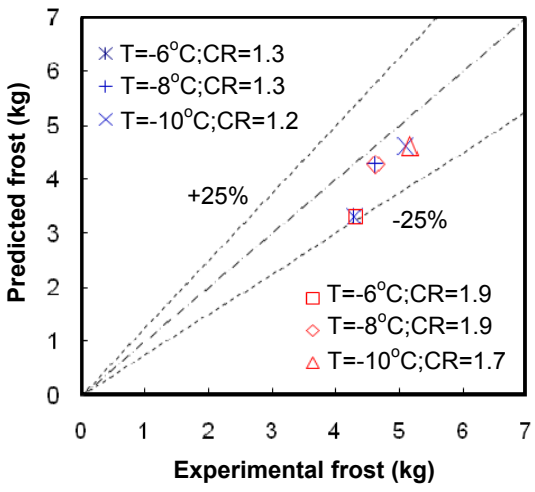

(b) Comparison between experimental and predicted frost accumulation

Figure 5.16 Predicted and experimental frost accumulation on the flooded MT evaporator coil for 4 hours defrost cycles

Figure 5.16a also shows the predicted frost accumulation determined from the evaporator model. It can be seen that the predictions from the model are slightly lower than the experimental test results and lie in the range between 0% and -25% (Figure 5.16b). The difference may be due to measurement of the relative humidity at only a single point whereas in practice the RH value may vary along the face of the coil and uncertainties in other measurements such as the amount of condensate after defrost.

5.4 Validation of the analytical results

The experimental test results were used to validate the numerical model. The validation includes comparison between predicted parameters and the experimental results. The performance parameters used for the validation were isentropic efficiency of the LT compressor and COP of the CO_2 refrigeration system which comprises COP_{MT}, COP_{LT} and $COP_{overall}$.

Figure 5.17 shows the variation of experimental isentropic efficiency of the LT compressor together with the results from the model at an evaporating temperature of -32 ^{o}C and condensing temperature of -7 ^{o}C. The average isentropic efficiency of the LT compressor determined from the test was to be around 0.69. This was slightly lower than the average isentropic efficiency predicted by the model which was around 0.72.

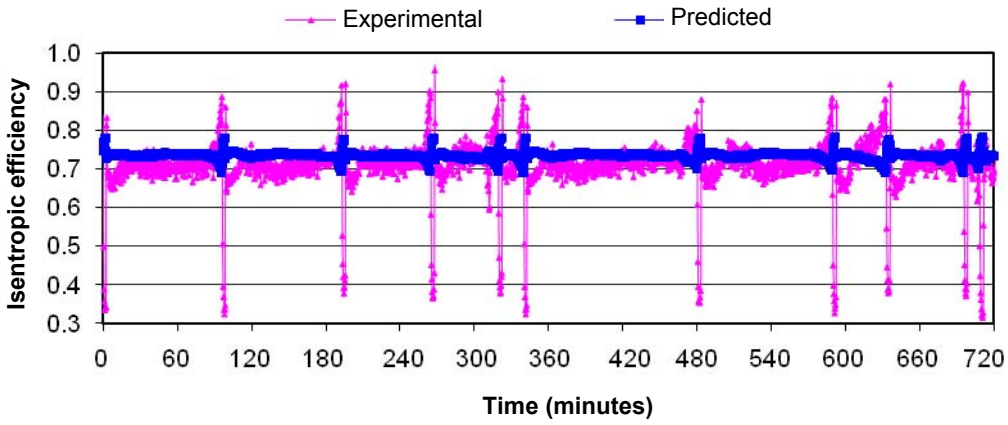

Figure 5.17 Isentropic efficiency of the LT compressor
(Evaporating temperature -32 ^{o}C and condensing temperature of -7 ^{o}C)

Comparisons of the predicted and experimental coefficient of performance of the CO_2 refrigeration system are shown in Figures 5.18, 5.19 and 5.20. Figure 5.18 shows the

comparison for the COP_{MT} at evaporating temperature -7 °C and circulation ratio *CR* = 1.3. The number of data points used for the comparison was 2160. All of the data points fall within ± 25% and 85.5% within ± 20%.

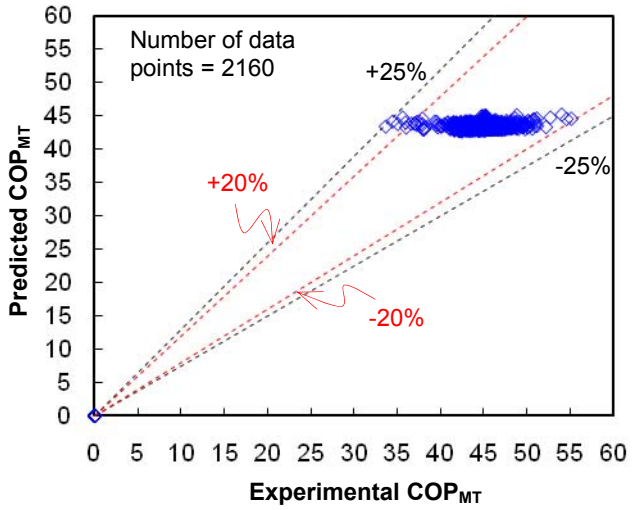

Figure 5.18 Comparison between the predicted and actual COP of the MT system
(Evaporating temperature, $T_{evap,MT}$ = -7 °C and *CR* = 1.3)

Figure 5.19 presents comparison of the experimental and predicted COP_{LT} at evaporating temperature -32 °C and condensing temperature -7 °C. It can be seen that 100% of the predicted COP_{LT} data points fall within ± 20% of the experimental values.

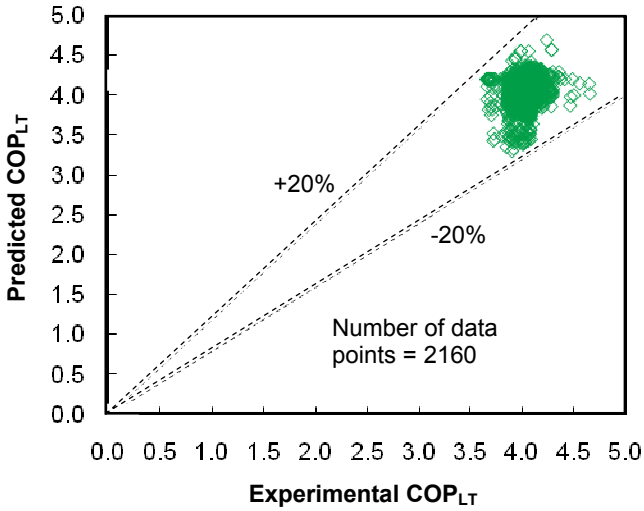

Figure 5.19 Comparison between the predicted and actual COP of the LT system
(Evaporating and condensing temperatures, $T_{evap,LT}$ = -32 °C and T_{cond} = -7 °C)

Figure 5.20 shows comparison of the actual and predicted overall COP of the CO_2 refrigeration system. It can be seen that the predicted overall COP values are within ± 20% of the experimental data.

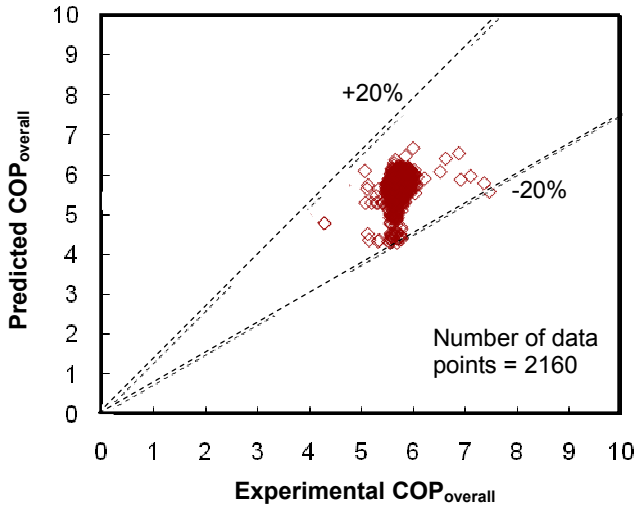

Figure 5.20 Comparison between the predicted and actual overall COP of the CO_2 system ($T_{evap,MT}$ = -7 °C; *CR* = 1.3; $T_{evap,LT}$ = -32 °C and T_{cond} = -7 °C)

The predicted COP_{MT}, COP_{LT} and $COP_{overall}$ have mean error value of 3.25%, 3.53% and 6.18% respectively. This indicates that the numerical model can predict the performance of the refrigeration system quite accurately. Statistical analysis of the predicted COP_{MT}, COP_{LT} and $COP_{overall}$ is given in Table 5.4.

Table 5.4 Statistical analysis of the predicted COP of the CO_2 refrigeration system

Parameters	Number of data points	Percentage of predicted points within ± 20%	Mean error (%)	Standard deviation of the error (%)
COP_{MT}	2160	85.5	3.25	3.76
COP_{LT}	2160	100	3.53	2.61
$COP_{overall}$	2160	100	6.18	3.89

$$Error = \frac{predicted - measured}{measured} \; x \; 100\%$$

5.5 Summary

This chapter has briefly reviewed the test facility of the integrated trigeneration and CO_2 refrigeration system and has reported the experimental test results which include the

performance of volatile medium temperature (MT) CO_2 refrigeration, low temperature (LT) direct expansion refrigeration and the overall CO_2 refrigeration system. This chapter has also described temperature and frost performance of the CO_2 display cabinets and validation of the numerical models including statistical analysis of the predicted performance parameters.

Chapter 6 will present a case study of the application of the integrated trigeneration and CO_2 refrigeration system in a supermarket. The approach covers simulation studies that investigate the seasonal energy and environmental performance of the integrated trigeneration and CO_2 refrigeration system arrangement.

Chapter 6

ANALYSIS OF THE INTEGRATED SYSTEM IN A SUPERMARKET APPLICATION: A CASE STUDY APPROACH

This chapter presents results of simulation studies that investigate the seasonal energy and environmental performance of integrated trigeneration and CO_2 refrigeration system in a case study supermarket. The trigeneration system considered is as described in Chapter 3. For comparison purposes, the energy and environmental performance of the case study supermarket with a conventional energy and refrigeration systems using R-404A refrigerant is also presented.

6.1 The case study supermarket

The supermarket considered in the study is a medium size store with a net sales area of 4,700 m^2 and a gross area of 7,290 m^2. The store is located at Cheetham Hill in Manchester. It was developed as an environmental format store to reduce the carbon footprint by integrating energy efficiency initiatives such as: mixed mode ventilation with roof mounted wind-catchers, building fabric improvement and lighting scheme incorporating day-lighting. The store also uses a cascade transcritical CO_2 refrigeration plant and

Figure 6.1 The case study supermarket
(Source: Besant-Roberts, 2009)

bio-fuel engine based CHP. All refrigerated display cabinets in the store, both chilled and frozen food employ glass doors (Campbell and Riley, 2009). A photograph of the store is shown in Figure 6.1.

From half hourly monitoring data in 2009, the annual electricity consumption of the store was 2,731 MWh with peak and average demand of 463 kW_e and 312 kW_e respectively, while gas consumption was 874 MWh with peak demand during the winter time of 492 kW. Annual average gas consumption was 100 kW. There was also a significant variation between daytime and night time electrical and gas energy consumption. Figure 6.2 shows the daily variation of the electricity and gas consumptions rate of the store.

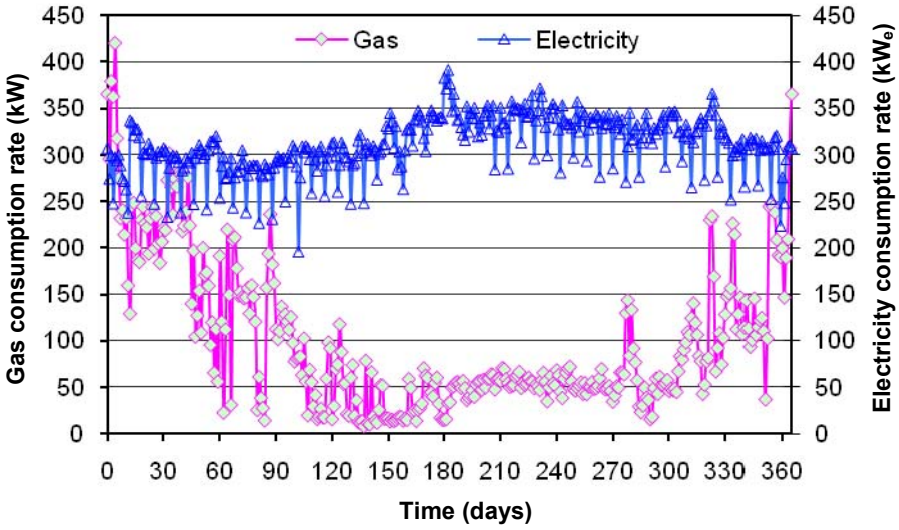

Figure 6.2 Daily average of the energy consumption rate of the case study supermarket
(Data source: Tesco, 2009)

Figure 6.3 shows the daily variation of energy rate demand of the case study supermarket during a whole year. The cooling energy demand is for air conditioning in the summer and was found to be 202 MWh with peak cooling demand of 210 kW_{th}. Heating is mainly used for space heating with only a very small proportion for domestic hot water. The annual heat energy demand was found to be 706 MWh with peak and average demand of 398 kW_{th} and 81 kW_{th} respectively. It can be seen from Figure 6.3 that there is a large variation of heat demand during the year with maximum in the winter months and minimum, of the order of 50 kW_{th}, in the summer months. The

heating demand was calculated from the gas consumption assuming thermal efficiency for the gas boilers of 80.8% (Tesco, 2009).

Refrigeration demand is fairly constant all year round, as the sales area is air conditioned and the store uses glass door chilled and frozen food display cabinets. Annual refrigeration demand was 1,761 MWh, 25% of which was for LT refrigeration and the reminder for MT refrigeration. Hourly MT and LT refrigeration load was 152 kW_{th} and 49 kW_{th} respectively.

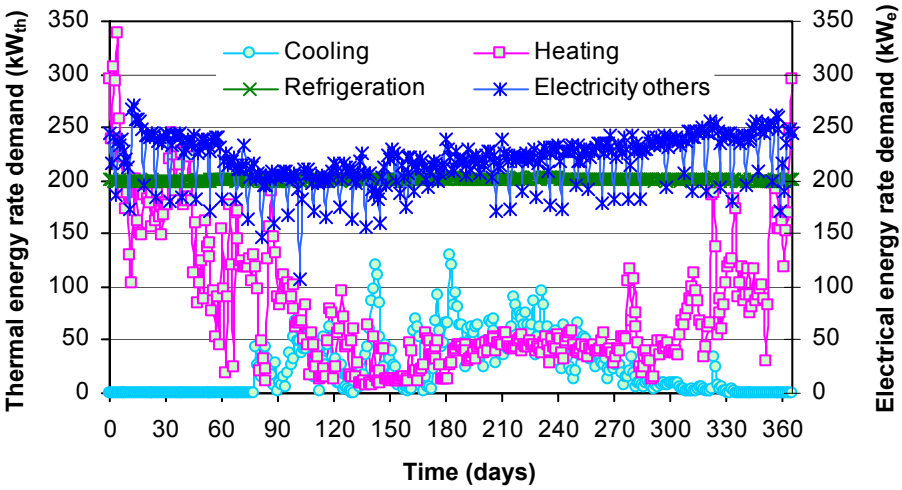

Electricity others = electrical energy rate demand excluding electricity consumed by food refrigeration equipment and refrigeration system for the HVAC plant

Figure 6.3 Daily average energy rate demand of the case study supermarket

Electrical energy demand (electricity others) is all the electricity consumed by the store excluding that used to drive food refrigeration equipment and the refrigeration system for the HVAC plant. Annual electrical energy demand for this was 1,923 MWh which accounted for 70.4% of total electricity of the store.

Electrical energy rate demand is higher in the winter months. This is because the electrical energy consumption for lighting is high in the winter and lower in the summer because the store utilises day-lighting which reduces the use of electrical energy for this service. The electricity consumption rate for the other services such as: preparation, food and services (PFS); HVAC equipment excluding electric chiller; display cabinets; and miscellaneous equipment is relatively constant over the year. Daily average of the electrical energy consumption rate of all services is shown in Figure 6.4.

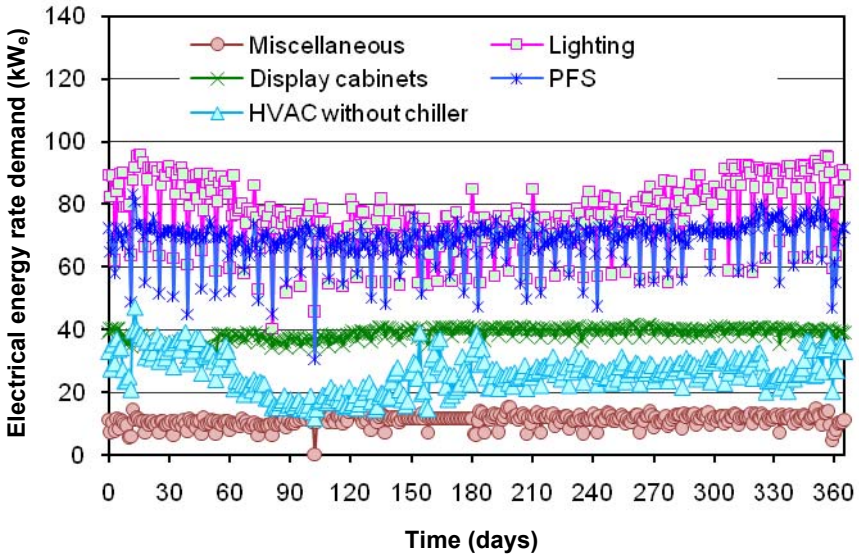

PFS = preparation, food and services

Figure 6.4 Daily average electrical-energy rate demand of all services apart from refrigeration systems (Data source: Tesco, 2009)

6.2 Supermarket energy system and simulation models

Energy systems in supermarkets are considered to comprise heating for HVAC (heating, ventilation and air conditioning) and domestic hot water and electrical power for refrigeration, cooling, lighting, food preparation and HVAC systems. In the UK, the heat demand is normally satisfied by gas boilers and the electrical demand by power 'imported' from the national grid. Most supermarkets utilise R-404A as refrigerant in multi-compressor 'remote' type refrigeration systems with separate parallel systems employed for the MT and LT refrigeration loads.

The models developed to simulate refrigeration system in supermarkets are based on the Engineering Equation Solver (EES) software and a spread sheet programme. The models consider a conventional energy system using refrigeration systems with R-404A refrigerant and a new energy system using CO_2 refrigeration in a trigeneration arrangement (trigeneration-CO_2 energy system). Energy demands of the conventional energy system are satisfied from a gas boiler, conventional refrigeration with R-404A refrigerant, an electric chiller and national grid as shown in Figure 6.5. The system is also backed up by a standby generator to supply electricity in the event electricity supply from the grid is disrupted.

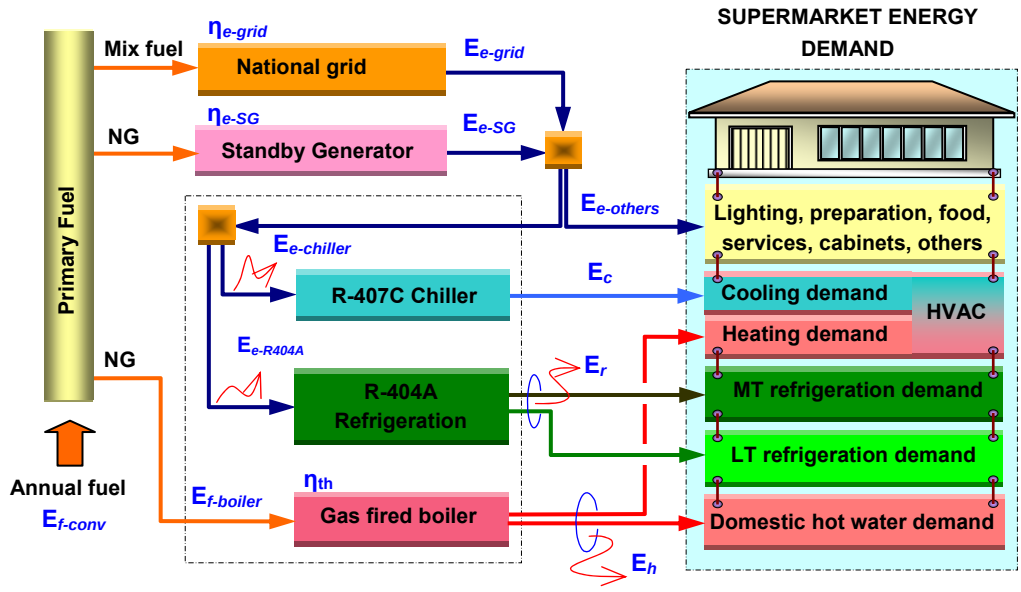

Figure 6.5 Energy flow diagram of the case study supermarket with a conventional energy system

The conventional refrigeration system with R-404A is a parallel system comprising two circuits: one serving the MT cabinets and the other serving the LT cabinets, as shown in Figure 6.6. Direct expansion evaporator coils using electronic expansion valves and single stage compression are used for both MT and LT circuits. An internal heat exchanger is used for the LT circuit only (Figure 6.6b).

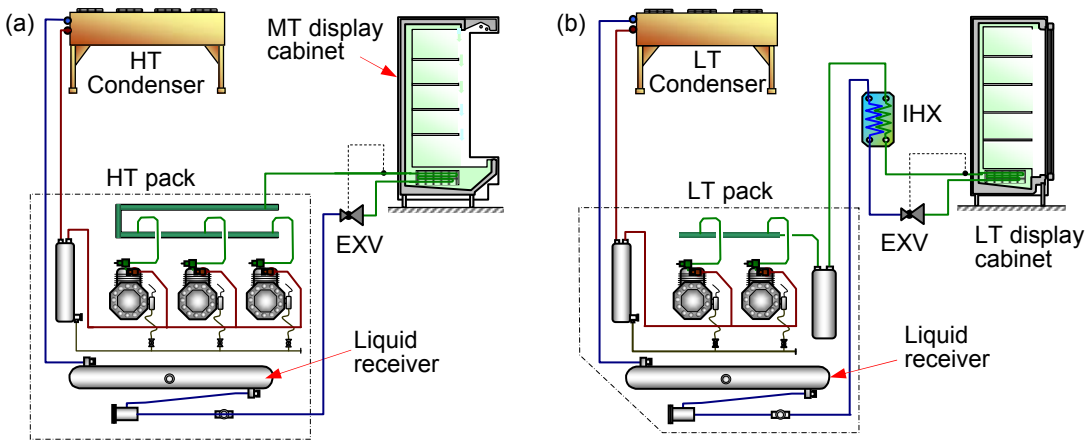

Figure 6.6 Simplified schematic diagram of a parallel conventional refrigeration system with R-404A refrigerant

The integration of CO_2 refrigeration and trigeneration involves a subcritical MT volatile secondary and LT DX CO_2 system in a cascade arrangement with an ammonia-water

absorption refrigeration system driven by the heat generated by a microturbine based CHP system. A schematic diagram of the arrangement is shown in Figure 3.6 (Chapter 3). The absorption chiller of the arrangement can provide delivery water-glycol temperature at -10 ^{o}C with heat input to the generator at 120 ^{o}C. This arrangement can achieve evaporating temperature at MT cabinet coils in the range -5.5 to -8 ^{o}C which is low enough for the MT cabinets.

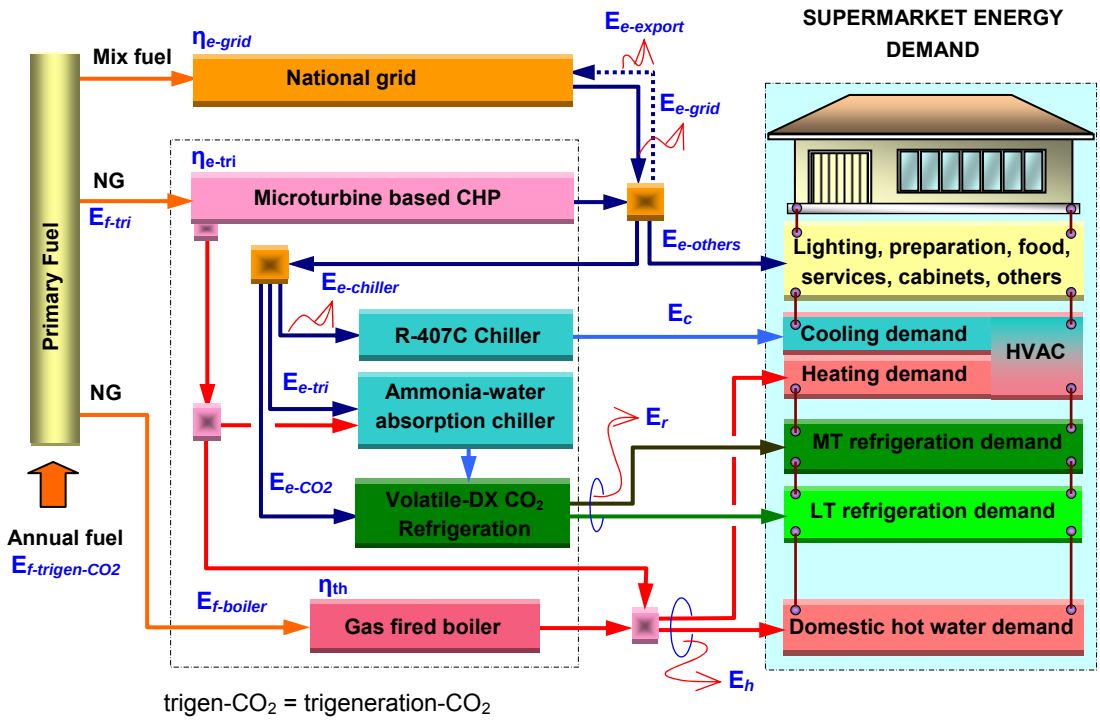

Figure 6.7 Energy flow diagram of the case study supermarket with energy system applying a volatile-DX CO_2 refrigeration in trigeneration arrangement

Figure 6.7 shows the energy flow diagram for the trigeneration-CO_2 supermarket energy system. It comprises subcritical MT volatile secondary and LT DX CO_2 refrigeration systems, trigeneration arrangement with ammonia-water absorption chiller, electric chiller and auxiliary boiler. Two gas-liquid heat exchangers are required on the exhaust gas of the microturbine. The first heat exchanger recovers heat from the exhaust gases to drive the absorption refrigeration system and the second one, installed in series downstream of the first heat exchanger, recovers heat for heating. The exhaust gas temperature leaving the first heat exchanger and the stack temperature from the second heat exchanger were assumed to be 130 ^{o}C and 95 ^{o}C respectively. An auxiliary boiler supplies heat only for domestic hot water and space heating. The auxiliary boiler will

run when the heat recovered in the heat exchanger cannot satisfy the total heat demand. The electric chiller with R-407C refrigerant is needed to satisfy the supermarket cooling demand. The plant comprises several systems arranged in parallel. Each system comprises one integrated trigeneration and CO_2 refrigeration system. The number of systems in operation can be modulated based on heat required for the refrigeration demand.

To simulate the energy consumption of the two energy systems, some assumptions were made as follows: refrigeration capacity of LT system is 32.5% of that of MT system; evaporating temperatures of -8 ^oC and -32 ^oC for the MT and LT cabinets respectively; temperature difference between ambient and condensing temperatures for the conventional R-404A refrigeration system of 9.5 K with minimum condensing temperature for a floating head pressure control of 25 ^oC for the MT system and 20 ^oC for the LT system. Weather data for the Manchester area of the United Kingdom (Met Office, 2009) were used for the simulations.

The main equations used in the simulations for the trigeneration-CO_2 energy system are described in Section 3.2 (Chapter 3). For the conventional system, the efficiency of R-404A semi-hermetic reciprocating compressor was calculated using a curve fit equation from experimental and modelling results by Navarro et al. (2007).

$$\eta_s = -0.0072.R_p^2 - 0.048.R_p + 0.5262 \tag{6.1}$$

$$\eta_v = -0.0735.R_p + 0.9741 \tag{6.2}$$

The overall *COP* of the conventional refrigeration system is determined from:

$$COP_{conv} = \frac{Q_{r-MT} + Q_{r-LT}}{W_{MT-comp} + W_{LT-comp}} \tag{6.3}$$

In this analysis, primary fuel energy utilisation ratio (*FEUR*) is used to express the useful energy efficiency of the energy systems. The overall primary fuel energy utilisation ratio (*FEUR*) is the ratio of the summation of the useful energy used in the store to primary fuel energy consumed. The *FEUR* of the conventional energy system can be calculated from:

$$FEUR_{conv} = \frac{E_h + E_r + E_c + E_{e-others}}{E_{f-conv}} \; x\; 100\% \tag{6.4}$$

The *FEUR* of the integrated trigeneration and CO_2 refrigeration system was calculated from:

$$FEUR_{trigen-CO2} = \frac{E_h + E_r + E_c + E_{e-others} + E_{e-export}}{E_{f-trigen-CO2}} x\ 100\% \quad (6.5)$$

where E_h, E_r, E_c, $E_{e\text{-}others}$, $E_{e\text{-}export}$ are energy useful for heating, refrigeration, cooling, electricity others and electricity exported respectively; $E_{f\text{-}conv}$ and $E_{f\text{-}trigen\text{-}CO2}$ are primary fuel energy used for conventional and integrated trigeneration-CO_2 refrigeration energy system respectively.

The primary energy consumption of the conventional and trigeneration-CO_2 energy systems was determined from:

$$E_{f-conv} = \frac{1}{\eta_{e-grid}}.E_{e-grid} + \frac{1}{\eta_{e-SG}}.E_{e-SG} + E_{f-boiler} \quad (6.6)$$

$$E_{f-trigen-CO2} = \frac{1}{\eta_{e-grid}}.\ E_{e-grid} + E_{f-tri} + E_{f-boiler} \quad (6.7)$$

The fuel energy saving ratio (*FESR*) was calculated from:

$$FESR_{trigen-CO2} = \frac{E_{f-conv} - E_{f-trigen-CO2}}{E_{f-conv}} x\ 100\% \quad (6.8)$$

The electrical efficiency of the UK national grid was assumed to be 33% (Sugiartha et al., 2006) and the efficiency of commercial gas boilers, 80.8% (Tesco, 2009). Electrical efficiency of the microturbine based CHP was determined to be 28.7% from test data in the laboratory.

The total impact of the conventional and trigeneration-CO_2 systems on the environment was calculated over the life time of the systems and was assumed to be equally distributed over their life time. The calculation was based on the direct effect of the refrigerant leakage and recovery losses as well as indirect effect of the energy consumed by the systems. These effects are combined and expressed as a total equivalent warming impact (*TEWI*) as defined by British Standard BS EN 378-1 (2008).

$$TEWI = GWP.L_{annual}.n + GWP.m_{charge}.\left(1 - \alpha_{recovery}\right) + n.E_{annual}.\beta \quad (6.9)$$

where:

GWP is the global warming potential of the refrigerant ($kgCO_2/kg$); L_{annual} = the annual refrigerant leakage (kg/year); m_{charge} = mass of the refrigerant charge (kg); α = life time refrigerant recovery factor; n = system operating time (years); E_{annual} = annual energy consumption (kWh/year); and β = CO_2 emission factor ($kgCO_2/kWh$).

To calculate the environmental impact of the supermarket some assumptions were made. These are detailed in Table 6.1.

Table 6.1 Assumptions for TEWI calculation of the case study supermarket

Parameters	Assumptions	References	
		Range	Source
Annual refrigerant leakage for centralised refrigeration system (% of charge)	15	15 - 30	TOC, 2006
Refrigerant charge for DX centralised refrigeration system:			
- Charged with HFC or HCFC (kg/kW refrigeration capacity)	3.5	2 - 5	MTP, 2008
- Charged with CO_2 (kg/kW refrigeration capacity)	1.75	1 – 2.5	MTP, 2008
CO_2 emissions factor:			
- Grid electricity ($kgCO_2/kWh$)	0.547		DEFRA, 2009
- Natural gas ($kgCO_2/kWh$)	0.184		DEFRA, 2009
Global warming Potential (100 years interval time horizon):			
- R-404A ($kgCO_2/kg$)	3900		TOC, 2006
- R-407C ($kgCO_2/kg$)	1800		TOC, 2006
- R-744 ($kgCO_2/kg$)	1		TOC, 2006
Refrigerant recovery factor (%)	70		
Useful life of conventional and trigen-CO_2 system (years)*	15		

*Trigen-CO_2 = integrated trigeneration and CO_2 refrigeration system

6.3 Energy performance of the conventional system

Simulation results of the conventional R-404A refrigeration system show an average seasonal *COP* for the MT refrigeration of 2.51. The *COP* of the LT refrigeration system was found to vary between 1.14 in the summer to 1.62 in winter, giving an average seasonal value of 1.53. The combined seasonal *COP* of the LT and MT plant was determined to be 2.17. A display of the conventional refrigeration model is given in Figure L-1 (Appendix L).

Figure 6.8 shows the average daily fuel energy utilisation ratio (*FEUR*) of the conventional supermarket energy system. It can be seen that the overall FEUR in winter can reach 58% and then drops to about 44% in the summer due to lower heating demand and higher electrical power consumption of the refrigeration systems, giving an

overall seasonal *FEUR* of 49.6%. The lower heating demand reduces the contribution of the high efficiency gas boiler to the *FEUR* of the store. The higher electricity consumption of the refrigeration systems counterbalances the reduction of the primary fuel of the gas boiler which makes the primary fuel energy of the store relatively constant all year round. The effect can also be seen from the *FEURs* for refrigeration and electricity-others, which are quite stable throughout the year with annual averages of 19% and 21.2% respectively.

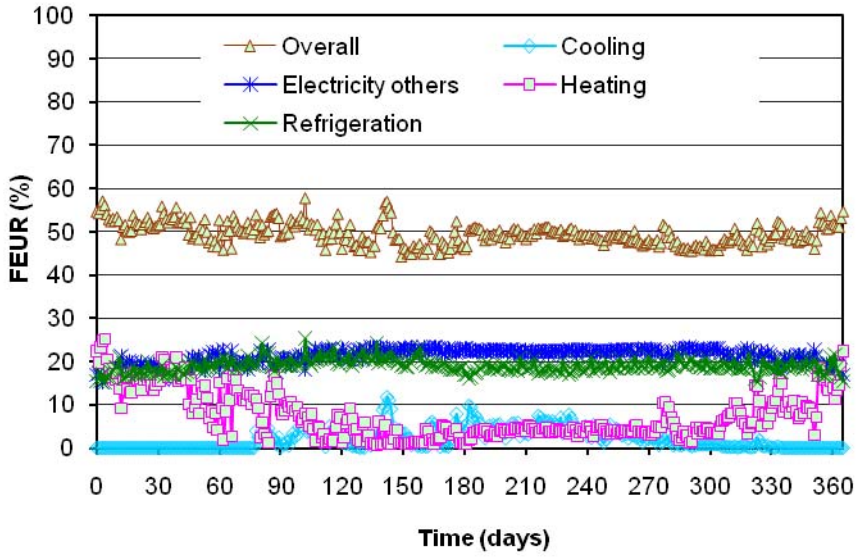

Figure 6.8 Daily average fuel utilisation ratio of the conventional energy system

Annual average *FEUR* of space cooling is only 2.1% and heating 7.3% because of the relatively low average demand for space cooling and heating respectively. The total primary fuel energy required by the conventional system is 9,411 MWh per year, 90.7% arising from electricity use (Table 6.2).

6.4 Energy and environmental performance of the trigeneration-CO_2 refrigeration system

The integrated trigeneration and CO_2 refrigeration system employs 5 systems operating in parallel each generating 80 kW of electrical power. This arrangement provides optimum fuel utilisation ratio with average load factor 85% (calculated from useful heat and total heat demand). The system can satisfy all refrigeration demand and 90% of the heating demand. The remainder of the heat requirement is provided by an auxiliary gas boiler system.

The daily variation of the *FEUR* of the system over a whole year is shown in Figure 6.9. The annual average *FEUR* was found to be 55.7%, made up of 21.1% for refrigeration, 2.5% for space cooling, 7.9% for heating, 24.2% for electricity (electricity others = 21.5% and electricity export = 2.7%). The total fuel demand of the system was found to be 8,081 MWh, providing savings of 1,331 MWh (14.14%) over the conventional system (Table 6.2). The total electricity consumption of the store reduces by 17.7% compared to the conventional system and most of the electricity consumption can be satisfied by the local power generation system. Only 8% of the electricity is required to be purchased from the national grid system. Because the control of the plant is based on meeting the refrigeration demand, the system also generates excess electricity giving a total electricity export to the grid of 261,221 kWh.

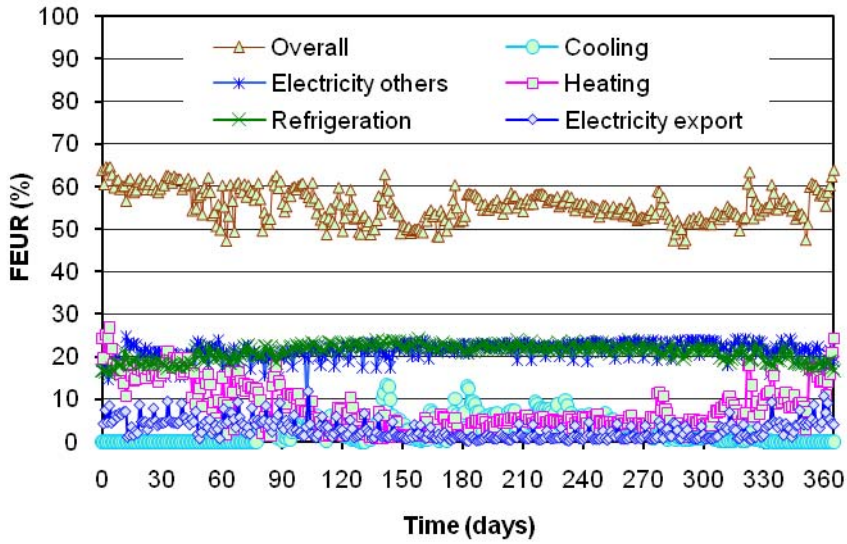

Figure 6.9 Daily average fuel energy utilisation ratio of the trigeneration-CO_2 energy system

Table 6.2 summarises the energy performance of the conventional and trigeneration-CO_2 energy systems. It can be seen that the latter provides significant energy savings over the conventional system. A detailed energy performance analysis of both energy systems is given in Appendix M.

Table 6.3 shows a comparison between the CO_2 emissions of the conventional and trigeneration-CO_2 systems for a 15% annual refrigerant leakage rate. It can be seen that the trigeneration-CO_2 energy system will result in annual emissions savings of 659 tCO_2

representing a reduction of 30.2% compared to the conventional system. Detailed CO_2 emissions analysis of both energy systems is given in Appendix M.

Table 6.2 Fuel saving analysis of conventional and trigeneration-CO_2 energy systems

Fuel utilization components	Supermarket energy systems		Unit
	Conventional	Trigen-CO_2	
Trigeneration fuel	-	8,340,339	kWh
Boiler fuel	874,068	91,090	kWh
Imported electricity	*2,817,321*	*184,408*	kWh
Fuel of imported electricity	8,537,338	558,811	kWh
Exported electricity	-	*261,221*	kWh
Fuel saving to grid supply	-	909,465	kWh
Total fuel required	9,411,406	8,080,776	kWh
Fuel energy savings	**-**	**1,330,630**	**kWh/year**
Fuel energy saving ratio (FESR)	**-**	**14.14**	**%**

Trigen-CO_2 = integrated trigeneration and CO_2 refrigeration system

Table 6.3 CO_2e emissions of conventional and trigeneration-CO_2 energy systems

CO_2 emissions	Conventional	Trigen-CO_2	Units
Indirect CO_2 emissions	1,702	1,509	tCO_2/year
Direct CO_2 emissions:			
• Refrigerant leakage	428	17	tCO_2/year
• Refrigerant recovery losses	55	0	tCO_2/year
Total annual emissions	2,185	1,526	tCO_2/year
Net emission savings		**659**	**tCO_2/year**
CO_2 emissions reduction		**30.2**	**%**

Trigen-CO_2 = integrated trigeneration and CO_2 refrigeration system

6.5 Summary

This chapter described the models which have been developed and used to investigate primary fuel utilisation of a conventional energy system with HFC based refrigeration and an integrated trigeneration and CO_2 refrigeration system. The chapter also evaluated the environmental impact of both energy systems.

Chapter 7 will investigate further integrated trigeneration and CO_2 refrigeration systems of different configurations. The evaluation will include energy and environmental performance as well as economic viability of the energy system alternatives.

Chapter 7

ENERGY SYSTEM ALTERNATIVES WITH INTEGRATED TRIGENERATION AND CO_2 REFRIGERATION

This chapter investigates energy and environmental performance of integrated trigeneration and CO_2 refrigeration system alternatives for supermarket applications. Different system arrangements are simulated and evaluated based on the energy demand of the case study supermarket described in Chapter 6. The analysis compares the performance of a conventional energy system using R-404A as the refrigerant, the existing energy system in the store which utilises CO_2 as refrigerant and alternative trigeneration and CO_2 refrigeration solutions.

7.1 Supermarket energy system alternatives

Three schemes are considered which utilise different CO_2 refrigeration and trigeneration system arrangements. Scheme-1 is the system currently employed in the case study supermarket and consists of: bio-fuel engine based CHP, sorption refrigeration system and electric chiller for air conditioning, cascade transcritical CO_2 refrigeration, and gas boiler. Heat released by the CHP system drives the sorption chiller in a trigeneration arrangement to generate cooling for the HVAC system. If cooling generated by the trigeneration system is not enough to satisfy the space cooling needs, the balance is provided by the electric vapour compression chiller with R-407C refrigerant. The cascade transcritical CO_2 refrigeration system is utilised to satisfy the MT and LT refrigeration demands. The schematic diagram of the CO_2 refrigeration system is as

shown in Figure 2.12 (Chapter 2). In this scheme, heat from the CO_2 refrigeration system is directly rejected to the atmosphere through an air cooled gas cooler. The heat demand is satisfied by heat from the CHP system, when it is not used for cooling, and the balance by the gas fired boiler. The electrical demand is satisfied by a combination of local power generated by the CHP system and power imported from the grid. The energy flow diagram of the energy system of Scheme-1 is shown in Figure 7.1.

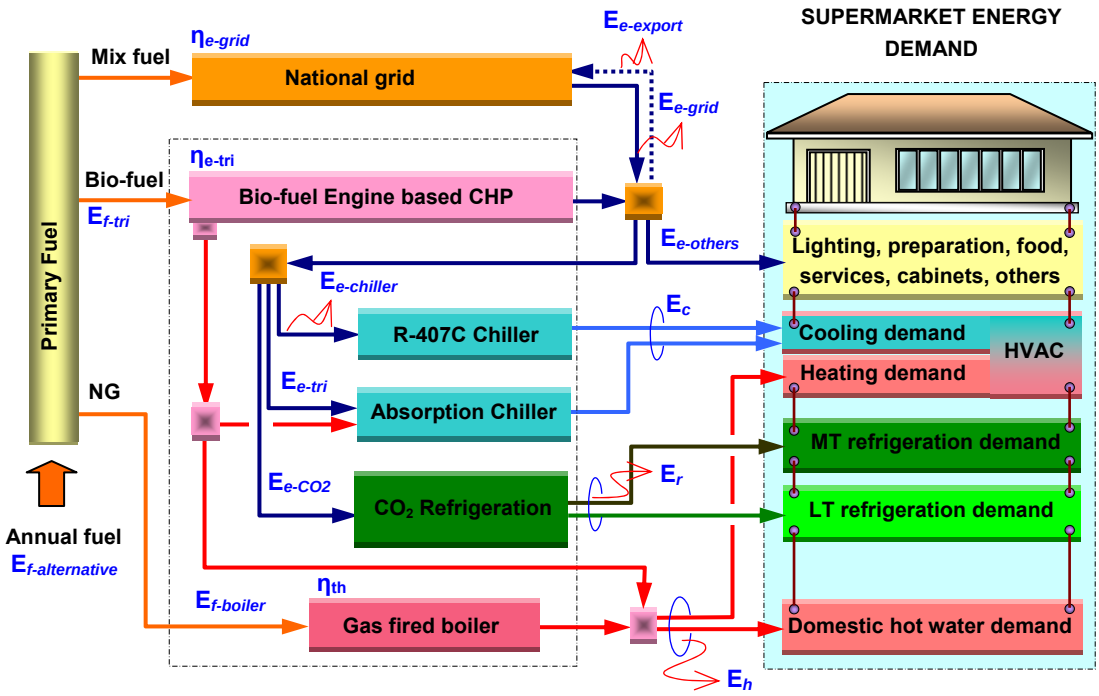

Figure 7.1 Energy flow diagram of existing energy system (Scheme-1)

Scheme-2 is a supermarket energy system which integrates cascade transcritical CO_2 refrigeration and trigeneration systems. The energy released by the gas engine CHP system is used to drive a sorption chiller which is cascaded to a CO_2 condenser to cool and condense the CO_2 refrigerant of the cascade transcritical CO_2 refrigeration system. Chilled water temperature from the sorption chiller of the trigeneration system is considered to be at 7 ^oC. This integration arrangement is shown in Figure 7.2. It ensures operation of the CO_2 refrigeration system in the subcritical region but the system can revert to transcritical operation in the event of trigeneration system failure.

From Figure 7.2, it can be seen that the integration mode of Scheme-2 can be set by opening valves SV1 and SV3; closing valve SV2; and switching off the ICMT valve. This allows cooling from the trigeneration system to condense the CO_2 gas in the HT condenser. The liquid CO_2 then flows from the condenser to the liquid receiver through valve SV3 without expansion. When the ambient temperature is below 7 ^oC, valve SV1 can be closed and valve SV2 opened to allow the CO_2 gas to be cooled by ambient air in the air-cooled condenser. In order to switch the system to the transcritical operation mode, valves SV1 and SV3 must be closed, valve SV2 opened; and the ICMT valve energised.

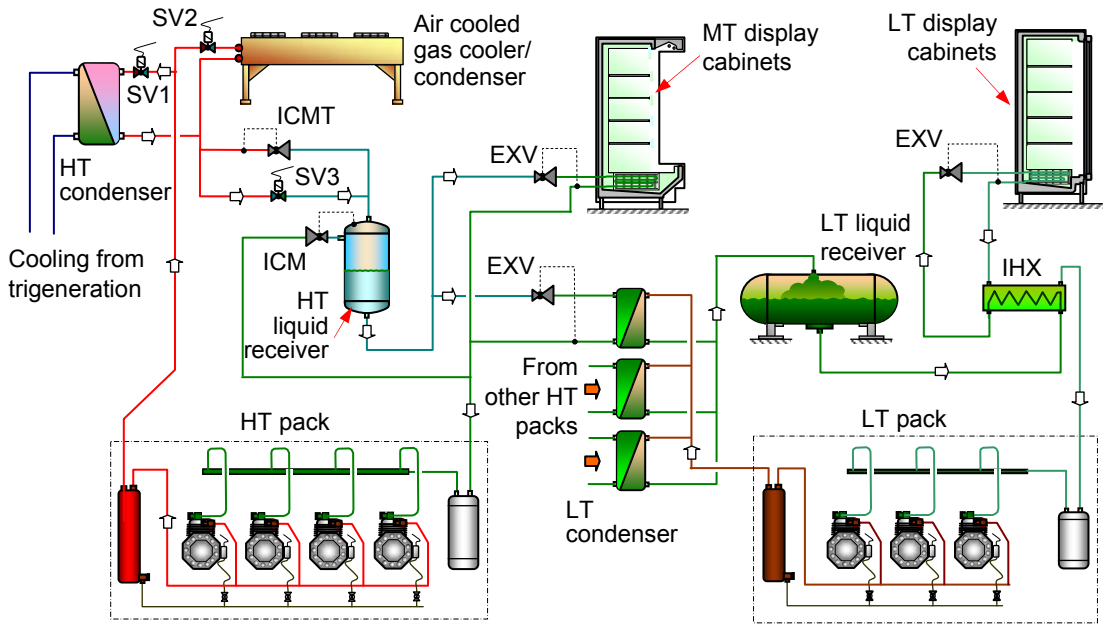

SV1 = solenoid valve of the HT condenser; SV2 = solenoid valve of the air cooled gas cooler/condenser; SV3 = bypass solenoid valve

Figure 7.2 Simplified schematic diagram of a cascade transcritical CO_2 refrigeration integrated with trigeneration system (Scheme-2)

Scheme-3 is an improvement on the energy system considered in Chapter 6. It utilises integrated CO_2 refrigeration and trigeneration employing a high temperature sorption chiller. A schematic diagram of scheme-3 is shown in Figure 7.3. The trigeneration system consists of a natural gas engine based CHP system and a sorption refrigeration system. The heat rejected by the CHP system is used to drive the sorption chiller, with the cooling energy produced employed to condense the CO_2 refrigerant of the

subcritical CO_2 refrigeration system. This ensures operation of the CO_2 refrigeration system in the subcritical region all the time and at a constant condensing temperature which ensures high energy efficiency throughout the year. The sorption refrigeration system considered in this study is a single effect lithium bromide-water system which can deliver chilled water at 7°C. The system can equally use an adsorption refrigeration system but the absorption system was chosen in this case due to its lower capital cost.

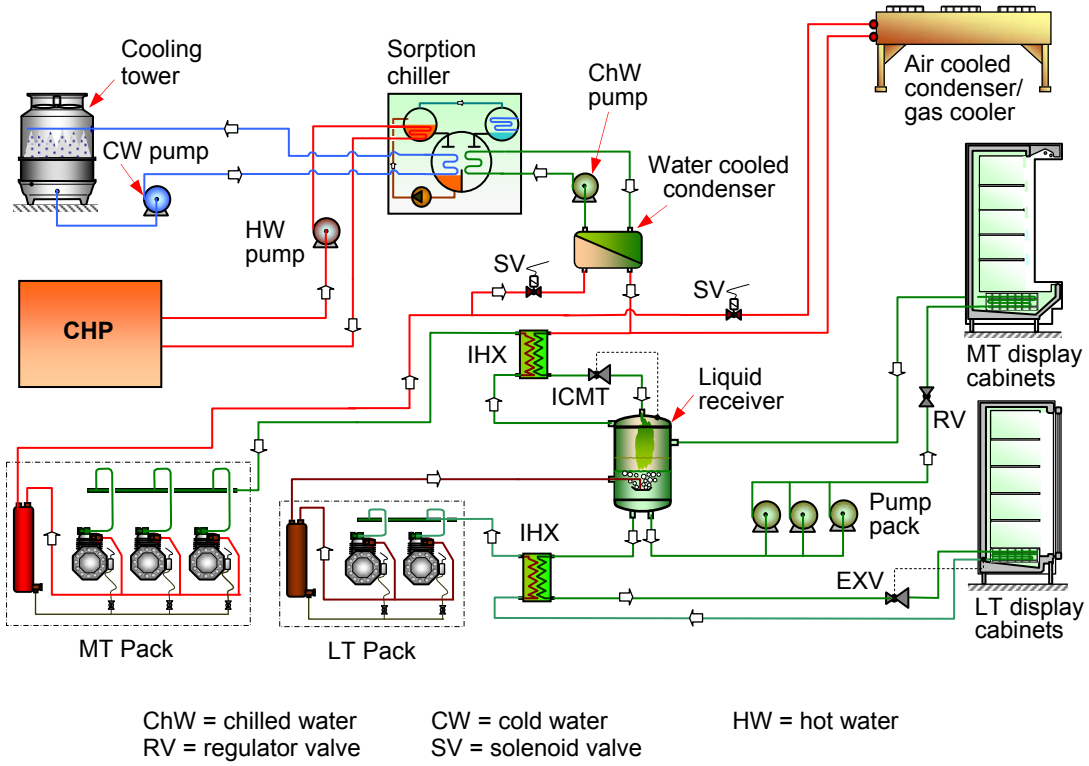

Figure 7.3 Simplified schematic diagram of integrated trigeneration and CO_2 refrigeration systems (Scheme-3)

The CO_2 refrigeration system employs a pumped CO_2 arrangement for the MT cabinets and direct expansion for the LT cabinets. This maximises the system efficiency as the compressor power for MT refrigeration, which is the predominant load in a supermarket, is replaced by a much lower pump power to circulate the liquid refrigerant to the refrigerated cabinets. The cooling energy for condensation of the CO_2 refrigerant is provided by the sorption chiller. A medium temperature CO_2 circuit (MT pack) is used to bridge the difference in temperature between that provided by the sorption chiller (7 °C) and the temperature required to condense the CO_2 refrigerant of the LT

and MT circuits (-8 ^{o}C). To ensure operation of the refrigeration system in the event of trigeneration system failure, the system design also employs a gas cooler which can be brought into operation to take over from the sorption refrigeration system. The arrangement can also provide an advantage of free cooling when the ambient temperature is below 7 ^{o}C.

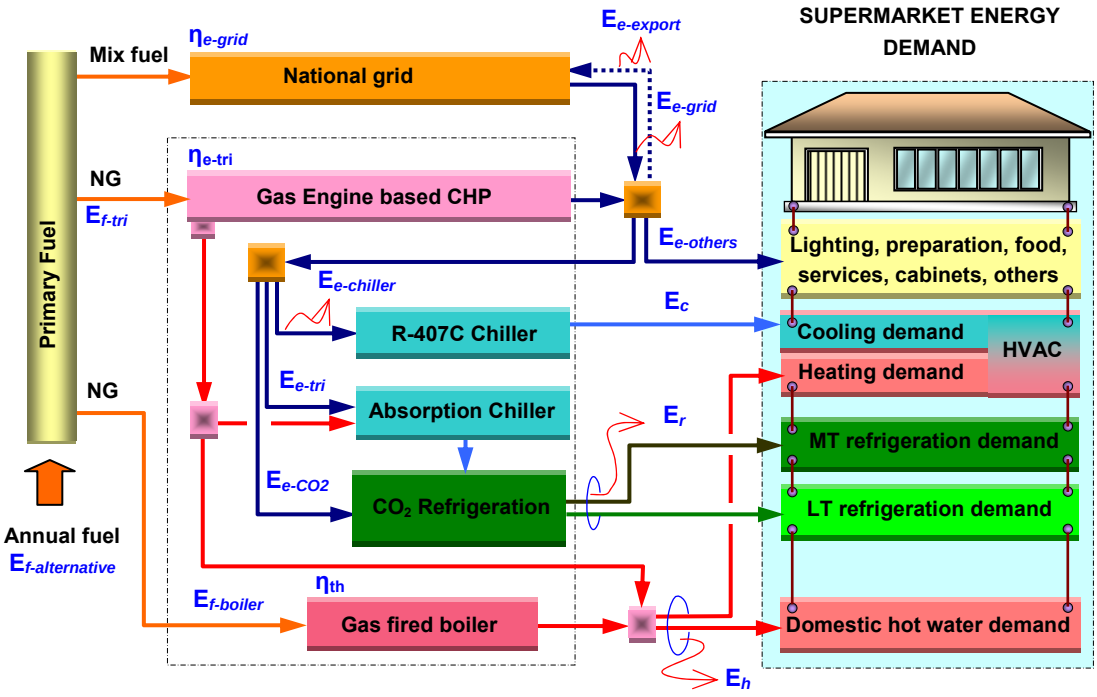

CO_2 refrigeration: Scheme-2 is a modified cascade transcritical CO_2 refrigeration system; Scheme-3 is a modified volatile-DX CO_2 refrigeration system

Figure 7.4 Energy flow diagram of energy system alternatives
(Scheme-2 and Scheme-3)

Figure 7.4 shows the energy flow diagram of Schemes-2 and 3. In order to satisfy all refrigeration demand of the store, the trigeneration system is modulated based on the heat required by the sorption chiller to cool the CO_2 refrigeration system. This also means that the HVAC cooling demand is satisfied by an electric chiller with R-407C refrigerant. A gas boiler is used to supply heat for the HVAC system and domestic hot water system, if the heat from the trigeneration arrangement is not enough particularly in the winter. The electrical demand is satisfied by a combination of local power generated by the CHP system and power imported from the grid. In periods of excess local power generation, the extra power is exported to the national grid.

7.2 Simulation models

Simulation models based on the Engineering Equation Solver (EES) software and a spread sheet programme were established to determine the performance of the alternative energy systems for the case study supermarket in terms of primary fuel energy utilisation, GHG emissions and economic viability. Pressure - enthalpy diagrams of the refrigeration systems applied in the schemes are shown in Figure 7.5. The primary fuel energy utilisation ratio (FEUR) of the energy system alternatives can be calculated from:

$$FEUR_{alternative} = \frac{E_h + E_r + E_c + E_{e-others} + E_{e-export}}{E_{f-alternative}} \, x\, 100\% \tag{7.1}$$

The primary energy was determined from:

$$E_{f-alternative} = \frac{1}{\eta_{e-grid}} . \, E_{e-grid} + E_{f-tri} + E_{f-boiler} \tag{7.2}$$

The fuel energy saving ratio (*FESR*) was calculated from:

$$FESR_{alternative} = \frac{E_{f-conv} - E_{f-alternative}}{E_{f-conv}} x\, 100\% \tag{7.3}$$

The payback period (years) is determined from:

$$Payback = \frac{Extra\ investment\ of\ energy\ system\ alternative}{Annual\ net\ saving} \tag{7.4}$$

The electrical efficiency of the bio-fuel engine based CHP was assumed to be 35.1% (Tesco, 2009) and the gas fuel engine based CHP to be 36.6% (Cogenco, 2008). Other assumptions for the energy and environmental performance analysis are given in Appendix N.

(a) Scheme-1: Cascade transcritical CO_2 refrigeration system

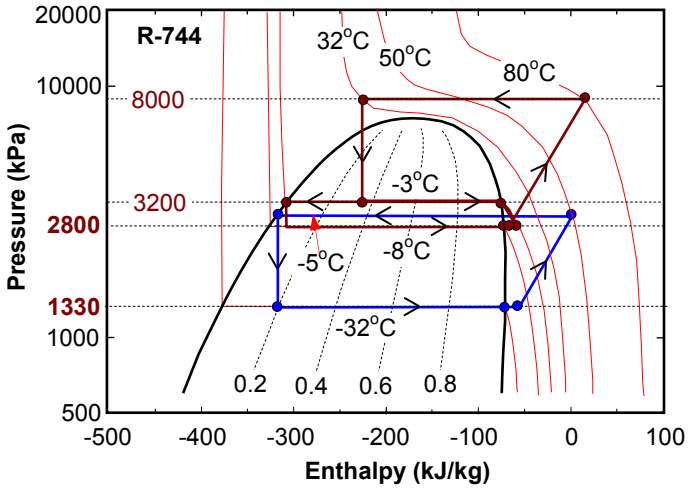

(b) Scheme-2: Transcritical CO_2 refrigeration system of Scheme-1 cascaded with high temperature sorption chiller of a trigeneration system

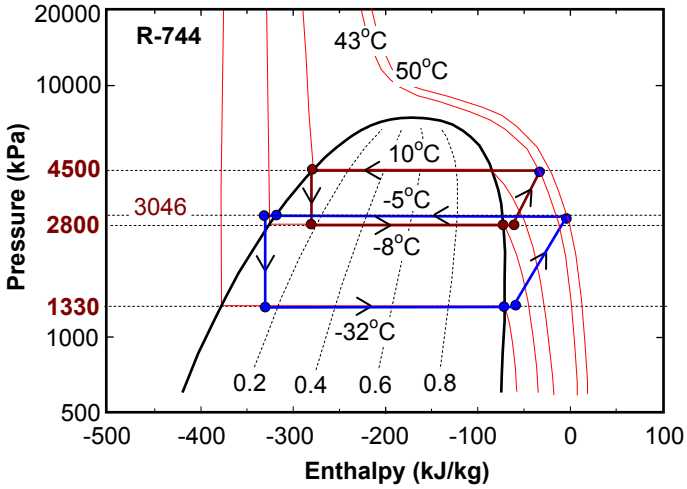

(c) Scheme-3: Modified volatile-DX CO_2 refrigeration system cascaded with high temperature sorption chiller of a trigeneration system

THE HIGH STAGE OF SCHEMES 2 AND 3 IS A TRIGENERATION SYSTEM WITH A HIGH TEMPERATURE SORPTION CHILLER FOR THE HEAT REJECTION

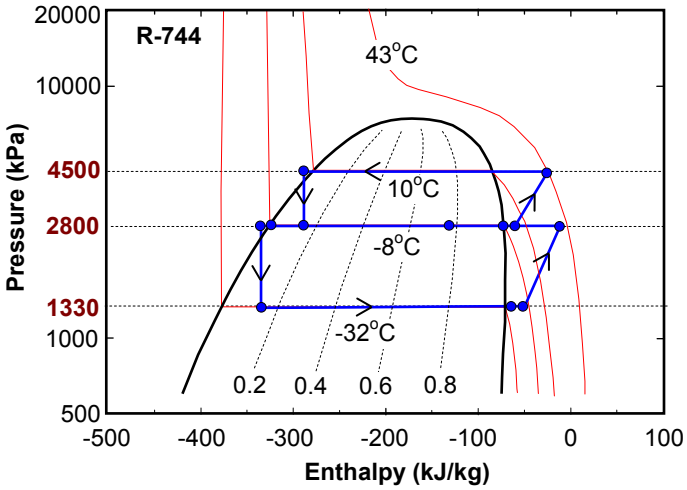

Figure 7.5 Thermodynamic models of the refrigeration system of Schemes 1 to 3 at ambient temperature of 27 °C

7.3 Model results and discussion

Scheme-1 is the current system in the supermarket which employs: i) a trigeneration arrangement with bio-fuel engine based CHP of 200 kW_e capacity; ii) a sorption chiller with a cooling capacity 250 kW_{th}; iii) 2 cascade transcritical CO_2 refrigeration systems; each system comprises of two HT circuits with MT load @ 38 kW_{th} cascaded with an LT circuit of capacity 25 kW_{th}; iv) a 200 kW_{th} R-407C electric chiller for air conditioning and; v) 2 gas boilers of 200 kW_{th} capacity each.

The *COP* of the cascade transcritical CO_2 refrigeration system calculated using data from the store was found to vary between 1.1 and 5.1 for MT system giving a seasonal average *COP* of 2.4. The *COP* of the LT CO_2 refrigeration system was in the range between 2.5 and 4.9 with seasonal average *COP* of 3.5. The overall seasonal *COP* of the cascade CO_2 transcritical system was determined to be 2.5.

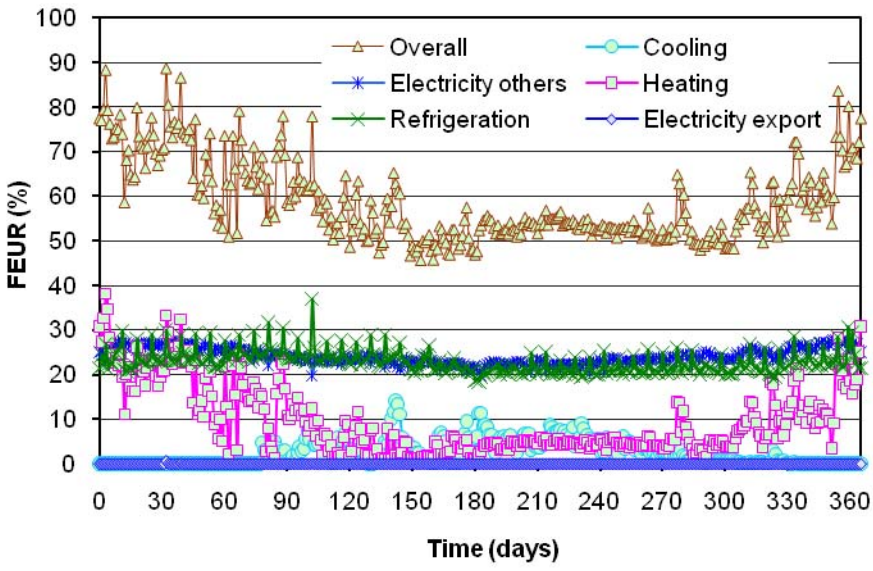

Figure 7.6 Daily average fuel energy utilisation ratio of scheme-1

Daily average fuel energy utilisation ratio (FEUR) of scheme-1 is shown in Figure 7.6. It can be seen that the FEUR of refrigeration and electricity are quite stable throughout the year with annual averages of 23% and 24% respectively, but the FEUR of heating varies from 0% in the summer to 47% in winter giving a seasonal FEUR of 9.4%. The figure also shows that the FEUR of cooling is relatively low with a seasonal average of only 2.4%. Most of the cooling demand can be satisfied by the trigeneration

arrangement and only 1% is provided by the electric chiller. The arrangement has average overall FEUR of 58.7%.

The energy analysis has also shown that with scheme-1, the trigeneration system can satisfy 97.5% of the heat demand with only 2.5% provided by the gas boilers. The electricity generated by the trigeneration arrangement in this scheme is 1,555 MWh which is 57.3% of the total electricity requirement of the store. The annual primary fuel requirement of scheme-1 is 7,967 MWh. Compared to the conventional energy system, scheme-1 can provide primary fuel energy saving of 1,445 MWh with FESR of 15.3% (Table 7.1).

Scheme-2 is a modification to the existing scheme of the case study supermarket. It utilises a trigeneration arrangement with a 342 kW_e gas engine based CHP and a sorption chiller of 310 kW_{th} integrated with a CO_2 refrigeration plant similar to that of Scheme-1. Scheme-2 also employs a 200 kW_{th} R-407C refrigeration system for space cooling and 2 x 200 kW_{th} gas boilers for space and domestic hot water heating.

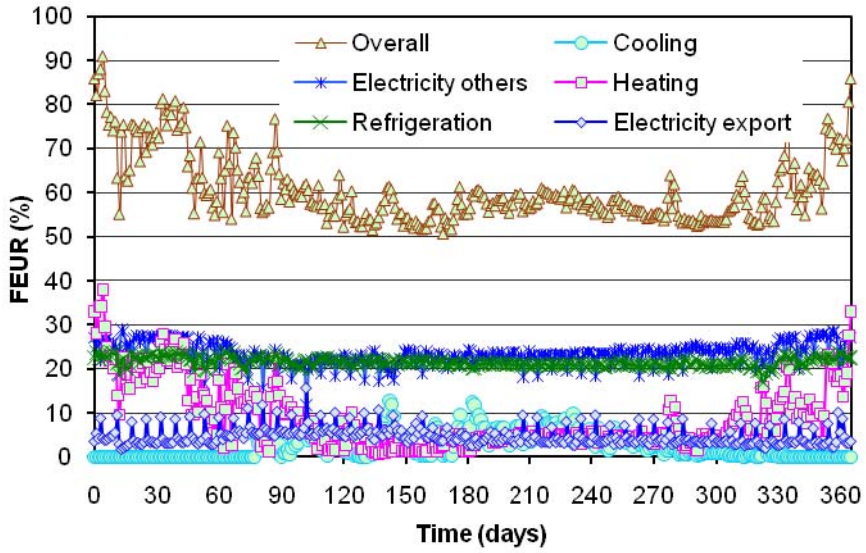

Figure 7.7 Daily average fuel energy utilisation ratio of scheme-2

Simulation results show a stable performance for both MT and LT refrigeration systems all year round with COP of 5.4 and 4.1 respectively. This can provide an overall seasonal COP of 5.0. With this arrangement, the CO_2 refrigeration system can operate subcritically at condensing temperature of 10 ^oC (assumed ΔT between chilled water

from the trigeneration and the liquid CO_2 to be 3 K). A display of the EES simulation of the CO_2 refrigeration system is given in Figure L-2 (Appendix L).

Figure 7.7 shows the variation of the daily average FEUR of scheme-2. Overall FEUR varies in the range 48.6% in the summer and 90% in winter with the average being 60.7%. Seasonal FEUR of electricity others, refrigeration, heating, cooling and export electricity are 23.3%, 21.5%, 8.7%, 2.4% and 4.8% respectively. Total electricity consumption of the store is 2,560 MWh which is 9.1% lower than the conventional energy system. Scheme-2 will import 44 MWh and will export 378 MWh to the grid in a year. The trigeneration arrangement generates electricity of 2,894 MWh. This scheme was found to have a fuel energy saving ratio (FESR) of 24.7% compared to the conventional system.

Preliminary sizing for an optimised trigeneration-CO_2 refrigeration arrangement (scheme-3) has shown the following system sizes to provide best results: trigeneration arrangement with a 342 kW_e gas engine based CHP and an absorption chiller with a design cooling capacity of 310 kW_{th}. Refrigeration capacity of 152 kW_{th} for the MT volatile CO_2 refrigeration packs and 50 kW_{th} refrigeration capacity for the LT packs. The scheme is backed up by an electric 200 kW_{th} capacity R-407C chiller for space cooling and 2 x 200 kW_{th} capacity gas boilers for heating.

Simulation on the modified volatile-DX CO_2 refrigeration system integrated with the trigeneration system also shows a stable performance for both MT and LT systems. The COPs of the MT and LT systems are 5.0 and 5.6 respectively, giving an annual overall COP of 5.1. Detailed simulation is given in Figure L-3 (Appendix L).

The daily variation of the FEUR of Scheme-3 over a whole year is shown in Figure 7.8. The annual average FEUR of the scheme was found to be 64.4% comprising FEUR of the electricity (for other services), refrigeration, heating and cooling of 25.1%, 23.1%, 9.2% and 2.6% respectively and FEUR of the export electricity of 4.4%. The scheme has total fuel consumption 6,655 MWh, providing savings of 2,757 MWh (29.3%) over the conventional system (Table 7.1). With Scheme-3, 96.8% of the electricity demand of the supermarket can be satisfied by the local power generation system. The trigeneration system can also satisfy 97% of the store's heat demand with the remainder supplied by the gas boiler system.

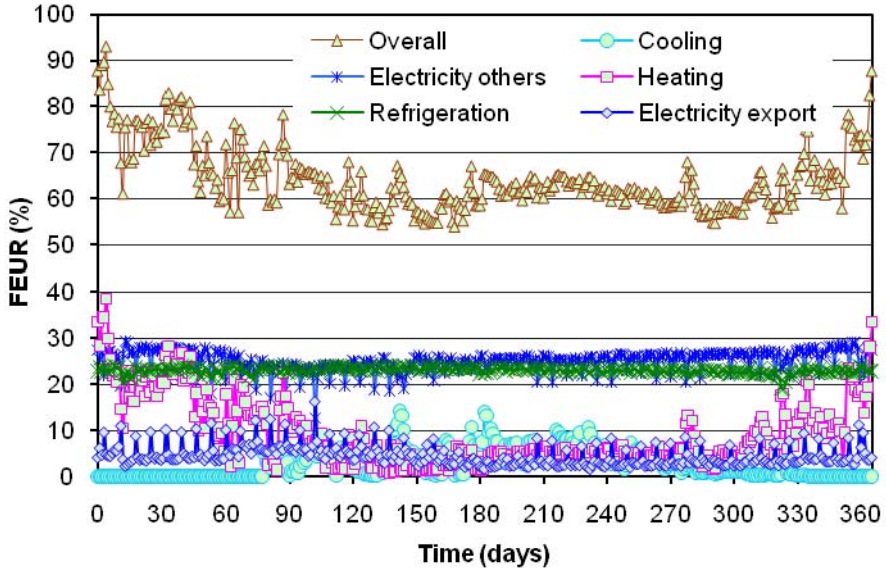

Figure 7.8 Daily average fuel energy utilisation ratio of scheme-3

Table 7.1 summarises the energy performance of the 3 alternative schemes. It can be seen that all schemes provide significant energy savings over the conventional system with scheme-3 resulting in the highest fuel savings and FESR.

Table 7.1 Results of fuel energy saving analysis

Fuel utilization components	Supermarket energy systems				Unit
	Conventional	Scheme-1	Scheme-2	Scheme-3	
Trigeneration fuel	-	4,431	7,907	7,450	MWh
Boiler fuel	874	21	194	25	MWh
Imported electricity	*2,817*	*1,160*	*44*	*62*	MWh
Fuel of imported electricity	8,537	3,515	135	189	MWh
Exported electricity	-	*0.12*	*379*	*333*	MWh
Fuel saving to grid supply	-	0.36	1,148	1,009	MWh
Total fuel required	9,411	7,967	7,088	6,655	MWh
Fuel energy savings	**-**	**1,444**	**2,323**	**2,756**	**MWh/year**
Fuel energy saving ratio (FESR)	**-**	**15.3**	**24.7**	**29.3**	**%**

(Detailed analysis is given in Appendix N)

Table 7.2 shows a comparison between CO_2e emissions of the conventional and the three energy system alternatives. The analysis assumed annual refrigerant leakage rate of 15% of system charge. It can be seen that scheme-3 will lead to CO_2e emissions savings of 941 tCO_2e which represents 43% savings over the conventional system.

Scheme-1 will result in savings of 1530 tCO_2e mainly because of the use of bio-fuel and the assumption that the emissions factor of bio-fuel is zero.

Table 7.2 CO_2e emissions of investigated energy systems

CO_2 emissions	Annual leakage 15% of charge				Units
	Conventional	Scheme-1	Scheme-2	Scheme-3	
Indirect CO_2 emissions	1,702	638	1,308	1,227	tCO_2/year
Direct CO_2 emissions:					
Refrigerant leakage	428	17	17	17	tCO_2/year
Refrigerant recovery losses	55	-	-	-	tCO2/year
Total annual emissions	2,185	655	1,325	1,244	tCO_2/year
Net CO_2 emissions saving		**1,530**	**860**	**941**	**tCO_2/year**
		70.0	**39.4**	**43.1**	**%**

(Detailed analysis is given in Appendix N)

7.4 Economic analysis

To establish the economic viability of the energy system alternatives, prices of fuel energy and the capital cost of the equipment were based on UK prices obtained from equipment suppliers and end users. The results of the economic analysis are shown in Table 7.3 for the installed cost and Table 7.4 for the annual energy and operational costs of the conventional and alternative energy systems. Assumptions and data used in the calculations are shown in Appendix O.

Table 7.3 Results of economic analysis: investment comparison

Cost components	Supermarket energy system			
	Conventional	Scheme-1	Scheme-2	Scheme-3
Installed cost (include VAT)				
HT R-404A refrigeration packs	£62,342.21			
LT R-404A refrigeration packs	£34,796.69			
HT transcritical CO_2 refrigeration packs		£111,325.38	£111,325.38	
MT Volatile-DX CO_2 refrigeration packs				£111,325.38
LT CO_2 refrigeration packs		£73,459.67	£73,459.67	£73,459.67
Electric chiller R-407C for air conditioning	£29,375.00	£29,375.00	£29,375.00	£29,375.00
Gas boilers	£47,000.00	£47,000.00	£47,000.00	£47,000.00
Gas engine based generator	£67,812.19			
Bio-fuel engine based CHP		£158,625.00		
Gas engine based CHP			£271,248.75	£271,248.75
Water-LiBr absorption chiller		£73,437.50	£91,091.68	£91,091.68
Total installed cost	**£241,326.08**	**£493,222.54**	**£623,471.29**	**£623,500.48**
Extra investment		**£280,052.40**	**£382,145.21**	**£382,174.40**

Calculation based on trigeneration capacity:
Scheme-1 (current system): CHP = 200 kW_e and sorption chiller = 250 kW_{th}
Schemes 2 and 3 (optimised capacity): CHP = 342 kW_e and sorption chiller = 310 kW_{th}
(Assumptions used for investment cost analysis are shown in Table O-1, Appendix O)

Table 7.4 Results of economic analysis: annual energy and operational cost

Energy and operational cost components	Supermarket energy system			
	Conventional	Scheme-1	Scheme-2	Scheme-3
Energy and operational cost (Incl. VAT)				
Electricity cost/supplemental electricity cost	£329,909.74	£135,828.75	£5,203.93	£7,300.44
Electricity sold back		-£11.61	-£36,605.51	-£32,166.76
Fuel cost for operating boilers	£28,431.62	£686.11	£6,321.38	£802.47
Bio-fuel cost for bio-fuel engine based CHP		£216,163.36		
Gas fuel cost for gas engine based CHP			£257,181.29	£242,333.51
Standing charge	£1,253.94	£1,253.94	£1,253.94	£1,253.94
Availability charge (700 kVA of supply capacity)	£9,080.40	£9,080.40	£9,080.40	£9,080.40
Operation and maintenance cost	£12,066.30	£32,592.38	£31,175.02	£31,175.02
Total energy and operational cost	**£380,742.01**	**£395,593.33**	**£273,610.99**	**£259,779.03**
Annual net savings		**-**	**£107,127.59**	**£120,962.98**
Payback period (years)		**-**	**3.6**	**3.2**

(Assumptions used for energy and operational cost analysis are given in Tables O-2 and O-3, Appendix O)

For the data used, it can be seen that scheme-3 will need additional investment of £382,000 compared to the conventional energy system but will produce running cost savings of the order of £121,000 per year, giving a payback period of 3.2 years. Scheme-1 will require approximately the same annual energy and operational cost as the conventional system due to the high cost of bio-fuel. The payback period of this scheme will be very long. Scheme-2 provides annual running cost savings of the order of £107,000. The payback period of Scheme-2 will be 3.6 years. The payback period is strongly influenced by the ratio of electricity to gas prices known as the `spark ratio'.

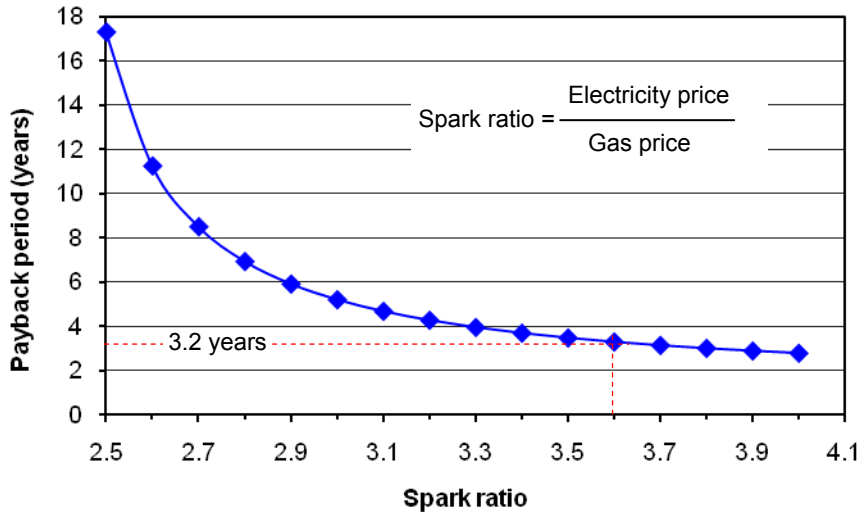

Figure 7.9 Variation of payback period with spark ratio

Figure 7.9 shows the variation of the payback period of scheme-3 with spark ratio. It can be seen that the payback period drops sharply as the spark ratio increases with the payback period reducing from 8 years at a spark ratio of 2.7 to 2.5 years at a spark ratio of 4.0. The spark ratio in the UK varied between 2.7 and 4.6 in the period 2007-2009 (Moorjani, 2009). The spark ratio used in the analysis was 3.6 for natural gas and 2.4 for bio-fuel.

7.5 Summary

This chapter has used modelling to investigate the energy and environmental performance as well as economic viability of three supermarket energy system alternatives. The energy system alternatives considered the application of trigeneration and CO_2 refrigeration systems of different arrangements including the integrated trigeneration and CO_2 refrigeration system proposed in this study. These investigations have shown that the proposed energy system can provide substantial carbon savings and a good payback period to HFC systems.

Chapter 8 will summarise the results and findings of the investigations in this study and will provide some recommendations for future work.

Chapter 8

CONCLUSIONS AND RECOMMENDATIONS FOR FUTURE WORK

The environmental impact of the food retail industry, particularly supermarkets, is high due to their high electrical energy consumption and indirect CO_2 emissions from the power stations and the direct emissions arising from refrigerant leakage to the atmosphere. The use of CO_2 as refrigerant offers the opportunity to reduce the direct emissions.

The application of trigeneration can reduce the environmental impacts through a substantial improvement in the overall energy efficiency over the conventional overall supermarket energy approach. One solution through which the overall energy efficiency of supermarkets can be increased and the environmental impacts reduced is through the integration of trigeneration and CO_2 refrigeration systems.

This thesis investigated experimentally and theoretically proof of concept of the integration of trigeneration and CO_2 refrigeration systems to maximise the reduction of the environmental impacts of supermarkets. The concept combines the advantages of CO_2 refrigeration in reducing direct environmental impacts and trigeneration in reducing indirect impacts through optimisation of fuel energy utilisation.

The research work involved the investigation and development of CO_2 refrigeration technologies for food retail refrigeration applications as well as the integration of CO_2 refrigeration with trigeneration systems to eliminate the use of HFC refrigerants and

produce both energy savings and significant reductions in CO_2 emissions. The work can be detailed as follows:

- Investigation of the advantages of CO_2 as a refrigerant over HFC (hydro-fluorocarbon) refrigerants including the investigation of design approaches for CO_2 refrigeration solutions for supermarket applications.
- Analytical investigations to determine the refrigeration capacity for a test CO_2 refrigeration system and its components and to evaluate the performance of the CO_2 refrigeration system and its integration with the trigeneration system.
- Modelling and design of direct expansion and secondary CO_2 coils for display cabinet applications.
- Design and construction of a primary low temperature and secondary medium temperature CO_2 refrigeration facility for frozen and chilled food refrigeration applications including the integration of the facility with the trigeneration system.
- Experimental investigation to establish the performance of the CO_2 refrigeration system and the performance of the integrated trigeneration and CO_2 refrigeration system.
- Evaluation of the energy performance, environmental impacts and economic viability of the integrated trigeneration and CO_2 refrigeration systems in a case study supermarket application.

This chapter summarises the findings arising from the research work and provides recommendations for future work.

8.1 Conclusions

1 CO_2 (R-744) is an environmentally benign refrigerant. It has an ODP of zero and a very low global warming potential (GWP) of 1 which is much lower than the GWP values of HCFC and HFC refrigerants. The CO_2 refrigerant is non-toxic and non-flammable which make it advantageous over other natural refrigerants such as ammonia and hydrocarbons. Based on thermo-physical properties, theoretical investigation of the comparative performance of CO_2 and other refrigerants for supermarket refrigeration applications showed that:

i) the CO_2 refrigerant to provide good heat transfer in heat exchangers which allows selection of smaller equipment than HCFC and HFC refrigerants;

ii) CO_2 refrigeration systems to operate with low pressure ratio and operate with a very small suction-gas specific volume and low pressure drop leading to smaller size compressors and smaller suction pipe diameters for the same operating conditions;

iii) the smaller components and pipe diameter that can be employed with CO_2 lead to a significant reduction in the refrigerant charge required for a given refrigeration load compared to HCFC and HFC refrigerants;

iv) the main disadvantage of CO_2 refrigerant to be its high working pressures. This can be overcome by using smaller and stronger components.

2 CO_2 refrigeration system solutions for supermarket applications fall into two major categories: subcritical cascade systems and transcritical systems. Subcritical cascade systems operate at moderate pressures and employ two refrigerants one for refrigeration and another for heat rejection. Transcritical systems operate at high pressures and high ambient temperatures but employ only CO_2 as refrigerant. A subcritical CO_2 refrigeration system comprising a primary low temperature circuit for frozen food refrigeration and a secondary medium temperature circuit for chilled food refrigeration was identified to offer distinct advantages for an integrated trigeneration and CO_2 refrigeration system. With this arrangement, the trigeneration system is used to condense the CO_2 refrigerant vapour from both the LT and MT circuits and ensure subcritical operation at all times.

3 Prior the construction of the CO_2 refrigeration system and its integration with the existing trigeneration system, an analytical investigation was performed to determine the capacity of the CO_2 refrigeration system and components. For this purpose, mathematical models were developed for all components which influenced the performance of the integrated system. The models were also used to investigate the performance characteristics of the individual components and integrated system and have led to the following results and conclusions:

1. The refrigeration capacity of the CO_2 refrigeration system that matched with the capacity of the existing trigeneration plant was determined to be 5 kW MT refrigeration and 3 kW LT refrigeration.

2. The investigation of the performance of the CO_2 refrigeration and integrated systems at different condensing temperature showed that: i) increasing the condensing temperature reduced the MT refrigeration capacity and increased the pump power which subsequently reduced the *COP* of the MT refrigeration system; ii) the increase of the condensing temperature also significantly reduced the *COP* of the LT system and the overall *COP* of the refrigeration system (combined LT and MT); iii) increasing the condensing temperature enabled the absorption system to operate at higher delivery brine temperature which improved the *COP* of the absorption and integrated systems.
3. The LT evaporating temperature was also found to affect the performance of the CO_2 refrigeration system. Increasing the LT evaporating temperature improved the *COP* of the LT system but did not have any effect on the *COP* of the MT system. The overall COP of the system increased slightly due to the impact of the increase in the LT system COP. The load ratio of LT to MT refrigeration in a system (*LRLM*) was also found to influence the overall *COP* of the CO_2 system. The overall *COP* increases with reducing *LRLM.*
4. The circulation ratio (*CR*) of the volatile MT system was found to influence the *COP* of the MT and overall CO_2 system. Increasing the circulation ratio above the optimum of between 1.1 and 1.3 reduced the *COP* of the MT and the overall CO_2 system due to the power of the pump.
5. The COP of the integrated trigeneration-CO_2 refrigeration system was found to be highly depended on the COP of the sorption chiller.

4 Investigation of MT CO_2 flooded evaporator coils and CO_2 DX (direct-expansion) evaporator coils for the MT and LT temperature levels was carried out with simulation models developed using EES (Engineering Equation Solver) software. The models were also used to design the geometry and tube arrangement of evaporator coils for the test facility and were validated using data obtained from the experimental investigations. The results showed:

i) for the same refrigeration duty the physical size of the flooded CO_2 evaporator coil was smaller compared to the direct expansion CO_2 evaporator coil;

ii) increasing the evaporating temperature of the CO_2 DX coil increased its refrigeration capacity and reduced the pressure drop;

iii) increasing the circulation ratio of the flooded CO_2 evaporator coil was found to slightly improve the refrigeration duty of the coil but increased the refrigerant mass velocity and pressure drop.

Investigation of the comparative performance of CO_2 DX evaporator coils and conventional coils using R-404A showed that for the same capacity and operating conditions, the CO_2 evaporator coils require smaller size and lower refrigerant charge compared to coils using R-404A refrigerant.

5 Based on the simulation model results, the CO_2 refrigeration system was designed and integrated with the existing trigeneration system to form a complete test facility. The test facility consists of three main modules: CHP module, absorption refrigeration module and retail refrigeration system module. The CHP module is based on an 80 kW_e recuperated micro gas turbine generation package with in-built boiler heat exchanger. The absorption refrigeration module is based on a packaged direct gas fired ROBUR chiller which was re-engineered to operate with a heat transfer fluid heated by the exhaust gases of the microturbine in the CHP module. The retail refrigeration system module consists of a cascade volatile MT and direct expansion LT CO_2 refrigeration system and associated test facilities which include an environmental test chamber and chilled and frozen food display cabinets located in the chamber to provide controlled load to the refrigeration system. The test facility is equipped with Danfoss controllers and was comprehensively instrumented for monitoring and evaluation.

6 The test facility was used to investigate and evaluate the energy performance of the CO_2 refrigeration system as well as that of the overall trigeneration-CO_2 refrigeration system. Tests were performed with different circulation ratios (*CR*) and different evaporating temperatures for the MT CO_2 refrigeration system. The experimental test results demonstrated the following: i) the MT CO_2 refrigeration system was found to be able to achieve very high *COPs* ranging from 32 to 60, due to the low power consumption of the CO_2 pump; ii) the increase in the circulation ratio caused an increase in the power consumption of the pump and influenced the *COP* of the MT system which was found to be in good agreement with the simulation results. The optimum circulation ratio was found to be in the range between 1.1 and 1.3; iii) the

LT CO_2 refrigeration system was found to deliver a steady state *COP* of 4.0; iv) the average overall *COP* of the CO_2 refrigeration system, MT and LT was found to vary in the range between 5.5 and 6.

7 A simulation study was carried out to investigate the seasonal energy and environmental performance of a supermarket energy system using an integrated trigeneration-CO_2 refrigeration based on similar equipment and arrangement as the one used for the laboratory tests and consisting of: i) CO_2 refrigeration system with a DX refrigeration circuit for LT and a pumped CO_2 circuit for MT; ii) a trigeneration system with a microturbine based CHP and ammonia-water absorption refrigeration system. The performance of the energy system was compared with the for a conventional energy system with R-404A parallel refrigerant circuits for MT and LT. The integrated trigneration-CO_2 refrigeration system was found to provide energy savings of the order of 15 % and CO_2 emission savings of the order of 30% compared to the conventional energy system.

8 Further investigations were carried out to optimise the configuration of trigeneration and CO_2 refrigeration systems for supermarkets. Three supermarket energy system alternatives to a conventional system were investigated using experimental data from the test facilities and simulation studies. The results indicated that:

1. Integration of CO_2 refrigeration with trigeneration systems can produce significant energy and GHG emission savings over conventional systems that utilise electricity from the national grid and thermal energy from gas fired boilers.
2. From the 3 alternative systems investigated, the most energy efficient configuration was found to be the one that utilises a trigeneration system based on a natural gas engine based CHP system and a single effect lithium bromide water sorption system which can deliver chilled water at 7 ^{o}C. The cooling produced by the sorption system of the trigeneration plant is used to condense the CO_2 refrigerant of the MT and LT refrigeration systems. The MT system is a secondary 'volatile' pumped system whereas the LT system is a direct expansion system. To bridge the difference in temperature provided by the sorption system and that required to condense the CO_2 refrigerant of the LT

and MT circuits, an MT CO_2 compressor pack is used to operate between the two temperature levels of 7 ^oC delivered by the sorption system and the -8 ^oC condensing temperature required by the CO_2 system. This system was shown to provide fuel energy savings of the order of 30% and CO_2 emission savings of 43% compared to the conventional system. The payback period of the system was found to be of the order of 3.2 years.

3. The use of bio-fuels to drive the trigeneration plant can be attractive in terms of the overall reduction in GHG emissions. However, the cost of bio-fuels can be higher than that of conventional fuels which would have a negative impact on the economic attractiveness of the system.

9

The research work carried out during the course of this project makes a contribution to the overall effort to reduce the energy consumption and environmental impact of the food retail industry, particularly supermarkets, in the UK. The work also delivered specific contributions as follows:

1. The individual test results in the laboratory on the performance of cascade volatile - DX CO_2 refrigeration and trigeneration systems improve confidence in the performance of the individual technologies and integrated systems.
2. The design approach proposed, where CO_2 refrigeration can operate independently of tri-generation when needed, should improve confidence in the reliability of practical application of the concept in supermarkets.
3. The models developed and knowledge gained enable the design and sizing of systems for given applications to ensure maximum performance and utilisation efficiency.
4. Very high performance of CO_2 when used as a secondary fluid in flooded evaporator systems can lead to significant energy savings for high frozen food loads. The optimum circulation ratio was determined to be in the range 1.1 to 1.3.
5. The unique test facility developed enables the in-depth investigation and optimisation of component and system designs and controls. Significant knowledge has been gained from the difficulties encountered in the commissioning of the facility and matching of the capacities of the various

components which is much more critical in CO_2 refrigeration systems compared to conventional R-404A systems.

6. Technical knowledge gained and already disseminated or to be disseminated with further publications includes better understanding of the behaviour of CO_2 as a heat transfer fluid in flooded and direct expansion evaporator coils in display cabinets, component operational characteristics and efficiencies as well as oil management system requirements for the high pressure compressors. These provide significant contributions to the development of more efficient and reliable CO_2 refrigeration technologies.

8.2 Recommendations for future work

The experimental investigations carried out as part of this project were mainly concentrated on obtaining test results for the validation of the component and system models developed. The unique test facilities developed enable the detailed investigation and optimisation of the performance of individual components in the system, optimisation of the matching of the capacities of these components as well as optimisation of the controls.

The evaporator coil models developed enable the prediction of frost accumulation on the coils during operation of the refrigeration system. The predictions of the rate of frost accumulation, however, were found to be lower than the actual test results and the differences which can be due to a variety of reasons such as measurement inaccuracies, and inaccuracies in the frost accumulation algorithms used from the literature need to be investigated further. It will be more appropriate to develop frost formation and accumulation algorithms based on controlled tests in the laboratory for both flooded and DX CO_2 evaporator coils and use these to optimise the defrost cycle.

The Circulation Ratio was found to be a key parameter of the performance of a secondary CO_2 refrigeration system because of its influence on the heat transfer of the coil and the pump power. An optimum circulation ratio enables the secondary refrigeration system to achieve very high two phase heat transfer coefficients. Continuous automatic adjustment of the circulation ratio for each display cabinet and the MT refrigeration system as a whole could lead to higher overall system COP and

further work should be carried out to investigate efficient and economical ways to continuously control the circulation ratio in commercial applications.

CO_2 refrigeration and trigeneration technologies are in their early stages of development and many years of research and development work are still required both at component and system level for these technologies to reach the state of development of conventional systems. The facilities at Brunel and the design and simulation tools developed will play a key role in these developments over the next few years.

REFERENCES

Aidoun, Z., and Ouzzane, M., 2009. A model application to study circuiting and operation in CO_2 refrigeration coils. *Appl. Therm. Eng.* 29, 2544-2553.

Arteconi, A., Brandoni, C., Polonara, F., 2009. Distributed generation and trigeneration: Energy saving opportunities in Italian supermarket sector. *Appl. Therm. Eng*. 29, 1735-1743.

ASHRAE Standard 34, 2007. Designation and safety classification of refrigerants. ASHRAE, Inc., Atlanta. 53 pgs.

ASHRAE Standard 62.1, 2007. Ventilation for acceptable indoor air quality. ASHRAE, Inc., Atlanta, 49 pgs.

ASHRAE Standard 15, 2007. Safety standard for refrigeration system. ASHRAE, Inc., Atlanta, 36 pgs.

ASHRAE, 2010. ASHRAE handbook of refrigeration. ASHRAE, Inc., Atlanta, 749 pgs.

ATMOsphere, 2010. How to bring natural refrigerants faster to market: A summary report. *International workshop on Natural Refrigerants*, Brussels, Belgium, 42 pgs.

Bansal, P.K., and Jain, S., 2007. Cascade systems: past, present, and future. *ASHRAE Transactions* 113, 245-252.

Bassols, J., Kuckelkorn, B., Langreck, J., Schneider, R., Veelken, H., 2002. Trigeneration in the food industry. *Appl. Therm. Eng.* 22, 595–602.

Bayer, 2007. Diphyl-THT: High performance heat transfer fluid for pressureless operation. Available from http://www.bayer.com (accessed 03/06/2007).

Bell, K.J., and Mueller, A.C., 2001. Engineering data book II. Wolverine Tube, Inc., p. 230.

Bellstedt, M., 2008. Carbon dioxide systems for supermarkets review. Green Cooling Council (GCC), 5 pgs, available from: http://www.r744.com (accessed 23/07/2009).

Bellstedt, M., Elefsen, F., Jensen, S.S., 2002. Application of CO_2 (R744) refrigerant in industrial cold storage plant. Forum, 25-30 (also available online from www.airah.org.au).

Bertelsen, P., and Christensen, K., 2003. Use of natural refrigerants in supermarkets. Danish Environmental Protection Agency.

Besant-Roberts, A., 2009. Tesco Thomas Street, Cheetham Hill, Great Manchester: Shortlisted for project of the year. Vinci Construction, UK.

Bingming, W., Huagen, W., Jianfeng, L., and Ziwen, X., 2009. Experimental investigation on the performance of NH_3/CO_2 cascade refrigeration system with twin-screw compressor. *Int. J. Refrigeration* 32, 1358-1365.

Bock, 2009. Product information HGX12P CO_2 subcritical. Available from: http://www.bock.de.

Bodinus, W.S., 1999. The rise and fall of carbon dioxide systems. *ASHRAE Journal*, 37-42.

BS EN 12735-1, 2001. Copper and copper alloys, seamless, round copper tubes for air-conditioning and refrigeration: Part 1 - Tubes for piping systems. BSI, UK, 18 pgs.

BS EN 13136, 2001. Refrigerating systems and heat pumps: Pressure relief devices and their associated piping - methods for calculation, 28 pgs.

BS EN 378-1, 2008. Refrigerating systems and heat pumps - Safety and environmental requirements: Part 1 - Basic requirements, definitions, classification and selection criteria. BSI, UK, 68 pgs.

Campbell, A., Maidment, G.G., Missenden, J.F., 2006. A natural refrigeration system for supermarkets using CO_2 as a refrigerant. *Proc. CIBSE National Conference*, London, UK.

Campbell, A., 2009. Working with CO_2 supermarkets. Available from: http:// www.atmosphere2009.com/speakers.presentations.php (Accessed 14/01/2010).

Campbell, A., and Riley, O., 2009. Building services for low carbon supermarkets. *Proc. Inst. R.* 2009-10, 3/1-8.

CanmetENERGY, 2009. CO_2 as a refrigerant in a Sobeys Supermarket, a case study. Natural Resources Canada, 8 pgs, available from: http://canmetenergy.nrcan.gc.ca (accessed 02/05/2010).

CCC, 2008. Building a low-carbon economy-The UK's contribution to tackling climate change. The 1st report of the Committee on the Climate Change, 511 pgs, available from: http://www.theccc.org.uk (accessed 12/03/2010).

CCC, 2010. The fourth carbon budget, reducing emissions through the 2020s, 376 pgs, available from: http://www.theccc.org.uk (accessed 12/03/2010).

Chandrasekharan, R., Verma, P., Bullard, C.W., 2006. Development of a design tool for display case evaporators. *Int. J. Refrigeration* 29, 823-832.

Cheng, L., Ribatski, G., Moreno-Quiben, J., Thome, J.R., 2008a. New prediction methods for CO_2 evaporation inside tubes: Part I - A two-phase flow pattern map and a flow pattern based phenomenological model for two-phase flow frictional pressure drops. *Int. J. Heat and Mass Transfer* 51, 111-124.

Cheng, L., Ribatski, G., Thome, J.R., 2008b. New prediction methods for CO_2 evaporation inside tubes: Part II - An updated general flow boiling heat transfer model based on flow patterns. *Int. J. Heat and Mass Transfer* 51, 125-135.

CIBSE CHP Group, 2005. Spark ignition gas engine CHP. Available from: www.cibse.org/chp, (accessed 18/03/2009).

CIBSE Guide F, 2004. Energy efficiency in buildings. 2nd edition, London, The Chartered Institution of Building Services Engineers Publications, London, 261 pgs.

Cogenco, 2008. Cogenco cogeneration units 50 Hz range on natural gas. Available from: http://www.cogenco.com, (accessed 09/06/2010).

Coleman, H.W., and Steele, W.G., 2009. Experimentation, validation and uncertainty analysis for engineers. 3rd edition, John Wiley & Sons, Inc., ISBN: 978-0-470-16888-2.

Coulomb, D., 2008. Refrigeration and cold chain serving the global food industry and creating a better future: two key IIR challenges for improved health and environment. *Trends in Food Science & Technology* 29, 413-417.

Cowan, D., Chaer, I., Maidment, G., 2010. Reducing refrigerant emissions and leakage – An overview and feedback from two EU projects. *Proc. Sustainable Refrigeration and Heat Pump Conference*, Stockholm, Sweden, ISBN 978-2-913149-81-6, 16 pgs.

Danfoss, 2008a. Transcritical CO_2 systems in a small supermarket. Available from www.danfoss.com/CO_2 (accessed 12/01/2009).

Danfoss, 2008b. Product catalogue. Available from: www.danfoss.co.uk.

Danfoss, 2010. Experience significant savings with the Danfoss pumped CO_2 solution. Available from www.danfoss.com/CO_2 (accessed 28/11/2010).

Dean & Wood, 2011. Available from: http://dean-wood.com/products/refrigerant-price/ (accessed 22/04/2011).

DEFRA, 2005. The validity of food miles as an indicator of sustainable development: final report. ED50254, Issue 7, available from: http://statistics.defra.gov.uk/esg/ reports/foodmiles/default.asp/ (accessed 24/09/2009).

DEFRA, 2009. Guidelines to DEFRA / DECC's GHG conversion factors for company reporting: Methodology paper for emission factors. DEFRA, London, 59 pgs.

Dopazo, J.A., Fernández-Seara, J., Sieres, J., and Uhía, F.J., 2009. Theoretical analysis of a CO_2-NH_3 cascade refrigeration system for cooling applications at low temperatures. *Appl. Therm. Eng*. 29, 1577–1583.

EES, 2010. Engineering equation solver. www.fChart.com

ESK Schultze, 2008. Components for CO_2, available from: www.esk-schultze.de.

Estrada-Flores, S., 2010. Achieving temperature control and energy efficiency in the cold chain. *Proc. 1st IIR International cold chain conference, Sustainability and the Cold Chain*, Cambridge, workshop paper, ISBN 978-2-913149-75-5, 13 pgs.

Evans, J.A., 2008, Frozen food science and technology. FRPERC University of Bristol, UK, Blackwell Publishing Ltd, ISBN 978-1-4051-5478-9, 355 pgs.

Evans, J.A., 2010. Retail display. *Proc. 1st Conference on Sustainability and the Cold Chain*, Cambridge, UK, ISBN 978-2-9193149-75-5, workshop paper, 13 pgs

Fernandez-Seara, J., Sieres, J., and Va´zquez, M., 2006. Compression-absorption cascade refrigeration system. *Appl. Therm. Eng.* 26, 502-512.

Gartshore, J., and Benton, S., 2010. Cool concerns and Waitrose to support the use of hydrocarbons. Available from: http://www.hydrocarbons21.com/content/articles/ 2010-07-22-cool-concerns-and-waitrose-to-support-the-use-of-hydrocarbons.php.

Getu, H.M., and Bansal, P.K., 2007. Modeling and performance analyses of evaporators in frozen-food supermarket display cabinets at low temperatures. *Int. J. Refrigeration* 30, 1227-1243.

Getu, H.M., and Bansal, P.K., 2008. Thermodynamic analysis of an R744–R717 cascade refrigeration system. *Int. J. Refrigeration* 31, 45-54.

Girotto, S., Minetto, S., Neksa, P., 2004. Commercial refrigeration system using CO_2 as the refrigerant. *Int. J. Refrigeration* 27, 717-723.

Heerup, C., 2009. Industrial systems. In: Reulens, W., Natural refrigerant CO_2, KHLim, Belgium, 43-99.

Hinde, D., Shitong Zha, S., Lan, L., 2009. Carbon dioxide in North American supermarkets. *ASHRAE Journal* 51, 18-26.

Hinde, D., 2011. Applying natural refrigerants in supermarket refrigeration. ASHRAE winter conference, Las Vegas, USA, reported in: http://www.ammonia21.com.

Hong, K.T., and Webb, R.L., 1996. Calculation of fin efficiency for wet and dry fins. *HVAC&R Research* 2, 27-41.

IEA, 2009. World energy outlook. Available at http://www.worldenergyoutlook.org/ (accessed 03/12/2010).

IIR, 2000. 5th Informatory note on refrigerants: Carbon dioxide as a refrigerant. Available from www.iifiir.org (accessed 02/01/2009).

Inlow, S.W., and Groll, E.A., 1996. Analysis of secondary loop refrigeration systems using carbon dioxide as volatile secondary refrigerant. *HVAC&R Research* 2, 107-120.

IPCC, 2005. Safeguarding the ozone layer and the global climate system. UN-Intergovernmental Panel on Climate Change, 478 pgs, available from: http:// arch.rivm.nl/env/int/ipcc/pages_media/SROC-final/SpecialReportSROC.html (accessed 12/08/2008).

Ismail, K.A.R., and Salinas, C.S., 1999. Modelling of frost formation over parallel cold plates. *Int. J. Refrigeration* 22, 425-441.

ISO 23953-1, 2005. International Standard - Refrigerated display cabinets: Part 1 - Vocabulary, 36 pgs.

ISO 23953-2, 2005. International Standard - Refrigerated display cabinets: Part 2 - Classification, requirements and test conditions, 86 pgs.

Jiang, H., Aute, V., Radermacher, R., 2006. Coil designer: a general-purpose simulation and design tool for air-to-refrigerant heat exchangers. *Int. J. Refrigeration* 29, 601-610.

Jokar, A., Hayes, N., Ayub, Z.H., 2010. Recent developments in CO_2 cascade condenser. *Proc. Sustainable Refrigeration and Heat Pump Technology Conference*, Stockholm, Sweden, 2010, 8 pgs.

Kakac, S., and Liu, H., 2002. Heat exchanger selection, rating and thermal design. 2nd edition, United State of America: CRC Press LLC.

Kays, W. M., and London, A. L., 1998. Compact heat exchangers. 3rd edition, Krieger Publishing, Malabar, FL.

Kim, N.H., Youn, B., Webb, R.L., 1999. Heat transfer and friction correlations for plain fin-and-tube heat exchangers. *Proc. 11th Int. Heat Transfer Conference*, Kyongju, Korea, 209-213.

Lawrence, J.M.W., and Gibson, D., 2010. Energy use across supermarket refrigeration. *Proc. 1st IIR International cold chain conference, Sustainability and the Cold Chain*, Cambridge, ISBN 978-2-913149-75-5, paper no. 242, 12 pgs.

Lee, T.S., Liu, C.H., Chen, T.W., 2006. Thermodynamic analysis of optimal condensing temperature of cascade-condenser in CO_2/NH_3 cascade refrigeration systems. *Int. J. Refrigeration* 29, 1100-1108.

Liang, S.Y., Wong, T.N., Nathan, G.K., 2001. Numerical and experimental studies of refrigerant circuitry of evaporator coils. *Int. J. Refrigeration* 24, 823-833.

Lidl, 2011. Two hundred Lidl stores to feature R290 technology by 2012. Available from: http://www.hydrocarbons21.com//content/articles/2011-01-14-200-lidl-stores-to-feature-r290-technology-by-2012.php.

Lommers, C.A., 2003. Air conditioning and refrigeration industry refrigerant selection guide. 7th ed. Melbourne, AIRAH, 66 pgs.

Lorentzen, G., 1995. The use of natural refrigerant: a complete solution to the CFC/HCFC predicament. *Int. J. Refrigeration* 18, 190-197.

M. Conde Engineering, 2002. Properties of working fluids–brines. Zurich, Switzerland, 9 pgs.

Maidment, G.G. and Tozer, R.M., 2002. Combined cooling heat and power in supermarkets. *Appl. Therm. Eng.* 22, 653-665.

Maidment, G.G., Zhao, X., Riffat, S.B. and Prosser, G., 1999. Application of combined heat and power and absorption cooling in a supermarket. *Applied Energy* 63, 169-190.

Maidment, G.G., Zhao, X. and Riffat, S.B., 2001. Combined cooling and heating using a gas engine in a supermarket. *Applied Energy* 68, 321–335.

Maidment, G.G., and Prosser, G., 2000. The use of CHP and absorption cooling in cold storage. *Appl. Therm. Eng.* 20, 1059–1073.

Mattsson, S.E., 1997. On modelling of heat exchangers in modelica. Proc. the 9th European Simulation Symposium, ESS'97, Oct 19-23, 1997, Passau, Germany.

Melinder, A., and Granryd, E., 2010. What to consider when using secondary fluids in indirect systems. *Proc. Sustainable Refrigeration and Heat Pump Conference*, Stockholm, Sweden, ISBN 978-2-913149-81-6, 12 pgs.

Met Office, 2009. Weather data for the London and Manchester area of the United Kingdom. Available from: www.metoffice.gov.uk

Moorjani, M., 2009. CHP in industrial and commercial sectors, a case study. Available from: http://chp.decc.gov.uk/cms/presentations-archive/ (accessed 03/09/2010).

Moreno-Quiben, J., and Thome, J.R., 2007a. Flow pattern based two-phase frictional pressure drop model for horizontal tubes: Part I - Diabatic and adiabatic experimental study. *Int. J. Heat and Fluid Flow* 28, 1049-1059.

Moreno-Quiben, J., and Thome, J.R., 2007b. Flow pattern based two-phase frictional pressure drop model for horizontal tubes: Part II - New phenomenological model. *Int. J. Heat and Fluid Flow* 28, 1060-1072.

MTP, 2008. BNCR36: Direct emission of refrigerant gases. Market Transformation Programme, available from: http://efficient-products.defra.gov.uk/cms/product-strategies/subsector/commercial-refrigeration (accessed 24/12/2009).

Navarro, E., Granryd, E., Urchueguia, J.F., Corberan, J.M., 2007. A phenomenological model for analyzing reciprocating compressors. *Int. J. Refrigeration* 30, 1254-1265.

PAS 2050, 2008. Specification for the assessment of the life cycle greenhouse gas emissions of goods and services. BSI Group, London, 43 pgs, available from: http://shop.bsigroup.com/en/Browse-by-Sector/Energy-Utilities/PAS-2050/ (accessed 03/12/2010).

Pearson, A., 2005. Carbon dioxide - new uses for an old refrigerant. *Int. J. Refrigeration* 28, 1140-1148.

Pearson, A., 2008. Refrigeration with Ammonia. *Int. J. Refrigeration* 31, 545–551.

PolySMART, 2008. Polygeneration in Europe – a technical report. 200 pgs, available from: http://www.polygeneration.org/.

Proklima, 2008. Natural refrigerants. GTZ GmbH, Eschborn, Germany, 208 pgs.

Rhiemeier, J.M., Harnisch, J., Ters, C., Kauffeld, M., Leisewitz, A., 2009. Comparative assessment of the climate relevance of supermarket refrigeration systems and equipment. Federal Environment Agency, 270 pgs, available from: http:// www.umweltbundesamt.de.

Riffat, S.B., Afonso, C.F., Oliveira, A.C., Reay, D.A., 1997. Natural refrigerants for refrigeration and air-conditioning system. *Appl. Therm. Eng.* 17, 33-42.

Rivet, P., 2002. A green and up to date retail store. *Proc. International Conference New Technologies in Commercial Refrigeration*, Urbana, IL, USA, pp. 31-34.

Robur, 2006. Gas fired absorption chiller for cooling medium-large area: installation, use and maintenance manual. 7th edition, available from http://www.robur.com (accessed 30/05/2007).

Rogstam, J., 2010. Ice rinks using carbon dioxide as secondary refrigerant. *Proc. Sustainable Refrigeration and Heat Pump Conference, Stockholm*, Sweden, ISBN 978-2-913149-81-6, 9 pgs.

Romero-Mendez, R., Sen, M., Yang, K.T., McClain. R., 2000. Effect of fin spacing on convection in plate fin and tube heat exchanger. *Int. J. Heat and Mass Transfer* 43, 39-51.

Sawalha, S., Soleimani, K.A., Rogstam, J., 2006. Experimental and theoretical evaluation of NH_3/CO_2 cascade system for supermarket refrigeration in laboratory environment. *Proc. 7th IIR Gustav Lorentzen Conference on Natural Working Fluids*, Trondheim, Norway.

Sawalha, S., 2008. Theoretical evaluation of transcritical CO_2 systems in supermarket refrigeration. Part I: Modelling, simulation and optimization of two system solutions. *Int. J. Refrigeration* 31, 516-524.

Schmidt, T.E., 1945. La production calorifique des surfaces munies d'ailettes. Bulletin de l'Institut International du Froid, Annexe G-5; cited in: Hong, K.T., and Webb, R.L., 1996. Calculation of fin efficiency for wet and dry fins. *HVAC&R Research* 2, 27-41.

Schmidt, T.E., 1949. Heat transfer calculation for extended surfaces. Refrigerating Engineering 57, 351-357; cited in: Perrotin, T., and Clodic, D., 2003. Fin efficiency calculation in enhanced fin and tube heat exchangers in dry conditions. *Proc. International Congress of Refrigeration*, Washington, D.C., US, paper no. ICR-0026, 8 pgs.

Shah, R.K., and Seculic, D.P., 2003. Fundamental of heat exchanger design. John Wiley & Sons Inc., New Jersey, 564-574.

Shilliday, J.A., and Tassou, S.A., 2010. Numerical analysis of a plate fin and tube evaporator using the natural refrigerant CO_2. *Proc. 1st IIR International cold chain conference, Sustainability and the Cold Chain*, Cambridge, ISBN 978-2-913149-75-5, 8 pgs.

SRC, 2001. Refrigerant evaporator (DX) coil. Available from: http://www.srcoils.com/File/PDF/Evap%20Coil%20Primer.pdf (Accessed 12/03/2010).

SRC, 2010. Standard plate fin coil specifications. Available from: http://www.srcoils.com /wp-content/blogs.dir/1/files/2010/05/Coil_Specs_Nomenclature.pdf (accessed 12/03/2010).

Stoecker, W.F., 1998. Industrial refrigeration handbook. McGraw-Hill, 782 pgs.

Suamir, IN. and Tassou, S.A., 2010. Trigeneration and its integration with CO_2 refrigeration systems for supermarket applications. In: the SIRAC meeting, Brunel University, 23rd June 2010, 17 pgs, available from: http://www.sirac.org.uk/.

Suamir, IN., Tassou, S.A., Hadawey, A., Chaer, I., Marriott, D., 2009. Investigation of the performance characteristics of an ammonia-water absorption chiller in a trigeneration system arrangement. *Proc. HPC Conference, Berlin, Germany*, ISBN 978-0-9563329-0-5, paper no. HPC430, 6 pgs.

Sugiartha, N., Tassou, S.A., Chaer, I., Marriott, D., 2008. Trigeneration in food retail: An energic, economic and environmental evaluation for a supermarket application. *Appl. Therm. Eng.* 29, 2624–2632.

Sugiartha, N., Chaer, I., Tassou, S.A., Marriott, D., 2006. Assessment of a micro-gas turbine based trigeneration system in a supermarket. *Proc. The International Conference of Fluid and Thermal Energy Conversion*, Jakarta, Indonesia, ISSN 0854 9346, 12 pgs.

Swain, M., 2006. Energy use in food refrigeration: calculation, assumptions and data sources. FRPERC JOB NO. 2006013, University of Bristol, 19 pgs.

Tassou, S.A., and Suamir, IN., 2010. Trigeneration – a way to improve food industry sustainability. *Proc. SEEP 2010 Conference*, Bari, ITALY, 14 pgs.

Tassou, S.A., Chaer, I., Sugiartha, N., Ge, Y.T., Marriott, D., 2007. Application of trigeneration systems to the food retail industry. *Energy Conversion & Management* 48, 2988-2995.

Tassou, S.A., Ge, Y., Hadawey, A., Marriott, D., 2011. Energy consumption and conservation in food retailing. *Appl. Therm. Eng.* 31, 147-156.

Tassou, S.A., Chaer, I., Sugiartha, N., Marriott, D., Suamir, IN., 2008. Trigeneration – a solution to efficient use of energy in the food industry. Proc. Inst. R. 2007-08 7/1-16.

Tassou, S.A., Lewis, J.S., Ge, Y.T., Hadawey, A., Chaer, I., 2010. A review of emerging technologies for food refrigeration applications. *Appl. Therm. Eng.* 30, 263-276.

Tesco, 2009. Available from: http://tesco_energyict.com/tesco_webclient/ (accessed 2010, username and password required).

Threlkeld, J.L., 1970. Thermal environmental engineering. 2nd edition, Prentice Hall Book Co., Englewood Cliffs, NJ, 1970, cited in: Getu, H.M., Bansal, P.K., 2007. Modelling and performance analyses of evaporators in frozen-food supermarket display cabinets at low temperatures. *Int. J. Refrigeration* 30, 1227-1243.

TOC, 2006. Report of the refrigeration, air conditioning and heat pumps. UNEP, Nairobi, 223 pgs.

Verdemar, 2010. The first supermarket in Latin America that uses CO_2 as a refrigerant. 9 pgs, available from: http://www.r744.com (accessed 24/12/2010).

Walravens, F., Hailes, J., Cox, N., 2009. ChillingFacts: The big supermarket refrigeration scandal. EIA, London, 8 pgs, available from: www.chillingfacts.org.uk (accessed 20/11/2010).

Wang, C.C., Chang, Y.J., Hsieh, Y.C., Lin, Y.T., 1996. Sensible heat and friction characteristics of plate fin and tube heat exchanger having plane fins. *Int. J. Refrigeration* 19, 223-230.

Wojtan, L., Ursenbacher, T., Thome, J.R., 2005a. Investigation of flow boiling in horizontal tubes: Part I - A new diabatic two-phase flow pattern map. *Int. J. Heat and Mass Transfer* 48, 2955-2969.

Wojtan, L., Ursenbacher, T., Thome, J.R., 2005b. Investigation of flow boiling in horizontal tubes: Part II - Development of a new heat transfer model for stratified-wavy, dryout and mist flow regimes. *Int. J. Heat and Mass Transfer* 48, 2970-2985.

APPENDIX A:

Trigeneration plant

This appendix presents the schematic diagram of the trigeneration plant prior integration with CO_2 refrigeration. The plant employs oil Diphyl-THT as heat transfer medium to transfer the recovered heat from the CHP unit to the absorption chiller as described in Chapter 1, Section 1.4.

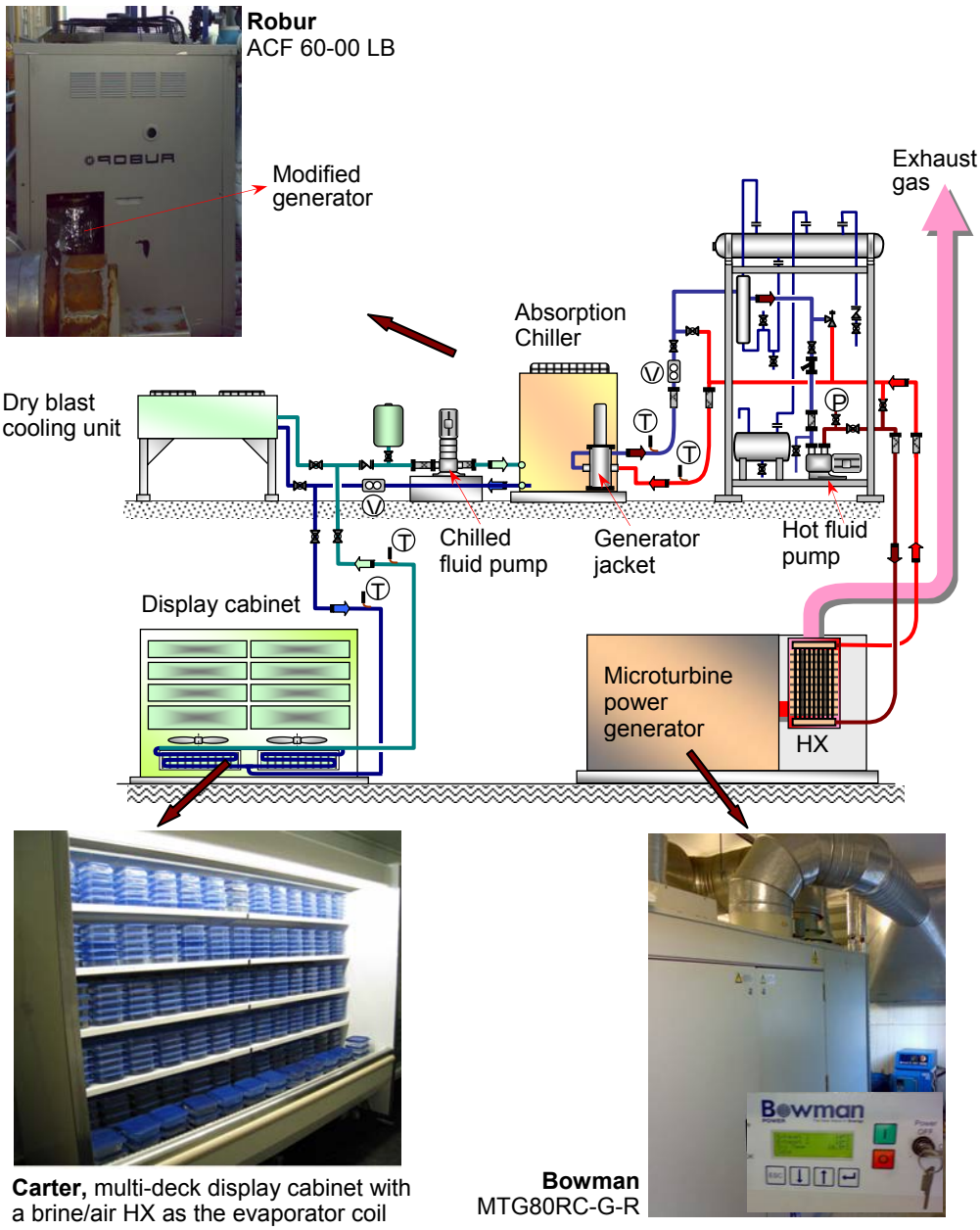

Figure A-1 The trigeneration plant prior integration with CO_2 refrigeration

APPENDIX B:

Mathematical model of integrated trigeneration and CO_2 refrigeration

This appendix provides supporting equations used in the mathematical models. Key equations of the model are presented in Chapter 3. The appendix also presents the displays of the EES models of the integration arrangements, pipe sizing and the liquid receiver.

HTF properties:

Best fit equations of the properties of oil Diphyl-THT (Bayer, 2007) used for heat transfer fluid (HTF) of the trigeneration system:

1. Density (kg/m^3) at temperature range 0 – 340 ^{o}C:

   $\rho = 0.652245603\ .\ T + 1017.526696$ (B.1)

   Coefficient of correlation $R^2 = 1.0000$

2. Specific heat transfer coefficient (kJ/kg.^{o}C) at temperature range 0 – 340 ^{o}C:

   $Cp = 0.003462118\ .\ T + 1.465115098$ (B.2)

   Coefficient of correlation $R^2 = 1.0000$

3. Thermal conductivity (W/m.^{o}C) at temperature range 0 – 340 ^{o}C:

   $k = -2.5315\ .\ 10^{-5}\ .\ T + 0.109809175$ (B.3)

   Coefficient of correlation $R^2 = 0.9914$

4. Dynamic viscosity (Pa.s) at temperature range 20 – 340 ^{o}C:

   $\mu = 20.0708312959\ .\ T^{-1.87016162771}$ (B.4)

   Coefficient of correlation $R^2 = 0.9865$

Temperature is in ^{o}C.

The equations of aqueous solution of the propylene glycol:

Density and specific heat of the propylene glycol can be determined from the equations described in M. Conde Engineering (2002) as below:

$$\rho_{brine} = 508.4 - 182.4\xi + 965.8\left[\frac{273.15}{T_{brine}}\right] + 280.3\xi\left[\frac{273.15}{T_{brine}}\right] - 472.2\left[\frac{273.15}{T_{brine}}\right]^2 \quad \text{(B.5)}$$

$$Cp_{brine} = 4.476 + 0.6086\xi - 0.715\left[\frac{273.15}{T_{brine}}\right] - 1.939\,\xi\left[\frac{273.15}{T_{brine}}\right] + 0.4787\left[\frac{273.15}{T_{brine}}\right]^2 \quad \text{(B.6)}$$

Where:

ρ_{brine} in kg/m^3; Cp_{brine} in kJ/kg K; $T_{brine} = \frac{T_i - T_o}{2}$ in K

ξ = mass fraction of propylene glycol in water (used ξ = 40%).

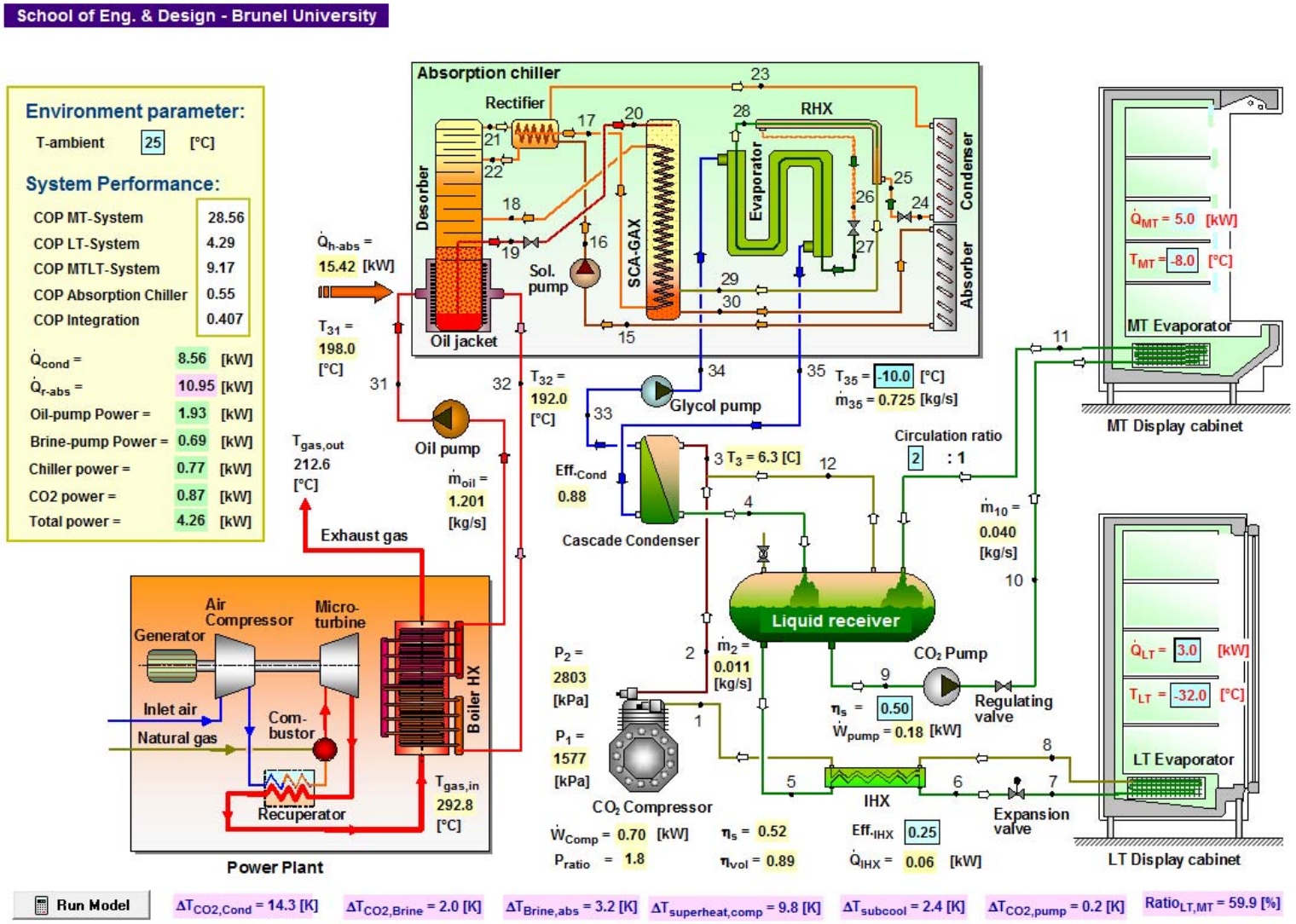

Figure B-1 A display of the EES model of the integration arrangement for component sizing

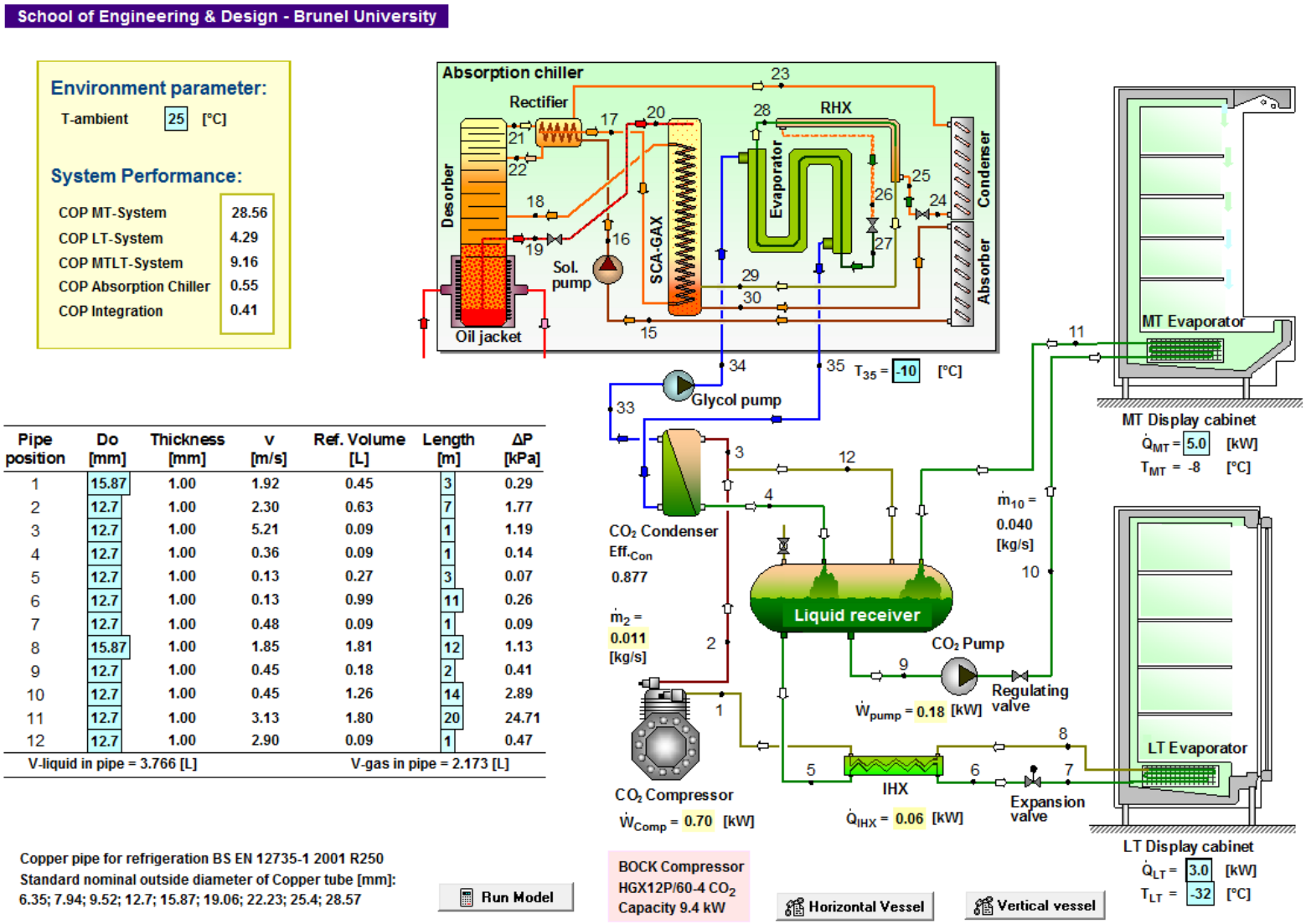

Figure B-2 EES model of pipe sizing and pressure drop simulation

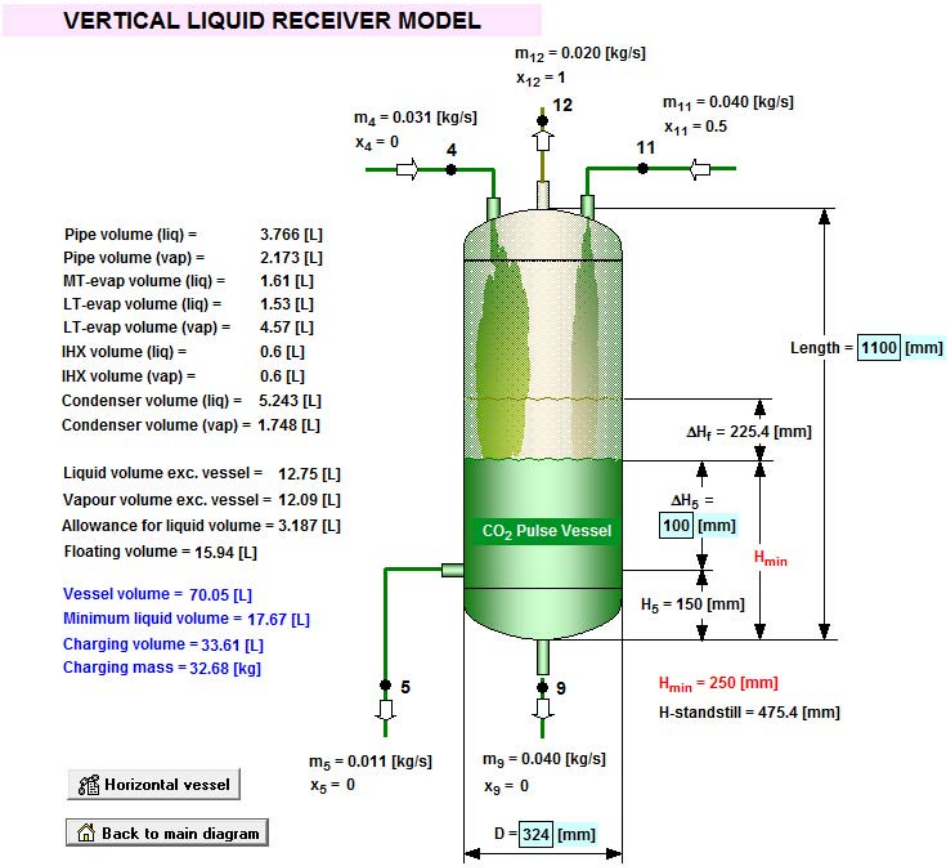

Figure B-3 Vertical liquid receiver model

APPENDIX C:
Mechanical components

This appendix provides drawing of the identification and numbering of the mechanical control of the CO_2 refrigeration system. The design drawings of the liquid receiver, MT and LT evaporator coils are also presented.

Legend for the symbol used in the mechanical control drawing:

V = flow control valve

PS = pressure transducer

SV = Solenoid valve

AKV = Danfoss electronic expansion valve

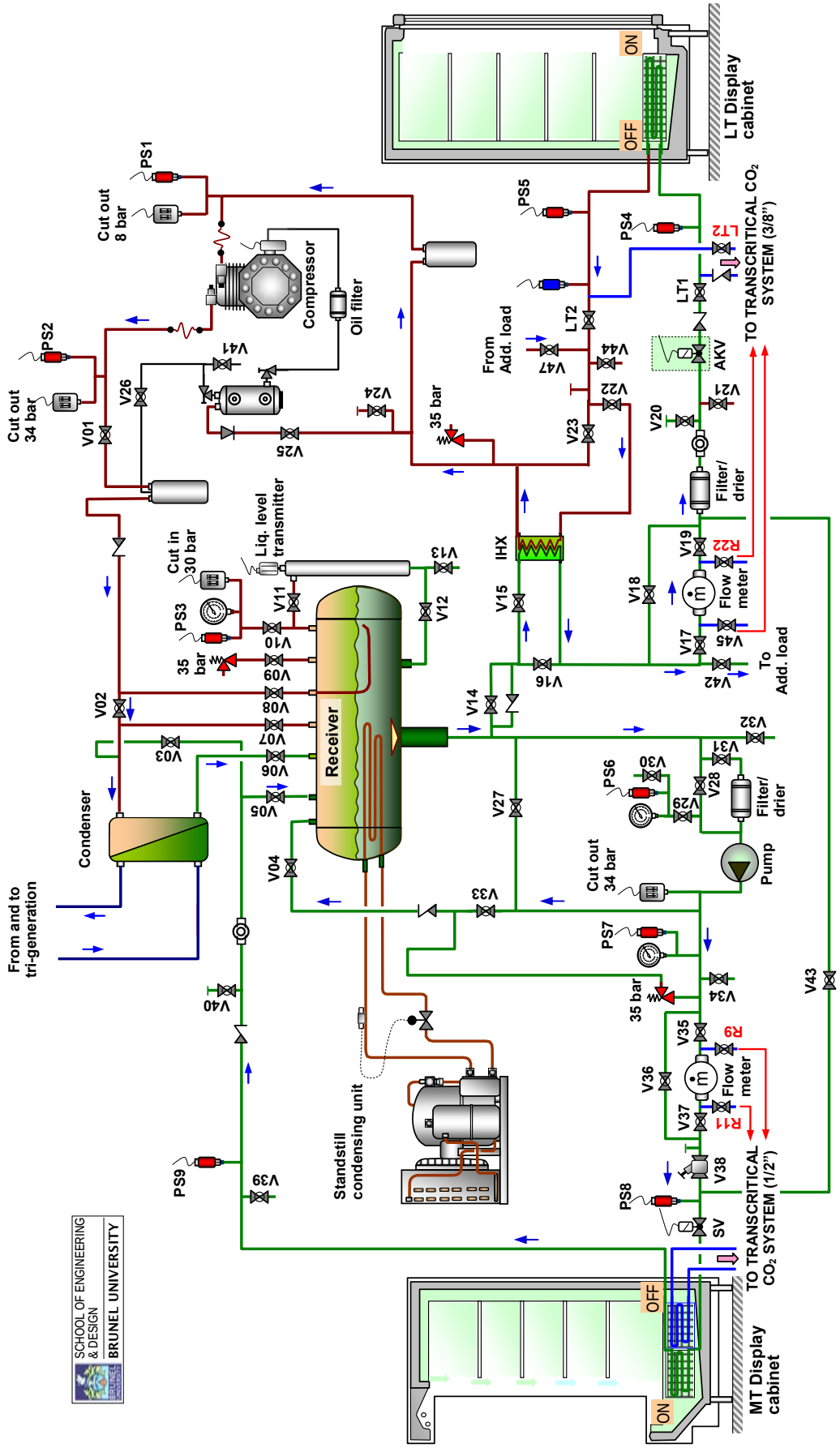

Figure C-1 Identification and numbering of the mechanical control components

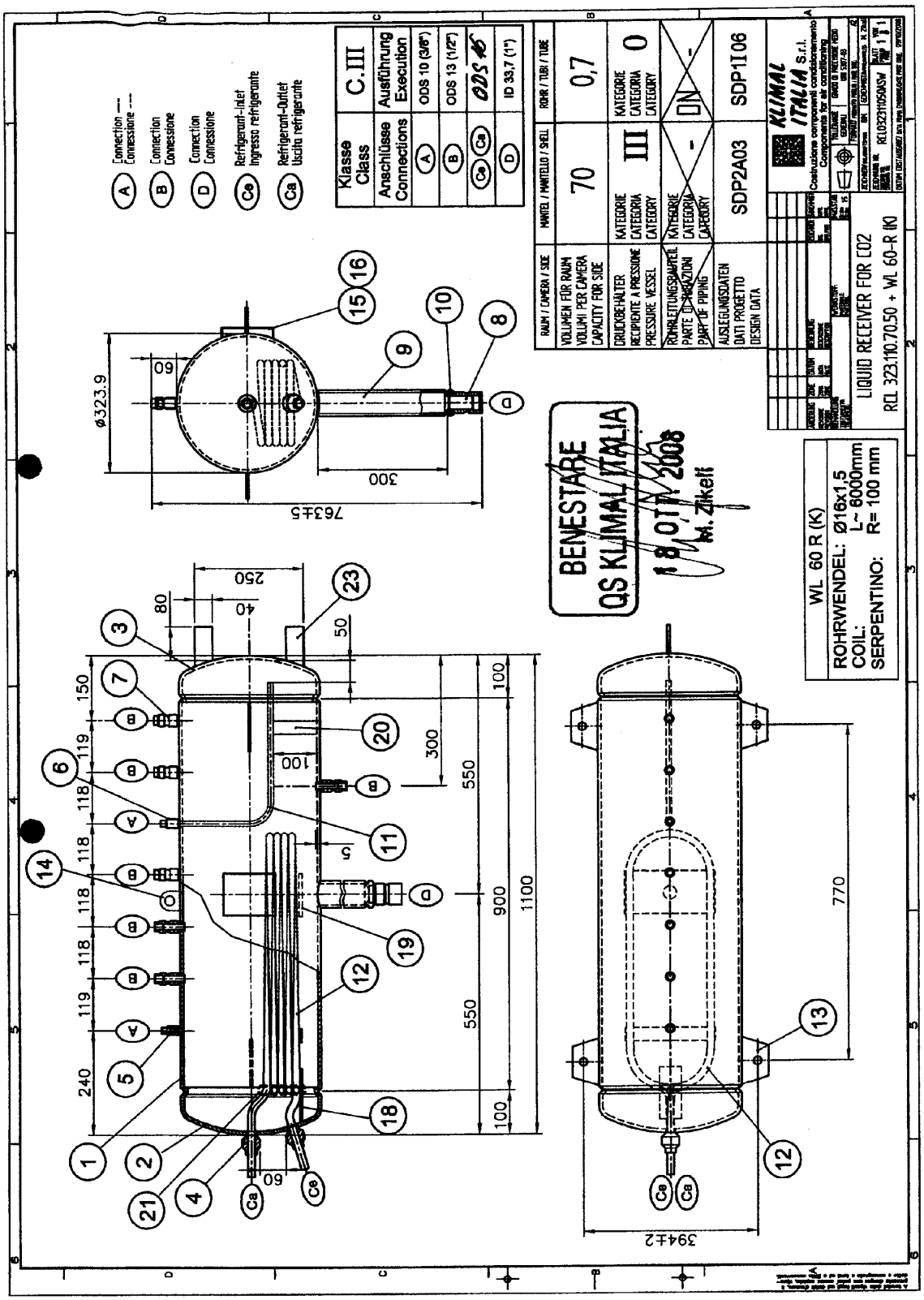

Figure C-2 Liquid receiver with the mounting of the liquid level transmitter

Technical data of the CO_2 compressor:

Type	Number of cylinders	Swept volume 50 / 60 Hz (1450/1740 1/min)	Electrical data ③				Weight	Connections		Oil charge
			Voltage ①	Max. working current ②	Max. power consumption ②	Starting current (rotor locked)		Discharge line DV	Suction line SV	
		m³/h		A	kW	A	kg	mm I inch	mm I inch	Ltr.
				Δ / Y		Δ / Y				
HGX12P/60-4 CO2	2	5,40 / 6,40	④	9,5 / 5,5	3,2	45 / 26	49	12 / 1/2	16 / 5/8	0,9

Explanations:

① Tolerance (± 10%) relates to the mean value of the voltage range. Other voltages and current types on request.

② Take account of the max. operating current / max. power consumption when designing contactors, leads and fuses. Switches: Service category AC3

③ All data are based on the mean value of the voltage range.

④ 220-240 V Δ / 380-420 V Y - 3 - 50 Hz
265-290 V Δ / 440-480 V Y - 3 - 60 Hz

Oil sump heater 110-240 V - 1 - 50/60 Hz
› HGX12P, HGX22P, HGX34P: 50-120 W
PTC heater, self-regulating, installation in housing bore
Oil sump heater 230 V - 1 - 50/60 Hz
› HGX4: 80 W
Permanently set version, installation in immersion sleeve

(Source: Bock, 2009)

CO_2 pump specification:

Manufacturer:	HERMETIC-Pumpen GmbH
Pump type	Rotary vanes
Model	HTP 1-400
Rated flow	0.44 m^3/h (approx. 108 gram/s at -8 ^oC)
NPSH required	3.5 mLC
Speed of pump	1450 rpm
Test pressure	37.5 bar
Suction port	3/8” (flange or weld connection)
Discharge port	3/8” (flange or weld connection)
Motor type	3 ph induction motor
Power output	0.37 kW
Voltage	230/400 Volt
Frequency	50 Hz
Motor speed	1450 rpm
Frequency converter	1450-750 rpm approx. flow 0.44-0.22 m^3/h

Manufacturer details:

Hermetic-Pumpen GmbH,
Gewerbestrrasse 51
79194 Gundelfingen, Deutschland
Phone +49-761-5830-0; Fax: +49-761-5830-180
lederle@lederle-hermetic.com; http://www.lederle-hermetic.com

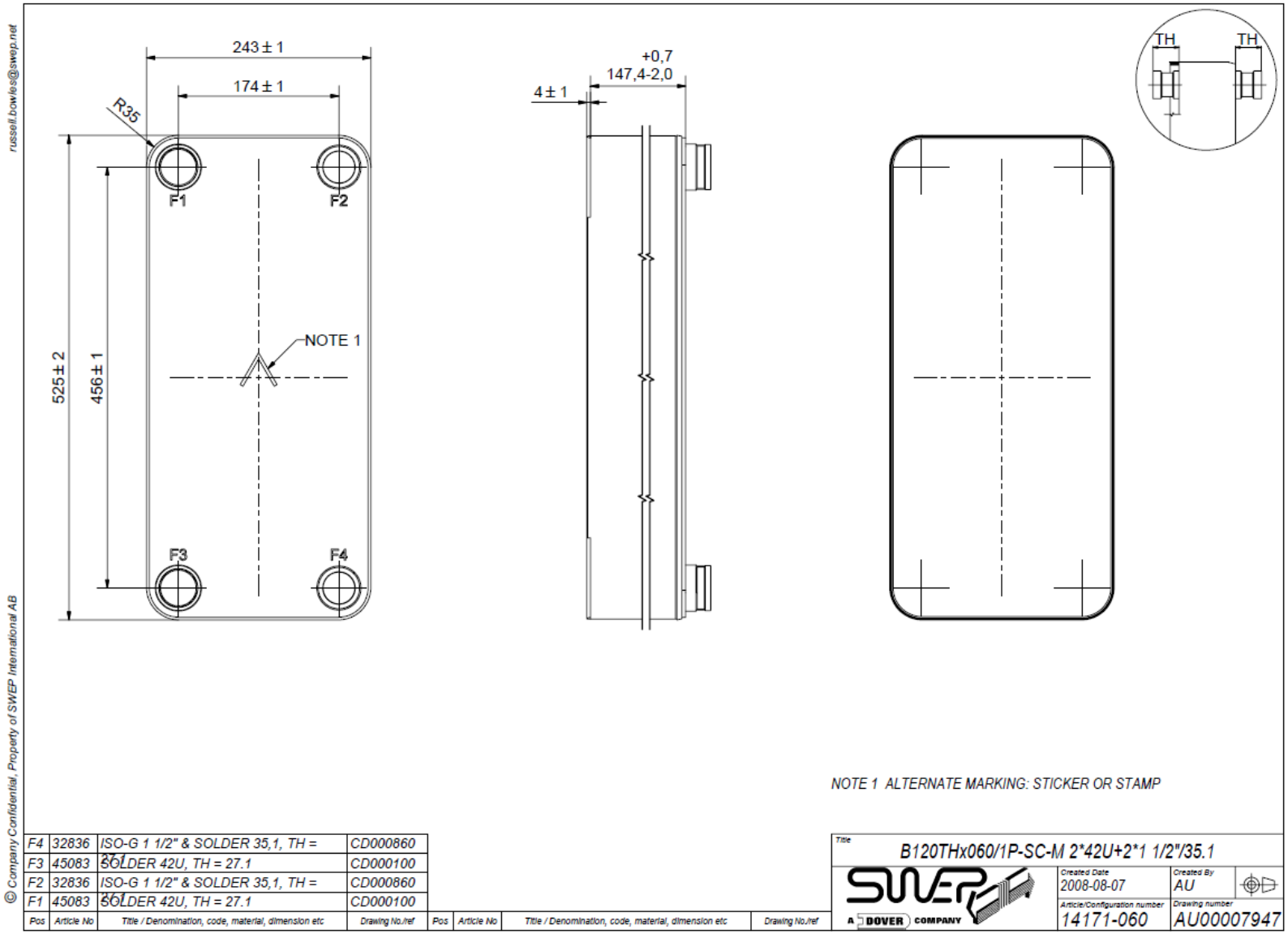

Figure C-3 Plate heat exchanger for the CO_2 condenser

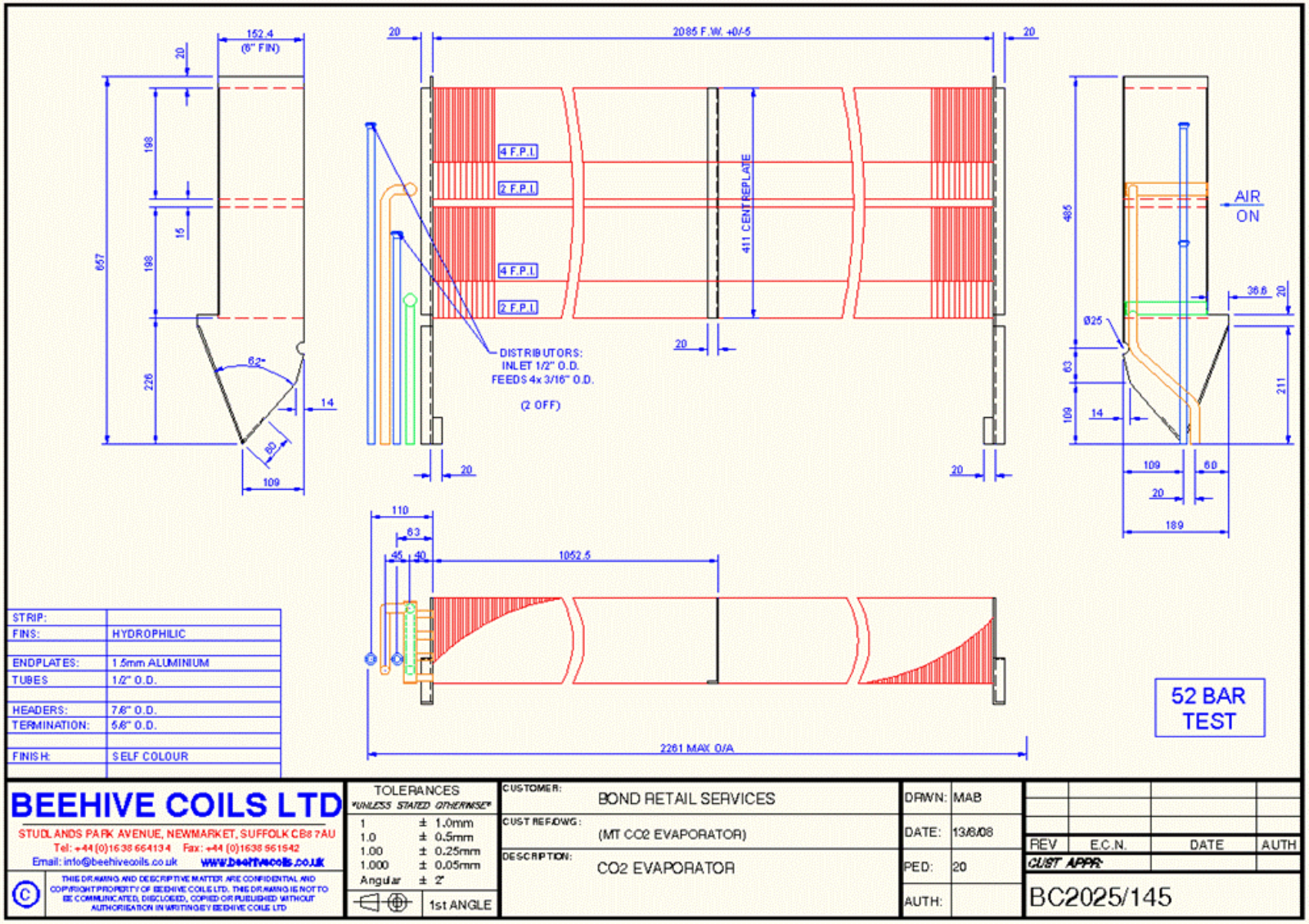

Figure C-4 Medium temperature evaporator coil

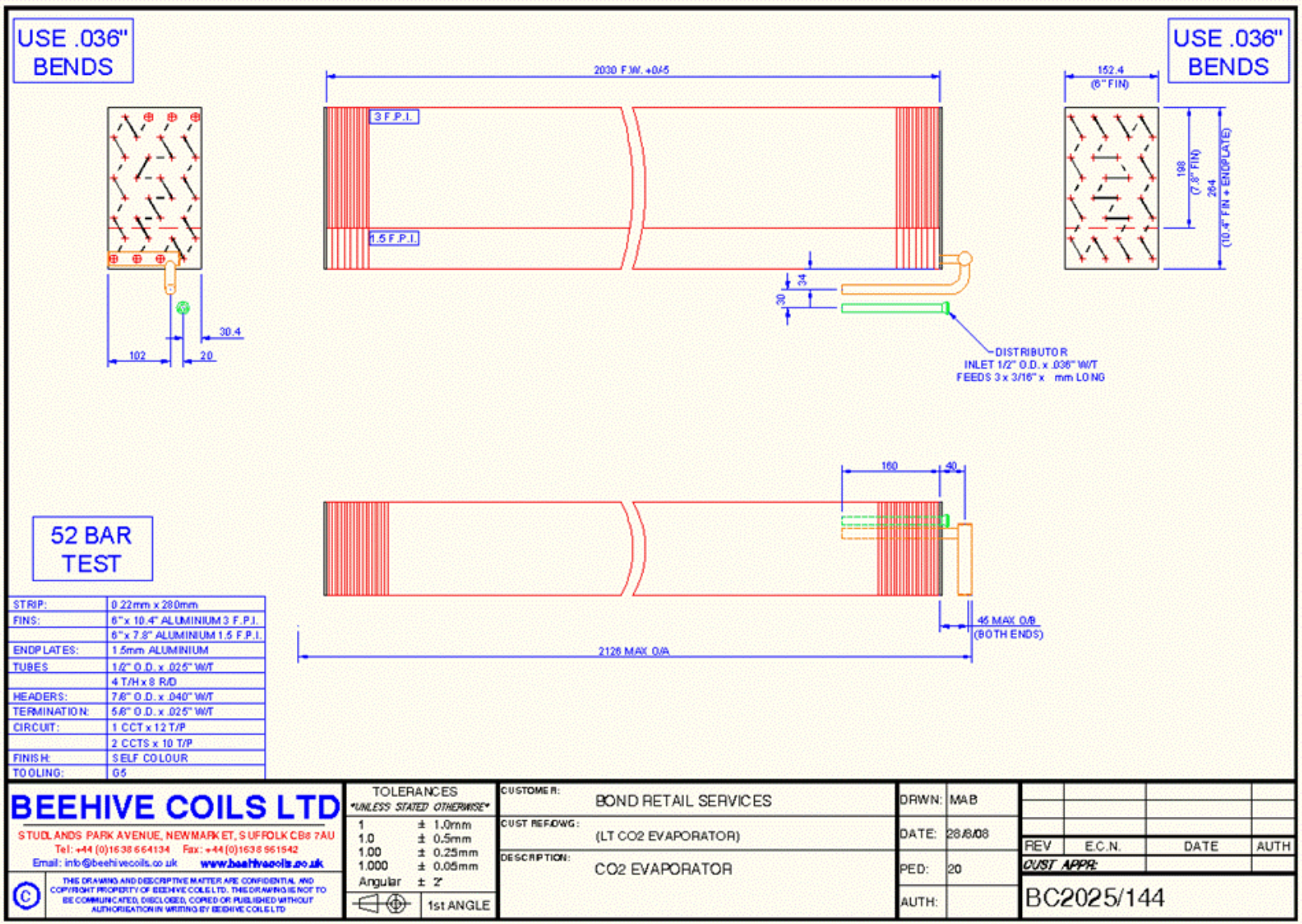

Figure C-5 Low temperature evaporator coil

APPENDIX D:

Electrical circuit diagrams of the CO_2 test system

This appendix presents wiring diagrams of the electrical installation circuit and cabinet controllers including electrical installation system of the additional load for the LT refrigeration system. The wiring diagrams include:

Main electrical installation circuit

LT control circuit

MT control circuit

Standstill control circuit

Additional load control circuit

LT cabinet controller (EKC-414A1)

MT cabinet controller (EKC-204A1)

LT additional load evaporator controller (AK-CC-550)

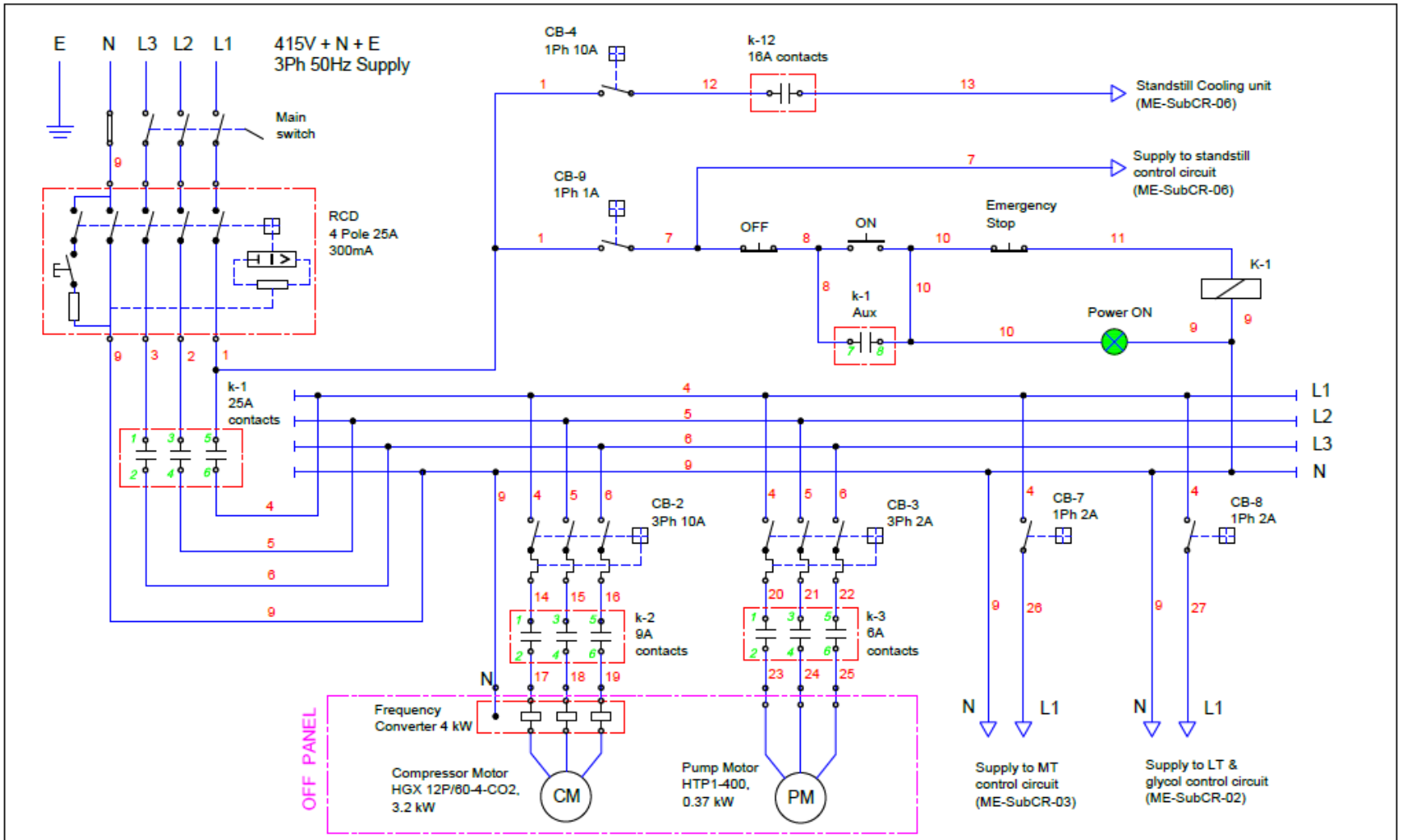

Drawn INS	Date 20-11-2008	Scale NTS	Title: **Figure D-1 Wiring diagram of the main electrical installation circuit**
No: ME-SubCR-01 Sheet: 1 of 8		Revision 2	

SCHOOL OF ENGINEERING & DESIGN
BRUNEL UNIVERSITY

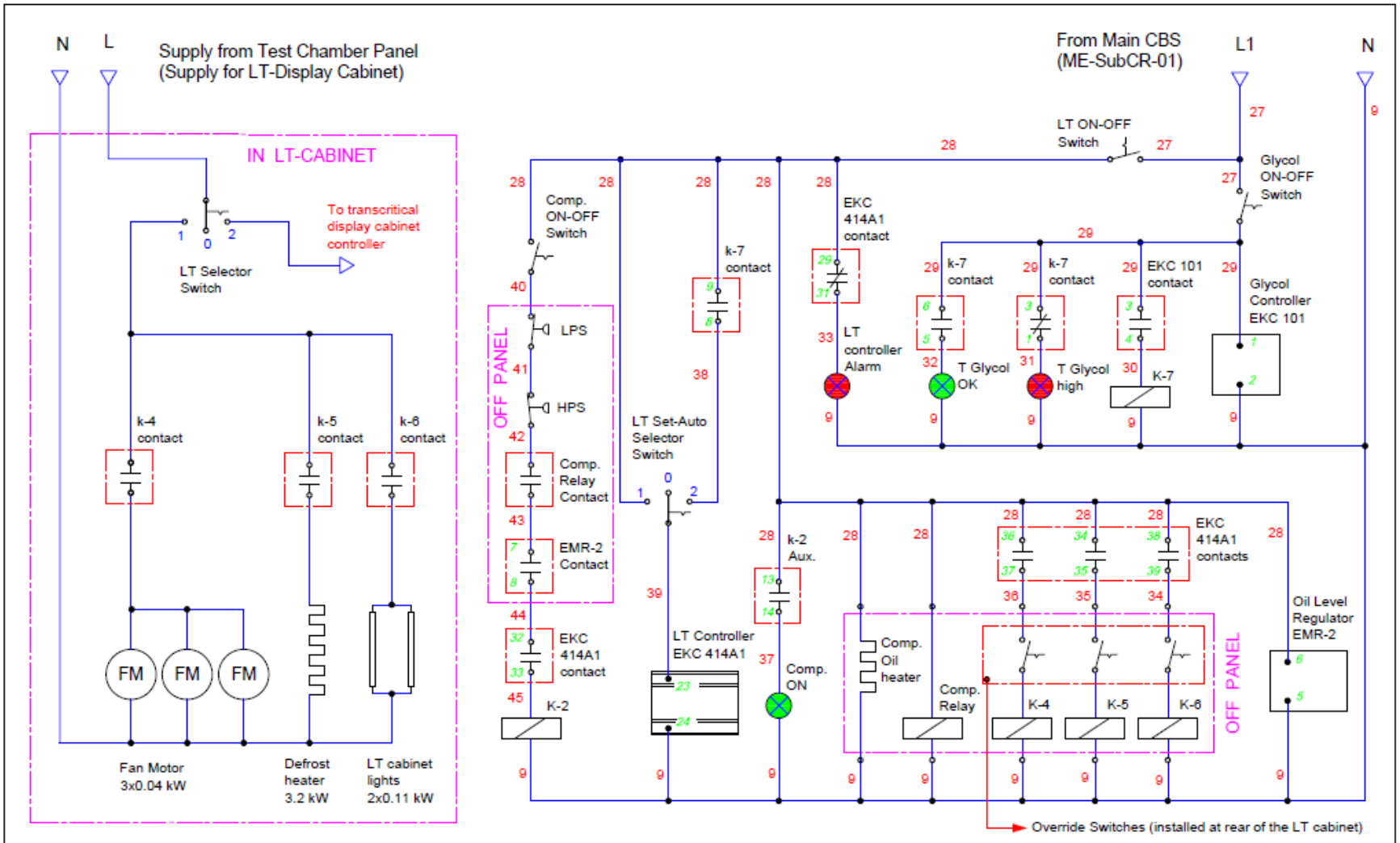

Drawn INS	Date 20-11-2008	Scale NTS	Title:
No: ME-SubCR-02 Sheet: 2 of 8		Revision 2	

Figure D-2 Wiring diagram of the LT control circuit

SCHOOL OF ENGINEERING & DESIGN
BRUNEL UNIVERSITY

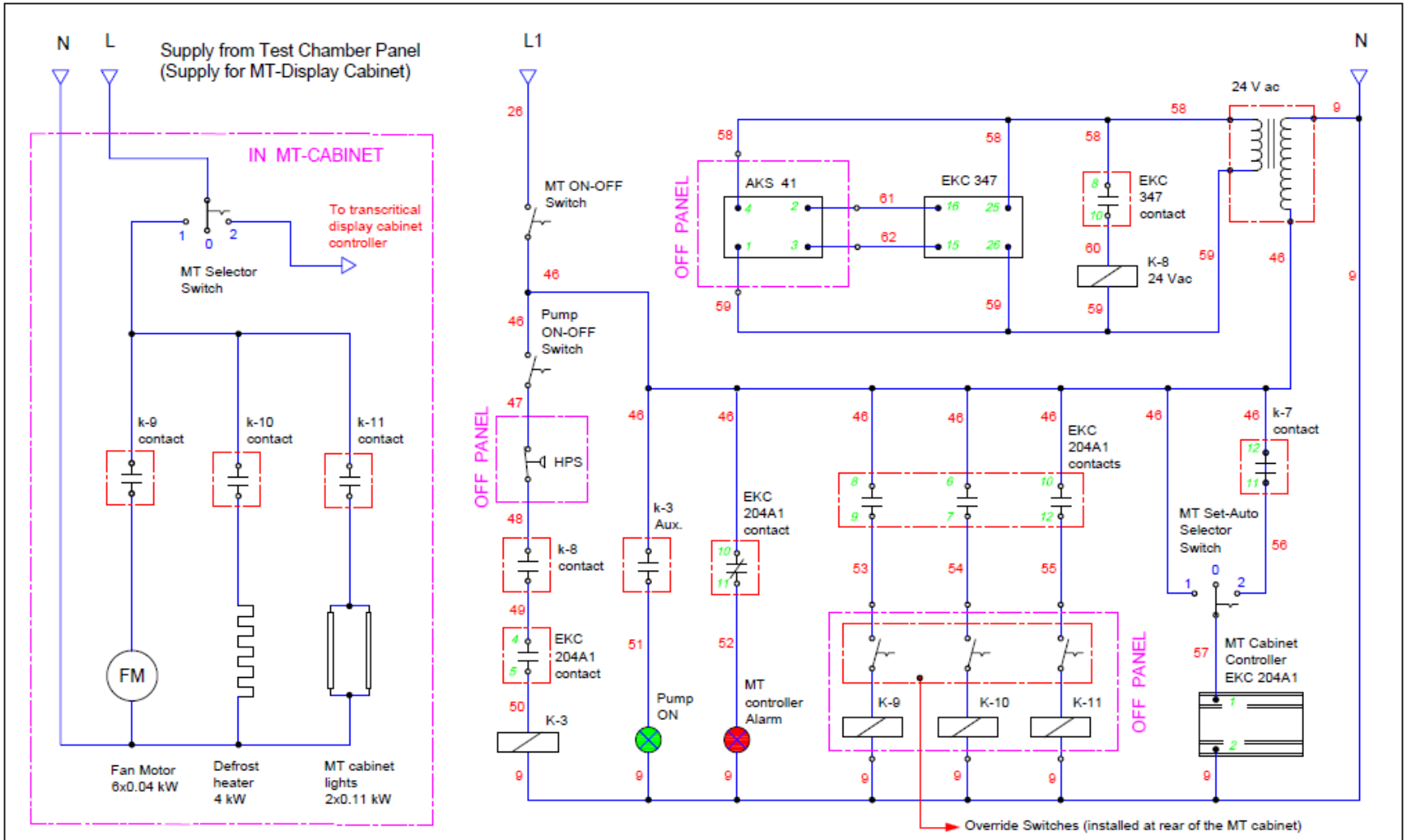

Drawn	Date	Scale	Title:
INS	20-11-2008	NTS	
No: ME-SubCR-03 Sheet: 3 of 8		Revision 2	

Figure D-3 Wiring diagram of the MT control circuit

SCHOOL OF ENGINEERING & DESIGN
BRUNEL UNIVERSITY

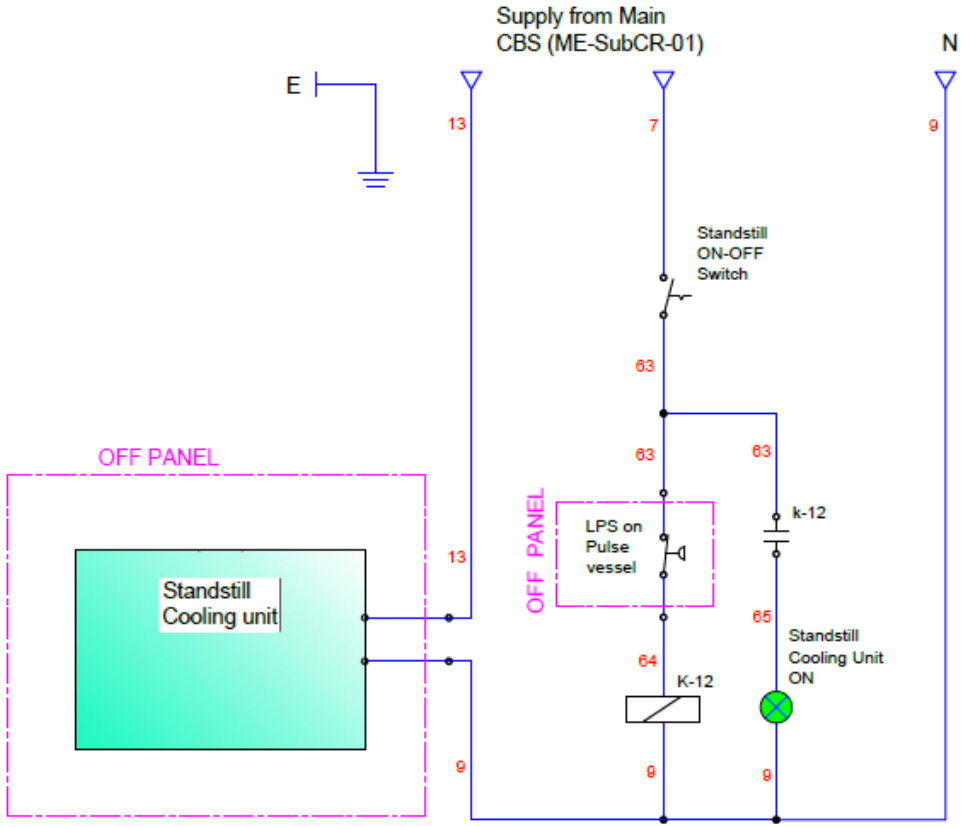

Drawn INS	Date 20-11-2008	Scale NTS	Title:
No: ME-SubCR-06 Sheet: 6 of 8		Revision 2	

Figure D-4 Wiring diagram of the standstill control circuit

SCHOOL OF ENGINEERING & DESIGN

BRUNEL UNIVERSITY

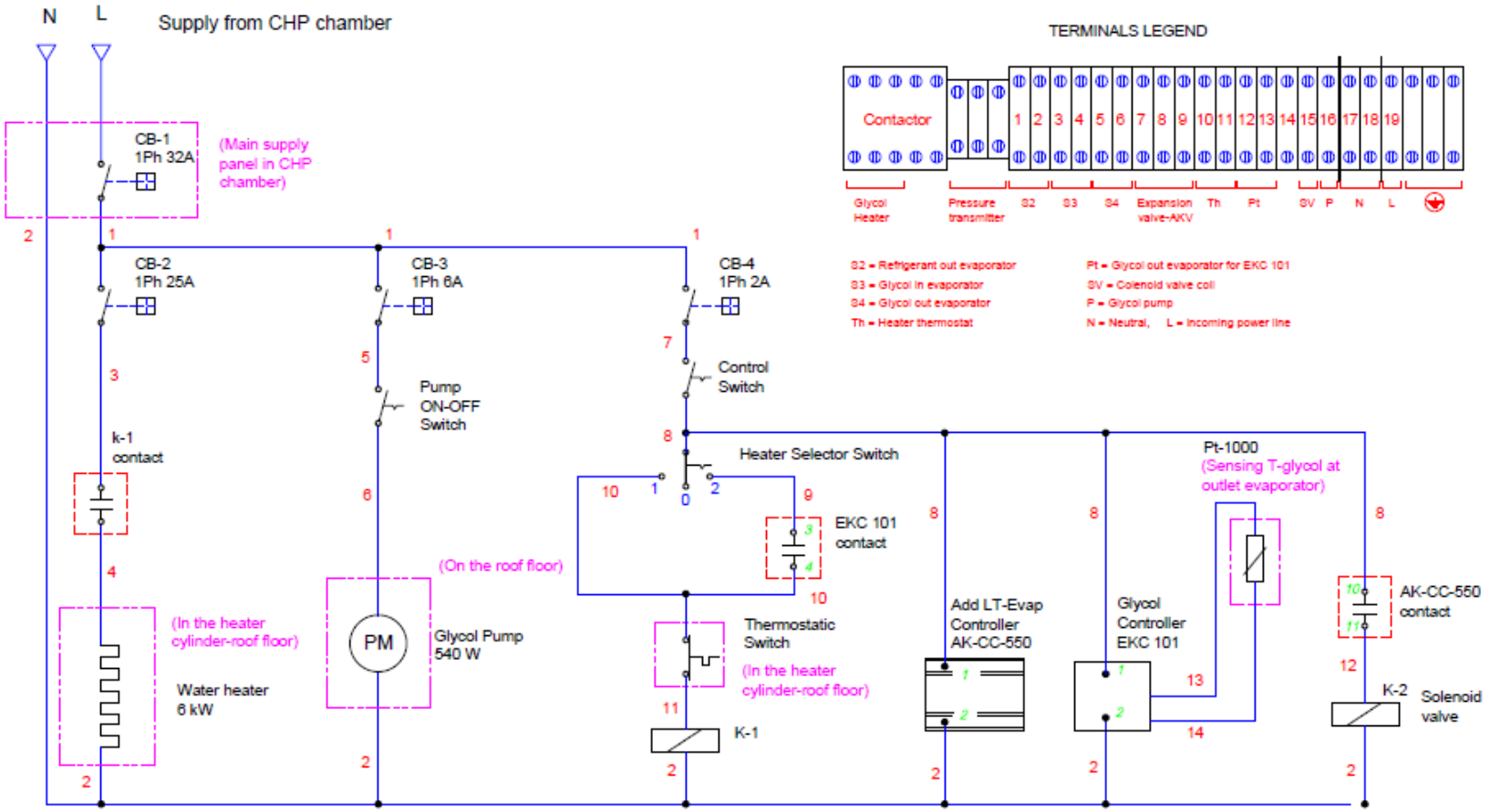

Drawn	Date	Scale	Title:
INS	14-07-2009	NTS	**Figure D-5 Wiring diagram of the LT additional load control circuit**
No: ME-AddLoad-01 Sheet: 1 of 2		Revision 0	

SCHOOL OF ENGINEERING & DESIGN

BRUNEL UNIVERSITY

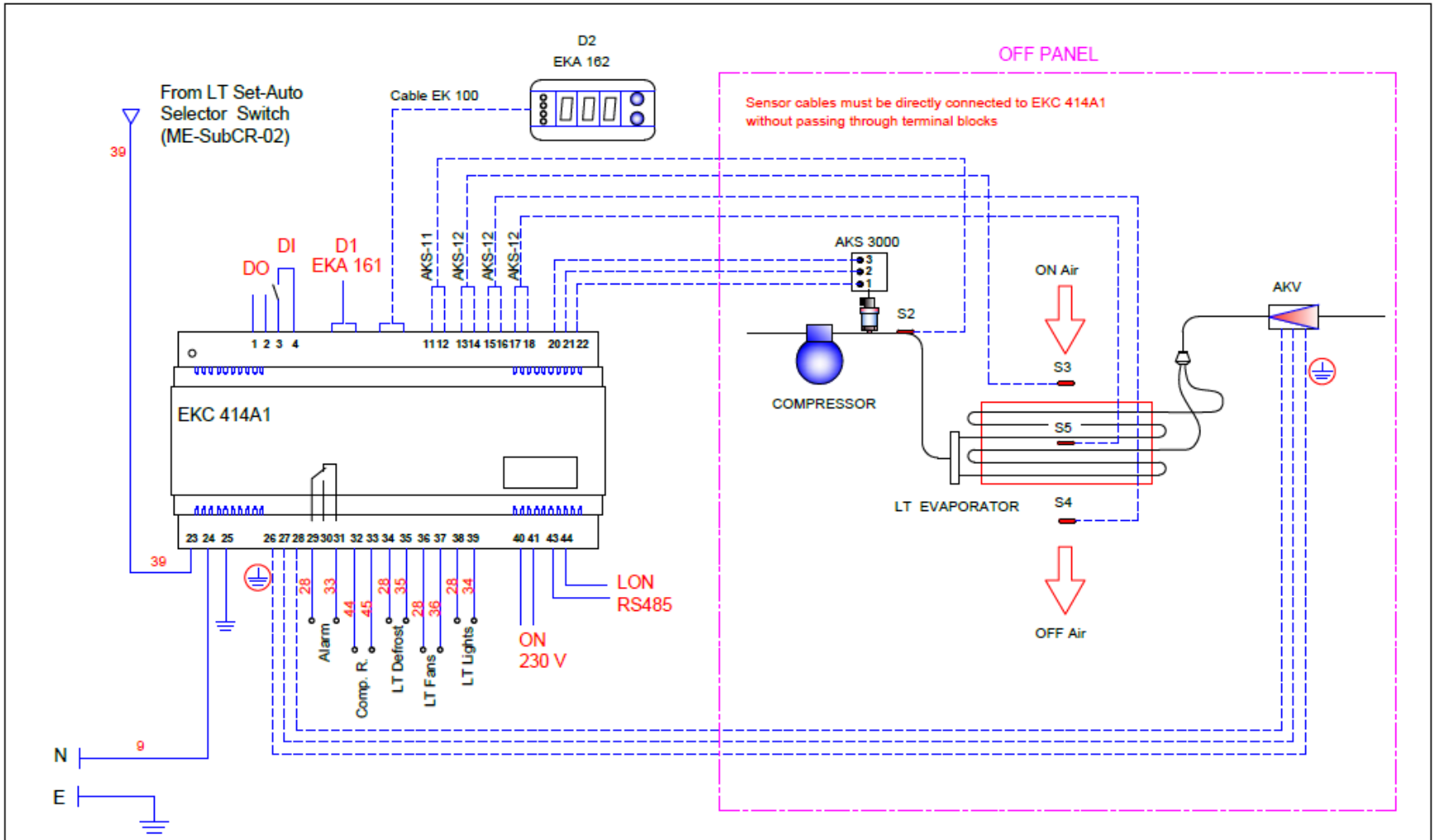

Drawn	Date	Scale	Title:
INS	20-11-2008	NTS	**Figure D-6 EKC 414A1 controller wiring diagram**
No: ME-SubCR-04 Sheet: 4 of 8		Revision 2	

SCHOOL OF ENGINEERING & DESIGN
BRUNEL UNIVERSITY

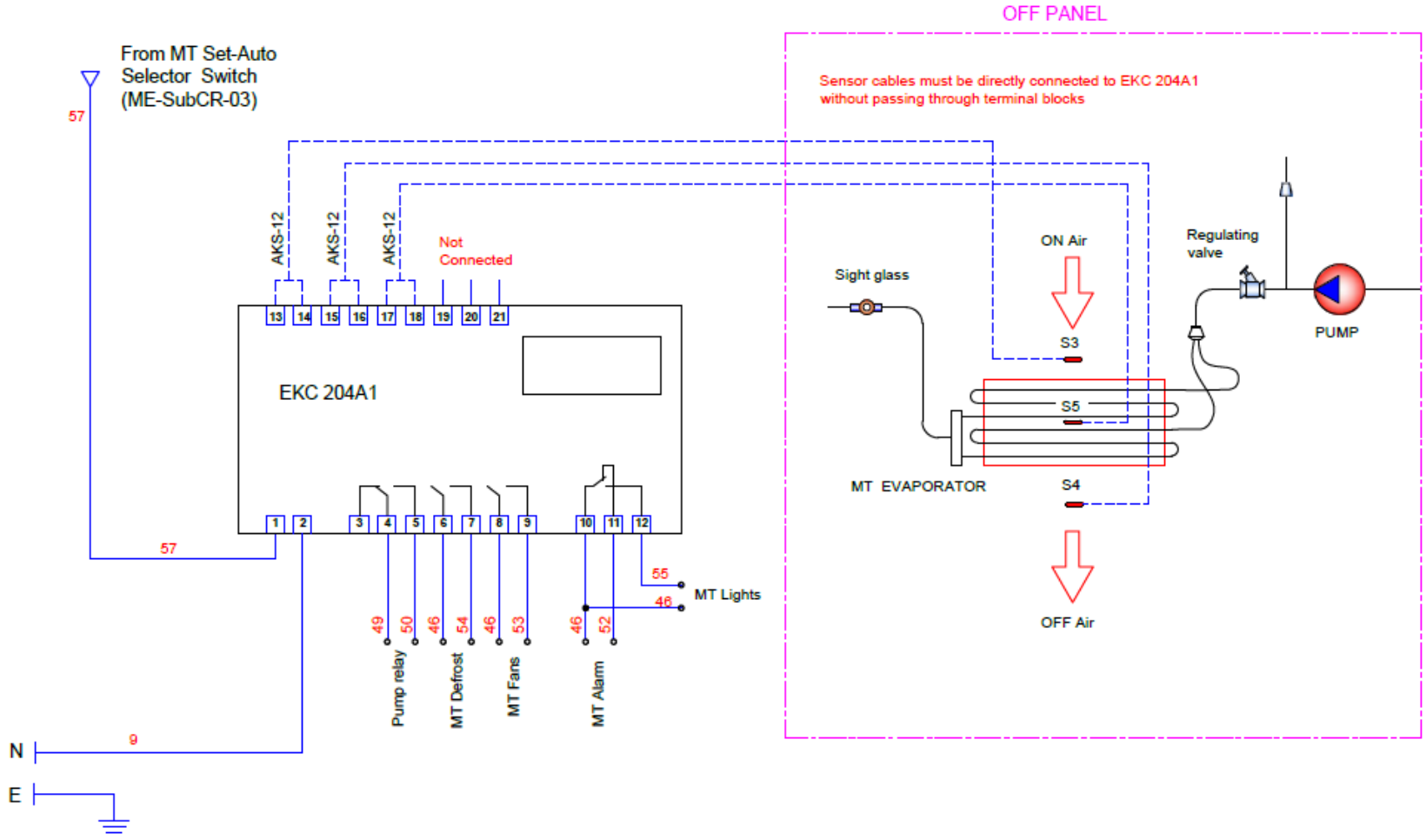

Drawn	Date	Scale	Title:
INS	20-11-2008	NTS	**Figure D-7 EKC 204A1 controller wiring diagram**
No: ME-SubCR-05		Revision	
Sheet: 5 of 8		2	

SCHOOL OF
ENGINEERING & DESIGN
BRUNEL UNIVERSITY

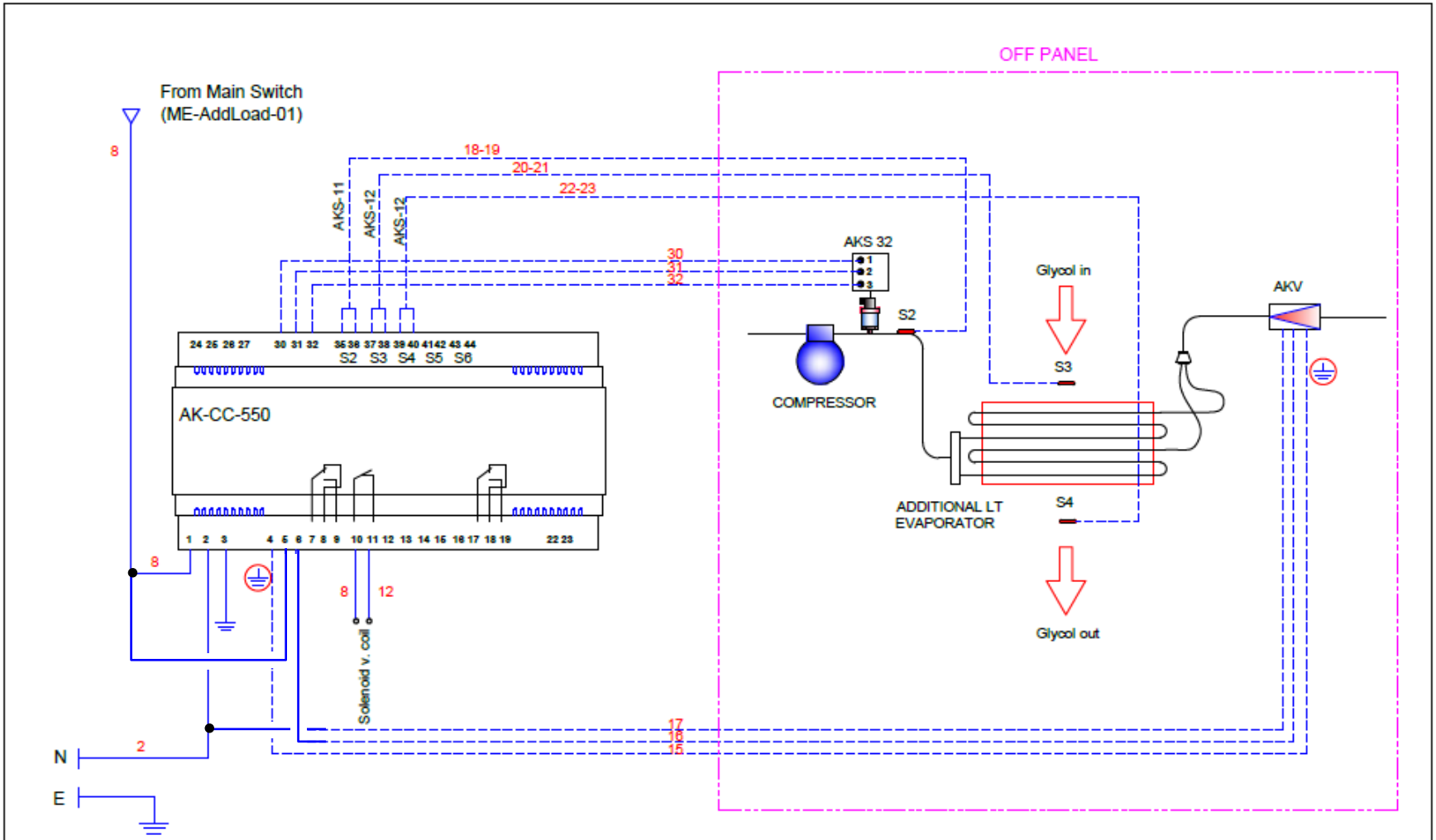

Drawn	Date	Scale	Title:
INS	14-07-2009	NTS	
No: ME-AddLoad-02		Revision	
Sheet: 2 of 2		0	

Figure D-8 AK-CC-550 controller wiring diagram

SCHOOL OF
ENGINEERING & DESIGN

BRUNEL UNIVERSITY

APPENDIX E:
Instrumentation and data logging systems

This appendix provides the positions of the measurement points in the test rig, a display of the monitoring system, identification of the measurement points and calibration equations of the measurement devices.

Identification of the measurement points on the Datascan logger, which include the measurement system of the subcritical and transcritical CO_2 test rigs, is presented in Table E-1.

Legend for Table E-1:

- L = left
- LT = low temperature
- M = middle
- MT = medium temperature
- PS = pressure transducer for the subcritical test system
- PT = pressure transducer for the transcritical test system
- R = right
- RH = relative humidity
- SC = subcritical test system
- T = temperature
- TC = transcritical test system

The calibration equations of the thermocouples are presented in Table E-2 and the graphs together with the calibration equations of the pressure transducers are shown in Figure E-3.

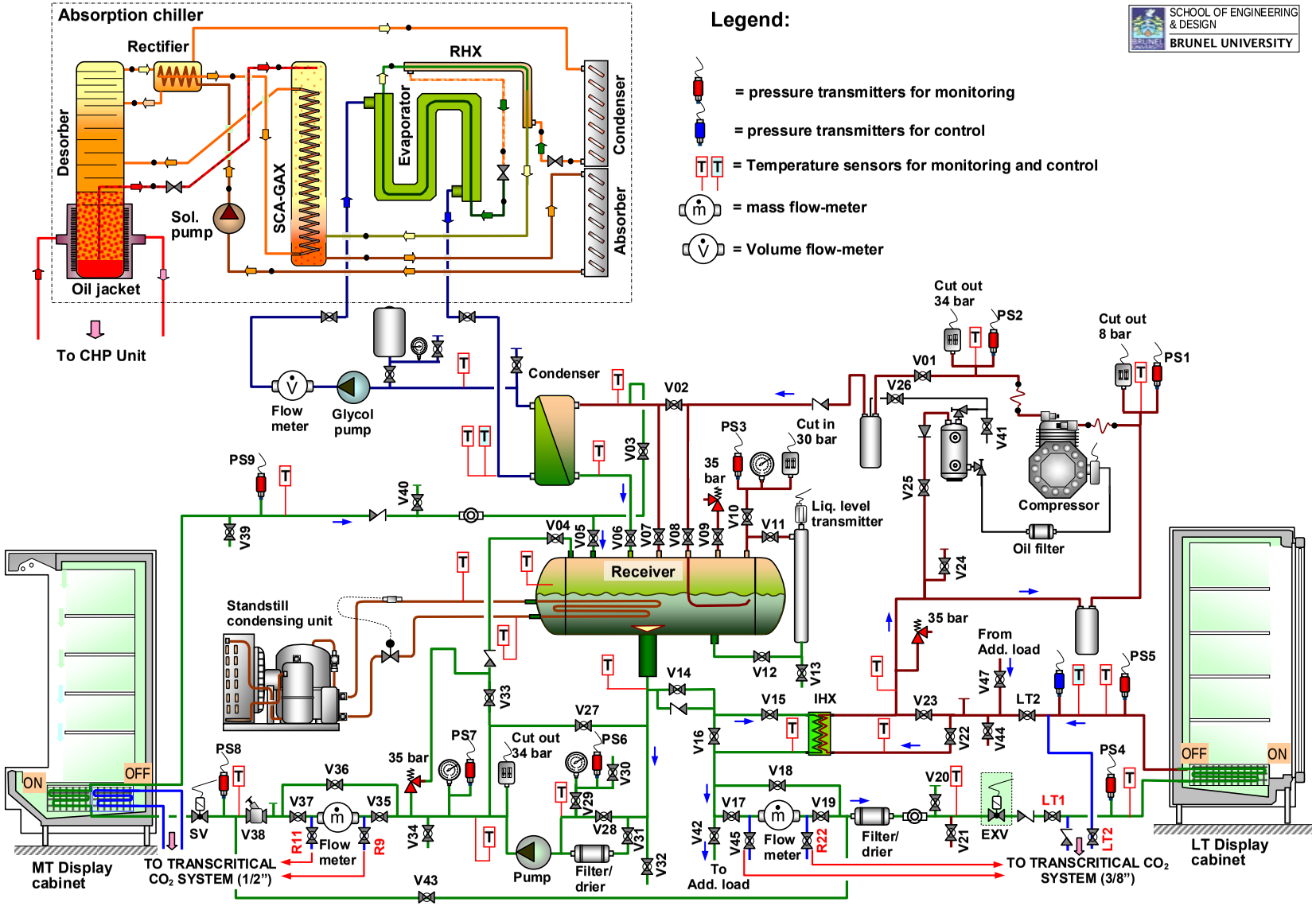

Figure E-1 Instrumentation of the control and monitoring systems

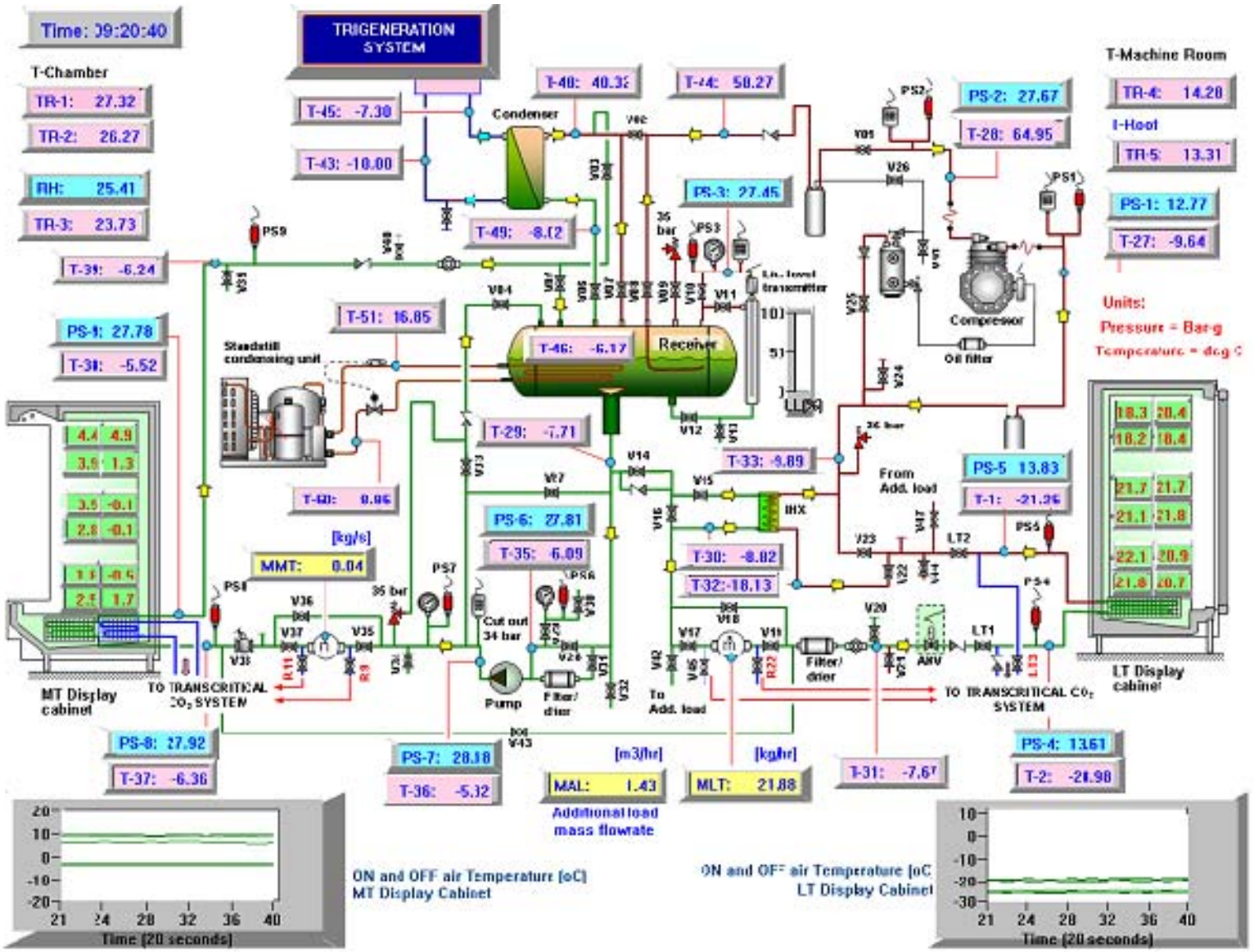

Figure E-2 Display of the measurement and monitoring systems

Table E-1 Channel identification on the DataScan logger

Channel No.	Sensor No.	Description	Channel No.	Sensor No.	Description
1	T27	SC Comp. IN	49	PT1	TC/SC Press. LT Evap. OUT
2	T28	SC Comp. OUT	50	PT2	TC Press. LT Comp. OUT
3	T29	Downleg pipe	51	PT3	TC Press. HT Comp.1a IN
4	T30	SC IHX-hot OUT	52	PT4	TC Press. HT Comp.1b IN
5	T31	SC EXV IN	53	PT5	TC Press. HT Comp. OUT
6	T32	SC IHX-cold IN	54	PT6	TC Press. GasCooler OUT
7	T33	SC IHX-cold OUT	55	PT7	TC Press. ICMT IN
8	T34	SC Out regulator valve	56	PT8	TC Press. ICMT OUT
9	T35	SC Pump IN	57	PT9	TC Press. MT Evap. OUT
10	T36	SC Pump OUT	58	PT10	TC Press. MT Evap. IN
11	T37	SC MT Evap. IN	59	PT11	TC/SC Press. LT Evap. IN
12	T38	SC MT Evap. OUT-1	60		
13	T39	SC MT Evap. OUT-2	61	MMT	MT Flowmeter
14	T40	Ambient M. Room	62	LLV	CO2 liquid level
15	T41	Brine evaporator chiller IN	63	MAL	Add. Load Flowmeter
16	T42	Brine evaporator chiller OUT	64	MLT	LT Flowmeter
17	T1	LT Evap. OUT	65	T43	Brine Condenser IN
18	T2	LT Evap. IN or EXV OUT	66	T44	SC Vessel IN from comp.
19	T2'	LT EXV IN	67	T45	Brine Condenser OUT
20	T3	MT Air ON - L	68	T46	SC Vessel-Mid
21	T4	MT air OFF - L	69	T47	SC Vessel-Top
22	T5	TC Gas cooler IN	70	T48	SC Condenser IN
23	T6	TC Gas cooler OUT-1	71	T49	SC Condenser OUT
24	T7	Ambient - Roof	72	T50	Standstill TXV IN
25	T8	LT air ON - L	73	T51	Standstill Evap. OUT
26	T9	LT air OFF - L	74	T52	MT Air MID-L
27	T10	TC LT-Comp. IN	75	T53	MT Air ON-M
28	T11	TC LT-Comp. OUT	76	T54	MT Air ON-R
29	T12	TC HT-Comp.1a IN	77	T55	MT Air MID-M
30	T13	TC HT-Comp.1b IN	78	T56	MT Air MID-R
31	T14	TC HT-Comp. OUT	79	T57	MT Air OFF-M
32	T15	TC ICMT IN	80	T58	MT Air OFF-R
33	T16	TC Receiver OUT	81	T59	MT Bot-Shelf-Frnt-L Up
34	T17	TC MT-EXV IN	82	T60	MT Bot-Shelf-Frnt-L Low
35	T18	TC MT-EXV OUT or Evap IN	83	T61	MT Bot-Shelf-Rear-L Up
36	T19	TC MT Evap. OUT-1	84	T62	MT Bot-Shelf-Rear-L Low
37	T136	T. Chamber-1	85	T63	MT Bot-Shelf-Frnt-M Up
38	T20	TC IHX2-hot OUT	86	T64	MT Bot-Shelf-Frnt-M Low
39	T21	TC MT Evap. OUT-2	87	T65	MT Bot-Shelf-Rear-M Up
40	T22	TC IHX3-cold IN	88	T66	MT Bot-Shelf-Rear-M Low
41	T23	TC Oil separator OUT	89	T67	MT Bot-Shelf-Frnt-R Up
42	T24	TC GasCooler OUT-2	90	T68	MT Bot-Shelf-Frnt-R Low
43	T25	TC Receiver-Top or ICM IN	91	T69	MT Bot-Shelf-Rear-R Up
44	T26	TC ICM OUT	92	T70	MT Bot-Shelf-Rear-R Low
45	T137	TC ICMT OUT	93	T71	MT Mid-Shelf-Frnt-L Up
46	T138	Add. Load IN	94	T72	MT Mid-Shelf-Frnt-L Low
47	T139	Add. Load OUT	95	T73	MT Mid-Shelf-Rear-L Up
48	T140	Brine add. Load IN	96	T74	MT Mid-Shelf-Rear-L Low

Box 1: All OFF

Box 2: S6 ON

Box 3: S5 ON

Box 4: S5 & S6 ON

Box 5: S4 ON

Box 6: S4 & S6 ON

Table E-1 Channel identification on the DataScan logger (Continued)

Channel No.	Sensor No.	Description	Channel No.	Sensor No.	Description
97	PS-1	SC Press. Compressor IN	145	T111	LT Mid-Shelf-Frnt-L Up
98	PS-2	SC Press. Compressor OUT	146	T112	LT Mid-Shelf-Frnt-L Low
99	PS-3	SC Press. Vessel	147	T113	LT Mid-Shelf-Rear-L Up
100	PS-6	SC Press. CO2 pump IN	148	T114	LT Mid-Shelf-Rear-L Low
101	PS-7	SC Press. CO2 pump OUT	149	T115	LT Mid-Shelf-Frnt-M Up
102	PS-8	SC Press. MT evap. IN	150	T116	LT Mid-Shelf-Frnt-M Low
103	PS-9	SC Press. MT evap. OUT	151	T117	LT Mid-Shelf-Rear-M Up
104			152	T118	LT Mid-Shelf-Rear-M Low
105	T75	MT Mid-Shelf-Frnt-M Up	153	T119	LT Mid-Shelf-Frnt-R Up
106	T76	MT Mid-Shelf-Frnt-M Low	154	T120	LT Mid-Shelf-Frnt-R Low
107	T77	MT Mid-Shelf-Rear-M Up	155	T121	LT Mid-Shelf-Rear-R Up
108	T78	MT Mid-Shelf-Rear-M Low	156	T122	LT Mid-Shelf-Rear-R Low
109	T79	MT Mid-Shelf-Frnt-R Up	157	T123	LT Top-Shelf-Frnt-L Up
110	T80	MT Mid-Shelf-Frnt-R Low	158	T124	LT Top-Shelf-Frnt-L Low
111	T81	MT Mid-Shelf-Rear-R Up	159	T125	LT Top-Shelf-Rear-L Up
112	T82	MT Mid-Shelf-Rear-R Low	160	T126	LT Top-Shelf-Rear-L Low
113	T83	MT Top-Shelf-Frnt-L Up	161	T127	LT Top-Shelf-Frnt-M Up
114	T84	MT Top-Shelf-Frnt-L Low	162	T128	LT Top-Shelf-Frnt-M Low
115	T85	MT Top-Shelf-Rear-L Up	163	T129	LT Top-Shelf-Rear-M Up
116	T86	MT Top-Shelf-Rear-L Low	164	T130	LT Top-Shelf-Rear-M Low
117	T141	Brine add. Load OUT	165	T131	LT Top-Shelf-Frnt-R Up
118	T135	T. Chamber-2	166	T132	LT Top-Shelf-Frnt-R Low
119	RH-LT OFF	RH Air OFF LT	167	T133	LT Top-Shelf-Rear-R Up
120	T-LT OFF	T Air OFF LT	168	T134	LT Top-Shelf-Rear-R Low
121	T87	MT Top-Shelf-Frnt-M Up	169	RH-LT ON	RH Air ON LT
122	T88	MT Top-Shelf-Frnt-M Low	170	T-LT ON	T Air ON LT
123	T89	MT Top-Shelf-Rear-M Up	171	RH-1	RH Chamber pos. MT cab.
124	T90	MT Top-Shelf-Rear-M Low	172	T-142	T-Chamber pos. MT cab.
125	T91	MT Top-Shelf-Frnt-R Up	173	RH-2	RH air OFF MT
126	T92	MT Top-Shelf-Frnt-R Low	174	T-143	T-air OFF MT
127	T93	MT Top-Shelf-Rear-R Up	175	RH-3	RH air ON MT
128	T94	MT Top-Shelf-Rear-R Low	176	T-144	T-air ON MT
129	T95	LT Air ON-M	177		
130	T96	LT Air ON-R	178		
131	T97	LT Air OFF-M	179		
132	T98	LT Air OFF-R	180		
133	T99	LT Bot-Shelf-Frnt-L Up	181		
134	T100	LT Bot-Shelf-Frnt-L Low	182		
135	T101	LT Bot-Shelf-Rear-L Up	183		
136	T102	LT Bot-Shelf-Rear-L Low	184		
137	T103	LT Bot-Shelf-Frnt-M Up	185		
138	T104	LT Bot-Shelf-Frnt-M Low	186		
139	T105	LT Bot-Shelf-Rear-M Up	187		
140	T106	LT Bot-Shelf-Rear-M Low	188		
141	T107	LT Bot-Shelf-Frnt-R Up	189		
142	T108	LT Bot-Shelf-Frnt-R Low	190		
143	T109	LT Bot-Shelf-Rear-R Up	191		
144	T110	LT Bot-Shelf-Rear-R Low	192		

Box 7: S4 & S5 ON

Box 8: S4, S5 & S6 ON

Box 9: S3 ON

Box 10: S3 & S6 ON

Box 11: S3 & S5 ON

Box 12: S3, S5 & S6 ON

Table E-2 Calibration equations of the thermocouples

General Equation:

$$Y = mX + b$$

Legend:

Y = estimated actual value of temperature ^{o}C — m = slope of Y and X corelation (linear regression)

X = measured temperature by thermocouple — b = constant or Y intercept

SE-m = Standard error of m — R^2 = coefficient of correlation

SE-b = standard error of b — SE-Y = standard error of estimated Y

Thermocouples	m	b	R^2	SE-m	SE-b	SE-Y
T27	0.996288	0.838253	0.998507	0.014559	0.241621	0.493266
T28	0.996873	0.917977	0.998537	0.014424	0.238908	0.486442
T29	0.997392	0.926840	0.998534	0.014443	0.239068	0.487008
T30	0.996485	1.007307	0.998551	0.014348	0.237383	0.483115
T31	0.996903	1.020488	0.998573	0.014244	0.235510	0.477880
T32	0.998242	1.051715	0.998577	0.014242	0.235041	0.476889
T33	1.000665	1.096362	0.998594	0.014190	0.233437	0.472780
T34	1.001412	1.146833	0.998559	0.014377	0.236130	0.481116
T35	0.996806	0.994470	0.998630	0.013952	0.230813	0.464066
T36	0.995816	1.066011	0.998665	0.013760	0.227594	0.455604
T37	0.998530	1.070330	0.998637	0.013943	0.229967	0.462488
T38	0.998970	1.058034	0.998639	0.013941	0.229874	0.462081
T39	0.998481	0.793385	0.998651	0.013870	0.229875	0.459045
T40	0.998982	0.803464	0.998676	0.013749	0.227727	0.453003
T41	1.011096	0.691332	0.998721	0.013674	0.224221	0.441661
T42	1.011714	0.764923	0.998719	0.013693	0.224102	0.442168
T5	1.003983	0.047941	0.998522	0.014597	0.244007	0.489775
T6	1.005148	0.043130	0.998563	0.014411	0.240632	0.480171
T7	1.005325	0.050396	0.998555	0.014455	0.241296	0.482145
T20	1.006869	-0.227677	0.998509	0.014706	0.246498	0.492923
T21	1.006422	-0.224810	0.998533	0.014578	0.244443	0.487189
T22	1.006125	-0.244091	0.998509	0.014693	0.246538	0.492799
T23	1.006597	-0.297907	0.998624	0.014124	0.237160	0.465705
T24	1.006529	-0.313855	0.998572	0.014387	0.241658	0.478105
T25	1.006209	-0.357100	0.998654	0.013964	0.234862	0.458439
T26	1.007656	-0.377674	0.998653	0.013988	0.235025	0.458610
T137	1.005084	-0.366662	0.998594	0.014254	0.240039	0.472816
T138	1.005240	-0.378429	0.998573	0.014363	0.241901	0.477865
T139	1.005009	-0.385253	0.998653	0.013950	0.235045	0.458561
T140	1.004826	-0.384303	0.998636	0.014034	0.236493	0.462631
T141	1.002380	-0.259961	0.998428	0.015033	0.253269	0.511478
T43	1.016260	-0.804837	0.998531	0.014733	0.247707	0.487759
T44	1.009519	-0.678186	0.998561	0.014482	0.244441	0.480586
T45	1.016917	-0.800334	0.998578	0.014503	0.243673	0.476630
T46	1.008868	-0.656974	0.998564	0.014461	0.244128	0.480032
T47	1.009174	-0.691975	0.998577	0.014400	0.243218	0.476978
T48	1.009247	-0.663899	0.998545	0.014559	0.245720	0.484362
T49	1.009185	-0.643462	0.998554	0.014515	0.244884	0.482338
T50	1.008918	-0.643991	0.998617	0.014192	0.239512	0.467365
T51	1.009197	-0.652264	0.998629	0.014132	0.238470	0.464343
T52	1.009030	-0.610201	0.998620	0.014176	0.239044	0.466548
T53	1.009542	-0.631277	0.998627	0.014149	0.238568	0.464918
T54	1.008963	-0.642083	0.998610	0.014229	0.240122	0.469091
T55	1.008861	-0.640687	0.998629	0.014129	0.238445	0.464440
T56	1.008694	-0.644177	0.998636	0.014089	0.237835	0.462691
T57	1.008963	-0.638842	0.998629	0.014128	0.238392	0.464319

Table E-2 Calibration equations of the thermocouples (Continued)

Thermocouples	m	b	R^2	SE-m	SE-b	SE-Y
T58	1.008353	-0.632173	0.998618	0.014180	0.239376	0.467158
T59	1.010924	-0.713968	0.998634	0.014130	0.238358	0.463136
T60	1.010447	-0.683936	0.998622	0.014188	0.239287	0.466155
T61	1.010024	-0.676273	0.998612	0.014234	0.240130	0.468616
T62	1.010466	-0.684766	0.998635	0.014122	0.238186	0.463080
T63	1.010357	-0.663061	0.998589	0.014354	0.241993	0.473996
T64	1.010359	-0.650000	0.998618	0.014204	0.239401	0.466969
T65	1.010123	-0.649104	0.998658	0.013995	0.235931	0.457316
T66	1.010484	-0.652083	0.998605	0.014277	0.240613	0.470312
T67	1.009404	-0.710182	0.998674	0.013899	0.234807	0.453313
T68	1.009879	-0.670779	0.998684	0.013857	0.233774	0.451000
T69	1.010261	-0.669156	0.998646	0.014061	0.237126	0.460356
T70	1.010034	-0.687574	0.998665	0.013955	0.235487	0.455528
T71	1.007995	-0.665754	0.998666	0.013925	0.235336	0.455418
T72	1.010419	-0.690479	0.998620	0.014197	0.239491	0.466630
T73	1.008126	-0.638037	0.998600	0.014266	0.240923	0.471383
T74	1.007786	-0.641638	0.998579	0.014370	0.242775	0.476490
T75	1.005102	-0.607275	0.998627	0.014087	0.238461	0.464966
T76	1.004906	-0.612683	0.998626	0.014087	0.238533	0.465089
T77	1.004027	-0.614769	0.998643	0.013988	0.237078	0.461002
T78	1.007630	-0.666963	0.998704	0.013719	0.231954	0.445984
T79	1.004642	-0.728074	0.998748	0.013445	0.228298	0.434954
T80	1.004826	-0.757554	0.998711	0.013645	0.231810	0.444304
T81	1.006584	-0.752051	0.998690	0.013781	0.233677	0.449569
T82	1.004779	-0.744378	0.998634	0.014044	0.238513	0.463123
T83	1.006029	-0.584418	0.998579	0.014345	0.242465	0.476465
T84	1.005678	-0.581317	0.998583	0.014319	0.242109	0.475517
T85	1.005771	-0.596321	0.998569	0.014390	0.243355	0.478771
T86	1.006373	-0.637317	0.998611	0.014187	0.239997	0.468812
T87	1.008531	-0.728030	0.998594	0.014303	0.241921	0.472836
T88	1.008854	-0.713885	0.998664	0.013946	0.235745	0.455869
T89	1.007804	-0.727061	0.998614	0.014192	0.240217	0.468114
T90	1.008799	-0.759998	0.998592	0.014320	0.242311	0.473447
T91	1.007704	-0.766771	0.998573	0.014398	0.243926	0.477834
T92	1.008302	-0.779651	0.998646	0.014031	0.237646	0.460198
T93	1.008223	-0.777688	0.998601	0.014262	0.241564	0.471109
T94	1.008354	-0.810320	0.998634	0.014096	0.238903	0.463240
T95	1.008650	-0.554843	0.998736	0.013564	0.228542	0.438034
T96	1.008062	-0.561418	0.998667	0.013918	0.234670	0.455046
T97	1.008530	-0.568245	0.998700	0.013755	0.231847	0.447072
T98	1.008026	-0.590051	0.998669	0.013907	0.234634	0.454541
T99	1.008064	-0.597276	0.998625	0.014139	0.238586	0.465459
T100	1.007922	-0.627917	0.998693	0.013781	0.232735	0.448710
T101	1.009413	-0.642028	0.998750	0.013499	0.227711	0.434516
T102	1.008360	-0.648860	0.998661	0.013956	0.235698	0.456670
T103	1.008867	-0.689146	0.998582	0.014370	0.242761	0.475750
T104	1.008742	-0.708548	0.998650	0.014017	0.236935	0.459254
T105	1.008667	-0.709277	0.998639	0.014076	0.237959	0.462092
T106	1.008591	-0.734869	0.998597	0.014288	0.241689	0.472092
T107	1.009206	-0.781258	0.998592	0.014325	0.242408	0.473401
T108	1.009734	-0.805710	0.998640	0.014082	0.238312	0.461665
T109	1.009126	-0.817441	0.998570	0.014431	0.244426	0.478462
T110	1.008841	-0.837981	0.998583	0.014364	0.243462	0.475477
T111	1.002716	1.175075	0.998613	0.014123	0.231555	0.468236
T112	1.001583	1.203327	0.998668	0.013827	0.226858	0.454989
T113	1.004092	1.157879	0.998680	0.013795	0.225936	0.451834

Table E-2 Calibration equations of the thermocouples (Continued)

Thermocouples	m	b	R^2	SE-m	SE-b	SE-Y
T114	1.000264	1.185578	0.998659	0.013853	0.227646	0.457071
T115	1.003079	1.124538	0.998731	0.013516	0.221725	0.439331
T116	1.000417	1.157030	0.998611	0.014103	0.231826	0.468816
T117	1.003063	1.100321	0.998672	0.013825	0.226879	0.453925
T118	1.003502	1.098576	0.998709	0.013638	0.223719	0.444799
T119	1.005694	0.500755	0.998716	0.013632	0.225517	0.443111
T120	1.005713	0.485195	0.998663	0.013908	0.230151	0.456134
T121	1.005153	0.483058	0.998643	0.014006	0.231904	0.461107
T122	1.002501	0.483082	0.998628	0.014044	0.233150	0.464658
T123	1.005028	0.411832	0.998645	0.013995	0.232054	0.460646
T124	1.002706	0.420698	0.998646	0.013953	0.231861	0.460208
T125	1.003458	0.416978	0.998634	0.014027	0.232922	0.463183
T126	1.002815	0.399485	0.998623	0.014077	0.233980	0.465973
T127	1.001188	3.770771	0.998599	0.014174	0.225485	0.471645
T128	1.000440	3.783498	0.998582	0.014250	0.226847	0.475766
T129	1.001976	3.762256	0.998602	0.014171	0.225283	0.471002
T130	1.002695	3.747141	0.998590	0.014242	0.226262	0.473842
T131	1.002419	3.738011	0.998533	0.014522	0.230789	0.487273
T132	1.002008	3.737103	0.998622	0.014069	0.223691	0.466133
T133	1.002238	3.720344	0.998631	0.014025	0.222967	0.463892
T134	1.002734	3.721418	0.998591	0.014235	0.226194	0.473507
T135	1.001583	-0.195296	0.998405	0.015132	0.254790	0.516708

Table E-3 Pressure range of the pressure transducers and resistors used for data logging

Pressure range and resistor used		
Number	**Pressure range**	**Resistor (ohm)**
PS-1	0 to 18 bar	250
PS-2	0 to 60 bar	500
PS-3	0 to 30 bar	500
PS-4/PT-11	0 to 18 bar	250
PS-5/PT-1	0 to 18 bar	250
PS-6	0 to 60 bar	500
PS-7	0 to 30 bar	500
PS-8	0 to 30 bar	500
PS-9	0 to 30 bar	500

General form of the best fit equations between the measured pressure and the output voltage of the pressure transducers is as follows:

$y = mx + b$

where y is the measured pressure (bar), x is the output voltage (V), b and m are a constant and rate of the pressure change with voltage respectively.

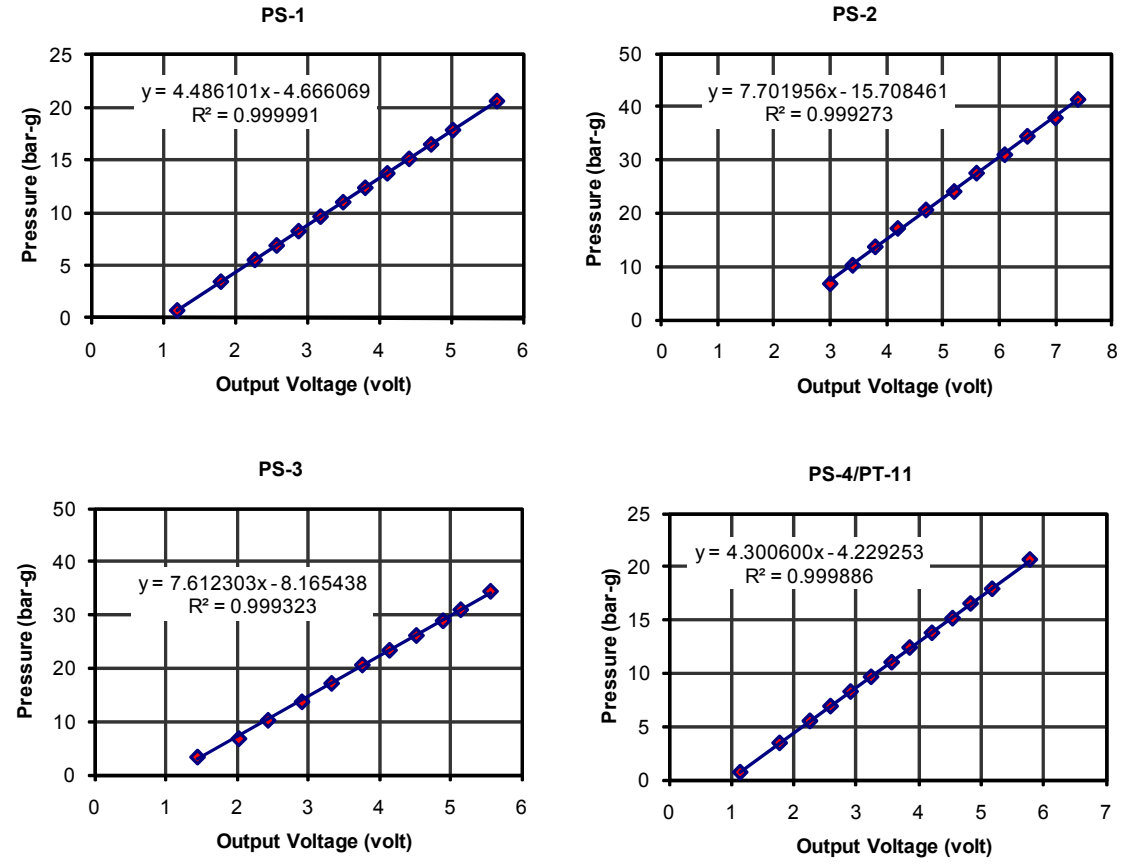

Figure E-3 Calibration graph and equation of the pressure transducers

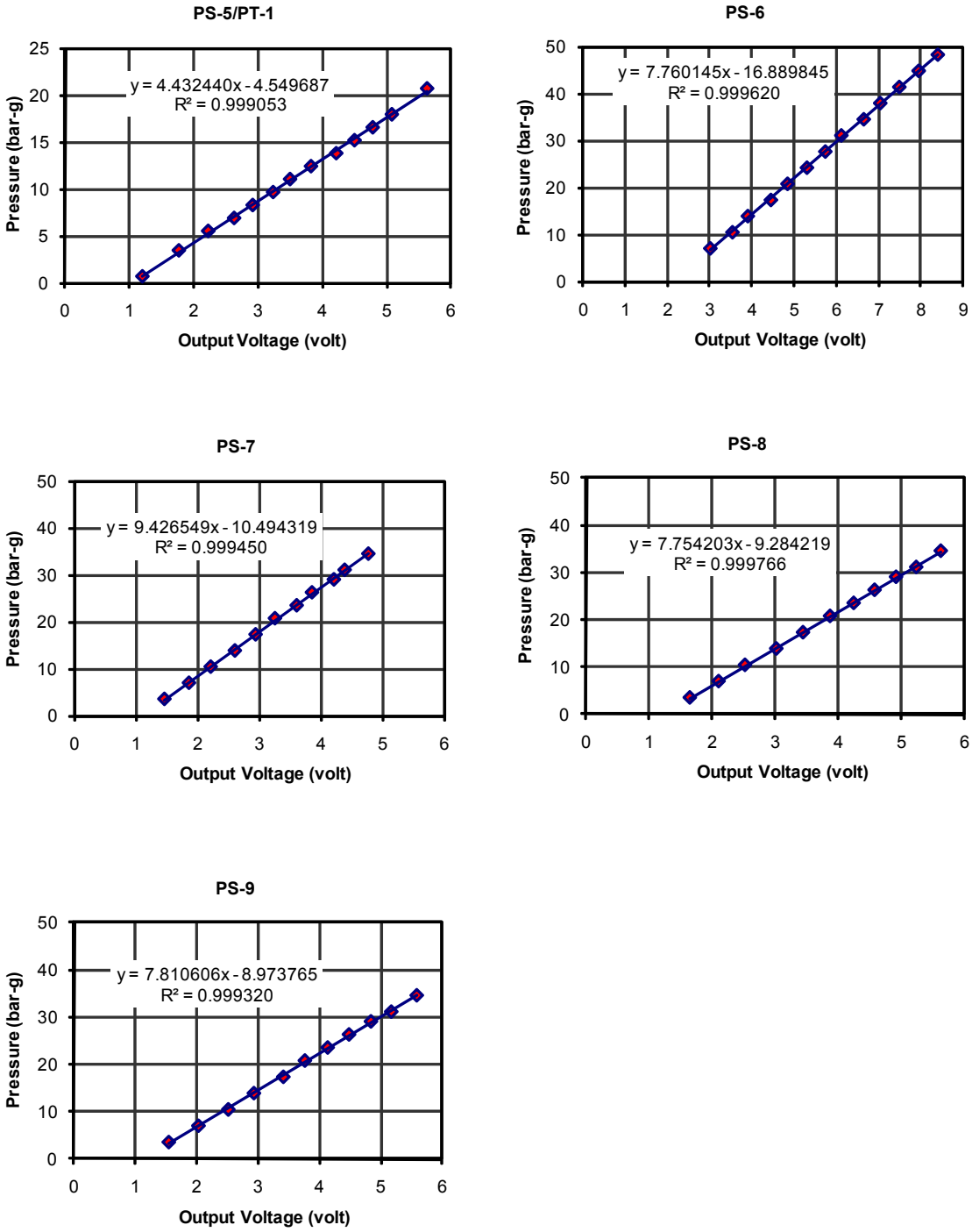

Figure E-3 Calibration graph and equation of the pressure transducers (Continued)

APPENDIX F:
CO_2 test chamber

This appendix presents the layout of the CO_2 test chamber including the position of the LT and MT display cabinets. A display of the design of the air handling unit (AHU) and a map of air velocity within the test area of the test chamber are also presented. The following drawings are also included:

Layout of the CO_2 test chamber with a 3.75 m long vertical door type cabinet

Layout of the CO_2 test chamber with a 2.5 m long MT vertical open type cabinet

Layout of a possible extension of the test chamber

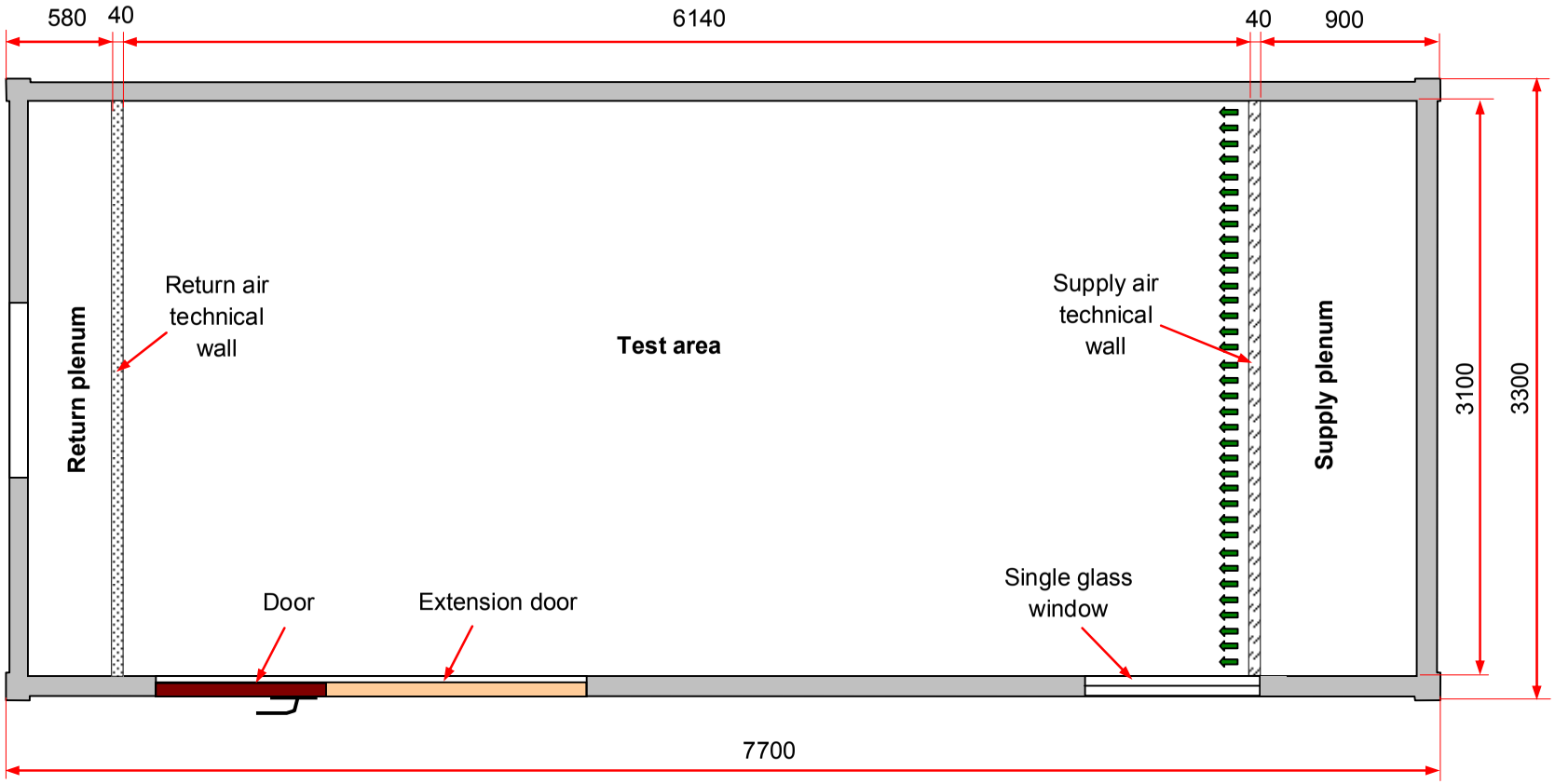

No : -	TITLE:	SCHOOL OF ENGINEERING AND DESIGN
Scale : NTS	**Figure F-1 Layout of the CO_2 test chamber**	BRUNEL UNIVERSITY
Date : July 2008		

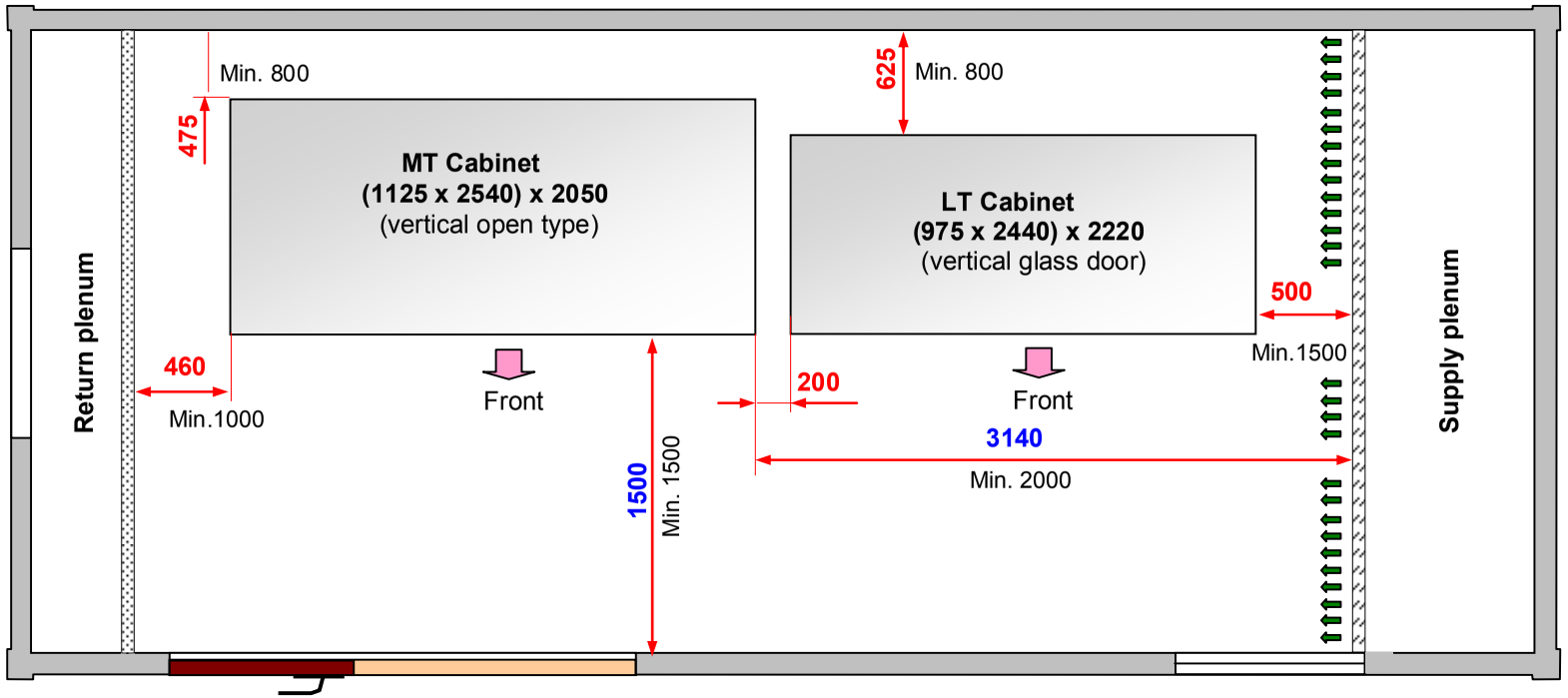

Minimum distance according to
BS EN ISO 23953-2-2005

MT Cabinet: Carter ELFM
LT Cabinet : Costan-Elephant H2200-3P

No : -	TITLE:	SCHOOL OF ENGINEERING AND DESIGN
Scale : NTS	**Figure F-2 Layout of the MT and LT cabinets in the test chamber**	BRUNEL UNIVERSITY
Date : July 2008		

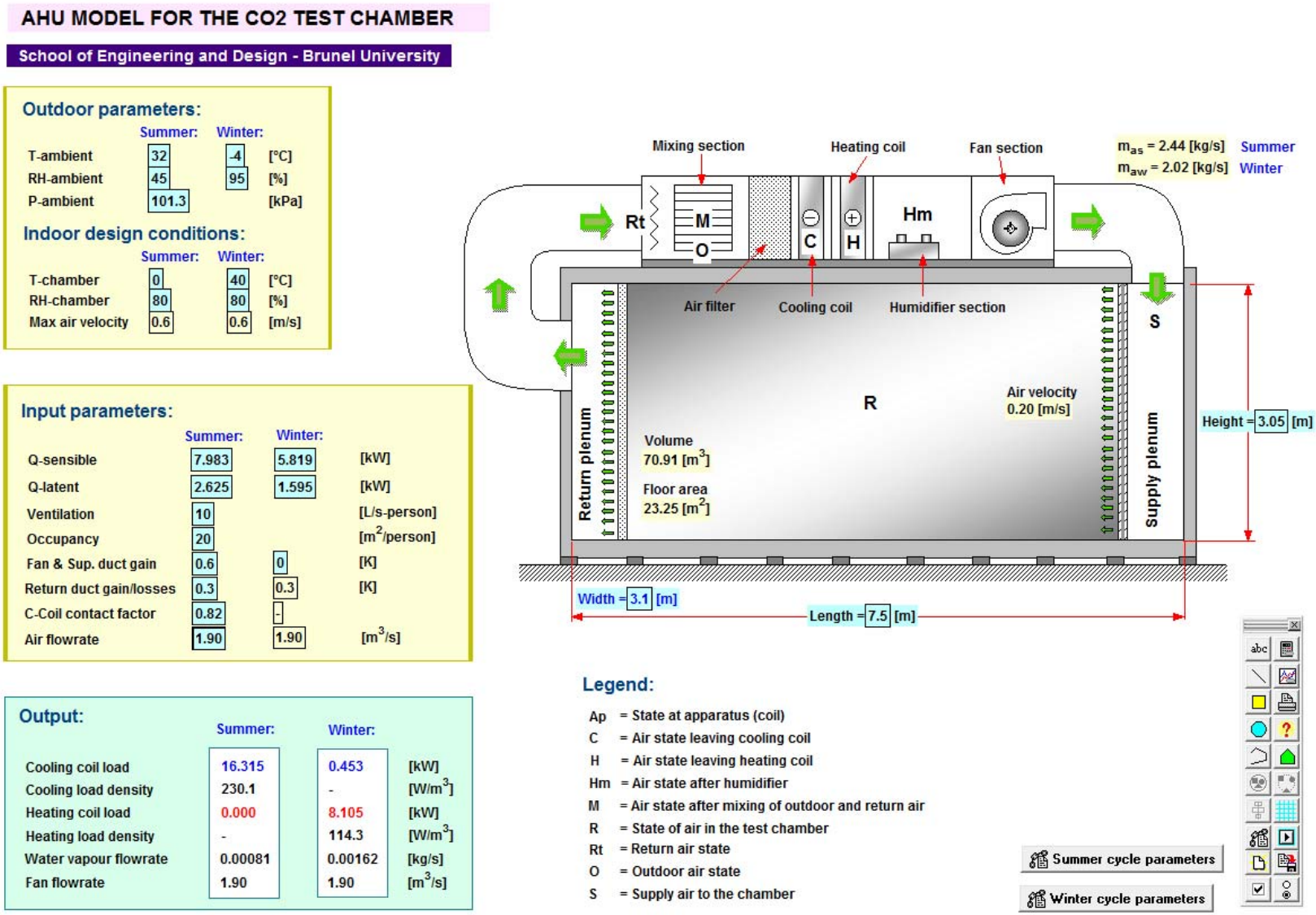

Figure F-3 A design simulation of the AHU of the CO_2 test chamber

CO_2 Chamber Layout

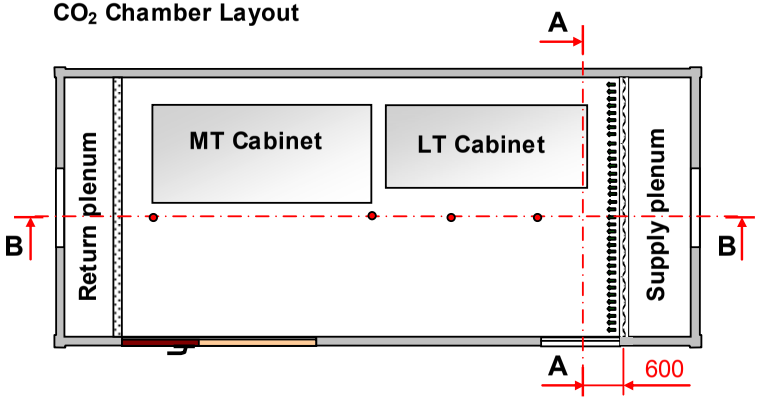

Section A – A
(rotated to be floor at the bottom)

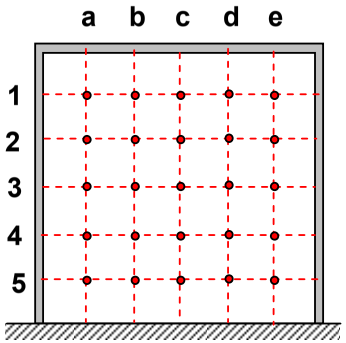

Section B – B

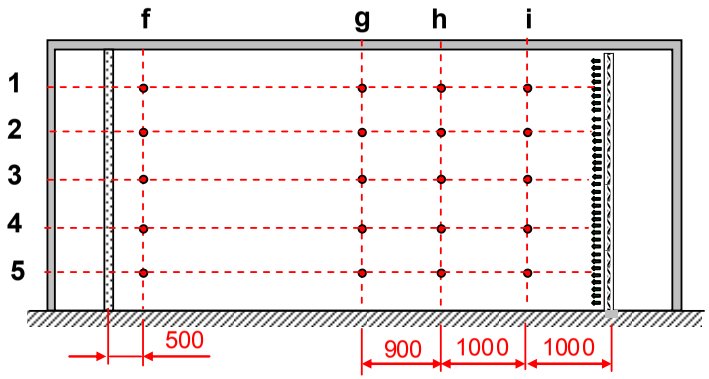

Ref. BS EN ISO 23953-2-2005

Tested on the 18th January 2011

3D measurement

Position	Air velocity (m/s)	Position	Air velocity (m/s)
f1	0.18	f4	0.13
g1	0.18	g4	0.20
h1	0.17	h4	0.20
i1	0.15	i4	0.19
f2	0.18	f5	0.10
g2	0.19	g5	0.14
h2	0.18	h5	0.18
i2	0.15	i5	0.24
f3	0.18		
g3	0.18		
h3	0.19		
i3	0.18		

86% comply with standard

Measurement plane parallel to plenum

Position	Air velocity (m/s)
a1	0.11
b1	0.17
c1	0.12
d1	0.14
e1	0.11
a2	0.14
b2	0.18
c2	0.15
d2	0.14
e2	0.14
a3	0.18
b3	0.20
c3	0.16
d3	0.18
e3	0.18
a4	0.17
b4	0.16
c4	0.15
d4	0.18
e4	0.17
a5	0.18
b5	0.20
c5	0.20
d5	0.18
e5	0.16

100% comply with standard

Results based on 40% fan speed

No	: -
Scale	: NTS
Date	: January 2011

TITLE:

Figure F-4 Air velocity map of the air flow in the CO_2 test chamber

SCHOOL OF ENGINEERING AND DESIGN
BRUNEL UNIVERSITY

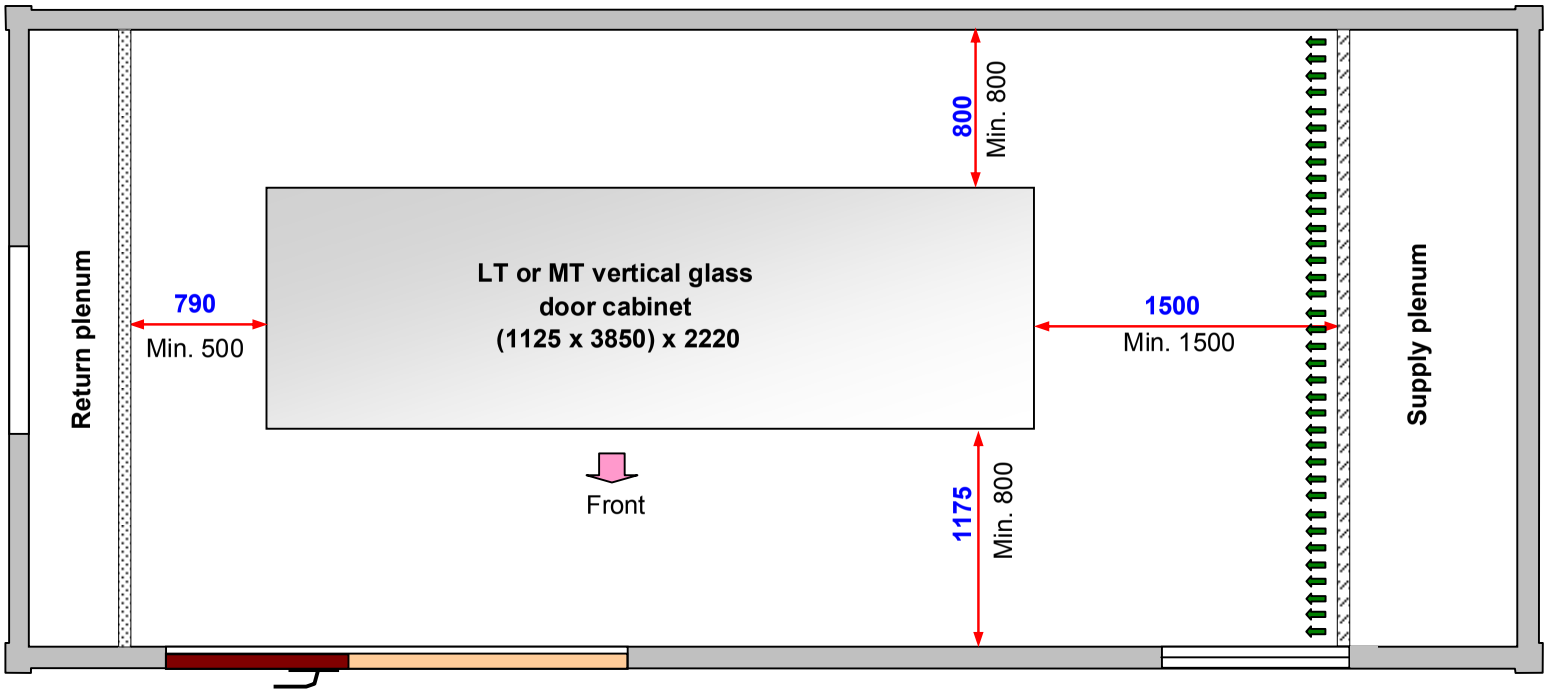

Minimum distance according to
BS EN ISO 23953-2-2005

No : -	TITLE: **Figure F-5 Layout of a 3.75 m long LT or MT vertical door type cabinet in the CO_2 test chamber**	SCHOOL OF ENGINEERING AND DESIGN BRUNEL UNIVERSITY
Scale : NTS		
Date : July 2008		

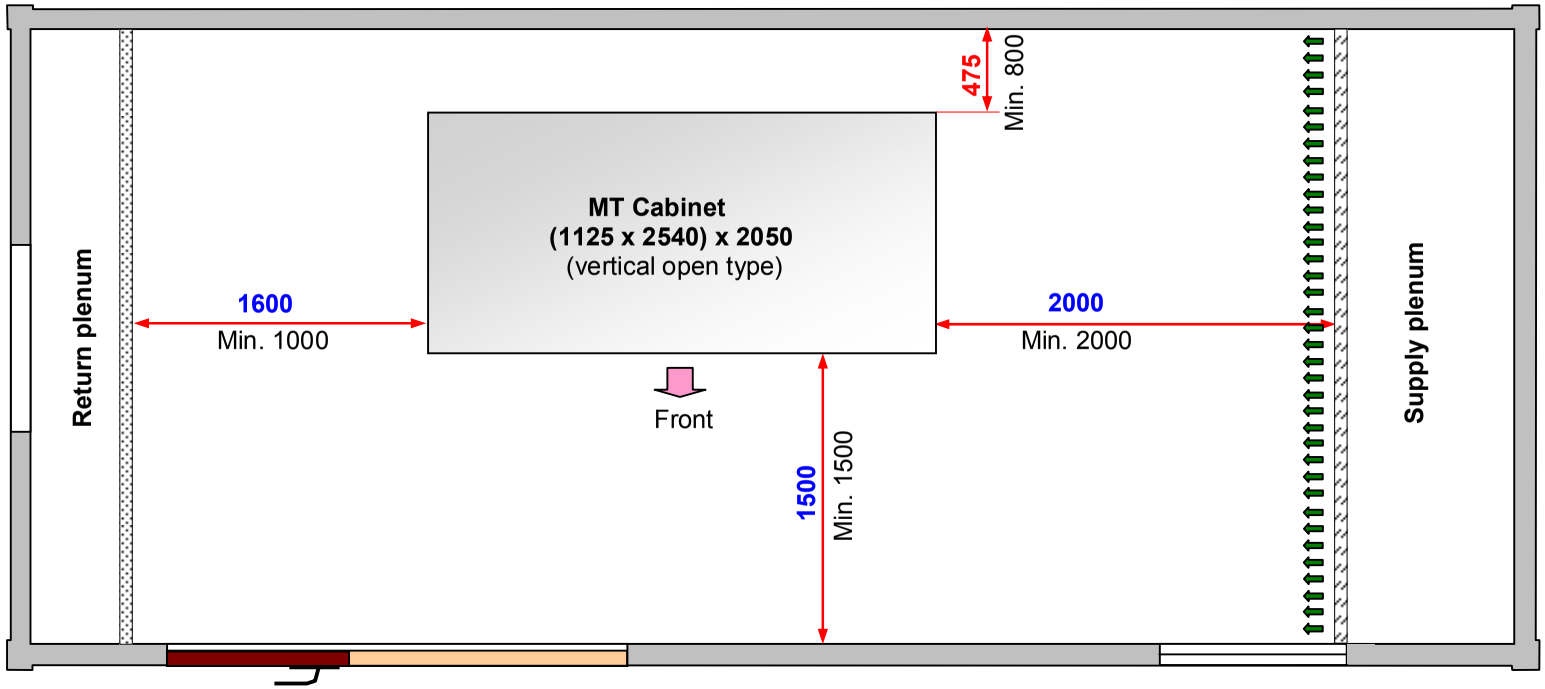

Minimum distance according to
BS EN ISO 23953-2-2005

No : -	TITLE: **Figure F-6 Layout of a 2.5 m long vertical MT open type cabinet in the CO_2 test chamber**	SCHOOL OF ENGINEERING AND DESIGN BRUNEL UNIVERSITY
Scale : NTS		
Date : July 2008		

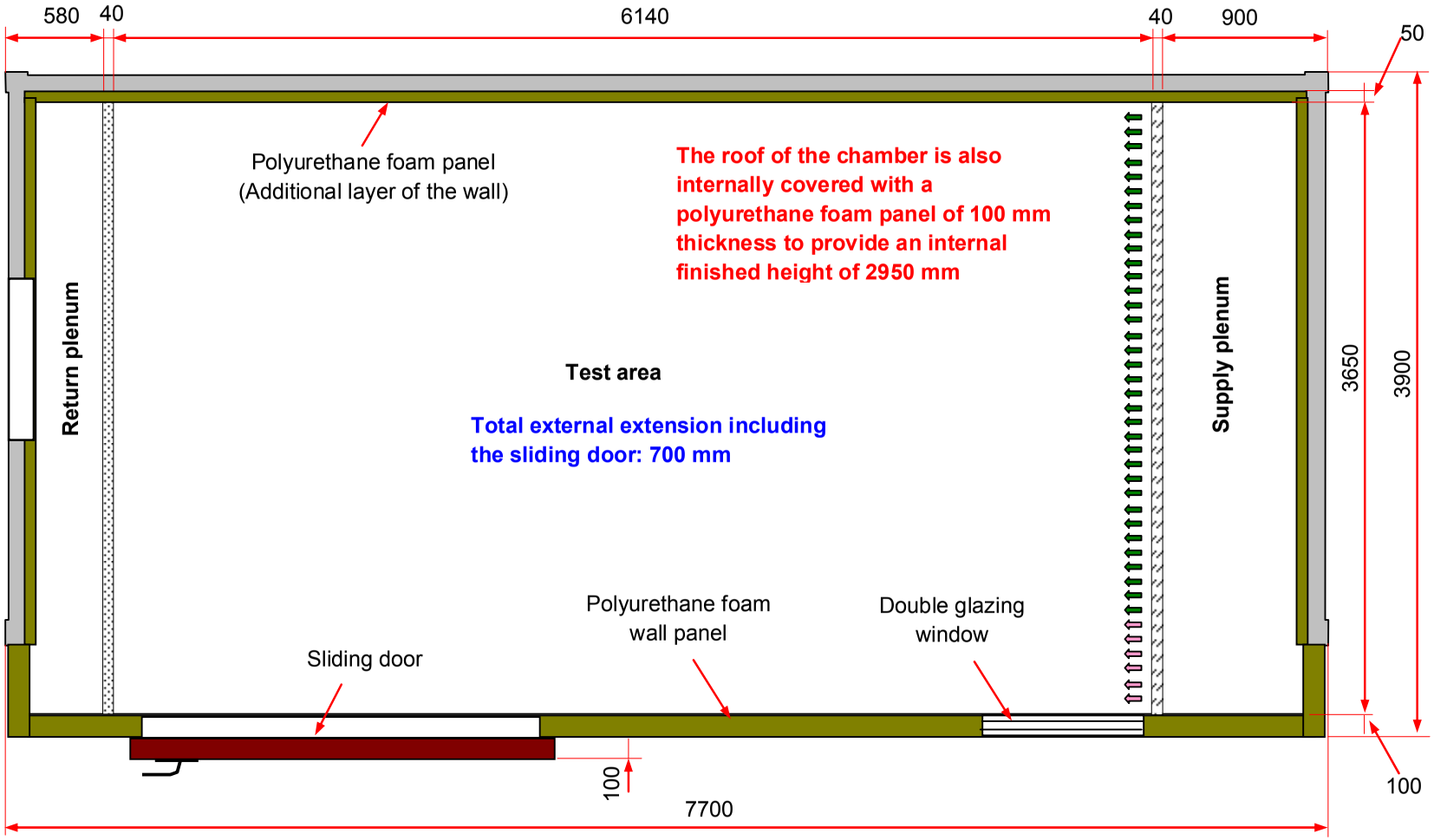

No : -	TITLE:	SCHOOL OF ENGINEERING AND DESIGN
Scale : NTS	**Figure F-7 Layout of a possible extension of the CO_2 test chamber**	BRUNEL UNIVERSITY
Date : March 2012		

APPENDIX G:
Operational modes and procedures

This appendix describes four modes of system operation. The valve arrangement for each mode, operational procedures and some precautions are also presented.

The explanations in this appendix refer to Figure C-1 (Appendix C).

G.1 Operational modes

The operational arrangements refer only to the CO_2 refrigeration system. The high stage system is operating at steady state conditions at the designed delivery water glycol temperature.

The four modes of the system operations can be described as below.

Normal operation mode:

The refrigerant circulates in both the LT and MT refrigeration systems. For the LT circuit the refrigerant flows from the liquid receiver through the internal HX, LT flow meter, LT evaporators (LT display cabinet and additional load), suction accumulator, LT compressor, oil separator, condenser and returns back to the receiver as liquid.

For the MT circuit the liquid refrigerant circulates from the receiver to the CO_2 pump through the suction filter/drier. At discharge of the pump, the flow is divided into two branches, one directly returns the liquid refrigerant back to the liquid receiver through the bypass valve (V-33) and the other circulates the liquid through the MT flow meter, regulator valve (V-38), MT evaporator and returns back to the receiver as a mixture of liquid and vapour. The saturated vapour in the receiver circulates to the condenser through a *thermosiphon loop* (valve V-07, condenser, and valve V-06). In this operation the saturated vapour from the receiver is mixed with the hot gas from the LT circuit just before entering the cascade condenser. The liquid from the condenser flows back into the receiver by forced flow and gravity.

Valve arrangement for normal operation mode
(Valve numbers refer to Figure C-1, Appendix C):

Valve no.	V-01	V-02	V-03	V-04	V-05	V-06	V-07	V-08	V-09	V-10	V-11	V-12
Position	O	O	C	O	O	O	O	C	O	O	O	O

Valve no.	V-13	V-14	V-15	V-16	V-17	V-18	V-19	V-20	V-21	V-22	V-23	V-24
Position	C	O	O	C	O	C	O	C	C	O	C	C

Valve no.	V-25	V-26	V-27	V-28	V-29	V-30	V-31	V-32	V-33	V-34	V-35	V-36
Position	O	O	C	C	O	C	O	C	OR	C	O	C

Valve no.	V-37	V-38	V-39	V-40	V-41	V-42	V-43	V-44	V-45		V-47	
Position	O	OR	C	C	C	O	C	C	C		O	

C = closed; O = fully open; OR = open with manual regulation

Operation with thermosiphon condensation

In this operation, the hot gas from the discharge of the LT compressor passes through the liquid receiver allowing the hot gas to be desuperheated by boiling some of the liquid. The two-phase refrigerant from the MT circuit also terminates in the receiver. The valve arrangement of the MT circuit is the same as in the normal operation mode. The flow of the saturated vapour refrigerant from the receiver to the condenser occurs solely due to the thermosiphon effect. The refrigerant vapour condenses in the condenser and returns back to the receiver as a saturated liquid by gravity.

Valve arrangement:

Most of the valves are arranged as for normal operation mode except valve V-02 is closed and valve V-08 is open.

Operation with forced condensation

The condensation of the CO_2 refrigerant in the condenser occurs in forced flow conditions. The condensation process is quite similar with the normal operation arrangement but the flow rate of the refrigerant in this operation is higher. The hot gas from the discharge of the LT compressor is connected in the same way as for normal operation. The saturated liquid-vapour mixture from the MT circuit, however, is directly circulated to the condenser after mixing with the hot gas from the LT circuit.

Valve arrangement:

The valves are arranged as those for normal operation except valve V-05 is closed and valve V-03 is open.

Operation with gravity mode

The aim of the gravity mode is to investigate the performance of the MT system in utilising the gravity force to circulate the liquid refrigerant and to provide refrigeration effect to the MT display cabinet. In this operation, the MT evaporator is fed with liquid refrigerant by gravity force. The pump is switched off. The bypass valve V-27 is open; valves V-33 and V-31 are closed. The solenoid valve (SV) upstream of the MT evaporator is in normal operation to enable the liquid refrigerant to flow through the evaporator. The other valve arrangements remain the same for the normal operation mode.

G.2 Operational procedures

The procedures consist of three stages which include starting up, testing and shutting down. The test system is assumed to be fully charged; in standby conditions; the standstill condensing unit is in operation to keep the CO_2 refrigerant in the system; and the test chamber is conditioned at 25 ^{o}C and 60% RH.

Starting up procedure

1. The procedure starts from the preparation of the high stage system (trigeneration system or water chiller) and visual check of the whole integrated system.
2. Prepare the high stage system and check the setting point of the water-glycol thermostat.
3. Position the control valves as set in the *normal operation mode*, except valves V-14 and V-31 are closed.
4. Ensure the oil level of the LT compressor in the range and there is sufficient oil in the oil reservoir.
5. Recheck the parameter settings of the display cabinets and the additional load.
6. Energise the flow meters and start up the monitoring and the data logging system.
7. Start up the high stage system and ensure the pump system and flow meter are in good working order. When the high stage system has been steady at the set point, the stand still condensing unit is automatically switched off (in standby conditions).

8. Switch on the display cabinets and the additional load system and ensure fans, lights, water-glycol pump, flow meter and expansion valve are in good working order.
9. Open valve V-31 to allow the liquid refrigerant to fill up the suction line of the CO_2 pump.
10. Start up the CO_2 pump and ensure the solenoid valve upstream of the MT evaporator has also been energised.
11. Monitor the refrigerant flow through the sight glass and the evaporator coil temperature of the MT cabinet. Adjust the regulator valve (V-38) and bypass valve (V-33) if required.
12. Monitor also the temperature and pressure of the whole system including the liquid level in the receiver to ensure the system is working in stable conditions.
13. The LT refrigeration system is now ready to start up.
14. Open the valve V-14 to allow the liquid refrigerant to fill up the liquid line of the LT circuit.
15. Switch on the LT compressor and observe the operation. The speed of the compressor can be adjusted to balance the capacity of the compressor and the LT refrigeration load.
16. Monitor the pressures of the CO_2 refrigeration system and the condensing temperature to ensure the high stage system can maintain the set point.
17. Monitor also the liquid level in the receiver after both LT and MT systems are in operation.
18. Regularly observe the oil level of the compressor to ensure the oil management system can work properly.
19. Monitor the LT and MT product temperatures and the defrost cycle. When the product temperatures have reached the M1 and L1 range for MT and LT cabinets respectively, the experimental tests can be arranged.

Experimental test procedure

1. Prior performing the experimental tests the starting up procedure needs to be completed and the system is kept running.
2. Rearrange the test rig according to the operation mode the test is performed.

3. Readjust the parameter set up according to the test requirements such as evaporating and condensing temperatures, defrost cycle, defrost termination temperature, temperature set point, degree of super heat for the LT evaporator and circulation ratio for the MT flooded system.
4. Monitor and record the performance parameters by restarting the data logging system.
5. Operate the system in a steady state conditions for 24 hours.
6. The test procedure can be repeated if other tests are performed.
7. When the tests have been completed the test rig must be shut down.

Shutting down procedure

1. Before shutting down, the CO_2 refrigeration system must be pumped down in order to store the liquid CO_2 back to the receiver.
2. Switch off the CO_2 pump if the pump is in operation. While the LT compressor is kept running.
3. Close all valves (V-14, V-27 and V-31) which supply the liquid CO_2 to the MT and LT circuits.
4. Open valve V-43 to allow the liquid refrigerant in the MT circuit to flow to the liquid line of the LT circuit.
5. Keep the LT compressor in operation until all liquid CO_2 is pump out from the liquid line. The compressor is automatically switched off when the system has been pumped down.
6. The compressor controller is safe to switch off.
7. Turn off the display cabinets and the additional load system.
8. Switch off the high stage system to complete the shutting down procedure. The liquid CO_2 is then kept in the system by the standstill condensing unit.

G.3 Precautions

For safety purposes, the test rig was designed to enable the CO_2 refrigerant to be released to the atmosphere when the pressure in the system is above 35 bar. During the operation, there is always a possibility that the CO_2 refrigerant escapes from the system due to system pressure rising above pressure limit. This may occur when the high stage system suddenly fails and the system is under full load conditions. The pressure in the

system can rise quickly and the standstill condensing unit cannot prevent the sudden increase of the system pressure. The pressure very quickly reaches the burst pressure of the safety valves which then open to allow the refrigerant to escape to the atmosphere. If this occurs, in order to avoid risks of injury the following precautions need to be taken:

- The machine room must be adequately ventilated by keeping the door open.
- Assess the situation carefully, especially the suction line pressure relief valve which releases the CO_2 to the machine room.
- Switch off the CO_2 pump and close all valves which supply the liquid CO_2 to the MT and LT systems.
- Don't stop the compressor before the LT system is pumped down.
- Turn off the display cabinets and the additional load system.
- By keeping the compressor running, the suction pressure can be maintained below the bursting pressure of the safety valve. The CO_2 refrigerant escape to the atmosphere from the pressure relief valve installed on the liquid receiver. This is safe because it is far from occupied areas.
- The compressor is automatically switched off by the low pressure switch. After that, switch off manually the compressor controller. The condensing unit is then gradually able to decrease the pressure of the system.

The CO_2 refrigerant will also escape from the system during standby conditions if the standstill condensing unit fails. In this case, the CO_2 refrigerant is released gradually from the pressure relief valve of the receiver. This is a normal safety action and is considered safe.

APPENDIX H:

Mathematical model of CO_2 evaporator coils

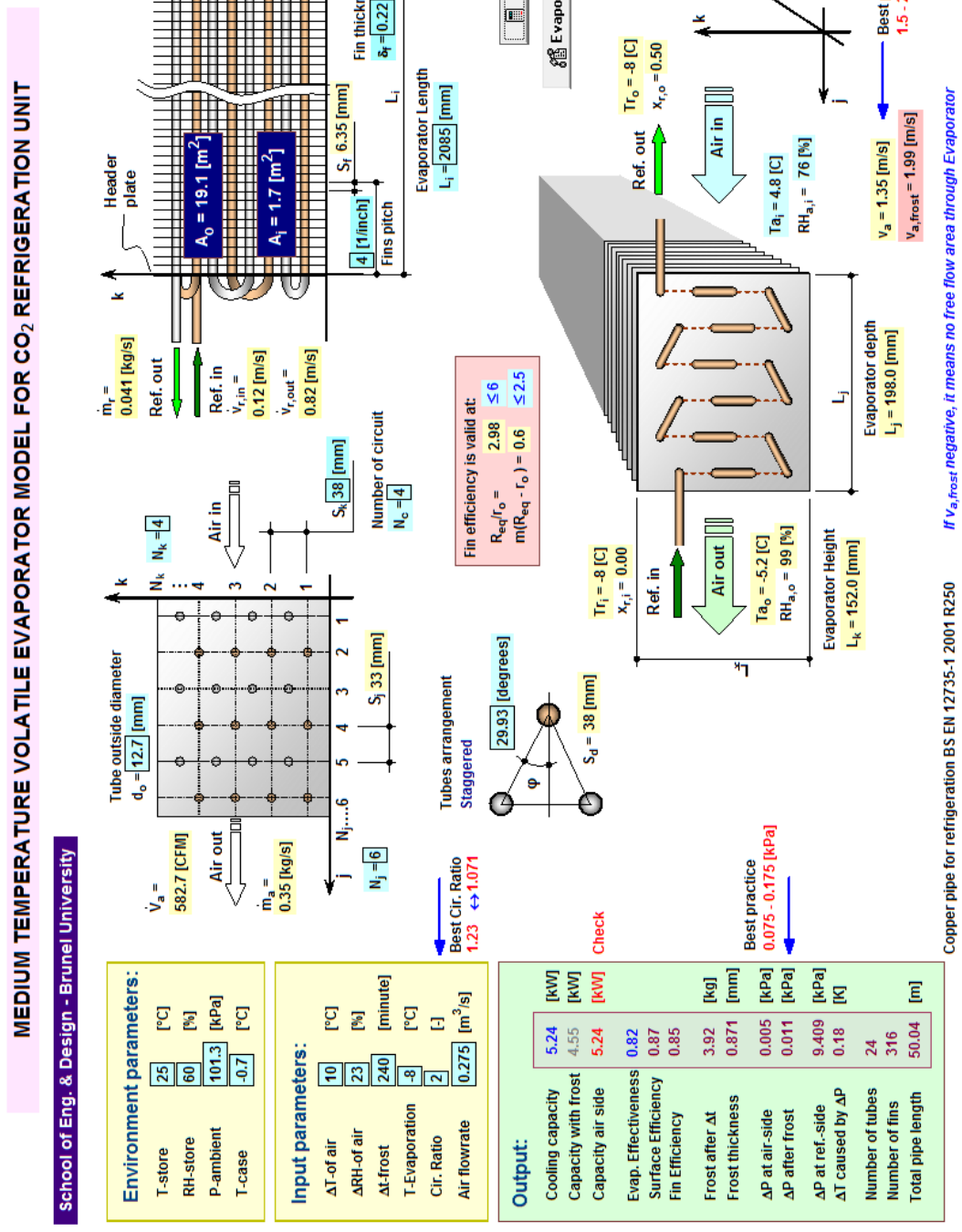

Figure H-1 EES model of the MT flooded evaporator coil

EVAPORATOR GEOMETRY AND PERFORMANCE

Volatile medium temperature

Geometrical Parameters	
Tube material	Copper
Fin Material	Aluminum
Fin type	Corrugated
Fin thickness [mm]	0.22
Fin pitch [fins/inch]	4
Fin spacing [mm]	6.35
Tube nominal outer diameter [mm]	12.7
Tube inner diameter [mm]	10.7
Tube wall thickness [mm]	1
Transverse tube spacing [mm]	38
Longitudinal tube spacing [mm]	33
Tube arrangement	Staggered
Number of transverse tube row	4
Number of longitudinal tube row	6
Number of circuit	4
Number of total tubes	24
Number of fins	316
Total tube length [m]	50.04
Evaporator height [mm]	152.0
Evaporator depth [mm]	198.0
Evaporator length exc. bend [mm]	2085
Evaporator volume [m^3]	0.063

Refrigerant Volume	
Straight pipe volume [L]	4.5
U-bend volume [L]	0.1234
Total volume [L]	4.623

Copper tube shall comply to BS EN 12735 R250

Operational and Performance Parameters			
Evaporator Capacity [kW]	5.24	Surface efficiency	0.87
Evaporation temperature [°C]	-8	Air flowrate required [m^3/s]	0.275
ΔT of air cross evaporator [°C]	10	Air face velocity [m/s]	1.35
Evaporator effectiveness	0.82	Design circulation ratio	2
Fin efficiency	0.85		

Heat transfer paramaters	Refrigerant side	Air side
Overall heat transfer transmittance [kW/m^2-K]	0.3658	0.03219
Heat transfer surface area [m^2]	1.7	19.1
Pressure drop [kPa]	9.409	0.005
Heat transfer coefficient [kW/m^2-K]	3.036	0.04981

Variation of heat transfer coefficient and pressure drop at refrigerant side

Vapour quality	Heat transfer coefficient [kW/m^2-K]	Pressure drop [kPa/m]
0.00	3.406	0.01967
0.14	3.403	0.07273
0.22	3.405	0.1043
0.31	3.408	0.1388
0.39	3.411	0.1757
0.48	3.413	0.2146
0.56	3.416	0.2551
0.64	1.719	0.2971
0.73	1.667	0.3402
0.81	1.88	0.3842
0.90	3.74	0.4289
0.93	2.874	0.3654
0.97	2.009	0.3018
0.97	1.143	0.2382
1.00	0.2769	0.1747

X_{out} 0.50

Back to Main window

Figure H-2 Geometry and estimated performance parameters of the MT evaporator coil

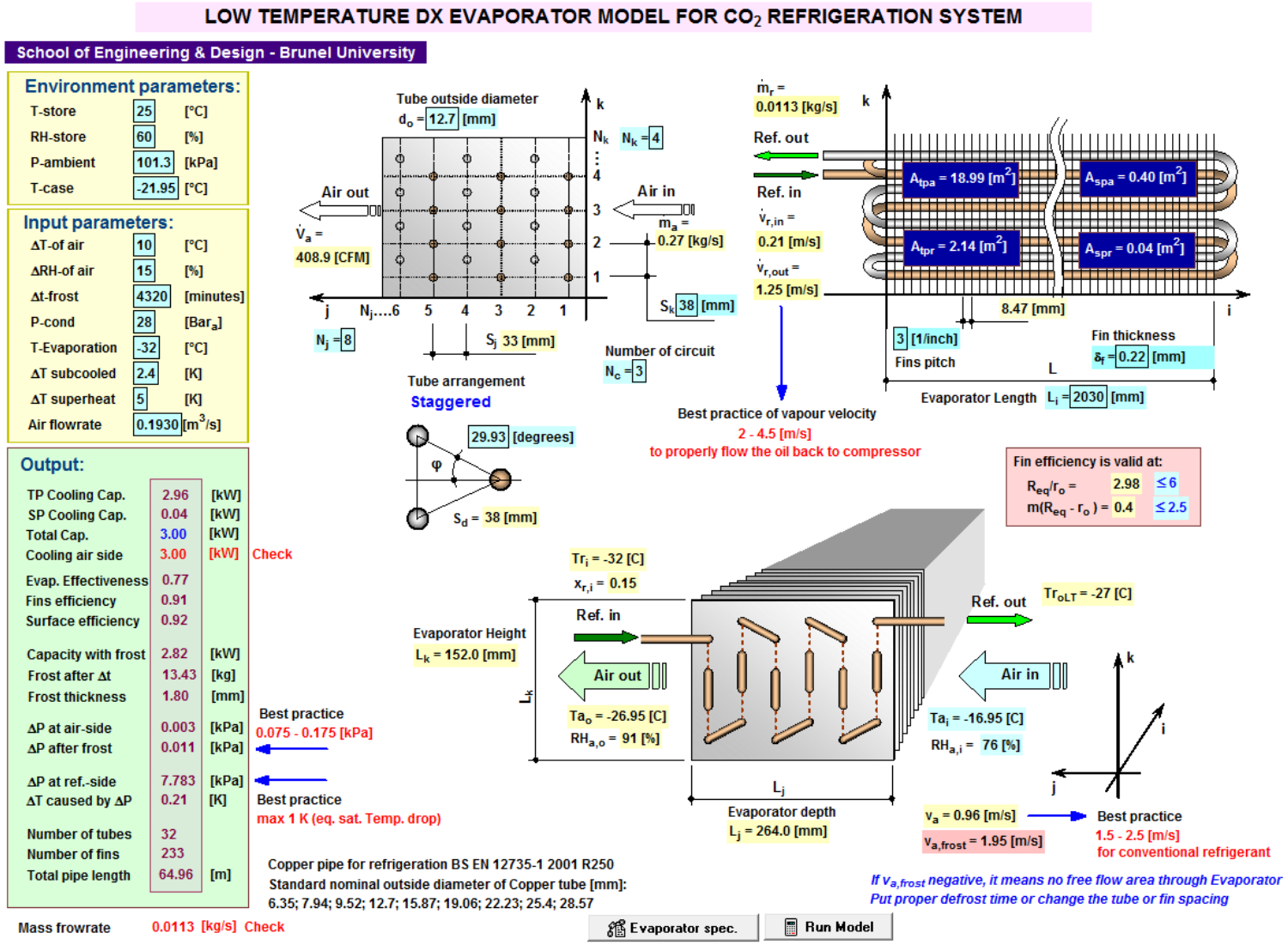

Figure H-3 EES model of the LT DX evaporator coil

EVAPORATOR GEOMETRY AND PERFORMANCE

DX Low Temperature

Geometrical Parameters	
Tube material	Copper
Fin Material	Aluminum
Fin type	Corrugated
Fin thickness [mm]	0.22
Fin pitch [fins/inch]	3
Fin spacing [mm]	8.47
Tube nominal outer diameter [mm]	12.7
Tube inner diameter [mm]	10.7
Tube wall thickness [mm]	1
Transverse tube spacing [mm]	38
Longitudinal tube spacing [mm]	33
Tube arrangement	Staggered
Number of transverse tube row	4
Number of longitudinal tube row	8
Number of circuit	3
Number of total tubes	32
Number of fins	233
Total tube length [m]	64.96
Evaporator height [mm]	152.0
Evaporator depth [mm]	264.0
Evaporator length exc. bend [mm]	2030
Evaporator volume [m^3]	0.081

Refrigerant Volume	
Straight pipe volume [L]	5.841
U-bend volume [L]	0.1664
Total volume [L]	6.008

Copper tube shall comply to BS EN 12735 R250

System operation condition to be considered:

P CO_2 intermediate = 28 [bar]
Degree of subcooled = 2.4 [K]
Degree of superheat = 5 [C]

Operational and Performance Parameters			
Evaporator Capacity [kW]	3.00	Surface efficiency	0.92
Evaporation temperature [°C]	-32	Air flowrate required [m^3/s]	0.1930
ΔT of air cross evaporator [°C]	10	Air face velocity [m/s]	0.96
Evaporator effectiveness	0.77	Design ΔT Superheat [K]	5
Fin efficiency	0.91		

Heat transfer paramaters	Refrigerant side	Air side
Overall heat transfer transmittance [kW/m^2-K]	0.189	0.02129
Heat transfer surface area [m^2]	2.2	19.4
Pressure drop [kPa]	7.783	0.003
Heat transfer coefficient [kW/m^2-K]	1.336	0.02938

Variation of heat transfer coefficient and pressure drop at refrigerant side

Vapour quality	Heat transfer coefficient [kW/m^2-K]	Pressure drop [kPa/m]
0.15	1.557	0.03264
0.23	1.558	0.0467
0.31	1.56	0.06205
0.39	1.562	0.07849
0.47	1.563	0.09583
0.55	0.7949	0.1139
0.63	0.8048	0.1327
0.71	0.8813	0.152
0.79	1.009	0.1717
0.87	1.211	0.1918
0.95	1.672	0.2121
0.98	1.263	0.1672
0.98	0.854	0.1222
1.00	0.4448	0.07722
1.00	0.03564	0.03225

Back to Main window

Figure H-4 Geometry and estimated performance parameters of the LT DX evaporator coil

APPENDIX I:

As built integrated trigeneration and CO_2 refrigeration

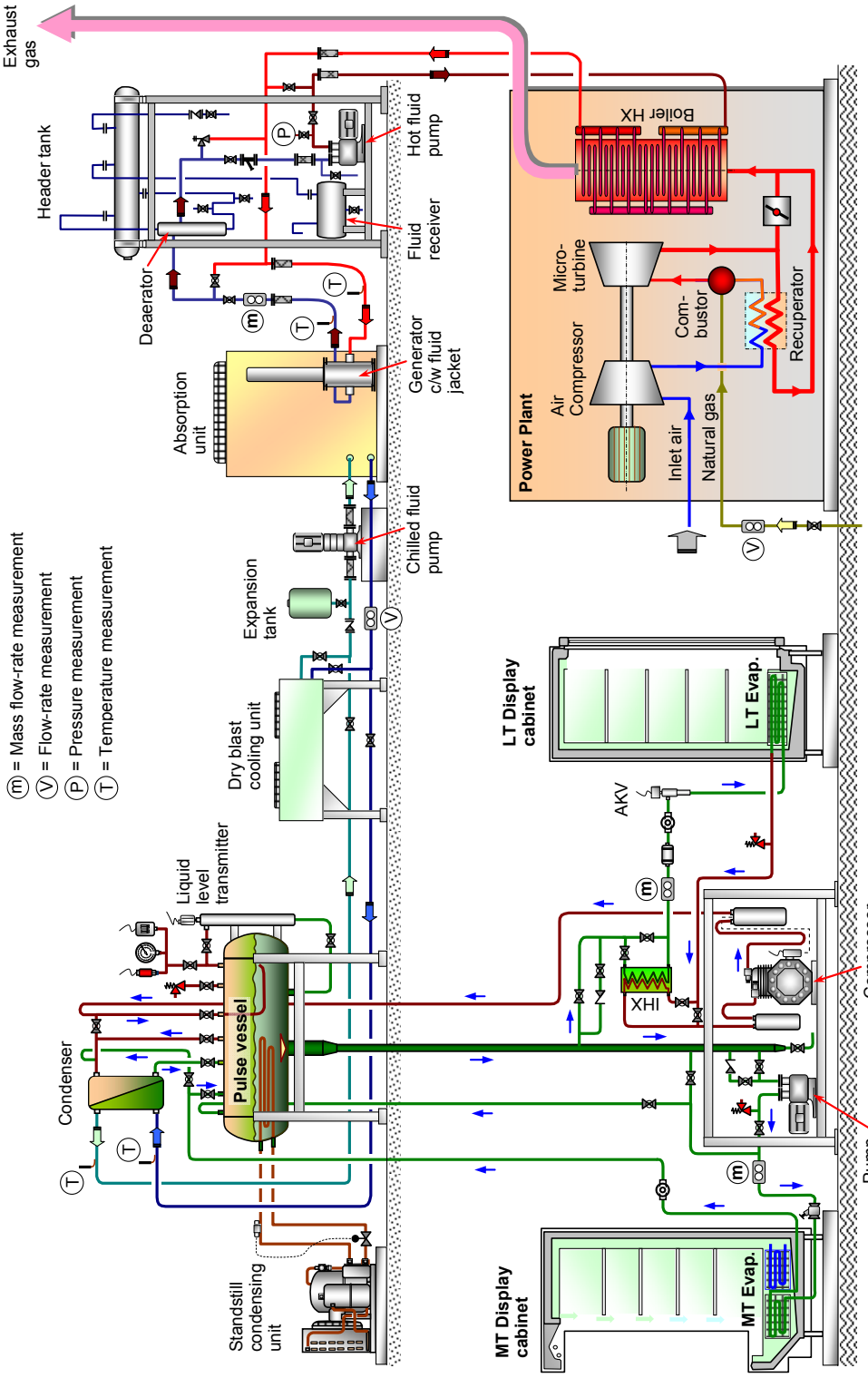

Figure I-1 Schematic diagram of the as-built test facility

APPENDIX J:
Uncertainty analysis

In the analysis of test results, key parameters such as: circulation ratio *CR* = 1 and coefficient of performance (*COP*) are not directly measured. They are calculated as a function of one or more variables that are directly measured. Each measured variable has a random variability which is referred to as its "uncertainty". This appendix describes the calculations of uncertainty propagation of measured variables into the calculated parameters which include: circulation ratio of 1, *COP* of the MT, LT and *COP* of the overall CO_2 refrigeration system. The uncertainty of reversed Carnot *COP* calculation is also presented.

The uncertainty propagation was determined using the EES software with an assumption that individual measurements are uncorrelated and random. In general, uncertainty of the calculated parameters can be determined from (EES, 2010):

$$U_Y = \sqrt{\sum_i \left(\frac{\partial Y}{\partial X_i} \right)^2 U_{X_i}^2} \tag{J.1}$$

Where:

Y = calculated parameter; X_i = measured variables; U_Y = uncertainty of calculated parameter; U_{Xi} = uncertainty of measured variables

J.1 Uncertainty of the calculation of the circulation ratio *CR* = 1

Circulation ratio is a function of measured variables as below:

$$CR = f(\dot{m}_{r,MT}, T_{evapMT}, RH_{a.ON}, RH_{a.OFF}, T_{a.ON}, T_{a.OFF}, L, w, v_a) \tag{J.2}$$

Refers to equations (5.6), (5.7) and (5.8) in Chapter 5.

Where: $\dot{m}_{r,MT}$ = MT refrigerant mass flow rate (kg/s); T_{evapMT} = MT evaporating temperature (^oC); $RH_{a.ON}$ and $RH_{a.OFF}$ are relative humidity of air-on and air-off; $T_{a.ON}$ and $T_{a.OFF}$ are temperature of air-on and off respectively (^oC); L and w are sectional dimensions of the air duct after the MT coil (m); v_a is air velocity at the measured sectional area of the air duct (m/s).

Uncertainties of the measured variables for calculation uncertainty of the circulation ratio CR = 1 are shown in Table J-1.

Table J-1 Uncertainties of the measured variables for calculation uncertainty of the circulation ratio *CR* = 1

Measured variable	Value at CR = 1	Unit	Absolute uncertainty	Relative uncertainty
$\dot{m}_{r,MT}$	0.019	kg/s		0.00035
T_{evapMT}	-7	°C	0.5	
$RH_{a.ON}$	0.76	-	0.015	
$RH_{a.OFF}$	0.91	-	0.015	
$T_{a.ON}$	5	°C	0.5	
$T_{a.OFF}$	-3	°C	0.5	
L	2.1	m	0.0005	
w	0.04	m	0.0005	
v_a	3.68	m/s		0.03

Uncertainty of *L* and *w* were assumed to be 0.5 mm
The uncertainties of the measured variables refer to Section 3.6.1 (Chapter 3)

Results of the uncertainty analysis for the CR obtained from EES:

Variable±Uncertainty	Partial derivative	% of uncertainty
CR = 1.031±0.111 [-]		
L = 2.1±0.0005 [m]	∂CR/∂L = -0.4911	0.00 %
$\dot{m}_{mes}$ = 0.019±0.00000665 [kg/s]	∂CR/∂$\dot{m}_{mes}$ = 54.28	0.00 %
RH_{airOFF} = 0.91±0.015 [-]	∂CR/∂RH_{airOFF} = 0.6533	0.78 %
RH_{airON} = 0.76±0.015 [-]	∂CR/∂RH_{airON} = -1.2	2.63 %
T_{airOFF} = -3±0.5 [C]	∂CR/∂T_{airOFF} = 0.1414	40.61 %
T_{airON} = 5±0.5 [C]	∂CR/∂T_{airON} = -0.1515	46.60 %
T_{evap} = -7±0.5 [C]	∂CR/∂T_{evap} = -0.01106	0.25 %
v_{air} = 3.68±0.1104 [m/s]	∂CR/∂v_{air} = -0.2803	7.78 %
w = 0.04±0.0005 [m]	∂CR/∂w = -25.78	1.35 %

Uncertainty of the circulation ratio was determined to be

- Absolute uncertainty: ± 0.111
- Relative uncertainty: ± 10.8%

J.2 Uncertainty of the COP calculation

Coefficient of performance (*COP*) of the refrigeration system is a function of the following measured variables:

$$COP = f(\dot{m}_{r,MT}, \dot{m}_{r,LT}, P_{MT}, P_{LT}, T_{evap.out.LT}, W_{comp}, W_{CO2pump}) \quad \text{(J.2)}$$

Uncertainties of the measured variables for the calculation of uncertainty of the COPs are shown in Table J-2

Table J-2 Uncertainties of the measured variables for uncertainty of the COP calculations

Measured variable	Value	Unit	Absolute uncertainty	Relative uncertainty
CR	1.3	-		0.108
$\dot{m}_{r,MT}$	0.026	kg/s		0.00035
$\dot{m}_{r,LT}$	0.032	kg/s		0.00035
P_{LT}	12.3	bar		0.03
P_{MT}	27.8	bar		0.03
$T_{evap.out.LT}$	-17	°C	0.5	
W_{comp}	2.55	kW		0.00036
$W_{CO2pump}$	0.11	kW		0.00036

The uncertainties of the measured variables refer to Section 3.6.1 (Chapter 3)

Results of the uncertainty analysis for COP obtained using EES:

- The uncertainty of the reversed Carnot COP
  - Absolute uncertainty: ± 0.0526
  - Relative uncertainty: ± 0.6%

  Detailed results:

Variable±Uncertainty	Partial derivative	% of uncertainty
COP_{carnot} = 9.616±0.05264		
CR = 1.3±0.1404	$\partial COP_{carnot} / \partial CR = 0$	0.00 %
$\dot{m}_{LT}$ = 0.032±0.0000112 [kg/s]	$\partial COP_{carnot} / \partial \dot{m}_{LT} = 0$	0.00 %
$\dot{m}_{MT}$ = 0.0259±0.000009065 [kg/s]	$\partial COP_{carnot} / \partial \dot{m}_{MT} = 0$	0.00 %
P_{LT} = 12.3±0.0369 [bar]	$\partial COP_{carnot} / \partial P_{LT} = 0.9305$	42.55 %
P_{MT} = 27.8±0.0834 [bar]	$\partial COP_{carnot} / \partial P_{MT} = -0.4784$	57.45 %
$T_{evapOUT,LT}$ = -17±0.5 [C]	$\partial COP_{carnot} / \partial T_{evapOUT,LT} = 0$	0.00 %
$W_{CO2comp}$ = 2.55±0.000918 [kW]	$\partial COP_{carnot} / \partial W_{CO2comp} = 0$	0.00 %
$W_{CO2pump}$ = 0.11±0.0000396 [kW]	$\partial COP_{carnot} / \partial W_{CO2pump} = 0$	0.00 %

- The uncertainty of the COP_{MT}
  - Absolute uncertainty: ± 4.921
  - Relative uncertainty: ± 10.8%

Detailed results of uncertainty of the COP_{MT}:

Variable±Uncertainty	Partial derivative	% of uncertainty
COP_{MT} = 45.43±4.921 [-]		
CR = 1.3±0.1404	$\partial COP_{MT} / \partial CR$ = -35.05	99.99 %
$\dot{m}_{LT}$ = 0.032±0.0000112 [kg/s]	$\partial COP_{MT} / \partial \dot{m}_{LT}$ = -7.930E-11	0.00 %
$\dot{m}_{MT}$ = 0.0259±0.000009065 [kg/s]	$\partial COP_{MT} / \partial \dot{m}_{MT}$ = 1754	0.00 %
P_{LT} = 12.3±0.0369 [bar]	$\partial COP_{MT} / \partial P_{LT}$ = -6.582E-16	0.00 %
P_{MT} = 27.8±0.0834 [bar]	$\partial COP_{MT} / \partial P_{MT}$ = -0.62	0.01 %
$T_{evapOUT,LT}$ = -17±0.5 [C]	$\partial COP_{MT} / \partial T_{evapOUT,LT}$ = -1.110E-16	0.00 %
$W_{CO2comp}$ = 2.55±0.000918 [kW]	$\partial COP_{MT} / \partial W_{CO2comp}$ = 0	0.00 %
$W_{CO2pump}$ = 0.11±0.0000396 [kW]	$\partial COP_{MT} / \partial W_{CO2pump}$ = -413	0.00 %

- The uncertainty of the COP_{LT}
  - Absolute uncertainty: ± 0.007
  - Relative uncertainty: ± 0.2%

  Detailed results of uncertainty of the COP_{LT}:

Variable±Uncertainty	Partial derivative	% of uncertainty
COP_{LT} = 4.018±0.007251 [-]		
CR = 1.3±0.1404	$\partial COP_{LT} / \partial CR$ = 0	0.00 %
$\dot{m}_{LT}$ = 0.032±0.0000112 [kg/s]	$\partial COP_{LT} / \partial \dot{m}_{LT}$ = 125.6	3.76 %
$\dot{m}_{MT}$ = 0.0259±0.000009065 [kg/s]	$\partial COP_{LT} / \partial \dot{m}_{MT}$ = -1.914E-13	0.00 %
P_{LT} = 12.3±0.0369 [bar]	$\partial COP_{LT} / \partial P_{LT}$ = -0.07179	13.35 %
P_{MT} = 27.8±0.0834 [bar]	$\partial COP_{LT} / \partial P_{MT}$ = -0.001157	0.02 %
$T_{evapOUT,LT}$ = -17±0.5 [C]	$\partial COP_{LT} / \partial T_{evapOUT,LT}$ = 0.01288	78.89 %
$W_{CO2comp}$ = 2.55±0.000918 [kW]	$\partial COP_{LT} / \partial W_{CO2comp}$ = -1.576	3.98 %
$W_{CO2pump}$ = 0.11±0.0000396 [kW]	$\partial COP_{LT} / \partial W_{CO2pump}$ = 0	0.00 %

- The uncertainty of the $COP_{overall}$
  - Absolute uncertainty: ± 0.204
  - Relative uncertainty: ± 3.6%

  Detailed results of uncertainty of the $COP_{overall}$:

Variable±Uncertainty	Partial derivative	% of uncertainty
$COP_{overall}$ = 5.731±0.2036 [-]		
CR = 1.3±0.1404	$\partial COP_{overall} / \partial CR$ = -1.449	99.87 %
$\dot{m}_{LT}$ = 0.032±0.0000112 [kg/s]	$\partial COP_{overall} / \partial \dot{m}_{LT}$ = 120.4	0.00 %
$\dot{m}_{MT}$ = 0.0259±0.000009065 [kg/s]	$\partial COP_{overall} / \partial \dot{m}_{MT}$ = 72.54	0.00 %
P_{LT} = 12.3±0.0369 [bar]	$\partial COP_{overall} / \partial P_{LT}$ = -0.06883	0.02 %
P_{MT} = 27.8±0.0834 [bar]	$\partial COP_{overall} / \partial P_{MT}$ = -0.02675	0.01 %
$T_{evapOUT,LT}$ = -17±0.5 [C]	$\partial COP_{overall} / \partial T_{evapOUT,LT}$ = 0.01235	0.09 %
$W_{CO2comp}$ = 2.55±0.000918 [kW]	$\partial COP_{overall} / \partial W_{CO2comp}$ = -2.154	0.01 %
$W_{CO2pump}$ = 0.11±0.0000396 [kW]	$\partial COP_{overall} / \partial W_{CO2pump}$ = -2.154	0.00 %

APPENDIX K:
Refrigerant charge and leak rate

This appendix presents a typical refrigerant charge for different sector of applications and reported annual leak rate of different refrigeration equipment for the UK. This appendix is related to Section 1.2 (Chapter 1) and Section 2.1 (Chapter 2).

Table K-1 Specific refrigerant charge for particular refrigeration system applications

Sector/ equipment	Specific refrigerant charge by refrigerant type (kg/kW)			
	HC	*HFC/HCFC*	*R717*	*R744* ‡
Domestic refrigeration	0.20 – 0.45	0.70 – 1.2	–	–
Retail refrigeration				
· Integral units	0.25 – 0.60	0.60 – 1.5	–	0.30 – 0.75
· Split/condensing units	–	0.40 – 0.70	–	0.20 – 0.35
· Central supermarket †	[0.15 – 0.35]	2.0 – 5.0	[0.09 – 0.21]	1.0 – 2.5
Stationary air conditioning				
· Unitary/split	0.10 – 0.15	0.25 – 0.70	–	0.15 – 0.35
· Chillers	0.13 – 0.15	0.27 – 0.35	0.04 – 0.25	–
· Heat pumps	0.08 – 0.11	0.19 – 0.53	–	0.10 – 0.25

† Values in square parentheses relate to indirect or secondary systems. ‡ Estimated from properties.

Source: MTP, 2008

Table K-2 Reported annual leakage rates for particular refrigeration system applications in the UK

Sector/ equipment	Reported annual leakage rates (% of charge per annum)			
	Johnson (1998)	*March (1999)*	*Haydock et al (2003)*	*ETSU (1997)*
Domestic refrigeration	1%	1%	0.3 – 0.7%	2.5%
Retail refrigeration	9 – 23%			
· Integral cabinets		1%	3 – 5%	2.5%
· Split/condensing units		10 – 20%	8 – 15%	15%
· Centralised supermarket		10 – 25%	10 – 20%	8%
Air conditioning	12 – 20%			
· Unitary/split		10 – 20%	8 – 12%	
· Chillers	15 – 22%	3 – 10%	3 – 5%	4%
· Heat pumps		3 – 10%	3 – 5%	4%

Source: MTP, 2008

APPENDIX L:

EES Models of the refrigeration systems for the conventional and trigeneration – CO_2 refrigeration energy systems

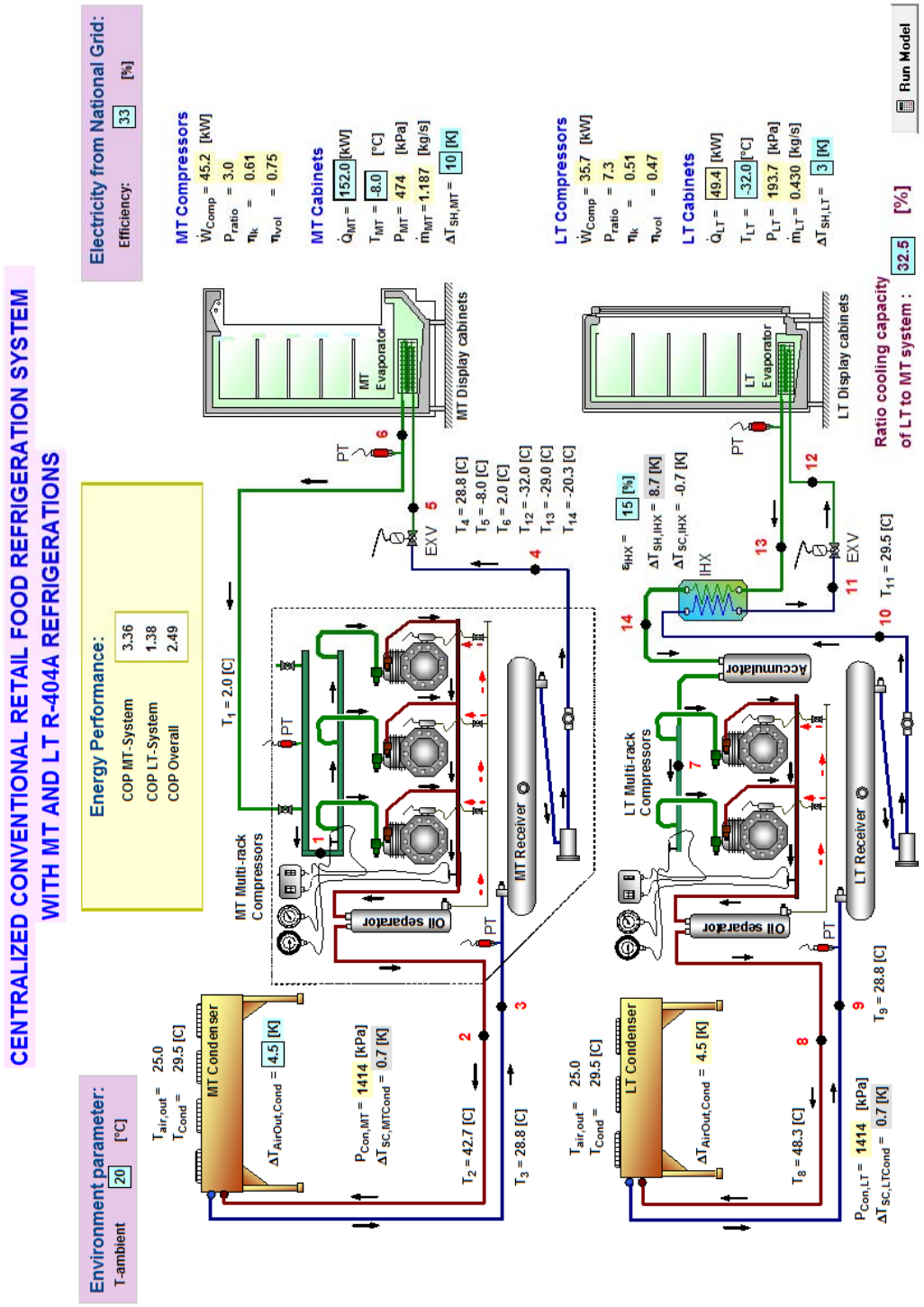

Figure L-1 A display of the EES model for the conventional supermarket refrigeration system using R-404A refrigerant

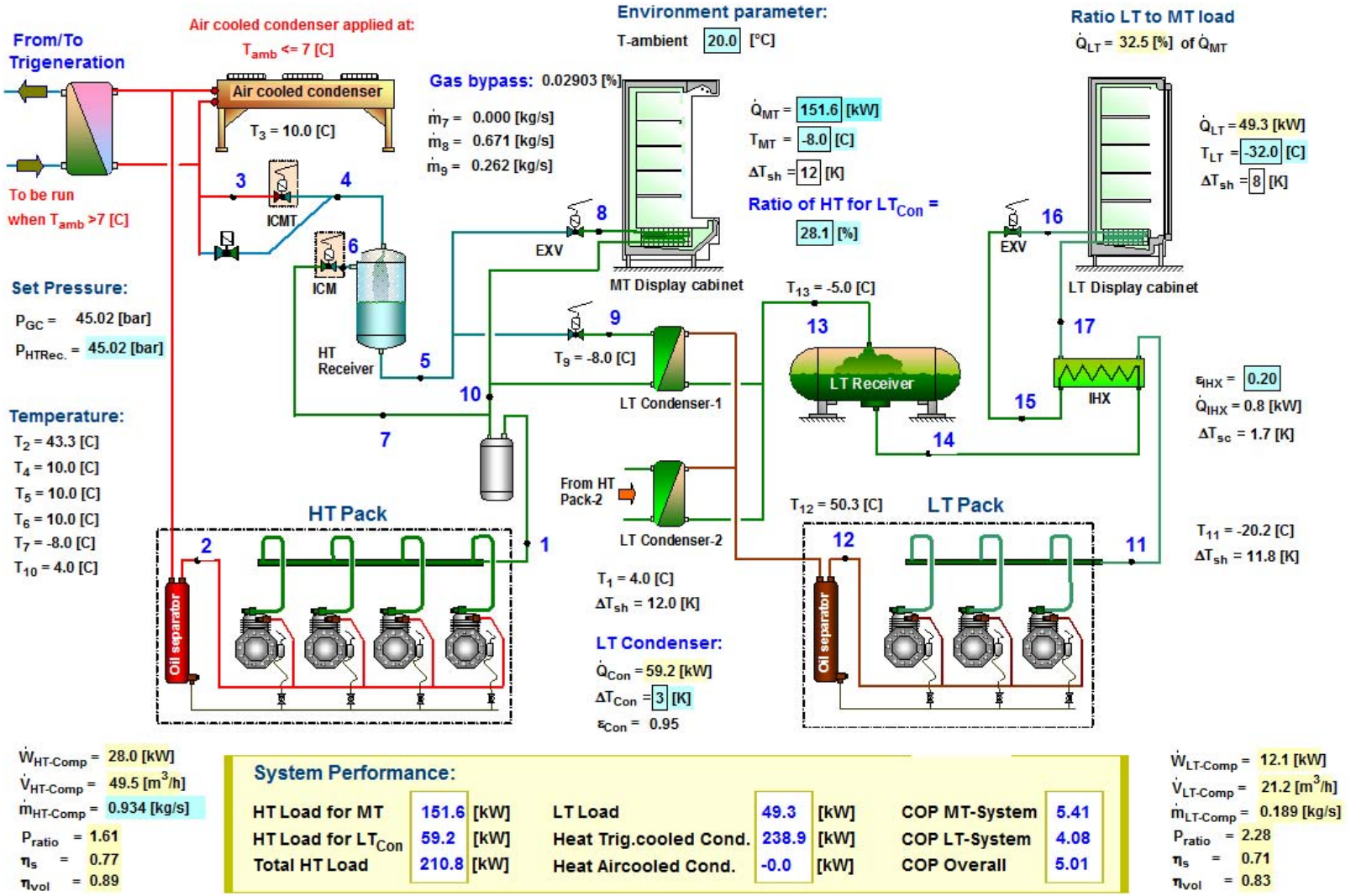

Figure L-2 A display of the EES model for the transcritical CO_2 refrigeration cascaded with a trigeneration system of Scheme-2 (Chapter 7)

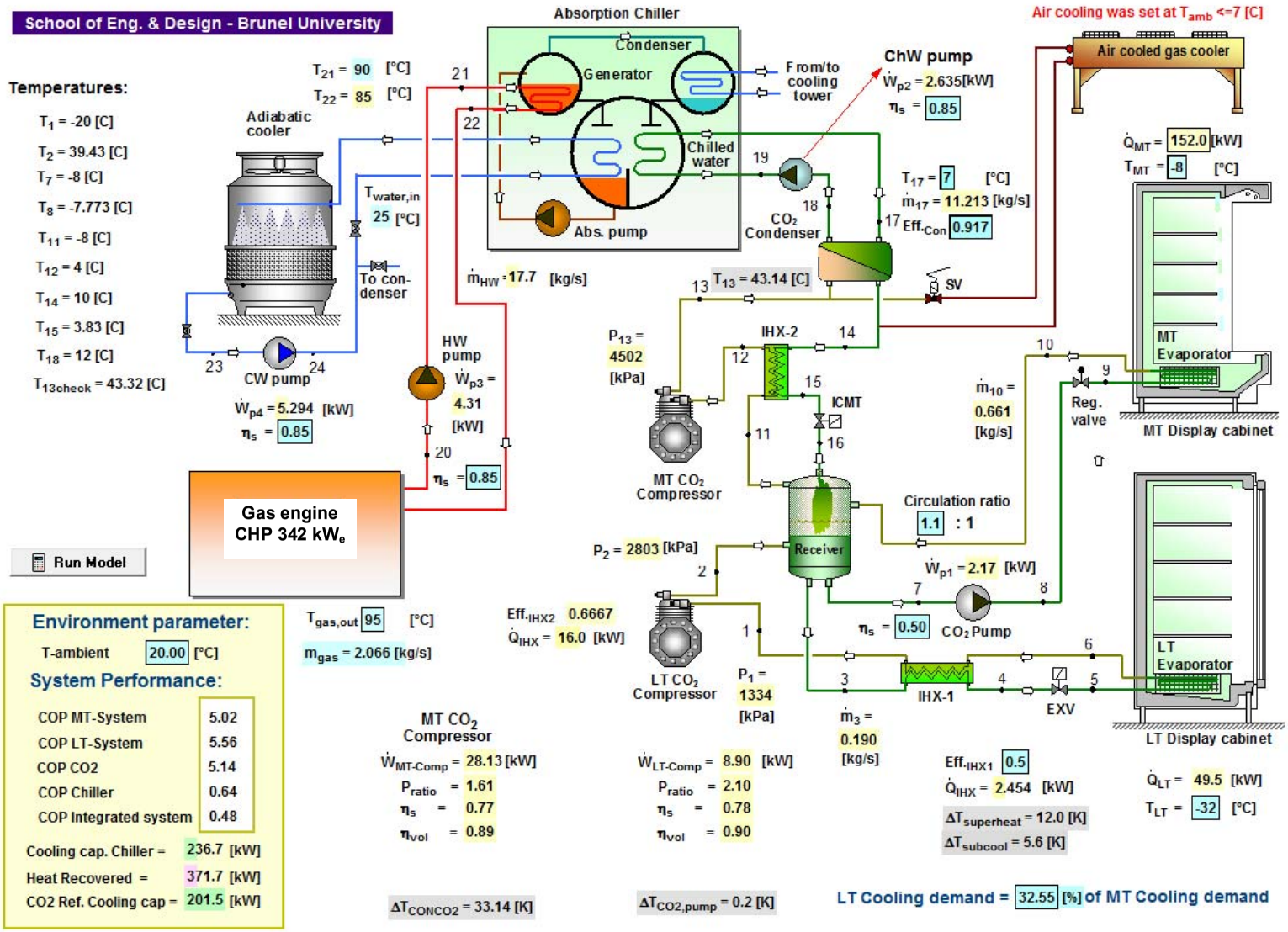

Figure L-3 A display of the EES model for the integrated CO_2 refrigeration and trigeneration system of Scheme-3 (Chapter 7)

APPENDIX M:

Detailed analysis of energy and environment performance of the conventional and trigeneration – CO_2 refrigeration energy systems

This appendix presents detailed analysis of the energy and environmental performance of the conventional energy system and the integrated CO_2 refrigeration and microturbine based trigeneration energy system of the case study supermarket described in Chapter 6.

Fuel energy saving analysis:

Conventional energy system with R-404A refrigerations, gas boilers and electric chiller		
Grid electricity supply	2,817,321	kWh
Electricity of R-404A refrigeration	816,636	kWh
Electricity of Air conditioning	77,467	kWh
Electricity of other than refrigeration and AC system	1,923,219	kWh
Fuel required for grid supply (a)	8,537,338	kWh
Fuel for boiler (b)	874,068	kWh
Total (a + b)	**9,411,406**	**kWh**
Energy system with integrated trigeneration and volatile-DX CO_2 refrigeration system, gas boiler and electric chiller		
CHP fuel (Natural gas) (c)	8,340,324	kWh
Auxiliary boiler fuel (d)	91,090	kWh
Imported electricity	184,408	kWh
Fuel required for grid supply (e)	558,811	kWh
Exported electricity	261,191	kWh
Fuel saving to grid supply (f)	909,370	kWh
Total (c + d + e - f)	**8,080,855**	kWh
Fuel energy savings	**1,330,551**	kWh/year
	152	kWh/hr
Fuel energy saving ratio	**14.14%**	
Ratio of electricity of CHP to total consumption	103.3%	

Assumptions:

Grid electricity efficiency	33.0%	
Self generated electricity efficiency	28.7%	
Boiler efficiency annual	80.8%	

CO_2 emission analysis for Chapter 6:

Conventional energy system with R-404A refrigerations, gas boilers and electric chiller		
Indirect CO_2 emissions	**kWh**	**kgCO_2**
Grid electricity consumption (A)	2,817,321	1,541,075
Natural gas consumption (B)	874,068	160,829
Direct CO_2 emissions	**kg**	**kgCO_2**
Annual R-404A refrigerant leakage (C1)	105	411,443
Annual R-404A refrigerant recovery losses (D)	14	54,859
Annual R-407C refrigerant leakage (C2)	9	16,740
Total (E) = (A)+(B)+(C1)+(D)+(C2)		**2,184,946**
Energy system with integrated trigeneration and volatile-DX CO_2 refrigeration system, gas boiler and electric chiller		
Indirect CO_2 emissions	**kWh**	**kgCO_2**
CHP fuel (F)	8,340,324	1,534,620
Boiler fuel (G)	91,090	16,761
Imported electricity (H)	184,408	100,871
Saving from exported electricity (I)	261,191	142,871
Total (K) = (F)+(G)+(H)-(I)		**1,509,380**
Direct CO_2 emissions	**kg**	**kgCO_2**
Annual refrigerant leakage of R-744 system (L)	53	53
Annual refrigerant leakage of the electric chiller R-407C (M)	9	16,740
Total (P) = (L)+(M)		**16,793**
Total (Q) = (K)+(P)		**1,526,173**
Net emission saving = (E)-(Q)		**658,773**
Percentage of the CO_2 emission savings		**30.15%**

APPENDIX N:

Detailed analysis of energy and environment performance of the energy system alternatives

This appendix details the energy and environment performance analysis of the energy system alternatives of the case study supermarket. The analysis compares the performance of the energy system alternatives to the conventional energy system with R-404A refrigerant.

Fuel energy saving analysis of Scheme-1:

Scheme-1		
CHP fuel (Biodiesel)	4,430,848	kWh
Auxiliary boiler fuel	21,096	kWh
Imported electricity	1,159,933	kWh
Fuel required for grid supply	3,514,949	kWh
Exported electricity	120	kWh
Fuel saving to grid supply	364	kWh
Total	**7,966,529**	kWh
Fuel savings	**1,444,877**	kWh/year
	165	kWh/hr
Fuel saving ratio	**15.35%**	
Ratio of electricity of CHP to total consumption	**57.3%**	

Assumptions:

Grid electricity efficiency	**33.0%**	
Self generated electricity efficiency	**35.1%**	
Boiler efficiency annual	80.8%	

Fuel energy saving analysis of Scheme-2:

Scheme-2		
CHP fuel (Natural gas)	7,907,431	kWh
Auxiliary boiler fuel	194,360	kWh
Imported electricity	44,440	kWh
Fuel required for grid supply	134,666	kWh
Exported electricity	378,908	kWh
Fuel saving to grid supply	1,148,206	kWh
Total	**7,088,252**	kWh
Fuel savings	**2,323,154**	kWh/year
	265	kWh/hr
Fuel saving ratio	**24.68%**	
Ratio of electricity of CHP to total consumption	**113.1%**	

Assumptions:

Grid electricity efficiency	**33.0%**	
Self generated electricity efficiency	**36.6%**	
Boiler efficiency annual	80.8%	

Fuel energy saving analysis of Scheme-3:

Scheme-3		
CHP fuel (Natural gas)	7,450,016	kWh
Auxiliary boiler fuel	24,670	kWh
Imported electricity	62,343	kWh
Fuel required for grid supply	188,919	kWh
Exported electricity	332,962	kWh
Fuel saving to grid supply	1,008,975	kWh
Total	**6,654,630**	kWh
Fuel savings	**2,756,776**	kWh/year
	315	kWh/hr
Fuel saving ratio	**29.29%**	
Ratio of electricity of CHP to total consumption	**111.0%**	

Assumptions:

Grid electricity efficiency	**33.0%**	
Self generated electricity efficiency	**36.6%**	
Boiler efficiency annual	80.8%	

CO_2 emission analysis of the energy system alternatives:

Scheme-1		
Indirect CO_2 emissions	**kWh**	**$kgCO_2$**
CHP fuel (F)	4,430,848	0
Boiler fuel (G)	21,096	3,882
Imported electricity (H)	1,159,933	634,483
Saving from exported electricity (I)	120	66
Total (K) = (F)+(G)+(H)-(I)		**638,299**
Direct CO_2 emissions	**kg**	**$kgCO_2$**
Annual refrigerant leakage of R-744 system (L)	53	53
Annual refrigerant leakage of electric chiller R-407C (M)	9	16,740
Total (P) = (L)+(M)		**16,793**
Total (Q) = (K)+(P)		**655,092**
Net emission savings = (E)-(Q)		**1,529,854**
Percentage of the CO_2 emission savings		**70.02%**

Scheme-2		
Indirect CO_2 emissions	**kWh**	**$kgCO_2$**
CHP fuel (F)	7,907,431	1,454,967
Boiler fuel (G)	194,360	35,762
Imported electricity (H)	44,440	24,309
Saving from exported electricity (I)	378,908	207,263
Total (K) = (F)+(G)+(H)-(I)		**1,307,776**
Direct CO_2 emissions	**kg**	**$kgCO_2$**
Annual refrigerant leakage of R-744 system (L)	53	53
Annual refrigerant leakage of electric chiller R-407C (M)	9	16,740
Total (P) = (L)+(M)		**16,793**
Total (Q) = (K)+(P)		**1,324,568**
Net emission savings = (E)-(Q)		**860,377**
Percentage of the CO_2 emission savings		**39.38%**

Scheme-3		
Indirect CO_2 emissions	**kWh**	**$kgCO_2$**
CHP fuel (F)	7,450,016	1,370,803
Boiler fuel (G)	24,670	4,539
Imported electricity (H)	62,343	34,102
Saving from exported electricity (I)	332,962	182,130
Total (K) = (F)+(G)+(H)-(I)		**1,227,314**
Direct CO_2 emissions	**kg**	**$kgCO_2$**
Annual refrigerant leakage of R-744 system (L)	53	53
Annual refrigerant leakage of electric chiller R-407C (M)	9	16,740
Total (P) = (L)+(M)		**16,793**
Total (Q) = (K)+(P)		**1,244,107**
Net emission savings = (E)-(Q)		**940,839**
Percentage of the CO_2 emission savings		**43.06%**

APPENDIX O:
Assumptions for the economic analysis

This appendix presents key assumptions used for the economic viability analysis of the energy system alternatives. The assumptions include investment, energy and operational costs of the system components for the energy system alternatives and the conventional energy system.

Table O-1 Assumptions for investment cost analysis

Equipment	Unit cost (£/kW capacity)			
	Conventional	Scheme-1	Scheme-2	Scheme-3
Installed cost				
HT R-404A refrigeration packs	350			
LT R-404A refrigeration packs	600			
HT transcritical CO_2 refrigeration packs		625	625	
Modified MT volatile-DX CO_2 packs				625
LT CO_2 refrigeration packs		1267	1267	1267
Electric chiller R-407C for air conditioning	125	125	125	125
Gas boilers	100	100	100	100
Gas engine based generator	169			
Bio-fuel engine based CHP		675		
Gas engine based CHP			675	675
Water-LiBr absorption chiller		250	250	250

Table O-2 Assumptions for energy rates

Electricity rate of National Grid	0.09966	£/kWh
Electricity sold back rate to National Grid	0.08222	£/kWh
Natural gas	0.02768	£/kWh
Bio-fuel	0.04152	£/kWh

Table O-3 Assumptions for other charges

Standing charge	88.9	£/month
Availability charge of electricity supply from grid	0.92	£/kW_e-month
VAT for energy rate and equipment	17.5	%
Percentage of annual O&M cost from the installed cost	5.0	%
Percentage of annual O&M cost for bio-fuel CHP	10.0	%

O&M = operational and maintenance